# Biochemical and Biophysical Studies on Guanylate Cyclase Activating Protein 1, a $Ca^{2+}$-sensor in Phototransduction

## Inaugural - Dissertation

**zur**
**Erlangung des Doktorgrades der**
**Mathematisch-Naturwissenschaftlichen Fakultät**
**der Heinrich-Heine-Universität Düsseldorf**

**vorgelegt von**


## Ji-Young Hwang

**aus Seoul, S. Korea**


**Jülich, März 2001**

Die in dieser Dissertation beschriebenen Arbeiten wurden in der Zeit vom 1. 10. 1997 bis 28. 2. 2001 am Institut für Biologische Strukturforschung des Forschungszentrum Jülich GmbH durchgeführt.

Referent : Prof. Dr. Georg Büldt

Koreferent : Priv. Doz. Dr. Torsten Friedrich

Tag der mündlichen Prüfung: 19. Juni 2001

*"**D**ream of that which cannot come true*
*__L__ove that which seems hopeless to love*
*__E__ndure the pains which seem unbearable*
*__S__eize the stars which seem unreachable"*

*– from 'Don Quijote de la Manch'*
*by Miguel de Cervantes Saavedra –*

# ZUSAMMENFASSUNG

GCAP-1 (Guanylatzyklase aktivierendes Protein 1) ist ein 24 kDa schweres, hydrophobes $Ca^{2+}$-Bindungsprotein. Es enthält drei funktionelle EF-Hand-Calcium-Bindungsmotive und wird *in vivo* N-terminal myristoyliert. Wildtyp GCAP-1 enthält vier Cysteinreste. Es wurden Cystein-Austauschmutanten hergestellt, um die Rolle der Cysteinreste in GCAP-1 für dessen Funktion zu klären. Diese wurden außerdem benutzt, Konformationsänderungen zu detektieren. Rekombinantes Wildtyp GCAP-1 und die Cystein-Mutanten wurden erfolgreich in *E. coli* überexprimiert und durch Gelfiltration und Anionenaustauschchromatographie gereinigt. GCAP-1 Mutanten mit nur einem Cystein-Austausch (Einzelmutanten) aktivierten die ROS-GC1 auf ähnliche Weise wie nichtmyristoyliertes Wildtyp GCAP-1 (halbmaximale Aktivität, $IC_{50}$, = 5.5 µM und Hill-Koeffizient, $n$, = 0.9). Die Mutanten mit drei mutierten Cysteinresten (Dreifachmutanten) aktivierten die ROS-GC1 auf ähnliche Weise wie myristoyliertes Wildtyp GCAP-1 ($IC_{50}$ = 706 nM und $n$ = 1.6). Die Vierfach-Cystein-Mutante ähnelte in ihrer ROS-GC1 Aktivierung am meisten dem nativen GCAP-1 ($IC_{50}$ = 293 nM and $n$ = 1.7). Zusätzlich zeigte diese Mutante einen inhibitorischen Effekt auf die ROS-GC1 bei hohen $[Ca^{2+}]_{frei}$ und ähnelte daher dem nativem GCAP-1. Es wurden verschiedene experimentelle Ansätze gewählt, um die $Ca^{2+}$-abhänigigen Eigenschaften von GCAP-1 zu untersuchen: Komplexierung von $Ca^{2+}$ mit 2 mM EGTA verursachte eine Änderung des Laufverhaltens von GCAP-1 im SDS-Gel. Während GCAP-1 in Gegenwart von $Ca^{2+}$ bei 21 kDa läuft, findet man $Ca^{2+}$-freies GCAP-1 bei 26 kDa. Der α-helikale Anteil in der Sekundärstruktur von nichtmyristoyliertem GCAP-1 verringerte sich in Abwesenheit von $Ca^{2+}$, während er bei myristoyliertem GCAP-1 durch $Ca^{2+}$-Komplexierung anstieg. GCAP-1 war in Gegenwart von $Ca^{2+}$ thermisch stabiler als in Gegenwart von EGTA. In Abwesenheit von $Ca^{2+}$ existierte GCAP-1 meist als Monomer, während in Anwesenheit von $Ca^{2+}$ die dimere Form überwog. In Abwesenheit von $Ca^{2+}$ zeigte GCAP-1 eine ausgeprägte Reaktivität gegenüber DTNB: alle vier Cysteinreste reagierten mit DTNB, während bei GCAP-1 in Anwesenheit von $Ca^{2+}$ nur drei Cysteinreste exponiert waren. Mit Hilfe der Cystein-Mutanten wurde die Thiol-Reaktivität jedes einzelnen Cysteinrestes detailliert untersucht. Zuerst wurden in Anwesenheit von $Ca^{2+}$ die Cysteinreste 18 und 125 exponiert, während das Cystein 29 erst langsam mit DTNB reagierte. Dagegen wurde der Cysteinrest 106 erst bei $Ca^{2+}$-Komplexierung mit EGTA exponiert, in Anwesenheit von $Ca^{2+}$ reagierte er nicht mit DTNB. Die Cystein-Mutanten wurden außerdem benutzt, die Interaktion zwischen GCAP-1 und der GCAP-1-Bindungsstelle der ROS-GC1 (d.h. Peptide, die die hypothetische GCAP-1-Bindungsregion darstellen) zu untersuchen. ROS-GC1 Peptide verringerten die Zugänglichkeit von zwei Cysteinresten, wenn GCAP-1 mit den Peptiden interagierte.

# CONTENTS

# ABBREVIATIONS

| | |
|---|---|
| ACN | acetonitrile |
| APS | ammonium persulfate |
| ATP | adenosine 5´-triphosphate |
| $A_x$ | Absorbance at wavelength *x* nm |
| Bis-Tris | bis(2-hydroxyethyl)-imino-tris-(hydroxymethyl)-methan |
| BSA | bovine serum albumin |
| CD | circular dichroism |
| cDNA | complementary deoxyribonucleic acid |
| cGMP | guanosine cyclic-3´, 5´-monophosphate |
| CNG | cGMP-gated cation channel |
| DMSO | dimethyl sulfoxide |
| DNA | deoxyribonucleic acid |
| DNase | deoxyribonuclease |
| DOC | sodium deoxycholate |
| DTNB | 5,5´-dithionitrobenzoic acid |
| DTT | dithiothreitol |
| ECL | enhanced chemiluminescence |
| *E. coli* | *Escherichia coli* |
| EDC | N-ethyl-N´(dimethylaminopropyl)carboiimide |
| EDTA | ethylenediaminetatraacetic acid |
| EGTA | ethylen glycol-bis(β-aminoethyl ether)-N,N,N´,N´-tetraacetic acid |
| $\varepsilon_x$ | molar absorbance at wavelength *x* nm |
| GAP | GTPase-accelerating protein |
| GC | guanylate cyclase |
| GCAP | guanylate cyclase activating protein |
| GST | glutathione S-transferase |
| HEPES | N-2-hydroxyethyl peperazine-N´-2-ethanesulfonic acid |
| HPLC | high-performance liquid chromatography |
| HRP | horseradish peroxidase |
| IAA | iodoacetic acid |
| IAM | iodoacetamide |
| IPTG | isopropyl-β-D-thiogalactoside |
| $K_{av}$ | partition coefficient of gel filtration |
| kb | kilobase |
| kDa | kilodalton |

| | |
|---|---|
| MALDI-TOF | matrix-assisted laser desorption/ionization time-of-flight |
| MOPS | 3-(N-morpholino)propanesulfonic acid |
| MS | mass spectrometry |
| MW | molecular weight (dimensionless) |
| Myr | myristoylation |
| NCKX | $Na^+/Ca^{2+}$, $K^+$ exchanger |
| ND | non denaturing |
| NHS | N-hydroxysuccinimide |
| NMR | nuclear magnetic resonance |
| NMT | N-myristoyl transferase |
| $OD_x$ | optical density at wavelength *x* nm |
| PAGE | polyacrylamide gel electrophoresis |
| PBS | phosphate-buffered saline |
| PCR | polymerase chain reaction |
| PDE | phosphodiesterase |
| PDEA | 2-(2-pyridinyldithio)ethaneamine |
| PEG | polyethylene glycol |
| pI | isoelectric point |
| PMSF | phenylmethylsulfonyl fluoride |
| PVDF | polyvinylidene difluoride |
| RGS | regulator of G protein signaling |
| ROS | rod outer segments |
| RU | resonance units |
| *S. cerevisiae* | *Saccharomyces cerevisiae* |
| SDS | sodium dodecylsulfate |
| SEC | size exclusion chromatography |
| Sinapinic acid | 3.5-dimethoxy-4-hydroxy cinnamic acid |
| SPR | surface plasmon resonance |
| $T_m$ | midpoint of temperature-induced transition |
| TBE | Tris-borate-EDTA |
| TEMED | N,N,N′,N′-tetramethylethylenediamine |
| TFA | trifluoroacetic acid |
| TNB | 5-thio-2-nitrobenzoic acid |
| Tricin | N-[Tris(hydroxymethyl)-methyl]-glycine |
| Tris | Tris(hydroxymethyl)-aminomethan |
| U | unit |
| UV/VIS | ultraviolet and visible |
| Zaprinast | 1,4-dihydro-5-(2-propoxyphenyl)-7H-1,2,3-triazolo[4,5-d]pyrimidin-7-one |

# ABSTRACT

The guanylate cyclase activating protein 1 (GCAP-1) is a hydrophobic 24 kDa, $Ca^{2+}$-binding protein with three putative functional EF-hands. Native GCAP-1 contains myristate on the N-terminus *in vivo* and four cysteines.

In order to evaluate whether the cysteines in GCAP-1 play a role in its function and can be used for monitoring conformational changes, several cysteine-exchange-mutants were constructed. Recombinant wild-type GCAP-1 and the cysteine mutants were successfully overexpressed in *E. coli* and purified by gel filtration and anion exchange chromatography.

The single cysteine mutants of GCAP-1 activated ROS-GC1 in a similar fashion as nonmyristoylated wild-type GCAP-1 (half maximal activity, $IC_{50}$, = 5.5 μM and Hill coefficient, $n$, = 0.9). The triple cysteine mutants of GCAP-1 activated ROS-GC1 in a similar fashion as myristoylated wild-type GCAP-1 ($IC_{50}$ = 706 nM and $n$ = 1.6). The quad cysteine mutant of GCAP-1 stimulated ROS-GC1 most similarly to native GCAP-1 ($IC_{50}$ = 293 nM and $n$ = 1.7) and also showed an inhibitory effect on ROS-GC1 in high $[Ca^{2+}]_{free}$.

Several $Ca^{2+}$-dependent properties of GCAP-1 were examined. On SDS-PAGE, complexing $Ca^{2+}$ with 2 mM EGTA in GCAP-1 solution caused a $Ca^{2+}$-dependent mobility shift of GCAP-1 from approx. 21 kDa to approx. 26 kDa. The α-helical content in the secondary structure of GCAP-1 decreased when the nonmyristoylated form was $Ca^{2+}$-free and when the myristoylated form was saturated with $Ca^{2+}$. Furthermore, GCAP-1 existed predominantly as a monomer in the absence of $Ca^{2+}$ and as a dimer in the presence of $Ca^{2+}$. $Ca^{2+}$-bound GCAP-1 was the most thermally stable form, compared with $Ca^{2+}$-free GCAP-1.

GCAP-1 showed a pronounced reactivity towards the thiol-modifying reagent, DTNB. When EGTA was added, all four cysteines rapidly reacted with DTNB, while only three cysteines in GCAP-1 were exposed in the presence of $CaCl_2$. Cysteine mutants of GCAP-1 were used to investigate the thiol reactivity of every single cysteine in more detail. The cysteines at position 18 and 125 were rapidly exposed in the presence of $Ca^{2+}$, whereas the cysteine at position 29 slowly reacted with DTNB in the presence of $Ca^{2+}$. Only the cysteine at position 106 was buried within GCAP-1 when $Ca^{2+}$ was bound, and it was exposed after EGTA addition.

Cysteine mutants were also used to study the interaction of GCAP-1 with target regions in ROS-GC1 (i.e. peptides representing hypothetical binding regions). ROS-GC1 peptides induced a shielding effect on two cysteines of GCAP-1, when they interacted with GCAP-1.

# 1. INTRODUCTION

## 1.1 Phototransduction in Vertebrate Photoreceptor Cells

In the vertebrate eye the lens focuses an image on the retina. The retina is composed of tightly stacked cell layers – including ganglion cells, bipolar cells, amacrine cells, horizontal cells, and photoreceptor cells (rods and cones). Light is converted into an electrical signal by the photoreceptor cells. The signal is relayed via horizontal cells, bipolar cells, and amacrine cells to the ganglion cells which convey the signal to the brain [1,2] (Fig. 1.1 *A*).

### 1.1.1 Vertebrate Photoreceptor Cells

A human retina contains approximately $1\times10^8$ rods and $5\times10^6$ cones. The rod cells are specialized for the detection of dim light, whereas the cone cells function in bright light and mediate color vision – there are three types of cones, each with different spectral response [3]. The human rod outer segment has a stack of about 500–2000 double membranous discs about 16 nm thick (Fig. 1.1 *B*). Each disc in humans contains $1\times10^4$–$10^6$ rhodopsins, the visual pigment molecules [4].

### 1.1.2 Phototransduction Cascade

A single photon absorbed by a dark-adapted rod outer segment closes hundreds of cation-selective channels. Upon illumination the rod hyperpolarizes to a membrane-potential of about −70 mV. The part of the electrophysiological response associated with the underlying biochemical events is called *the rising phase* (Fig. 1.2).

Rhodopsin (**R**) is composed of the apoprotein, opsin (**O**), and the chromophor, 11-*cis*-retinal, which is covalently linked to opsin. Absorption of a photon (***hv***) causes the isomerization of 11-*cis*-retinal to all-*trans*-retinal which leads to a conformational change of the protein moiety; rhodopsin changes its conformation and reaches an active state called metarhodopsin II (**R***). The photoactivated rhodopsin then enhances the exchange of GDP to GTP on a heterotrimeric G-protein, transducin (**T**). One single activated rhodopsin catalyzes the activation of ~500 molecules of transducin. The activated GTP-bound form of transducin

($T_\alpha$*-GTP) stimulates the hydrolytic activity of a phosphodiesterase (**PDE**) by relieving its inhibitory γ subunit ($PDE_\gamma$). The activated catalytic subunits of PDE ($PDE_{\alpha,\beta}$*) then hydrolyzes guanosine cyclic-3′-5′-monophosphate (**cGMP**) to 5′-GMP [5]. The decrease of the cGMP concentration leads to the closure of the cyclic nucleotide-gated (**CNG**) cation channels stopping the influx of $Ca^{2+}$ ions and thus hyperpolarizing the plasma membrane of the photoreceptor outer segment [6].

In light, closure of the channel stops the influx of $Ca^{2+}$, but the efflux continues and consequently reduces the free concentration of $Ca^{2+}$ from ~500 nM in the dark to ~50 nM in the outer segment. In darkness the CNG channels are open when 3–4 molecules of cGMP are bound per channel and sustain a dark current of which 80% is carried by $Na^+$ and 10–15% by $Ca^{2+}$. There is a steady circulation of $Ca^{2+}$ in the photoreceptor cell, which consists of an influx through the CNG channels and an efflux through a $Na^+/Ca^{2+}$, $K^+$ exchanger (**NCKX**) [7]. The NCKX operates by exchanging extracellular $Na^+$ with intracellular $Ca^{2+}$ and $K^+$.

Returning to the dark state during *the recovery phase* is mediated by the deactivation of the active intermediates in the phototransduction cascade [8]. Transducin is deactivated through its intrinsic GTPase activity, which hydrolyzes GTP to GDP, and allows $PDE_\gamma$ to reassociate with $PDE_{\alpha,\beta}$*. There is a GTPase-accelerating protein (GAP) or RGS9 which stimulates GTP hydroylsis by $T_\alpha$ which is enhanced by GAP activity of the PDE inhibitor γ subunit [9]. The deactivated phosphodiesterase no longer hydrolyzes cGMP. Meanwhile the photoactivated rhodopsin is phosphorylated by rhodopsin kinase (**RK**) and subsequently binds to arrestin (**Arr**), which terminates the activity of rhodopsin and suppresses further interaction of rhodopsin with transducin. The deactivation of phosphodiesterase through deactivation of transducin allows the cGMP concentration to return to high level and, thus, the CNG channels reopen [10].

When cytoplasmic calcium ($[Ca^{2+}]_i$) levels decrease as a result of the closure of CNG channels, the guanylate cyclase (**GC**) is stimulated to enhance its synthesis of cGMP. Thus the cGMP-gated channels reopen to allow $Ca^{2+}$ ions to flow into the cell [11].

The $Ca^{2+}$-mediated feedback pathway is regulated by different $Ca^{2+}$-binding proteins. 1) Recoverin (**Rec**) apparently regulates the phosphorylation of activated rhodopsin through the inhibition of rhodopsin kinase at high $[Ca^{2+}]_i$ [12]. 2) Guanylate cyclase activating proteins (**GCAP**) activate guanylate cyclase at low $[Ca^{2+}]_i$ and also mediate the inhibitory action of $Ca^{2+}$ at high concentration [13,14]. 3) The cGMP-gated channel is also a target of $Ca^{2+}$ feedback. When $[Ca^{2+}]_i$ decreases in light, the channels tend to reopen in spite of the drop in cGMP

level, because $Ca^{2+}$ decreases the apparent affinity of the channels to cGMP. This effect of $Ca^{2+}$ is mediated by calmodulin (**CaM**) [15].

The reciprocal relation between $Ca^{2+}$ and cGMP in photoreceptor outer segments is a mechanism of light adaptation. It plays a role in recovery after light stimulation in the transduction cascade and desensitization of the photoreceptor to light. Decline in $Ca^{2+}$ in the light induces stimulation of the guanylate cyclases. The guanylate cyclases responsible for the synthesis of cGMP are controlled by GCAPs which are sensitive to the $Ca^{2+}$ level [14].

The biochemical mechanism of phototransduction in a rod outer segment is shown in Fig. 1.3 and summarized in Table 1.1.

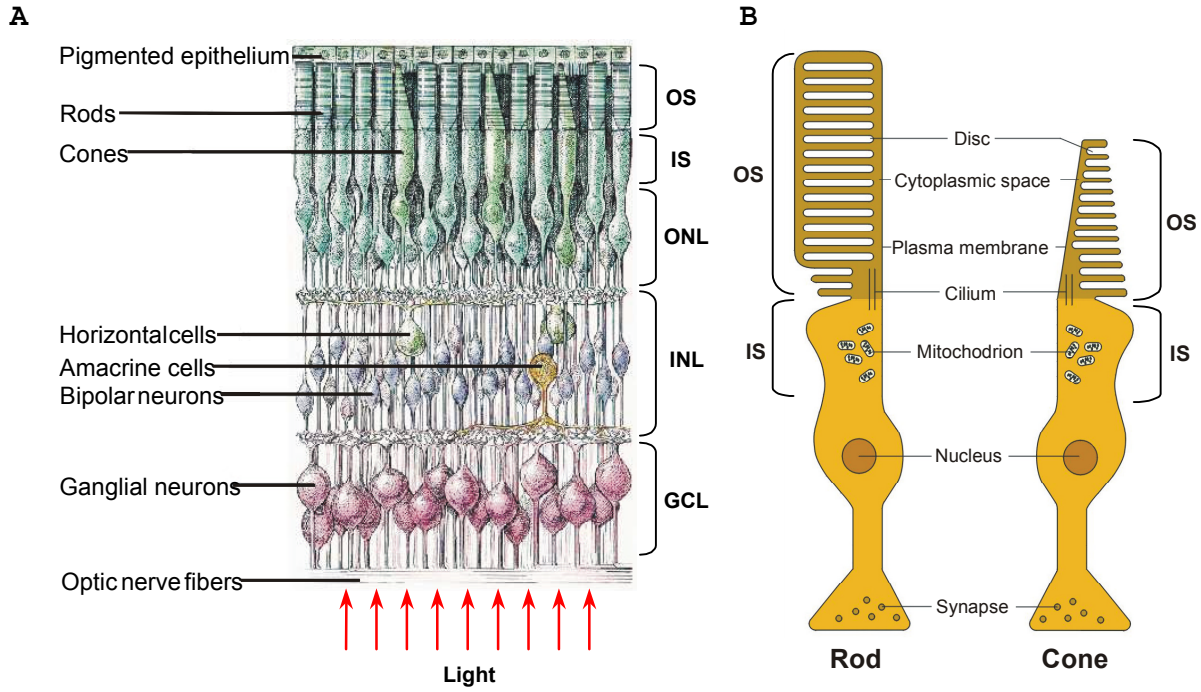


**FIG. 1.1.** The structure of the retina and the types of the photoreceptor cells. ***A.*** The retina is a tightly packed layer of cells, capable to transform light into nerve impulses and to integrate visual information. The retina layers are indicated as follows; OS, outer segments; IS, inner segments; ONL, outer nuclear layer; INL, inner nuclear layer; GCL, ganglion cell layer. ***B.*** The outer segment of human rods is slender, elongated, cylindrical element with length of ~20 µm and diameter of ~2 µm, while the human cones are short, stout cells with an outer segment tapering to its distal end. The peripheral cone outer segment is ~10 µm in length and ~2.5 µm across at its base [2,16].

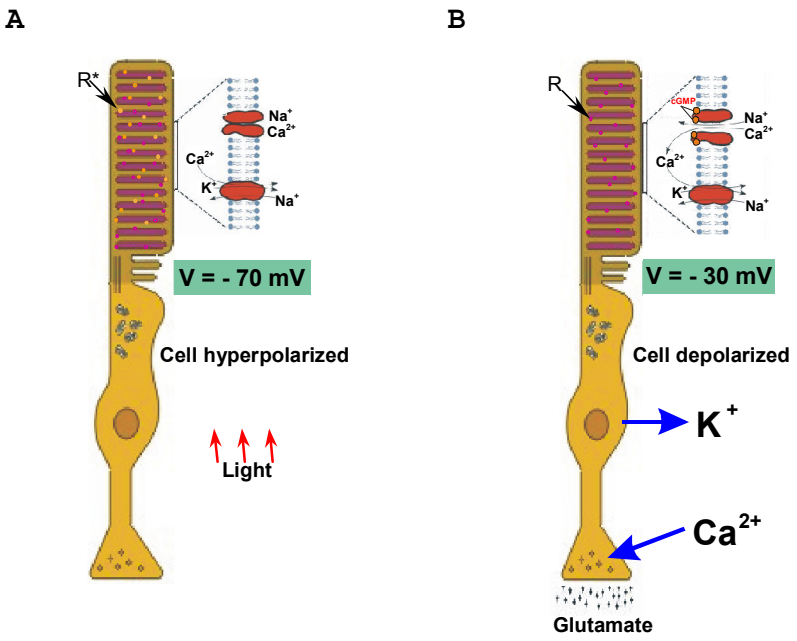


**FIG. 1.2.** Photoreceptors response to light and transmit the signals. ***A.*** In the light, the cGMP level decreases and the cation channels close, leading to a membrane hyperpolarization. ***B.*** In the dark, cGMP binds to and opens cation channels on the plasma membrane of the outer segment. Open CNG channels on the plasma membrane of the outer segment sustain an inward dark current, which keeps the cell partially depolarized and maintains a steady release of neurotransmitter from its synaptic terminal [2].

**TABLE 1.1** List of the key proteins of visual phototransduction in vertebrate photoreceptors

| **Protein** | **Mass (kDa)** | **Function** |
|---|---|---|
| Rhodopsin (R) | 36 | Light receptor, activation of transducin |
| Transducin (T) | 84; α (39), β (37), γ (8) | Activation of cGMP-PDE<br>$T_\alpha$ has an intrinsic GTPase activity. |
| Phosphodiesterase (PDE) | 200; α (88), β (84), γ (11), δ (17) | Hydrolysis of cGMP to 5′-GMP<br>$PDE_\gamma$ has GAP activity [9]. |
| Guanylate cyclase (GC) | 110–120 | Synthesis of cGMP from GTP |
| Cyclic nucleotide gated (CNG) cation channel | α (63), β (240) | Influx of $Ca^{2+}$ and $Na^+$ |
| $Na^+/Ca^{2+}$, $K^+$ exchanger (NCKX) | 230 | Electrogenic exchange of $Ca^{2+}$ and $K^+$ against $Na^+$ |
| $Na^+/K^+$ ATPase | 155; α (113), β (35), γ (6) | Hydrolysis of ATP coupled with the exchange of $Na^+/K^+$ |
| Rhodopsin kinase (RK) | 68 | Phosphorylation of R*<br>Initiation of deactivation of R* |
| Arrestin (Arr) | 48 | Inactivation of R* and prevention of T-mediated activation of PDE |
| Regulator of G protein signaling (RGS) protein | 57 | Activator of $T_\alpha$-GTPase activity as GAP [9] |
| Recoverin (Rec) | 23 | $Ca^{2+}$-sensitive inhibition of RK |
| Calmodulin (CaM) | 17 | $Ca^{2+}$-sensitive regulation of CNG |
| Guanylate cyclase activating proteins (GCAP-1 and -2) | 24 | $Ca^{2+}$-sensitive modulator of GC |

* The apparent molecular weight of ROS-GC1 is ~110 kDa on SDS-PAGE. The calculated molecular mass ~120 kDa containing the 56 amino acids of an N-terminal signal peptide (LS), which is cleaved of in the mature protein. For reviews, see References 2,5,10,11,17-25.

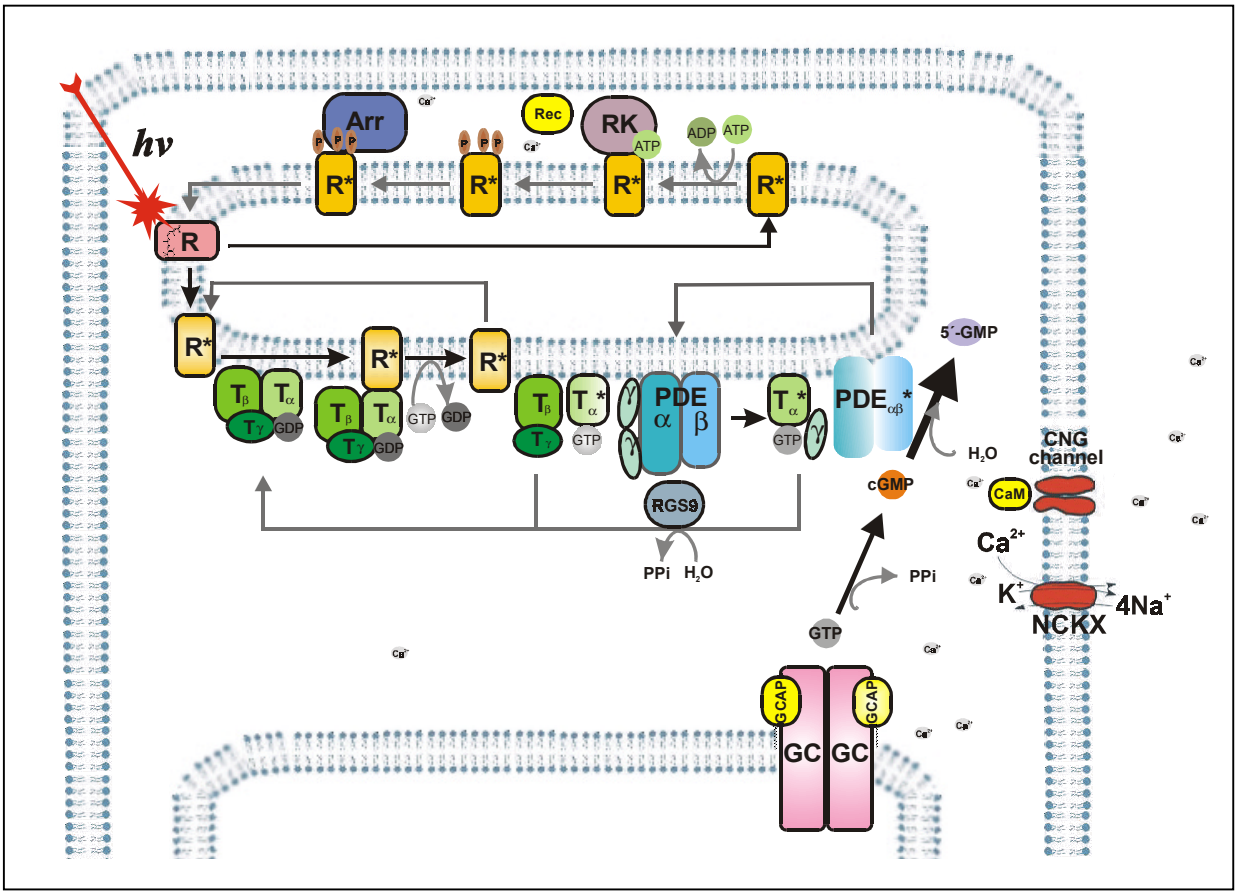


**FIG. 1.3.** Schematic description of the biochemical mechanism of phototransduction. When a photon of light (***hv***) hits 11-*cis*-retinal in the transmembrane protein rhodopsin (**R**), a conformational change occurs that allows transducin (**T**) to be activated. The activated transducin ($\mathbf{T_\alpha}$*) stimulates the hydrolytic activity of the phosphodiesterase (**PDE**) by removing its inhibitory γ-subunits. Hydrolysis of cGMP by the activated phosphodiesterase ($\mathbf{PDE_{\alpha\beta}}$*) causes the closure of cGMP-gated cation channels (**CNG**) in the plasma membrane and hyperpolarization of the photoreceptor cell. The light signal ends when $\mathbf{T_\alpha}$* becomes inactive by hydrolyzing its GTP and rhodopsin kinase (**RK**) phosphorylates rhodopsin by negating the inhibitory effect of recoverin (**Rec**). Interaction with $\mathbf{PDE_\gamma}$ and the RGS9 complex accelerates the intrinsic GTPase activity of $\mathbf{T_\alpha}$* which returns it into the inactive GDP-bound state. $\mathbf{T_\alpha}$-GDP releases the $\mathbf{PDE_\gamma}$, allowing the catalytic subunits of $\mathbf{PDE_{\alpha\beta}}$ to become re-inhibited. Reductions in calcium caused by light stimulate guanylate cyclase (**GC**) to replace the hydrolyzed cGMP. The GC is stimulated by $Ca^{2+}$-free sensor protein (**GCAP**), restores cGMP concentration, and the cGMP-gated channels reopen. The asterisks indicate the active forms of proteins in the cascade. For reviews, see References 2,5,10,19,21,25-27.

## 1.2 Guanylate Cyclase (GC)

Guanylate cyclases (EC 4.6.1.2) are enzymes which catalyze the formation of cGMP from GTP. They are found both in the soluble and the plasma membrane-bound forms with different structure, regulation, and properties. The known mammalian guanylate cyclases are listed in Table 1.2.

### 1.2.1 Classification of Guanylate Cyclases

The soluble forms of cytoplasmic guanylate cyclase are heterodimers. The two subunits, α and β, are proteins of 70–82 kDa which are highly homologous. Two isoforms of the subfamily of soluble guanylate cyclases have been found, $\alpha_1 \cdot \beta_1$ and $\alpha_2 \cdot \beta_1$ [28]. A heme group is bound to subunits, α and β, and the soluble guanylate cyclases are activated by binding of nitric oxide to the heme.

The membrane-bound and cytoplasmic forms of guanylate cyclase share a conserved domain which is important for the catalytic activity to synthesize cGMP. A subfamily of membrane-bound guanylate cyclases consists of the peptide receptors, atrial natriuretic factor receptor (ANP-A or **GC-A**) which is specific to atrial natriuretic peptide (ANP) [29], atrial natriuretic factor receptor (ANP-B or **GC-B**) which is stimulated more effectively by brain natriuretic peptide (BNP) than by ANP [30], and the intestinal receptor (**GC-C**) for *E. coli* heat-stable enterotoxin (STa), guanylin, and uroguanylin [31]. In vertebrate photoreceptor cells, there are two isoforms of the subfamily of retinal guanylate cyclases (ROS-GC), referred to as ROS-GC1 (RetGC-1 or **GC-E**) and ROS-GC2 (RetGC-2 or **GC-F**) [11,32,33]. In addition an olfactory GC (**GC-D**) [34] and a novel membrane form of GC (**GC-G**) have been cloned from rat [35].

### 1.2.2 Characteristics of ROS-GC1

ROS-GC1, one isoform of the subfamily of the retinal membrane-bound guanylate cyclase, has been isolated from the vertebrate photoreceptor outer segments and identified as a ~112 kDa protein. It was cloned from human [36], bovine [37], and rat [38] retinal cDNA libraries.

Immunocytochemistry has shown that ROS-GC1 is localized in cone outer segments and in rod outer segments and also detected in the plexiform layers of retina. ROS-GC1

appears to be more abundant than ROS-GC2 in the retina [39]. Only ROS-GC1 may contribute to the pool of cGMP, essential to support phototransduction in photoreceptors. The localization of ROS-GC2 within photoreceptors is not well known.

The ROS-GC1 activity of bovine ROS membranes is highly dependent on the concentration of $Ca^{2+}$ ions in the range between 20–400 nM. Its specific activity decreases from 11 to 2 nmol $cGMP \cdot min^{-1} \cdot mg^{-1}$ rhodopsin when free concentration of $Ca^{2+}$ ($[Ca^{2+}]_{free}$) is raised from 20 to 200 nM [13]. The decline in $[Ca^{2+}]_{free}$ causes activation of ROS-GC with $EC_{50}$ values ~100 nM and a Hill coefficient of 2–2.5. At $[Ca^{2+}]_{free} \leq 500$ nM, ROS-GC1 is activated by guanylate cyclase activating proteins (GCAPs; GCAP-1, GCAP-2, and GCAP-3) [40,41]. However, at $[Ca^{2+}]_{free} \geq 1$ μM, ROS-GC1 is stimulated by S100β (namely CD-GCAP) [42,43].

Several additional biochemical mechanisms are probably involved in the regulation of ROS-GC1, including ATP binding [44], actin and tubulin binding [45,46], as well as inhibition by RGS9 [47] and by guanylate-cyclase-inhibitory protein (called as GCIP) [48]. GCAPs activate ROS-GC1 by enhancing dimerization of ROS-GC1 [49]. Transition of the active form of ROS-GC1 to its inactive form is caused by either partial or complete dissociation of the dimeric form [50].

### 1.2.3 Structure of ROS-GC1

Several functional domains in ROS-GC1 have been predicted: an N-terminal signal peptide for leader sequence (**LS**), an extracellular domain (**ECD**), a transmembrane domain (**TM**), a juxtamembrane domain (**JMD**), an intracellular protein kinase homology domain (**KHD**), a dimerization domain (**DD**), a cyclase catalytic domain (**CCD**), and C-terminus (**C-T**) (Fig. 1.4).

Duda et al. suggested that the extracellular domain of ROS-GC1 may not regulate ROS-GC1 activity [51]. The activation of GCAP-2 was effected through the deletion of the extracellular domain domain, accordingly the extracellular domain has a regulatory function that has not yet been detected. However, deletion of extracellular domain had no effect on the regulation of GCAP-1 [51]. GCAPs interact constitutively with the kinase homology domain of ROS-GC1 and cGMP synthesis is controlled by $Ca^{2+}$-dependent conformational changes in the ROS-GC/GCAP complex [52]. Some mutations in the juxtamembrane domain of ROS-GC1 were found to be connected with Leber's congenital amaurosis (LCA1) [53] and others in the dimerization domain of ROS-GC1 were related to cone-rod dystrophy (CORD6) [54-56].

The primary structures of the cyclase catalytic domains of ROS-GC1 and of adenylate cyclase are very similar. Because of this similarity it has recently been possible to model the catalytic site of ROS-GC1 based on the crystal structure of an adenylate cyclase homodimer. The stereochemical data substantially define the conformation of the bound $Mg^{2+}$·ATP or $Mg^{2+}$·GTP complex, docked into the active sites [57].

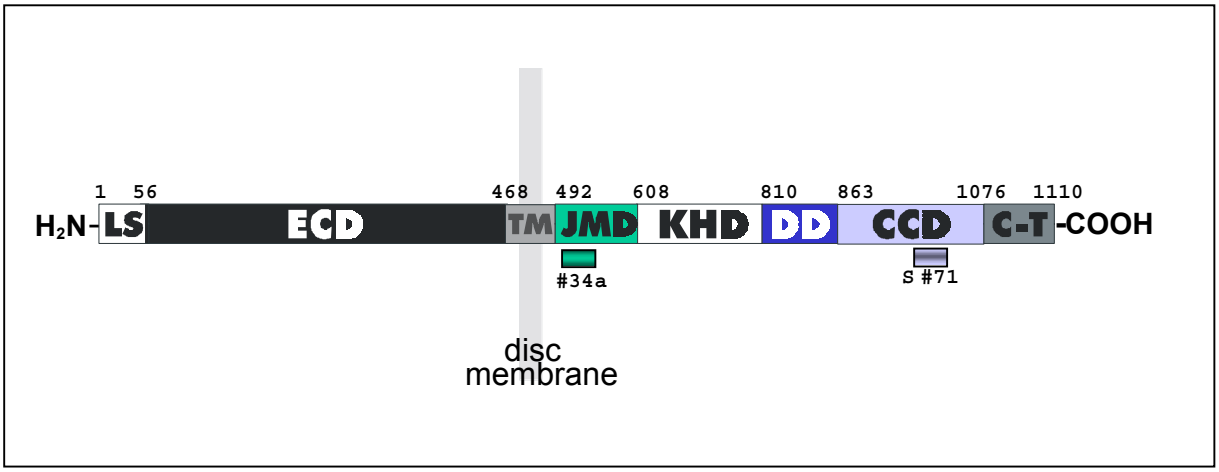


**FIG. 1.4.** Schematic representation of the topographic map of ROS-GC1: N-terminal signal peptides for leader sequence (LS), extracelluar domain (ECD), transmembrane domain (TM), juxtamembrane domain (JMD), kinase homology domain (KHD), putative dimerization domain (DD), catalytic cyclase domain (CCD), and C-terminus (C-T) [58]. The ECD resides in the intracellular domain and can also be assigned as intradiscal domain (IDD). The box with #34a indicates the peptide #34a ($Leu^{559}$–$Ile^{578}$) within the JMD of ROS-GC1 [59] and the box with S #71 indicates the peptide Sokal #71 ($Gly^{966}$–$Gly^{983}$) within the CCD of ROS-GC1 [60] (see Appendix 6.5.1).

**TABLE 1.2** Properties of mammalian guanylate cyclases

| Name | Mass (kDa) | Function | Ligand | Tissue Distribution |
|---|---|---|---|---|
| Soluble GC; | | activated by NO or CO | NO, CO | |
| subunit GC-$\alpha_2$ | 82 | | | smooth muscle, platelets, blood cells, aortic tissues |
| -$\beta_1$ | 71 | | | lung, brain |
| -$\alpha_1$ | 77 | | | - |
| -$\beta_2$ | 19 | | | kidney, liver |
| **GC-A** (ANP-A or NPR-A) | 130 | atrial natriuretic factor receptor | ANP | smooth muscle, kidney, adrenal, heart |
| **GC-B** (ANP-B or NPR-B) | 117 | atrial natriuretic factor receptor | BNP, CNP | fibroblasts, other tissues |
| **GC-C** (Intestinal GC) | 123 | guanylin receptor | STa, guanylin, uroguanylin | intestine |
| **GC-D** (Olfactory GC) | 122 | olfactory GC-D | - | olfactory neuroepithelium |
| **GC-E** (RetGC-1 or ROS-GC1) | 114 | photoreceptor membrane GC; activated by GCAPs | - | retina (rod/cone), pineal gland |
| **GC-F** (RetGC-2 or ROS-GC2) | 118 | photoreceptor membrane GC; | - | retina (rod/cone outer segments), pineal gland |
| **GC-G** | 122 | novel membrane form of GC from rat | - | skeletal muscle, lung, intestine |

## 1.3 Guanylate Cyclase Activating Proteins (GCAP)

The native GCAP-1, a 24 kDa acidic protein with a pI of 4.40, has four cysteine residues out of 204 amino acids. GCAP-1 is a hydrophobic, $Ca^{2+}$-binding protein with three putative functional EF-hands and contains a myristic acid modification on the N-terminus (Fig. 1.5) *in vivo.* It activates ROS-GC1 to synthesize cGMP from GTP under conditions of low cytoplasmic $Ca^{2+}$ concentration (≤500 nM).

### 1.3.1 Characteristics of GCAPs

Koch and Stryer reported in 1988 that a soluble protein imparts $Ca^{2+}$ sensitivity to ROS-GCs [13]. Later, one of the soluble activators, GCAP-1, was isolated from a fraction containing photoreceptor outer segment membranes and purified to apparent homogeneity based on its ability to activate ROS-GC activity in washed photoreceptor outer segment membranes [14]. Another activator, GCAP-2, was isolated from a heat-stable fraction of soluble retinal proteins and was also purified by the same criterion [61,62]. A third activator, GCAP-3, was cloned from a human retina library [41].

Genes encoding GCAP1 and GCAP2 in mammals are adjacent to each other in tail-to-tail orientation [63] on chromosome 6p21.1 in human [64,65]. The GCAP3 gene is located on 3q13.1, suggesting an ancestral gene duplication/translocation event [41].

GCAP-1 is detected in rod outer segments and cone outer segments and also observed in disc membrane regions. Less GCAP-1 is also found in synaptic regions and inner segments of cones. GCAP-2 is observed in outer and inner segments of rods and cones. Synaptic regions are also labeled by a GCAP-2 antibody [40,64,66,67].

GCAPs regulate their target enzyme, ROS-GCs, as a function of $Ca^{2+}$ which binds to their EF-hands. However, the unique property of GCAPs is not from their ability to inhibit ROS-GC activity in $Ca^{2+}$-bound forms but from becoming potent activators in $Ca^{2+}$-free forms. This phenomenon was not previously observed for other EF-hand proteins.

A mutation, $Tyr^{99}Cys$, in human GCAP-1 was recently found to be linked to an autosomal dominant cone dystrophy in British families [68-71]. The families with this mutation were shown to be ancestrally related. Decreased visual acuity and loss of color vision occurred after the age of 20 years, followed by progressive atrophy of the central 5 degrees to 10 degrees of vision angles.

### 1.3.2 $Ca^{2+}$-binding Proteins

The GCAPs belong to a family of $Ca^{2+}$-binding proteins that includes recoverin, neurocalcin, hippocalcin, visinin, VILIP, etc. A myristoylation signal is found at the N-termini of GCAPs and other members of this protein family [63,72].

GCAPs have three putative canonical $Ca^{2+}$-binding motifs (EF-hands) that undergo conformational change upon binding of $Ca^{2+}$. They also contain an additional EF-hand-like structure that lacks essential amino acid residues required to coordinate $Ca^{2+}$ [14,41,73]. Each domain contains a pair of EF-hands, the 29-residue helix-loop-helix motifs found in calmodulin, troponin C, parvalbumin, recoverin, and other members of the superfamily. The EF-hands are defined from N-terminus: EF-1 ($Glu^{17}$–$Lys^{46}$), EF-2 ($Tyr^{55}$–$Val^{83}$), EF-3 ($Lys^{91}$–$Ile^{119}$), and EF-4 ($Phe^{135}$–$Asp^{163}$). The N-terminus of GCAP-1 contains a consensus sequence (MGXXXS) recognized by N-terminal myristoyl transferase 1 (NMT1) [74]. GCAP-1 and several other GCAP-like proteins with myristoylate have shown their ability to bind biological membranes in a $Ca^{2+}$-dependent manner.

The mechanism called a '$Ca^{2+}$-myristoylated switch' has been described for recoverin that functions as $Ca^{2+}$-sensor into the membrane when its hydrophobic anchor is exposed at high $[Ca^{2+}]_{free}$ [75]. It operates via a $Ca^{2+}$-induced conformational change that is accompanied by the extrusion of the myristoyl moiety from the interior of the protein into the solvent phase. Nonmyristoylated recoverin does not associate with phospholipids irrespective of the free $Ca^{2+}$ concentration [76]. $Ca^{2+}$-induced extrusion of the myristoyl group causes recoverin to become solvent exposed, and thus recoverin may serve as a target-binding site of rhodopsin kinase [77,78].

The properties of GCAP-1, GCAP-like proteins, and some $Ca^{2+}$-binding proteins are summarized in Table 1.3. Figure 1.6 shows their sequence alignment.

### 1.3.3 Interaction of GCAP-1 with ROS-GC1

It is reported that GCAP-1 interacts with more than one site in ROS-GC1. GCAPs interact with the intracellular domain of ROS-GCs [51,52]. When $[Ca^{2+}]_{free}$ is less than 300 nM, ROS-GC1 is activated by GCAP-1, GCAP-2, and GCAP-3. ROS-GC2 has also been reported to be stimulated by GCAP-2 and GCAP-3 but not by GCAP-1 under similar $[Ca^{2+}]_{free}$ [41]. In addition, GCAPs appear to inhibit the basal GC activity in the presence of more than 500 nM of $[Ca^{2+}]_{free}$ [44].

Lange et al. reported that two regions represented by peptides #5 ($Leu^{497}$–$Thr^{516}$) and #34a ($Leu^{559}$–$Ile^{578}$) within the JMD of ROS-GC1 are critical for activation of ROS-GC1 by GCAP-1 [59]. The sequence covered by peptide #34a represents a main regulatory site for GCAP-1. This peptide showed a significant inhibitory effect on the ROS-GC1 activity at low $[Ca^{2+}]_{free}$, while it was slightly more efficient at high $[Ca^{2+}]_{free}$. Since peptide #5 inhibited the activated state of ROS-GC1 more effectively, this region represents a GCAP-1 dependent transducer motif of ROS-GC1. The other motif is necessary to cause $Ca^{2+}$-dependent activation of the CCD. A peptide ($Gly^{966}$–$Gly^{983}$; named 'peptide Sokal #71' or 'S #71' in this thesis) from the CCD of ROS-GC1 was a strong inhibitor of GCAP-1/GCAP-2 mediated activation [60]. The peptide #34a and the peptide Sokal #71 are at remote distances in the primary structure within the guanylate cyclase molecules. Therefore, the CCD and the JMD probably form a multipoint attachment site for GCAP-1 [59,60].

Schrem et al. have identified a 15-amino acid region located at EF-2 in GCAP-1 as the main interaction domain for ROS-GC1 [45]. The peptides #37/38 ($Phe^{73}$–$Lys^{87}$) from GCAP-1 interact with the GCAP-1 dependent activation of ROS-GC1 at low $[Ca^{2+}]_{free}$, which indicates that it critically disturbs the $Ca^{2+}$-dependent activation of ROS-GC1 by GCAP-1. In addition, they reported that ROS-GC1 and tubulin formed a complex with GCAP-1 from the co-immunoprecipitation experiments [45].

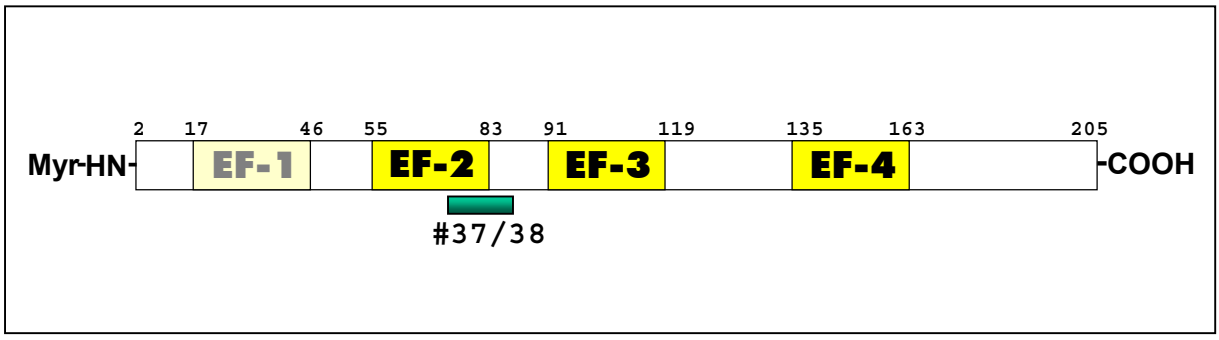


**FIG. 1.5.** Schematic diagram of the topographic map of GCAP-1. GCAP-1 contains one non-functional EF-hand (EF-1) and three distinct functional EF-hands (EF-2, EF-3, and EF-4). The amino acid numbers of each domain of GCAP-1 are indicated above the diagram. The peptides #37/38 ($Phe^{73}$–$Lys^{87}$) are located in EF-2 and between EF-2 and EF-3 [45].

**TABLE 1.3** Properties of GCAP-1 and some $Ca^{2+}$-binding proteins

| Protein | Mass (kDa) | Tissue Localization | Target | Homology | Myr | Cys | EF-hands | | | | Ref. |
|---|---|---|---|---|---|---|---|---|---|---|---|
| | | | | | | | 1 | 2 | 3 | 4 | |
| GCAP-1 | 22.9 | vertebrate retina (ROS/COS) | ROS-GC1 | 100% | + | 4 | - | + | + | + | 63 |
| GCAP-2 | 23.5 | vertebrate retina (rods/CIS) | ROS-GC1/GC2 | 44% | + | 3 | - | + | + | + | 61 |
| GCAP-3 | 23.8 | human retina | ROS-GC1/GC2 | 45% | + | 1 | - | + | + | + | 41 |
| GCIP [a] | 23.7 | frog cones | (ROS-GC1) | 35% | +? | 4 | - | + | + | - | 48 |
| NECD [b] | 22.1 | retina, brain stem, cerebellum | (ROS-GC1 or RK) | 41% | + | 2 | - | + | + | + | 79 |
| S100β * | 10.7 | ubiquitous | ROS-GC1 and others | - | - | 0 | - | + | | | 42 |
| Rec [c] | 23.1 | vertebrate retina | RK | 34% | + | 1 | - | + | + | - | 80 |
| CaM *[d] | 16.8 | ubiquitous | CNG channel and others | 26% | - | 0 | + | + | + | + | 81 |

a. Guanylate cyclase inhibitory protein

b. Neurocalcin δ

c. Recoverin

d. Calmodulin

* Calmodulin and S100β are not specific neuronal $Ca^{2+}$-binding proteins, but they are indicated for better comparison with other $Ca^{2+}$-binding proteins.

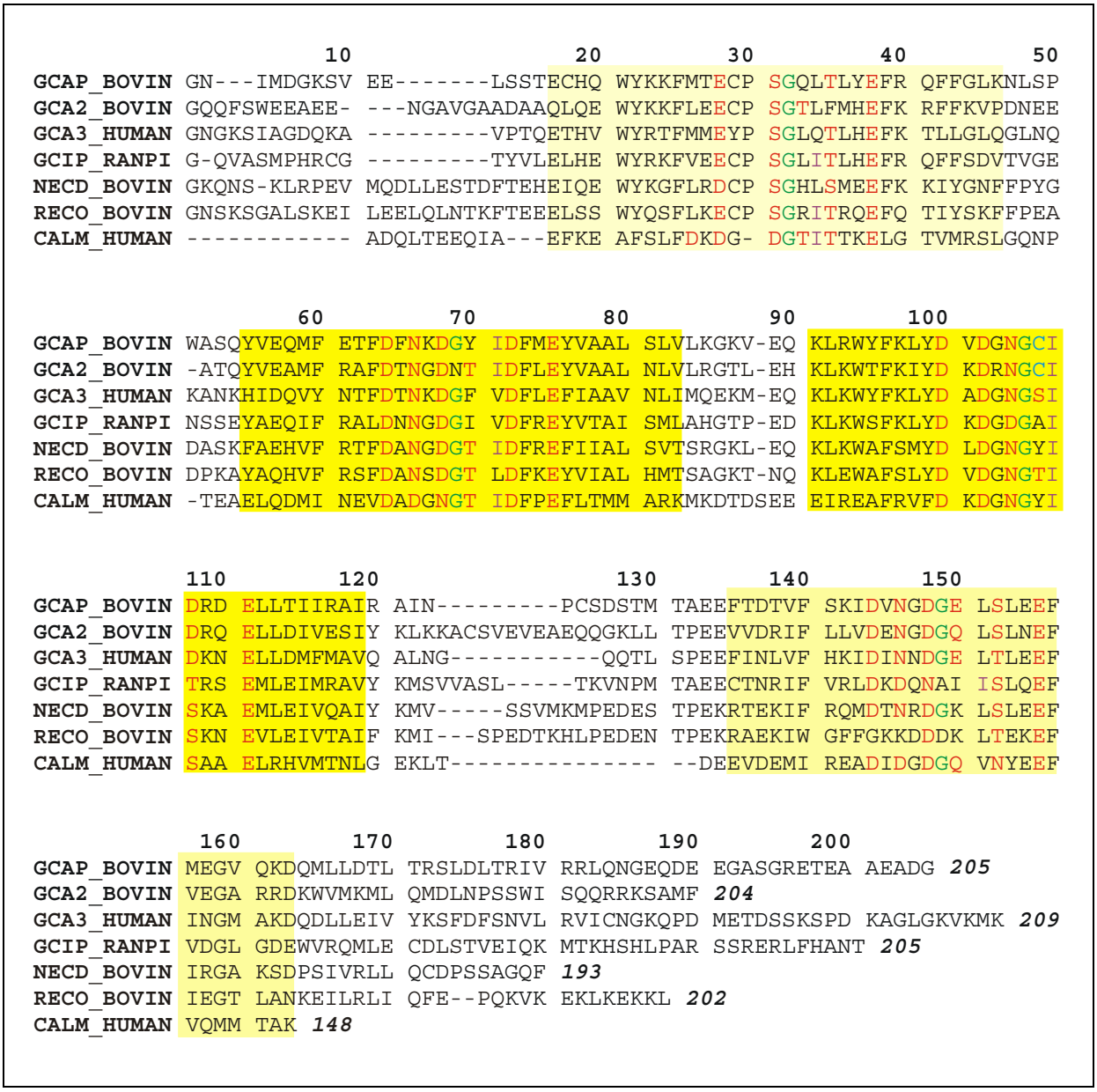


**FIG. 1.6.** Amino acid sequence alignment of GCAP-1 with other GCAPs, GCAP-like proteins, and calmodulin. GCAP_BOVIN (the access number: P46065), GCAP-1 from bovine; GCA2_BOVIN (P51177), GCAP 2 from bovine; GCA3_HUMAN (O95843), GCAP-3 from human; GCIP_FROG (O73763), GCIP from frog; NECD_BOVIN (P29554), neurocalcin δ from bovine; RECO_BOVIN (P21457), recoverin from bovine; CALM_HUMAN (P02593), calmodulin from human and bovine. The sequence of each protein was obtained from SWISS-PROT and TrEMBL Protein Sequence Databases (http://expasy.ch/cgi-bin/sprot-search-ac). The sequence alignment was carried out using CLUSTAL W (1.8) Multiple Sequence Alignment Software from the internet. The 29-residue EF-hand motifs are highlighted in yellow. The consensus sequence for $Ca^{2+}$-binding loops in EF-hands is shown with colored letters.

## 1.4 Purpose of This Thesis

The overall goal of the work presented here is to gain information about the structure and function of GCAP-1.

My initial work with GCAP-1 focused on the preparation of large quantities of pure protein to be used for crystallization and X-ray diffraction studies. Over the past half decade, there has been great progress in the functional and structural understanding of GCAPs. Several groups, including our laboratory, have tried to crystallize it, however no successful results of crystallization have been reported. To address the problems regarding why GCAP-1 is difficult to be crystallized, I investigated the extent and the roles of myristoyl group on the N-terminus, the roles of cysteine residues, and the $Ca^{2+}$-dependent conformational changes of GCAP-1.

Is myristoylation of GCAP-1 important for association with membrane surface, its stimulation of ROS-GC1 activity, and its structural stability? To examine the extent and the role of myristoylation, MALDI-TOF mass spectrometry and high-pressure liquid chromatography (HPLC) analysis were employed and HPLC methods for the assay of ROS-GC1, circular dichroism spectroscopy, UV/VIS spectrophotometer for monitoring cysteine reactivity with Ellman's reagent (DTNB) were carried out. Is aggregation of GCAP-1 assignable to particular cysteine residues? To further understand the role of each cysteine residue in the function and structure of GCAP-1, different cysteine mutants were constructed and characterized by chemical modification with iodoacetate derivatives and DTNB and by assay of ROS-GC1 activity. To observe the $Ca^{2+}$-dependent conformational changes, circular dichroism spectroscopy, gel electrophoresis, and size exclusion chromatography were used. Furthermore, the interaction of GCAP-1 and its mutants with peptides of ROS-GC1 was studied by cysteine reactivity and surface plasmon resonance spectroscopy.

# 2. MATERIALS AND METHODS

## 2.1 Materials

### 2.1.1 Equipment and Apparatus

**Agarose gel electrophoresis:**

Power Pack P25; Biometra, Göttingen

Transilluminator TI1; Biometra, Göttingen

**Autoclaver:**

Fedegari AutoclavisSPA; IntregraBioscience, Fernwald

**CD spectrometer: (Institute of Biochemistry, RWTH Klinikum Aachen)**

Model 62A DS CD Spectropolarimeter; AVIV, Lakewood, USA

JASCO J-600 CD Spectropolarimeter; JASCO, Tokyo, Japan

**Centrifuge:**

Centrifuge 5417R; Eppendorf, Hamburg

Biofuge 13 R with rotor HFA 14.2; Heraeus, Osterode

Megafuge 1.0 R with rotor BS4402/A; Heraeus, Osterode

Sorvall RC5C with rotor SS34, GS-3, KA-9000; DuPont, Wilmington, USA

Beckman J2-21 with rotor JA-20 and JS-13; Palo Alto, USA

Optima TL Ultracentrifuge with rotor TLA 45 and TLA 100; Beckman, Palo Alto, USA

Optima L-70K Ultracentrifuge with rotor Ti 70; Beckman, Palo Alto, USA

**DNA-sequencing:**

LI-COR 4200 Automatic Sequencer; MWG-Biotech, Ebersberg

**FPLC:**

ÄKTA™ FPLC; Amersham Pharmacia Biotech, Uppsala, Sweden

FPLC System; Pharmacia Biotech, Uppsala, Sweden

**French pressure:**

French Pressure Cell Press; SLM Aminco, Rochester, USA

French Press Cell 20K and 40K; SLM Aminco, Rochester, USA

**Electroblotting:**

Biometra-Festblotkammer B33; Biometra, Göttingen

**Gel documentation system:**

Gel Doc 1000, Molecular Analyst; Bio-Rad, München

**HPLC:**

HPLC; LKB, Bromma, Sweden

Waters; Millipore Corp. Bedford, USA

**Incubator:**

Multitron; Infos HT, Einsbach

Innova Model 4200; New Brunswick, New Jersey, USA

**Lyophilizer:**

Speedvac Plus SC110 Vacuum concentrator; Savant, Famingdale, USA

**MALDI-TOF mass spectrometry: (ICG-7, Forschungszentrum Jülich)**

Bruker REFLEX reflector TOF-MS instrument, Biflex III; Bruker Daltonik, Bremen

SCOUT multiprobe inlet and gridless delayed extraction ion source

**NMR: (IBI-2, Forschungszentrum Jülich)**

Digital NMR Bruker DMX600; Bruker, Bremen

**pH-Meter:**

pH-Meter 766 Calimatic; Knick, Berlin

Polyacrylamide gel electrophoresis:

Model 1000/500 Power Supply; Bio-Rad, München

Model 500/200 Power Supply; Bio-Rad, München

SE250 Mighty Small Mini Vertical Units; Hoefer Scientific Instruments, San Francisco, USA

SE400 Sturdier Vertical Units; Hoefer Scientific Instruments, San Francisco, USA

**Sonicator:**

Labsonic L with needle 40TL; Braun, Melsungen

Transsonic Digital; Elma, Singen

**SPR spectroscopy:**

BIAcore 1000; BIAcore, Uppsala, Sweden

**Thermocycler:**

PTC-200 Peltier Thermal Cycler; MJ Research, Watertown, USA

**UV/VIS spectrophotometer:**

Ultrospec 3000 UV/Visible Spectrometer; Pharmacia, Uppsala, Sweden

UV-2101PC UV-VIS Scanning Spectrometer; Shimadzu, Duisburg

DW-2000 Dual Wavelength UV/VIS Spectrophotometer; SLM-Aminco, Rochester, USA

## 2.1.2 Materials and Chemicals

Unless otherwise specified, all chemicals were purchased and used in the highest purity available.

### *2.1.2.1 Materials*

**Column materials for the chromatography:**

| | |
|---|---|
| Column PD-10 | Amersham Pharmacia Biotech, Freiburg |
| Superdex 75 HR 16/60 | Amersham Pharmacia Biotech, Freiburg |
| Superdex 75 HR 10/30 | Amersham Pharmacia Biotech, Freiburg |
| Uno Q-6 | Bio-Rad, München |
| Hibar LiChrospher 100 RP C18 column | Merck, Darmstadt |

**Dialyzer:**

| | |
|---|---|
| Dialyze tube, 10 kDa cut off | Life Technologies, Gaithersburg, USA |
| Slide-A-Lyzer dialysis cassettes | Pierce, Rockford, USA |

**Filters:**

| | |
|---|---|
| Filter GSWP04700, 0.2 µm | Millipore, Bedford, USA |
| Supor Acrodisc 32, 0.2 µm, 0.45 µm | Gelman Sciences, Ann Arbor, USA |

**Ultrafiltration:**

| | |
|---|---|
| Microcon-10, Centricon-10, Centriplus-10 Concentrators | Amicon, Beverly, USA |

### *2.1.2.2 Enzymes for cloning*

| | |
|---|---|
| Calf intestinal alkaline phosphatase | Boehringer Mannheim, |
| Expand high fidelity *Taq/Pwo* DNA polymerase | Boehringer Mannheim, |
| T4 DNA ligase | Gibco/BRL and New England Biolabs |

Restriction and other enzymes are obtained form New England Biolabs (Beverly, USA) and Life Technologies (Gaithersburg, USA) and used according to the manufacturers' recommendations.

### *2.1.2.3 Standards for electrophoresis*

| | |
|---|---|
| 1 kb, 100 bp DNA ladder | Gibco/BRL and New England Biolabs |
| 1 kDa protein standards for SDS-PAGE | Gibco/BRL, Karlsruhe |
| Low molecular weight standards for SDS-PAGE | Amersham Pharmacia AB |
| Molecular weight standards for ND-PAGE | Sigma |

#### *2.1.2.4 Two peptides from the cytoplasmic parts of ROS-GC1*

The following peptides from the cytoplasmic part of ROS-GC1 were reported previously to interact with GCAP-1 [59,60]. Both peptides were obtained from Dr. M. Beyermann (Forschungsinstitut für Molekulare Pharmakologie, Berlin).

Peptide #34a Ac-$^{559}$LYEGD WVWLK KFPGD RHIAI$^{578}$-$NH_2$ (MW = 2443 g/mol)

Peptide Sokal #71 Ac-$^{966}$GTFRM RHMPE VPVRI RIG$^{983}$-$NH_2$ (MW = 2152 g/mol)

## 2.1.3 Media and Buffers

#### *2.1.3.1 Media and antibiotics*

Additive of media:

Additives were filter-sterilized and stored as aliquots at −20°C.

IPTG stock solution: 1 M in water

Myristic acid stock solution: 50 mg/ml in water

Bacterial media: **(per liter)**

Media were sterilized by autoclaving for 20 min at 121°C.

BHI: 36 g brain heart infusion (BHI) broth

dYT: 16 g of bacto-tryptone, 10 g of bacto-yeast extract, 5 g of NaCl

SOB: 20 g of bacto-trypton, 5 g of bacto-yeast extract, 0.5 g of NaCl, 2.5 mM KCl, 10 mM $MgCl_2$, 10 mM $MgSO_4$

SOC: SOB medium + 20 mM glucose

Antibiotics: **(Table 2.1)**

Antibiotic solutions were sterilized by filtration through a 0.22 µm sterile filter and stored at −20°C.

**TABLE 2.1** Antibiotic solutions [82]

| **Antibiotic** | | **Stock solution concentration** | **Working concentration** |
|---|---|---|---|
| Ampicillin | (Amp) | 100 mg/ml in water | 100 µg/ml |
| Carbenicillin | (Car) | 50 mg/ml in water | 50 µg/ml |
| Chloramphenicol | (Cam) | 34 mg/ml in ethanol | 170 µg/ml |
| Kanamycin | (Kan) | 50 mg/ml in water | 50 µg/ml |
| Tetracycline | (Tet) | 5 mg/ml in ethanol | 50 µg/ml |

### *2.1.3.2 Buffers and solutions*

Milli-Q-purified water was used. Most solutions were degassed and filtered through a 0.22 µm sterile filter.

**Buffers for competent cells:**

| | |
|---|---|
| TFB I buffer: | 30 mM sodium acetate, 50 mM $MgCl_2$, 100 mM NaCl, 10 mM $CaCl_2$, 15% (v/v) glycerol |
| TFB II buffer: | 10 mM MOPS, 10 mM NaCl, 75 mM $CaCl_2$, 15% (v/v) glycerol |

**Buffers for cloning:**

| | |
|---|---|
| TE: | 10 mM Tris, pH 8.0, 1 mM EDTA |
| TAE: | 40 mM Tris-acetate, pH 8.0, 1 mM EDTA |
| 10× PCR buffer: | 200 mM Tris-HCl, pH 7.5, 1 M KCl, 10 mM DTT, 1 mM EDTA, 15 mM $MgCl_2$, 0.5% (v/v) Tween 20, 50% (v/v) glycerol |
| 10× Ligation buffer: | 500 mM Tris-HCl, pH 7.8, 100 mM $MgCl_2$, 100 mM DTT, 10 mM ATP, 250 µg/ml BSA |
| 10× DNA sample solution: | 1× TAE, 50% (w/v) saccharose, 0.25% (w/v) bromophenol blue |

**Buffers for sequencing:**

| | |
|---|---|
| TBE: | 50 mM Tris-borate, 1 mM EDTA, pH 7.8 |

**Buffers for purification of proteins:**

| | |
|---|---|
| Lysis buffer: | 20 mM Tris, pH 7.5, 1 mM DTT, 0.1 mM PMSF |
| Gel filtration buffer: | 20 mM Tris, pH 7.5, 150 mM NaCl, 2.5 mM EGTA, 2 mM DTT, 0.1 mM PMSF |
| Ion exchange starting buffer: | 20 mM Tris, pH 7.5, 2.5 mM EGTA, 2 mM DTT, 0.1 mM PMSF |
| Ion exchange washing buffer: | starting buffer + 150 mM NaCl |
| Ion exchange gradient buffer: | starting buffer + 500 mM NaCl |

**Solutions for SDS-PAGE:**

| | |
|---|---|
| Separating gel buffer: | 1.5 M Tris, pH 8.8 |
| Stacking gel buffer: | 0.5 M Tris, pH 6.8 |
| SDS sample solution: | 50 mM Tris, 2% (w/v) SDS, 2.5% (v/v) β-mercaptoethanol, 10% (v/v) glycerol, 0.01% (w/v) bromophenol blue |
| SDS electrophoresis buffer: | 25 mM Tris, 192 mM glycine, 0.1% (w/v) SDS, pH 8.3 |
| Coomassie staining solution: | 0.2% (w/v) Coomassie blue R-250, 5% (v/v) acetic acid, 25% (v/v) ethanol |
| Destaining solution: | 5% (v/v) acetic acid, 25% (v/v) ethanol |

**Solutions for ND-PAGE:**

| | |
|---|---|
| ND sample solution: | 50 mM Tris, 50% (v/v) glycerol, 0.01% (w/v) bromophenol blue |
| ND electrophoresis buffer: | 25 mM Tris base, 192 mM glycine, pH 8.8 |

**Solutions for immunoblotting:**

PBS buffer: 10 mM $Na_2HPO_4$, 1.8 mM $KH_2PO_4$, pH 7.3, 140 mM NaCl, 2.7 mM KCl

Blotting buffer: 25 mM Tris, pH 7.4, 192 mM glycine, 20% (v/v) methanol

Ponceau S staining solution: 0.2% (w/v) Ponceau S, 3% (w/v) trichloroacetic acid

PBS-T buffer: 1× PBS, 0.05% (v/v) Tween 20

PBS/milk solution 1× PBS, 3% (w/v) low fat dried milk, 0.2% (v/v) Tween 20

Amido black staining solution: 0.1% (w/v) amido black, 25% (v/v) methanol, 5% (v/v) acetic acid

Destaining solution: 90% (v/v) methanol, 2% (v/v) acetic acid

**Buffers for ROS-GC assay:**

Washing buffer: 10 mM HEPES, pH 7.4, 1 mM DTT

Resuspension buffer: 50 mM HEPES, pH 7.4, 500 mM KCl, 20 mM NaCl, 1 mM DTT

$Mg^{2+}$/GC buffer: 100 mM MOPS, pH 7.1, 140 mM KCl, 20 mM NaCl, 25 mM $MgCl_2$, 5 mM GTP

$Ca^{2+}$/EGTA buffer: (Table 2.2) [58]

**TABLE 2.2** The calculated free calcium concentration in $Ca^{2+}$/EGTA buffer [83]

| $[K_2Ca^{2+}EGTA]/[EGTA]_{total}$ | $[K_2H_2EGTA]$ | $[K_2Ca^{2+}EGTA]$ | $[Ca^{2+}]_{free}$ (calculated) * |
|---|---|---|---|
| 0 | 2.0 mM | - | 0.8 nM |
| 0.1 | 1.8 mM | 0.2 mM | 34.8 nM |
| 0.2 | 1.6 mM | 0.4 mM | 78.5 nM |
| 0.3 | 1.4 mM | 0.6 mM | 135 nM |
| 0.4 | 1.2 mM | 0.8 mM | 210 nM |
| 0.5 | 1.0 mM | 1.0 mM | 315 nM |
| 0.6 | 0.8 mM | 1.2 mM | 473 nM |
| 0.7 | 0.6 mM | 1.4 mM | 737 nM |
| 0.8 | 0.4 mM | 1.6 mM | 1.26 µM |
| 0.9 | 0.2 mM | 1.8 mM | 2.81 µM |
| 1.0 | - | 2.0 mM | 23.5 µM |

* $[Ca^{2+}]_{free}$ was calculated with the CHELATOR buffer program [84].

**Solution for thiol reactivity:**

IAA solution 10 mM iodoacetic acid in 250 mM Tris, pH 8.0, 500 mM KOH

IAM solution 10 mM iodoacetamide in 500 mM Tris, pH 8.0

| | |
|---|---|
| Denaturing solution: | 8 M urea in 100 mM Tris, pH 8.0, 1 mM EDTA |
| Ellman's reagent | 12.5 mM DTNB in 0.1 M Tris, pH 8.0 |
| **Running buffers for SPR:** | |
| HBS-$Ca^{2+}$ buffer: | 10 mM HEPES, pH 7.4, 150 mM KCl, 10 mM $MgCl_2$, 2 mM $CaCl_2$, 0.05% (v/v) BIAcore Surfactant P20 or 0.005% (v/v) Tween 20 |
| HBS-EGTA buffer: | 10 mM HEPES, pH 7.4, 150 mM KCl, 10 mM $MgCl_2$, 2 mM EDTA, 0.05% (v/v) BIAcore Surfactant P20 or 0.005% (v/v) Tween 20 |
| Regeneration buffer | 200 mM glycine, pH 2.0 |

# 2.2 Cloning of GCAP-1 and Its Mutants

## 2.2.1 Bacterial Strains and Plasmid Vectors

### *2.2.1.1 Bacterial strains*

*E. coli* strains TOP10 and DH5α were used for cloning and analysis of plasmids and BL21(DE3) and BL21-CodonPlus(DE3) were used for expression. Detailed genotype and reference for the bacterial strains used are listed in Table 2.3.

**TABLE 2.3** Host strains and genotypes.

| Strain | Genotype | Supplier | Ref. |
|---|---|---|---|
| One Shot™Top10 | *F⁻ mcrA Δ(mrr⁻hsdRMS⁻mcrBC) φ80dlacZΔM15 ΔlacX74 deoR recA1 araD139 Δ(ara⁻leu)7697 galU galK rpsL endA1 nupG* | Invitrogen | Invitrogen |
| DH5α | *F⁻ endA1 hsdR17 ($rk^-$, $mk^+$) supE44 thi⁻1 λ⁻ recA1 gyrA96 relA1 deoR [lacZYA⁻argF]⁻U169 (φ80dlacZDM15)* | ITC Biotechnology | 85 |
| BL21(DE3) | *B F⁻ dcm ompT hsdS($r_B^-$ $m_B^-$)gal λ (DE3)* | Novagen | 86 |
| Epicurian Coli® BL21-Codon Plus™(DE3)-RIL | *B F⁻ dcm ompT hsdS($r_B^-$ $m_B^-$)dcm⁻ Tet$^r$ gal λ (DE3) endA Hte [argU ileY leuW Cam$^r$]* | Stratagene | 87 |

#### *2.2.1.2 Storage of strains*

A single colony was inoculated into 50 ml dYT or SOC media in a 250 ml flask and incubated with vigorous shaking at 37°C until the $OD_{600}$ reached 0.6–0.8. An overnight culture volume of 0.9 ml was transferred to a cryovial, supplemented with 0.1 ml of 80% (v/v) glycerol, and then mixed well. It was stored at −80°C. To inoculate a culture from the frozen stock, a few µl were scraped or melted from the surface with a sterile pipette, and the remainder was returned to the −80°C deep freezer without thawing.

#### *2.2.1.3 Vectors*

Cloning, mutagenesis, and isolation of double-stranded DNA were carried out in the plasmid pCR-Blunt. This vector was supplied linearized and blunt-ended at a unique site in the polylinker. For expression of wild-type GCAP-1 and its variants in *E. coli*, the plasmid pET-11a was used, as it is designed to permit enhanced gene expression of target proteins in *E. coli* [88]. The pET-11a vector contains the T7*lac* promoter, the start codon (internal methionine codon; ATG) on *Nde*I (CA|TATG) restriction site, and the terminator T$\phi$ on the *Bam*HI (G|GATCC) cloning site downstream of the efficient T7 polymerase promoter [88]. For the myristoylation of the N-terminus of GCAP-1, the plasmid pBB-131 was used. This plasmid contains N-terminal myristoyl transferase 1 (NMT1) from *S. cerevisiae.* See Table 2.4 and Appendix 5.4.

**TABLE 2.4** Vectors and their properties.

| Vector | Properties | Supplier | Ref. |
|---|---|---|---|
| pCR®-Blunt | Cloning vector for blunt PCR fragments; $Kan^r$, $Zeo^r$ | Invitrogen | Invitrogen |
| pET-11a | Expression vector for GCAP1 in *E. coli*; $Amp^r$ | Novagen | 88 |
| pET-21a | Expression vector for GCAP1 in *E. coli*; $Amp^r$ | Novagen | 88 |
| pBB-131 | Expression vector for NMT1 from *S. cerevisiae* in *E. coli*; $Kan^r$ | Dr. J. I. Gordon | 89 |

## 2.2.2 Preparation and Analysis of Plasmid DNA

#### *2.2.2.1 Standard methods*

All standard DNA procedures were performed as described by Sambrook et al. [82] and according to the following manufacturer's instructions.

| | |
|---|---|
| Cloning of blunt-ended PCR products: | Zero Blunt™ PCR Cloning Kit, Invitrogen |
| Amplification of DNA by PCR: | Expand™ High Fidelity PCR System Kit, Boehringer Mannheim |
| Isolation of DNA-fragments from agarose gel: | QIAEX II Gel Extraction Kit, QIAGEN |
| Preparation of plasmids from *E. coli*: | QIAprep Spin Miniprep Kit, QIAGEN |
| DNA-sequencing reaction: | Thermo Sequenase Kit, Amersham Pharamcia Biotech |

#### *2.2.2.2 Agarose gel electrophoresis*

After polymerization of a 1.2–2% (w/v) agarose gel containing 0.075% (w/v) ethidium bromide, the DNAs were run with 1× DNA sample buffer at 80–120 V in TAE buffer. The DNA on the gel was visualized on a UV transilluminator and documented by Gel Doc 1000 (Bio-Rad).

#### *2.2.2.3 Automated DNA sequencing*

For each reaction a template/primer-premix was prepared containing 65 ng/kb of DNA, 5% (v/v) DMSO in water, and 1.2 pmol of IRD800 labeled primer in a total volume of 7 µl. The reaction was mixed with a half volume of the template/primer-premix and another half volume of the G, A, T and C termination mix containing dedeoxy nucleotides and thermosequenase (from Amersham) to the corresponding tube of each reaction. Chill Out Wax was added to each tube. PCR reaction was run in the followings:

| | | |
|---|---|---|
| Step 1: Pre-incubation | 94°C, 2 min | |
| Step 2: Denaturation | 94°C, 40 sec | ← |
| Step 3: Annealing | 50°C, 40 sec | 30 cycles |
| Step 4: Extension | 70°C, 60 sec | ← |
| Step 5: Stop | 4°C, until manual end | |

After running the PCR reaction, 3 µl of stop buffer were added to each tube and incubated for 2 min at 70°C to denature DNA, and then cooled down to room temperature. The reactions were separated on a denaturing high-resolution polyacrylamide gel in a LICOR DNA Sequencer Long ReadIR 4200 (MWG Biotech). The 4.6% (w/v) gel (66 cm × 0.25 mm) contained RapidGel (Amersham Pharmacia Biotech), 1% (v/v) DMSO, 7 M urea, 0.07% (w/v) APS, and 0.1% (v/v) TEMED in TBE buffer. The samples of about 1.5 µl were loaded onto the gel. The electrophoresis was run for 8–16 hours with 45 W at 45°C in TBE

buffer. During processing, the fluorescence of the labelled primers was detected. The sequencing data were analyzed with the program BaseImageIR (LICOR).

## 2.2.3 Polymerase Chain Reaction (PCR)

Mutagenesis of GCAP-1 was performed on exchange of the cysteine residues of putative importance for function and structure.

### *2.2.3.1 Primers*

The following primers were obtained from MWG-Biotech AG (Ebersberg) and Eurogenetech (Köln). Mutagenesis sites are shown in bold:

**PCR primers:**

#1 : FP-Nde I 5´-GCC ATA TGG GTA ACA TTA TGG ACG GTA AGT CG-3´

#2 : RP-T7 Term 5´-GCT AGT TAT TGC TCA GCG GTG G-3´

**Mutagenesis primers:**

#3 : RP-C18,29A 5´-GGG **CGC** CTC TGT CAT GAA CTT CTT GTA CCA CTG GTG **GGC** CTC GGT GCT GCT CAG-3´

#4 : FP-C29A 5´-GAA GTT CAT GAC AGA G**GC G**CC CTC CGG CCA GCT CAC CCT CTA CG-3´

#5 : FP-C106A 5´-CGT GGA CGG CAA CGG A**GC G**AT CGA CCG CGA CGA GCT GC-3´

#6 : RP-C125A 5´-GGC GGT CAT GGT CGA GTC GCT **CGC** GGG GTT AAT GGC TCG GAT GGC-3´

**Sequencing primers:**

#7 : IRD800-UP-90 5´-GGC CTC TTC GCT ATT ACG C-3´

#8 : IRD800-RP-80 5´-GGC ACC CCA GGC TTT ACA C-3´

#9 : IRD800-FP-T7 5´-TAA TAC GAC TCA CTA TAG GG-3´

#10: IRD800-RP-T7 5´-GCT AGT TAT TGC TCA GCG G-3´

### *2.2.3.2 Condition of reaction*

The GCAP1 gene was cloned into the plasmid pET-11a between the restriction sites *Nde*I and *Bam*HI [73]. PCR reactions were carried out in a MJ Research model PTC-200 (Watertown, USA) Thermocycler. Deoxynucleotides were mixed to create a stock solution of dNTP (dATP, dCTP, dGTP, and dTTP, each 5 mM). Enzyme mix contained thermally stable polymerases, *Taq* and *Pwo* (Expand$^{TM}$ High Fidelity PCR System; Boehringer Mannheim).

The constituents were added in the following order: 20 ng of template DNA, 1 pmol of forward primer, 1 pmol of reverse primer, 0.1 mM of dNTP mix, 10 µl of 10× PCR buffer, 1 µl of enzyme mix, and distilled sterilized water added to a total volume of 100 µl. The thermocycler settings used were as follows:

| | | |
|---|---|---|
| Step 1: Pre-incubation | 95°C, 3 min | |
| Step 2: Denaturation | 95°C, 1 min | 30 cycles |
| Step 3: Annealing | $T_m$ – 4°C, 1 min | |
| Step 4: Extension | 72°C, 1 min | |
| Step 5: Stop | 4°C, until manual end | |

$$T_m = 2\,(\#A + \#T) + 4\,(\#G + \#C) \qquad (2.1)$$

#### *2.2.3.3 Purification of PCR products*

After running a PCR reaction, the entire PCR reaction volume was loaded on a 2% (w/v) agarose gel with appropriate size markers. The correct band was cut out from the agarose gel and the proper double-stranded DNA was purified using QIAEX II Gel Extraction Kit according to the manufacturer's instructions.

### 2.2.4 Cloning into Plasmids

#### *2.2.4.1 Ligation of GCAP1 fragments*

Ligation of DNA blunt fragments was performed under the following conditions: 25 ng of linearized blunt pCR-Blunt vector, 0.2 pmol of blunt PCR products, 1 µl of 10× ligation buffer, 400 units of T4 DNA ligase, and sterile water to a total volume of 10 µl. This reaction was incubated at room temperature for 1.5 hours and placed on ice for transformation. After analysis of transformants in pCR-Blunt by *Eco*RI, the desired clone was digested by incubation at 37°C for 1–16 hours with *Nde*I and *Bam*HI. The appropriate band at about 640 bp was cut out from the agarose gel, and the desired fragments were purified using QIAEX II Gel Extraction Kit. The appropriate purified inserts were mixed with the vector pET-11a, restricted by *Nde*I and *Bam*HI, and dephosphorylated by calf intestinal alkaline phosphatase (CIP). This mixture was preincubated at 45°C for 5 min. The ligation reaction was carried out with 400 units of T4 DNA ligase (from Biolabs) at 16°C for 2 hours and then placed on ice for the preparation of transformation or stored at –20°C until use.

#### *2.2.4.2 Preparation of competent cells*

A tube of frozen stock or a single colony (2–3 mm in diameter) from a plate freshly grown overnight at 37°C was inoculated in 1 ml of SOB medium in a test tube and then incubated overnight at 37°C. This overnight culture was transferred into 100 ml of SOB in a 1 *l* flask and incubated for 2–3 hours at 37°C with vigorous shaking until $OD_{600}$ of 0.3 was reached. The cells were transferred to 50 ml polypropylene tubes (Falcon 2070), cooled to 0°C by storing the tubes on ice for 15 min, and then recovered by centrifugation at 3500 rpm for 15 min at 4°C in a Megafuge rotor. The pellets were resuspended carefully in 20 ml of ice-cold TFB I and placed on ice for 15 min. To recover the cells, the tubes were again centrifuged at 3500 rpm for 15 min at 4°C in a Megafuge rotor. The pellets were resuspended in 4 ml of ice-cold TFB II and placed on ice for 15 min. Aliquots of 100 µl or 200 µl of competent cells were distributed into chilled, sterile microcentrifuge tubes, frozen in liquid nitrogen, and stored at −80°C.

#### *2.2.4.3 Transformation of competent cells*

A tube of frozen competent cells was thawed on ice. The DNA solution (1−10 ng) was added to the competent cells and incubated on ice for 30 min. Each transformation tube was heat-pulsed for 25−60 sec in a 42°C and placed on ice for 2 min. Room temperature SOC medium was added to each tube to a final volume of 500−1000 µl and incubated at 37°C (250 rpm) for 60 min. 50−500 µl of each transformation were spread on BHI-agar plates containing appropriate antibiotics, 50 µg/ml kanamycin for pCR-Blunt and 100 µg/ml ampicillin for pET-11a. The plates were placed on the bench for several min to allow excess liquid to be absorbed and then inverted and incubated overnight at 37°C.

#### *2.2.4.4 Analysis of transformants*

Transformants selected on appropriate antibiotics were inoculated into 3 ml dYT medium containing appropriate antibiotics and then grown overnight at 37°C. The recombinant plasmids were isolated using QIAprep Spin Miniprep Kit according to the manufacturer's instructions, in order to confirm presence and correction of cloned insert by restriction, digestion, and sequencing. After digestion with *Nde*I and *Bam*HI or, alternatively, with *Nhe*I and *Xba*I at 37°C for 1−16 hours, the DNA reaction was run on an 1.2% (w/v) agarose gel.

## 2.2.5 Screening of GCAP-1 for Expression

Aliquots taken every hour from cultures were centrifuged for 5 min at 13000 rpm. The cell pellets were resuspended with 100 µl of 20 mM Tris, pH 7.5, 1 mM DTT, 1 mM PMSF. Lysozyme (3 mg/ml) was added and incubated for 2 hours at room temperature. Those samples were incubated with 0.05% (v/v) DOC for 20 min at room temperature. In order to screen expression by SDS-PAGE, 5× sample buffer were added and incubated for 10 min at 95°C.

## 2.2.6 Overexpression in *Escherichia coli*

Overexpression of the gene products was achieved in *Escherichia coli* strain BL21-Codon Plus(DE3).

### *2.2.6.1 Expression of GCAP-1 and its mutants without myristoylation*

Single colonies of bacterial strain BL21-Codon Plus(DE3) cells engineered with pET-11a/GCAP1 were used to inoculate 5 ml of dYT medium supplemented with 100 µg/ml ampicillin for overnight growth at 37°C. From this preculture mixture, 10 ml was added to 500 ml of dYT medium containing ampicillin (100 µg/ml) in 2 *l* Erlenmeyer flasks for aerobic growth at 37°C with vigorous agitation (150 rpm). In the mid-log phase of growth at 37°C, overproduction of unmyristoylated GCAP-1 was induced by isopropyl-thio-β-D-galactoside (IPTG) to a final concentration of 1 mM, when the culture had reached an $OD_{600}$ of 0.6–0.8. Cells were grown for additional 4 hours before harvesting. The cell pellets were resuspended in 5 ml of lysis buffer and stored at –20°C.

### *2.2.6.2 Coexpression of GCAP-1 and N-terminal myristoyl transferase*

For production of myristoylated GCAP-1, plasmid pBB-131 (a kind gift from Dr. J. I. Gordon) encoding yeast protein NMT has been transformed into BL21-Codon Plus(DE3)/pET-11a/GCAP1. The resulting BL21-Codon Plus(DE3)/pBB-131/pET-11a/ GCAP1 strain was inoculated in dYT media containing 100 µg/ml of ampicillin and 25 µg/ml of kanamycin at 37°C. One liter of dYT medium containing 100 µg/ml of ampicillin and 25 µg/ml of kanamycin was inoculated with the overnight preculture and cultured at 37°C. Myristic acid (50 µg/ml in ethanol) was added to the culture at $OD_{600}$ of 0.3. Production of myristolylated GCAP-1 was induced by 1 mM IPTG when the culture had reached an $OD_{600}$

of 0.6–0.8. After four hours, cells were harvested by centrifugation for 20 min at 9000 rpm in Sorvall RC5C with rotor KA-9000 at 4°C. Harvested cells from 1 *l* were resuspended in 250 ml of 50 mM Tris-Cl, pH 8.0, and stored at –20°C.

## 2.3 Preparation of GCAP-1 and Its Mutants

### 2.3.1 Purification of GCAP-1 and Its Mutants

GCAP-1 and its mutants were purified using ÄKTA FPLC and FPLC system from Pharmacia Biotech. All purification steps were performed at 4°C. Recombinant GCAP-1 was heterologeously expressed in *E. coli* and isolated from the soluble supernatant of cell cultures. The thawed, resuspended *E. coli* cells were added to a French pressure cell. The samples were ruptured by three passages through the apparatus at approximately 20000 psi. The cell lysate was then separated from cell wall debris and unbroken cells by centrifugation for 30 min at 17500 rpm in a Beckman J2-21 centrifuge with a JA-20 rotor at 4°C. The supernatant was ultracentrifuged for 30 min at 35000 rpm in Beckman Optima L-70K centrifuge with a Ti70 rotor at 4°C to remove some particles, aggregated proteins, and DNA.

HiLoad 16/60 Superdex 75 prep grade gel filtration column (1.6 × 60 cm) was equilibrated with two times of column volume of gel filtration buffer (see Methods 2.1.3.2) at a flow rate of 1.0 ml/min. Aliquots of 5 ml of the crude extracts were loaded and eluted. Fractions were collected on 2.0 ml per tube. After analysis by SDS-PAGE, the appropriate fractions were pooled.

An Uno Q-6 ion-exchange column (1.2 × 5.0 cm) was equilibrated with over 10 column volumes of starting buffer (see Methods 2.1.3.2) at a flow rate of 3.0 ml/min. The pooled GCAP-1 fractions from gel filtration column were loaded at a flow rate of 0.5 ml/min. Unbound proteins were washed out at a flow rate of 3.0 ml/min with 5 times of column volumes of washing buffer (see Methods 2.1.3.2). GCAP-1 was eluted with a linear gradient of NaCl (150–600 mM), using 10 column volumes of gradient buffer (see Methods 2.1.3.2) at a flow rate of 2.0 ml/min. Fractions of 1.0 ml were collected. The appropriate fractions identified by SDS-PAGE were pooled.

Purified GCAP-1 (0.5–3 ml protein solution of 1–3 mg/ml) was dialyzed using 10 kDa molecular weight cutoff tubing at least 12 hours in 5 *l* of 50 mM ammonium bicarbonate

buffer with two changes of buffer. After determining the protein concentration, each 1 mg aliquot was lyophilized by a Speedvac concentrator and then stored at −80°C till further use. Mutants of GCAP-1 were purified according to the same scheme.

## 2.3.2 Determination of GCAP-1 Concentration

### *2.3.2.1 Absorbance at 280 nm*

Protein concentrations can be measured by absorbance spectroscopy. The absorbance $A$ is a linear function of the molar concentration $c$ according to the Beer-Lambert relation:

$$A = \varepsilon \cdot c \cdot l \qquad (2.2)$$

Where $\varepsilon$ is the molar absorbance coefficient, and $l$ is the cell length.

Only tryptophan, tyrosine, and disulfide bonds contribute to the absorbance of a protein between 270 nm and 300 nm. The molar absorbance coefficient of a protein at 280 nm, $\varepsilon_{280}$, is calculated by using Equation 2.3 [90]:

$$\varepsilon_{280}\,(M^{-1} \cdot cm^{-1}) = 5500 \cdot \mathbf{n}(Trp) + 1490 \cdot \mathbf{n}(Tyr) + 125 \cdot \mathbf{n}(S\text{-}S) \qquad (2.3)$$

The molar absorbance coefficient at 280 nm of GCAP-1, $\varepsilon_{280}$, is 28378 $M^{-1}\cdot cm^{-1}$, measured with purified GCAP-1 (personal communication with Dr. K.-W. Koch).

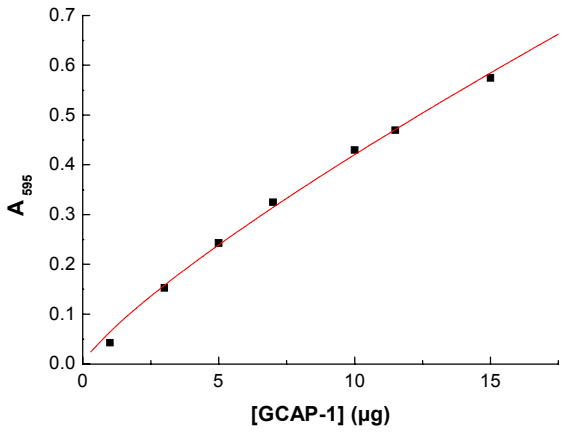


**FIG. 2.1.** The calibration curve of GCAP-1. Purified GCAP-1 was used to create the standard curve by plotting the absorbance at 595 nm against the known concentration of GCAP-1.

#### *2.3.2.2 Bradford assay* [91]

Purified GCAP-1 solutions (1–20 µg/ml) were mixed with buffer to a total volume of 800 µl. The absorbance of $\lambda$ = 595 nm was measured against a blank after 5 min and within one hour. The GCAP-1 concentration was determined using a GCAP-1 calibration curve. The calibration curve was created with a GCAP-1 stock solution that was adjusted to a purified GCAP-1 concentration using the absorbance coefficient of GCAP-1, $\varepsilon_{280}$ = 28378 $M^{-1} \cdot cm^{-1}$. The calibration curve of purified GCAP-1 is shown in Fig. 2.1.

### 2.3.3 Identification of GCAP-1

#### *2.3.3.1 SDS polyacrylamide gel electrophoresis (SDS-PAGE)*

On SDS-PAGE proteins are separated primarily due to their molecular weights. SDS-PAGE gels consisted of a 4% (w/v) acrylamide stacking gel and a 15% (w/v) acrylamide separating gel and were in a Tris/glycine buffer system according to Laemmli [92].

Approximately 1–10 µg of protein were mixed with SDS sample buffer and loaded onto the gel after boiling for 10 min at 95°C. The electrophoresis was carried out at 150–200 V for 1–2 hours. The proteins were stained with Coomassie staining solution for 1 hour and then destained overnight with destaining solution. If proteins could not be detected with Coomassie staining, the more sensitive silver staining (detection limit: ~2 ng) was carried out using silver staining kits from Roth.

Electrophoretic molecular mass determination of GCAP-1 was performed following the methods of Weber and Osborn [93] using the low molecular weight standards from Amersham Pharmacia AB: α-lactalbumin (14.4 kDa), soy bean trypsin inhibitor (20.1 kDa), carbonate anhydrase (30 kDa), ovalbumin (43 kDa), BSA (67 kDa), and phosphorylase b (94 kDa). Calibration proteins ('standards') are essential for determination of the molecular weight of unknown proteins. The calibration graph was obtained by plotting the logarithm of molecular weight (*log M.W.*) versus the relative migration distance ($R_f$), required for comparing results obtained from the separating gels.

$$R_f = \frac{distance\ of\ protein\ migration}{distance\ of\ tracking\ dye\ migration} \qquad (2.4)$$

**TABLE 2.5** Ingredients for SDS-PAGE

| Separating Gel | Stacking Gel |
|---|---|
| 0.375 M Tris-HCl, pH 8.8 | 0.125 M Tris-HCl, pH 6.8 |
| 15% (w/v) acrylamide/bis-acrylamide | 5 % (w/v) acrylamide/bis-acrylamide |
| 0.10% (w/v) SDS | 0.1% (w/v) SDS |
| 0.07% (w/v) APS | 0.2% (w/v) APS |
| 0.05% (v/v) TEMED | 0.1% (v/v) TEMED |

#### *2.3.3.2 Nondenaturing polyacrylamide gel electrophoresis (ND-PAGE)*

ND-PAGE is a method of identifying the molecular weight of natively folded protein without boiling and SDS. Gel electrophoresis was performed at 4°C to minimize denaturation [94,95]. Native PAGE separates proteins based on their size and charge properties. A 10% (w/v) acrylamide separating gel was used to separate proteins in the range 10–100 kDa. Approximately 5–20 µg of protein were mixed with sample buffer and loaded onto the gel. The protein gels were run at 100 V for 4–6 hours in the cold room, and then destained with destaining solution overnight. No exact molecular weight determination was possible because standards did not run sufficiently precise.

#### *2.3.3.3 Immunoblotting*

All incubation and washing steps were performed at room temperature with agitation. The GCAP-1 and its mutants were transferred from SDS-PAGE gels to Immobilon-P membranes (Millipore) by electroblotting at 0.8 mA/cm$^2$ for 1–1.5 hours in blotting buffer. After transfer, membranes were incubated in Ponceau S staining solution for 2 min and destained in distilled water until bands were visible. The non-reacted sites on the membrane were blocked by soaking the membrane in PBS/milk solution for 1 hour. The immunoblot was incubated with anti-GCAP-1 antiserum (1:10000 dilution, from Frins et al. [73]) in PBS/milk for 1 hour and rinsed with PBS-T buffer. The incubation was continued with horseradish peroxidase (HRP)-labeled anti-rabbit second antibody (1:5000 dilution, from Sigma) in PBS/milk for 1 hour and washed in an excess of PBS-T buffer. Finally the blot was treated with ECL substrate (Amersham) for 1 min according to the manufacturer's protocol. The immunoreactive band was detected by exposing the blot on Kodak (Rochester, NY) XAR-2 film for a few seconds. The membranes were stained by Amido black solution for documentation.

# 2.4 Biochemical Studies

## 2.4.1 ROS-GC Assay

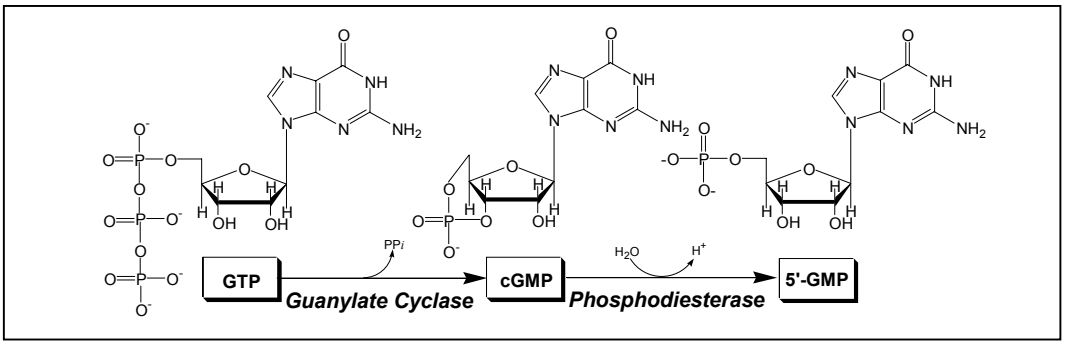


**FIG. 2.2.** Synthesis and hydrolysis of cGMP. In outer segments of vertebrate retinal photoreceptors, the concentration of intracellular cGMP is regulated through synthesis from GTP by guanylate cyclase and hydrolysis to 5′-GMP by phosphodiesterase [4].

### *2.4.1.1 Preparation of ROS-GCs*

Rod outer segments (ROS) were prepared from freshly collected bovine eyes by a standard protocol according to Lambrecht and Koch [96]. The predominant GC in ROS preparation is ROS-GC1 (personal communication with Dr. K.-W. Koch). The activity of ROS-GC was determined by a HPLC chromatography assay using a nucleotide separation and quantitation system [32,97].

The ROS-GC assay was performed under very dim red light. For reconstitution experiments, ROS-membranes were prepared by diluting them 5-fold with washing buffer and centrifugation for 10 min at 80000 rpm in a Beckman TLA100 centrifuge at 4°C. The resulting pellets were suspended in the same buffer using the same dilution, and the washing procedure was repeated. The pellet was resuspended in one half of the original ROS volume in resuspension buffer.

### *2.4.1.2 Effect of GCAP-1 on activity of ROS-GC1*

Varying concentration of GCAP-1 or its mutants were added to 10 µl of washed ROS-membranes to give a total volume of 20 µl. The reaction samples were preincubated with 10 µl of 2 mM $CaCl_2$ or 2 mM EGTA for 5 min at room temperature.

The reaction for cGMP synthesis of ROS-GC1 was started by adding 20 µl of $Mg^{2+}$/GC buffer containing ATP and PDE inhibitor zaprinast. Final concentration of ATP and

PDE inhibitor zaprinast (Sigma) were 100 µM and 0.4 mM, respectively. The resulting suspension containing GCAP-1and ROS-membranes was incubated for 5 min at 30°C. Incubation was stopped by adding ice-cold 50 mM EDTA and boiling for 5 min. Afterwards the solution was centrifuged for 5 min at 13000 rpm in a microcentrifuge to remove membranes and denaturated proteins. The supernatants (~95 µl) were injected into an HPLC reversed-phase C18 column (4 × 250 mm) and nucleotides were eluted with a gradient of 0–70% (v/v) methanol in 5 mM $KH_2PO_4$, pH 5.0 at a flow rate of 1.2 ml/min. The elution was monitored by absorbance at 254 nm. A typical chromatogram is shown in Figure 2.3. The retention time of some nucleotides is summarized in Table 2.7. The activity of ROS-GC1 is expressed as nmol cGMP·$min^{-1}$·$mg^{-1}$ rhodopsin.

**TABLE 2.6** Retention time ($R_t$) of nucleotides after separation on a HPLC reversed-phase C18 column (4 × 250 mm) (personal communication with Dr. K.-W. Koch).

| Nucleotide | $R_t$ |
|---|---|
| GTP | 2.10 min |
| GDP | 2.38 min |
| GMP | 4.46 min |
| cGMP | 7.38 min |
| Guanosine | 8.30 min |

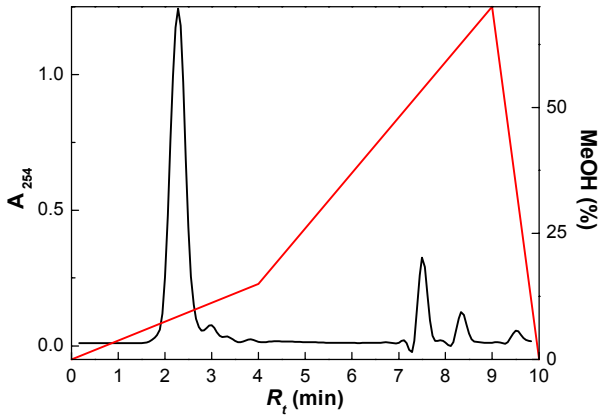


**FIG. 2.3.** Typical chromatogram showing the separation of some nucleotides on a HPLC reversed-phase C18 column.

### *2.4.1.3 Effect of calcium on stimulation of ROS-GC1 activity by GCAP-1*

GCAP-1 increases the ROS-GC1 activity at low $[Ca^{2+}]_{free}$. This regulation was tested on a range of varying free $[Ca^{2+}]$. The reaction samples, contained of ROS or ROS-membranes

and 10 µM of GCAP-1 or its variants, were preincubated in 10 µl of varying concentration of free $Ca^{2+}$ (see Table 2.2) for 5 min at room temperature. Subsequent procedures were carried out as described above (refer to Methods 2.2.1.2).

The free [$Ca^{2+}$] was adjusted by $Ca^{2+}$/EGTA buffer calculated with a $Ca^{2+}$ buffer program CHELATOR [84]. The values for the Hill coefficient *n* and the half maximum of $Ca^{2+}$-dependent ROS-GC1 activation $K_m$ ($IC_{50}$) were obtained by fitting data to the modified Hill equation using the program ORIGIN 6.1 (Microcal Software Inc., Northhampton, USA):

$$\frac{V}{V_{\max}} = \frac{1-[Ca^{2+}]^n}{[Ca^{2+}]^n + K_m^n} + Z \qquad (2.5)$$

Activity of ROS-GC1 is $V$, the maximum activity of ROS-GC1 is $V_{max}$, the half maximum of $Ca^{2+}$-dependent ROS-GC1 activation is $K_m$, and $Z$ is a constant taking into account that ROS-GC1 activity is not zero at high free [$Ca^{2+}$] [97].

## 2.4.2 High Performance Liquid Chromatography (HPLC)

To examine the extent of myristoylation of GCAP-1 and to confirm attachment of a myristoyl group to recombinant GCAP-1, the analytical HPLC was used. This experiment can complement the results of MALDI-TOF mass spectrometry. The degree of myristoylation in GCAP-1 was determinated by analytical HPLC. Fifty µl of each sample (1 mg/ml) were injected into an HPLC reversed-phase C18 column (250 × 4 mm; from Merck) and eluted with a gradient of 0–100% (v/v) acetonitrile / 0.13–0.1% (w/v) TFA at a flow rate of 0.8 ml/min. The elution was monitored by absorbance at a wavelength in the far-UV 214 nm.

## 2.4.3 Size Exclusion Chromatography (SEC)

Size exclusion chromatography was used to analyze the molecular weight estimation of GCAP-1 and to investigate the distribution of monomer and dimer of GCAP-1 in the presence and the absence of $Ca^{2+}$ and DTT. The Superdex 75 HR 10/30 gel filtration column (1.0 × 30 cm; from Pharmacia Biotech) was equilibrated with two column volumes of elution buffer (50 mM Tris, pH 7.5, 150 mM NaCl) at a flow rate of 0.5 ml/min using an automated fast protein liquid chromatography system (ÄKTA™ FPLC; Amersham Pharmacia Biotech). The Superdex 75 HiLoad 10/30 column was calibrated with the following proteins. Purified GCAP-1 was injected in a volume of 100 µl (1 mg/ml) containing 5 mM EGTA or

2 mM $CaCl_2$ and in the presence or the absence of DTT and eluted at 0.5 ml/min elution buffer.

The volume of solvent between the point of injection and the peak maximum of a solute is known as the elution volume ($V_e$). The elution volume is equal to the void/exclusion volume ($V_0$). The separation can be characterized in terms of the partition coefficient, $K_{av}$, defined by:

$$K_{av} = \frac{V_e - V_0}{V_t - V_0} \qquad (2.6)$$

Where $K_{av}$ describes the fraction of stationary column volume available for diffusion of a given proteins ($K_{av} = K_d$). Whereas $V_0$ and $V_t$ are the 'void volume' and 'total volume' of the column, respectively [98]. The $V_0$ of the column is 7 ml, determined by thyroglobulin and the $V_t$ is 24 ml.

**TABLE 2.7** The molecular weight standards for size exclusion chromatography (from Amersham Pharmacia Biotech)

| Standards | Molecular Weight |
|---|---|
| Thyroglobulin | 669 kDa |
| BSA | 67 kDa |
| Ovalbumin | 43 kDa |
| Chymotrysinogen A | 25 kDa |
| Ribonuclease A | 13.7 kDa |
| Aprotinin | 6.5 kDa |

## 2.4.4 Thiol Reactive Chemical Reactions

### *2.4.4.1 Counting disulfide bonds by iodoacetate derivatives*

To count the integral numbers of the disulfide bonds of GCAP-1, the method described by Hirose et al. and Hollecker was used [99,100]. This approach examines the charge differences that are introduced by specific chemical modification of the cysteine using the alkylation reagents iodoacetamide (IAM) and iodoacetic acid (IAA). After this treatment, the total number of disulfide bonds of proteins was determined by ND-PAGE, in which proteins were separate into distinct bands depending on the number of disulfide bonds cleaved [99]. Carboxymethylation with IAA results in a new acidic group at each free cysteine residue,

making the charge of the molecule more negative. When IAM reacts with thiol groups competitively, the residues remain neutral [100] (Fig. 2.4 *A*).

GCAP-1 (40 μM) was reduced by incubation at 37°C for 30 min in 0.5 ml of denaturing buffer in the presence of varying concentrations of DTT solutions (0–10 mM). For the first alkylation, 10 mM IAM of the solution were added and incubated at room temperature for 15 min. Each sample was desalted by gel filtration on a Sephadex G-25 column or PD-10 column. The dried samples after lyophilization were dissolved in 50 μl of denaturing solution, and mixed with the final concentration of 0.1 mM of DTT, and then incubated at 37°C for 30 min. For the second alkylation, the final concentration of 0.1 mM IAA of solution was added and incubated at room temperature for 15 min. After two alkylation steps, the samples were electrophoresed with ND-PAGE. Electrophoresis was performed at constant currents (20 mA) at 16°C for 12–20 hours and stained with Coomassie staining solution and then destained with destaining solution [99]. This gel electrophoresis was carried out according to the procedures of Goldenberg [95] and Hollecker [100].

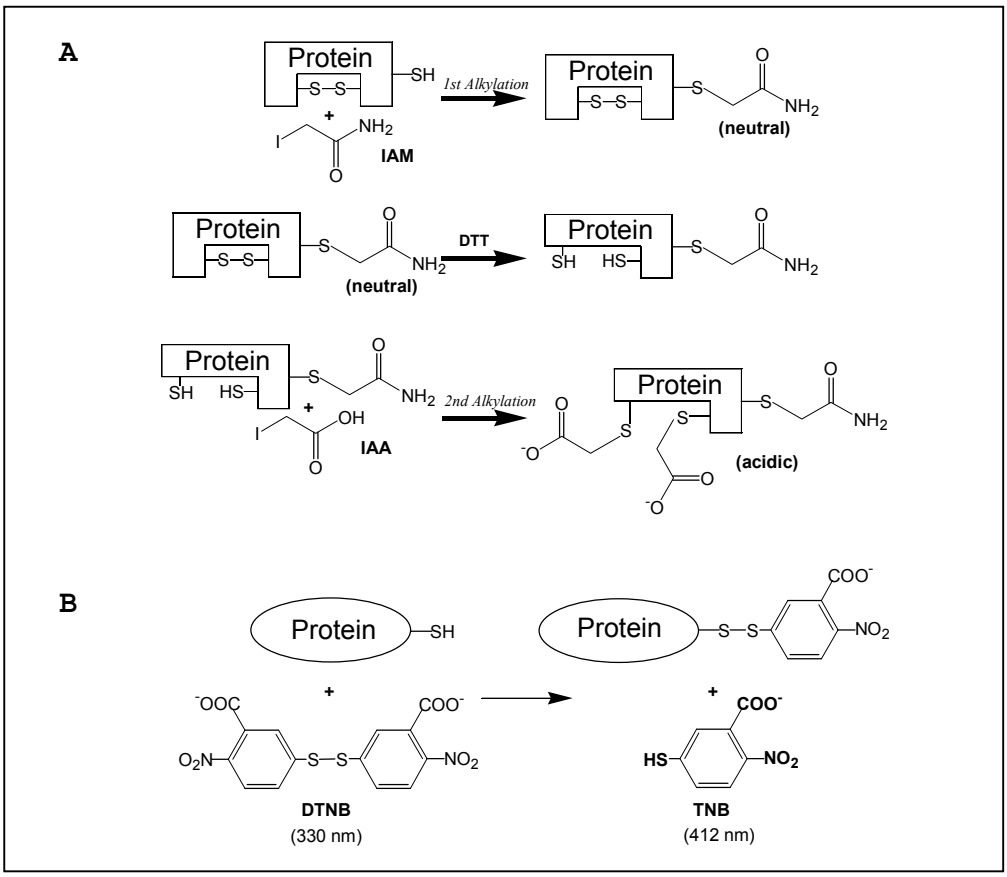


**FIG. 2.4.** Thiol reactive chemical reactions. ***A.*** Modification of SH groups with iodoacetic acid (IAA) to give the negative charge and with iodoacetamide (IAM) to remain the neutral charge. ***B.*** Reaction of Ellman's reagent with cysteine residue of protein.

### *2.4.4.2 Monitoring cysteine reactivity towards DTNB (Ellman's reagent)*

Ellman's reagent, 5,5′-dithio-bis-(2-nitrobenzoic acid), called DTNB, is a compound useful for the quantitative determination of thiol groups in solution [101]. The disulfide of DTNB undergoes disulfide exchange with a free thiol group to form a mixed disulfide with proteins and to release one molecule of the chromogenic substance 5-thio-2 nitrobenzoic acid, called TNB (Fig. 2.4 *B*). The intense yellow color produced by the TNB anion can be measured by its absorbance at 412 nm. Since each thiol group generates one molecule of TNB per molecule of DTNB, direct quantitation is easily done [102] (Fig. 2.5 *A*). This modification reaction is both specific and stoichiometric (Fig. 2.5 *B*).

**Measurement of *L*-cysteine for thiol standard calibration curve:** The thiol concentrations of *L*-cysteine standards were determined and then used to create a calibration curve of varying concentration (0.1–100 mM). A degassed 100 mM *L*-cysteine stock solution was diluted into 1 ml of 50 mM HEPES, pH 7.4, 100 mM NaCl to give the standard solutions. Ellman's reagent at 50–250 μM was added to each tube, mixed well and incubated at room temperature for 5 min. The absorbance at 412 nm of buffer was measured as a baseline and then the absorbance of the each solution at 412 nm was read.

$$[Thiol]\ (M) = \frac{\Delta A_{412}}{\varepsilon_{412} \cdot l} \qquad (2.7)$$

The thiol concentration of the *L*-cysteine working solution was calculated using the measured absorbance value, $\Delta A_{412}$ and the molar extinction coefficient, $\varepsilon_{412} = 13600\ M^{-1} \cdot cm^{-1}$ [101].

**Thiol reactivity of GCAP-1 and its cysteine mutants:** The fresh solution of DTNB (12.5 mM) was prepared by dissolving the Ellman's reagent (Pierce) in 0.1 M Tris, pH 8.0 and sonicating for 5 min at 80–100 W. Using 100 μM stock solutions of GCAP-1 and its mutants in 50 mM HEPES, pH 7.4, 100 mM NaCl, 2–10 μM of protein solutions and 50–250 μM of DTNB were prepared for each experiment. Each protein sample containing DTNB solution was mixed with 100 μM of $CaCl_2$ or 2 mM EGTA. The solution was stirred well and incubated in 50 mM HEPES, pH 7.4, 100 mM NaCl at room temperature for 5–15 min. The absorbance at 412 nm was read versus time using a Shimadzu UV-2101PC UV/VIS scanning spectrophotometer with appropriate baseline correction.

Thiol reactivity of GCAP-1 and its cysteine mutants was also measured as a function of the free [$Ca^{2+}$]. Varying concentrations of $Ca^{2+}$/EGTA buffer (refer to Table 2.2) were

adjusted and the reaction was started by the addition of DTNB directly to the cuvette to a final concentration of 100–250 μM. Spectral changes were immediately monitored using an SLM-Aminco DW-2000 UV/VIS spectrophotometer in dual wavelength mode with monochromators set at 412 nm and 750 nm.

Thiol reactivity of GCAP-1 was also tested in the presence of the peptide #34a and the peptide Sokal #71 (refer to Methods 2.1.2.4). For this purpose 10–100 μM of peptide solutions were prepared, using 1 M stock solutions of peptides in 50 mM HEPES, pH 7.4, 100 mM NaCl. Those experiments were undertaken as described above.

**Kinetic analysis of thiol reactivity of the cysteine mutants of GCAP-1 towards DTNB:** An affinity label characteristically forms a reversible protein-reagent complex prior to the irreversible modification. This behavior can be expressed as:

$$P + R \underset{k_{-1}}{\overset{k_1}{\rightleftarrows}} PR \xrightarrow{k_{max}} PR'$$

where *P* represents the free protein, *R* is the affinity label, *PR* the reversible protein-reagent complex, and *PR′* the covalently modified protein. The existence of a reversible protein-reagent complex is indicated by a 'rate saturation effect' in which the rate of modification increases with increasing reagent concentration until the protein is saturated with reagent; further increases in reagent concentration do not enhance that rate of modification. The observed rate constant ($k_{obs}$) at a particular reagent concentration is described by the equation:

$$k_{obs} = \frac{k_{\max}}{1+(K_m/[R]^n)} \qquad (2.8)$$

Where

$$K_m = \frac{k_{-1}+k_{\max}}{k_1} \qquad (2.9)$$

$K_m$ is the equivalent of the Michaelis constant of enzyme kinetics, and $k_{max}$ is the maximum rate of modification at saturating concentrations of reagent. The reciprocal form of equation 2.8 is:

$$\frac{1}{k_{obs}} = \frac{1}{k_{\max}} + \frac{K_m}{k_{\max}\cdot[R]^n} \qquad (2.10)$$

A double-reciprocal plot of $1/k_{obs}$ versus [R] provides values for $K_m$ and $k_{max}$ [103]. This can be also expressed as the following equation;

$$\frac{k_{obs}}{k_{\max}} = \frac{[Ca^{2+}]^n}{[Ca^{2+}]^n + K_m} \qquad (2.11)$$

The Hill coefficient is $n$ and the half maximum of $Ca^{2+}$-dependent affinity of GCAP-1 to DTNB is $K_m$. The kinetic traces for the affinity labeling reaction were fit to modified exponentials in varying concentrations of $Ca^{2+}$/EGTA buffer (see Table 2.2). The modified Hill equation was used for $Ca^{2+}$-dependent reactivity of GCAP-1 to DTNB. For this purpose, the program ORIGIN 6.1 (Microcal Software Inc., Northhampton, USA) was used.

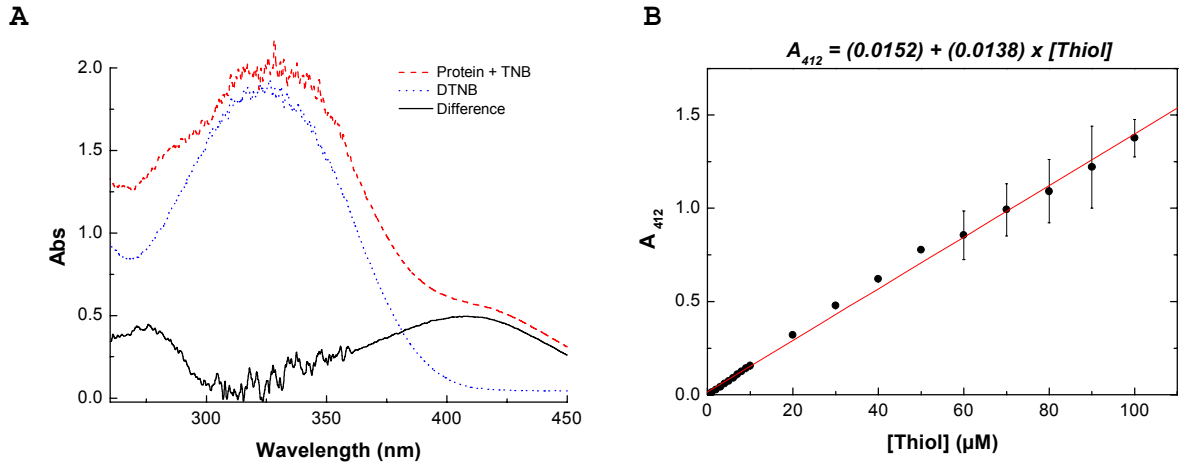


**FIG. 2.5.** The typical spectra of DTNB reaction and the standard curve of *L*-cysteine. ***A.*** The typical spectra of DTNB and proteins. ***B.*** The calibration curve of reactivity of cysteine with DTNB, plotting the absorbance at 412 against the concentration of thiol groups.

# 2.5 Biophysical Studies

## 2.5.1 Circular Dichroism (CD) Spectroscopy

In order to investigate the influence of $Ca^{2+}$, temperature and the myristoyl group on the conformation of GCAP-1 circular dichroism (CD) spectroscopy was used.

### *2.5.1.1 Introduction of circular dichroism* [104-106]

Circular dichroism is one aspect of optical activity, the other being optical rotation. An electronic transition is optically active if it is connected with both an electric and a magnetic transition moment, provided these are not perpendicular to each other. Proteins are optically active on the one hand because of their chiral building blocks, the amino acid residues. On the other hand, optical activity also results from the spatial distribution of the constituent chromophores in the protein structure. Therefore the phenomenon lends itself to structural analysis of proteins.

CD spectroscopy is the most widely used method to look into the conformation of proteins in solution. The main chain conformation, including periodic and non-periodic secondary structures, is reflected in the far UV, the absorption range of the main chain chromophores, i.e. of the transitions of the peptide bonds.

CD spectra can be analyzed in terms of the secondary structural composition of proteins, i.e. the percentage of α-helix, β-structure, β-bends etc., whereas it is not possible to localize these elements within the structure. Quantification of secondary structure, however, is much less the strength of CD spectroscopy than is its capacity to sensitively indicate conformational changes. These may concern the main chain, but in any case will affect the tertiary structure, altering distances and relative orientations of side chains. The near-UV CD originates in the chromophores of aromatic side chains and disulfide groups.

### *2.5.1.2 Measurement of circular dichroism*

The CD spectra were recorded on a JASCO J-20 CD spectropolarimeter in the near-UV and on an AVIV model 62A DS CD spectropolarimeter in the far-UV. Quartz cells with 0.01–0.1 cm path length were used. The protein concentration was 0.3–1.0 mg/ml in 20 mM Tris, pH 8.0. The $Ca^{2+}$-free proteins were measured with 2 mM EGTA, while the $Ca^{2+}$-bound proteins with 2 mM $CaCl_2$. Constant temperature was maintained at 25°C using a

circulating water bath. Samples were scanned in 1 nm increments at a scan rate of 0.5 m/min. Data were collected by a PC computer that averaged three spectra for each sample.

#### *2.5.1.3 Monitoring the conformational stability*

The conformational stability of GCAP-1 was measured by stepwise increasing the temperature and monitoring the ellipticity at 215 nm, increasing 1°C every 3 min from 25°C to 95°C. Samples of 0.2–0.3 mg/ml protein were measured in 0.01–0.03 cm path length cuvettes in 20 mM Tris, pH 8.0 with the presence or the absence of $CaCl_2$.

#### *2.5.1.4 Analysis of circular dichroism spectra*

CD spectrometers measure the difference in absorbance for left and right circularly-polarized light, $\Delta A = A_L - A_R$· CD spectra are reported either as the differential molar CD extinction coefficient, $\Delta\varepsilon_M = \varepsilon_L - \varepsilon_R$ or as the molar ellipticity, $[\Theta]_M$ which are interrelated by Equation 2.16:

$$[\Theta]_M = 3300 \cdot \Delta\varepsilon_M \qquad (2.12)$$

The molar ellipticity, $[\Theta]_M$, or the mean residue weight ellipticity, $[\Theta]_{MRW}$, are calculated by using Equation 2.13 or 2.14:

$$[\Theta]_M = \frac{100 \cdot \Theta_{obs} \cdot M_r}{c \cdot l} \qquad (2.13)$$

$$[\Theta]_{MRW} = \frac{100 \cdot \Theta_{obs} \cdot M_r}{c \cdot l \cdot N_A} = \frac{100 \cdot \Theta_{obs} \cdot MRW}{c \cdot l} \qquad (2.14)$$

where $\Theta_{obs}$ is measured ellipticity in degrees, $c$ is the protein concentration in mg/ml, $l$ is the optical path length in cm, $M_r$ is the protein molecular weight, and $N_A$ is the number of amino acids per protein. $MRW$ is the average molecular weight of an amino acid in the protein. $[\Theta]$ and $[\Theta]_{MRW}$ have the units $deg \cdot cm^2 \cdot dmol^{-1}$ [107,108].

## 2.5.2 MALDI-TOF Mass Spectrometry

To confirm attachment of a myristoyl group to the purified recombinant GCAP-1, matrix-assisted laser desorption/ionization time-of-flight (MALDI-TOF) mass spectrometry was performed.

### *2.5.2.1 Introduction of mass spectrometry* [4,109,110]

A mass spectrometer is an analytical device to determine the molecular weight of molecules by separating molecular ions according to their mass-to-charge ratio (*m/z*) in electric or magnetic fields. It usually consists of three parts; the ion source, the mass analyzer, and the detection system. To ionize non-volatile, thermally labile organic compounds, particularly high-molecular biomolecules, a soft ionization technique such as MALDI has to be applied.

In MALDI the macromolecular analyte is embedded in a solid low-molecular organic matrix on a metallic substrate and then inserted into the high vacuum of the ion source. By irradiating the sample with an UV laser the macromolecules are desorbed and ionized with the explicite assistance of the matrix. The mostly singly charged ions are accelerated in an electric field of about 20 kV where they pick up the same amount of energy. Accordingly, ions of lower mass enter the mass analyzer with a higher speed than the heavier ones, consisting essentially of a field-free tube in high vacuum. Due to the different drift velocities the ions arrive at the detector at different time after having passed the drift distance of 1–2 m, namely the time-of-flight mass spectrometer (TOF). From measuring the flight times with a transient recorder the molecular masses can be determined, using the fact that the mass or ratio mass/charge is proportional to the square of the flight time. For exact mass determination, calibration with known standard masses is necessary. MALDI-TOF MS permits the analysis of high molecular weight compounds with high sensitivity.

### *2.5.2.2 Measurement of mass spectrometry*

MALDI-TOF MS spectra were acquired on a Bruker Reflex TOF-MS instrument (Biflex III, Bruker Daltonik, Bremen, Germany) with delayed extraction of 200 ns. The mass spectrometer was equipped with a SCOUT multiprobe inlet and $N_2$ laser (337 nm, 3 ns pulse width). The acceleration voltage was 20 kV, and the reflectron voltage was 14.9 kV. The working matrix solution was prepared with a saturated sinapinic acid (3,5-dimethoxy-4-hydroxycinnamic acid) matrix dissolved in 0.1% (v/v) aqueous trifluoroacetic acid

(TFA)/acetonitrile (2:1). A five µl volume of solution without matrix containing 50–100 µM of protein was mixed with 5 µl of matrix solution. A solution of 1 µl volume of the resulting mixture was deposited on the target for the measurement (dried droplet method). For each sample, at least four spectra were averaged. Data were analyzed using the software XMASS 5.0 supplied with the instrument.

#### *2.5.2.3 Analysis of mass spectra*

The molecular weight of GCAP-1 can be calculated by adding the masses of each individual amino acid residue in GCAP-1 and adding the mass of the N-terminal groups and its respective additive:

$$\boldsymbol{m}(protein) = \sum_{i=1}^{n} n_i \, \boldsymbol{m}(aa_i) + \boldsymbol{m}(N\text{-}term) \qquad (2.15)$$

where $n_i$ is the total number of a given amino acid residue, $aa_i$, present in the protein sequence, $\boldsymbol{m}(protein)$ is the average or the monoisotopic molecular weight of the protein [109].

The following molecular weights of standards were used to calculate accurate protein average molecular masses: ~23312 Da (trypsin_$MH^+$) and ~29025 Da (carbonic anhydrase_$MH^+$).

### 2.5.3 Surface Plasmon Resonance (SPR) Spectroscopy

#### *2.5.3.1 Basic theory of surface plasmon resonance*

Surface plasmon resonance (SPR) spectroscopy is a non-invasive optical technique which measures the mass concentration of biomolecules in close proximity to a specially prepared surface to study protein-protein or protein-peptide interactions [111,112].

A glass slide is coated with a 50 nm gold film, which is in turn covered with a covalently bound hydrogel (carboxylated dextran), modified to facilitate immobilization of proteins. This glass/gold/dextran biosensor is docked on an optical unit, thus creating a flow-cell where the dextran is exposed to solution. A polarized monochromatic light beam is reflected off the surface, where a plasmon resonance phenomenon takes place at the gold surface. This means that at a specific angle of incidence, the intensity of reflected light decreases and a ‘dip’ appears. If every parameter is kept constant and only the composition of the buffer *etc* near the surface changes, a shift in the angle of incidence occurs, and

consequently a dip of the reflected light beam appears. Binding and dissociation of proteins can be monitored by measuring the time-dependent shift of the dip, i.e. time-dependent change of the refractive index.

Biophysical studies on the interaction between GCAP-1 and two peptides from ROS-GC1 were performed by surface plasmon resonance spectroscopy using a BIAcore 1000 instrument (BIAcore AB). Each of the purified triple mutants of GCAP-1 at a concentration of 10 µM were captured to an immobilization level of about 7000 RU on CM5 sensor chips via thiol coupling. All interaction experiments were carried out in either HBS-$Ca^{2+}$ buffer or HBS-EGTA buffer at a constant flow rate of 50 µl/min. The peptide #34a and the peptide Sokal #71 were injected at concentrations varying from 50 to 2000 µM. Nonspecific binding was subtracted using an unmodified sensor surface for each concentration individually. The association and dissociation phase were both monitored for 1 min. The resulting data were evaluated with the BIAevaluation software version 3.0 (BIAcore AB).

#### *2.5.3.2 Immobilization of cysteine mutants of GCAP-1*

The sensor chip CM5 (BIAcore AB) was first activated with a 2-min pulse of 50 mM *N*-hydroxysuccinimide (NHS) and 200 mM *N*-ethyl-*N′*-(dimethylaminopropyl)carbodiimide (EDC) at a flow rate of 5 µl/min. For introduction of a reactive disulfide group onto carboxyl groups thiol coupling reagent, 80 mM 2-(2-pyridinyldithio)ethaneamine (PDEA), was injected with a 7-min pulse at a flow rate of 5 µl/min in 0.1 M sodium borate buffer, pH 8.5. To immobilize the proteins, 10 µM of triple mutants of GCAP-1 were injected with a 7-min pulse at a flow rate of 5 µl/min in 50 mM sodium formate buffer, pH 4.0. Excess reactive groups remaining on the surface after immobilization were deactivated by a 7-min pulse of 50 mM *L*-cysteine at a flow rate of 5 µl/min in 50 mM sodium formate buffer, pH 4.0 containing 1 M NaCl [113]. The reaction of thiol coupling and a typical sensorgram are shown in Fig. 2.6.

#### *2.5.3.3 Interaction of peptides derived from ROS-GC1 with immobilized GCAP-1*

The peptide #34a and the peptide Sokal #71 (refer to Methods 2.1.2.4) were dissolved at concentrations ranging from 50–2000 µM in either HBS-$Ca^{2+}$ or HBS-EGTA running buffer (refer to Methods 2.1.3.2). Peptide was injected for 0.7 min at a flow rate of 50 µl/min. Complex formation between the immobilized GCAP-1 and the peptides was monitored by a change in refractive index, directly correlated to changes in resonance units (RU), and

recorded in real time to yield a sensorgram. Dissociation of the formed complex was initiated by washing with running buffer without peptides. After each cycle, the sensor chip was regenerated by injection of 10 µl of regeneration buffer (200 mM glycine, pH 2.0) at a flow rate 50 µl for 1.2 min.

#### *2.5.3.4 Analysis of sensorgrams*

Using BIAlogue software, the SPR signal is presented in resonance units (RU). The change in SPR signal is directly related to the change in surface concentration of biomolecules. A response of 1000 RU corresponds to a shift of 0.1° in the resonance angle, which in turn represents a change in surface protein concentration of about 1 ng/mm$^2$.

The change in *RU* with time is described by:

$$\frac{dRU}{dt} = k_a [p] \, (RU_{max} - RU_t) - k_d \, RU_t \qquad (2.16)$$

Where *dRU/dt* is the peptides binding rate, $RU_t$ the value of RU at time t, and $RU_{max}$ the maximum value of RU. *[p]* is the concentration of peptides used. Rearranging Equation 2.16 yields:

$$\frac{dRU}{dt} = k_a [p] \, RU_{max} - ( k_a [p] + k_d ) \, RU_t \qquad (2.17)$$

$$-\frac{dRU}{dt} = k_d \, RU_t \quad ( \text{if } [p] = 0 ) \qquad (2.18)$$

Thus the value of $k_d$ is determined directly from the dissociation phase [114].

Sensorgrams were analyzed by a curve-fitting program using BIAevaluation software 3.0. The data processing was performed with the program ORIGIN 6.1 (Microcal Software Inc., Northhampton, USA) and SigmaPlot 4.01 (SPSS, Inc).

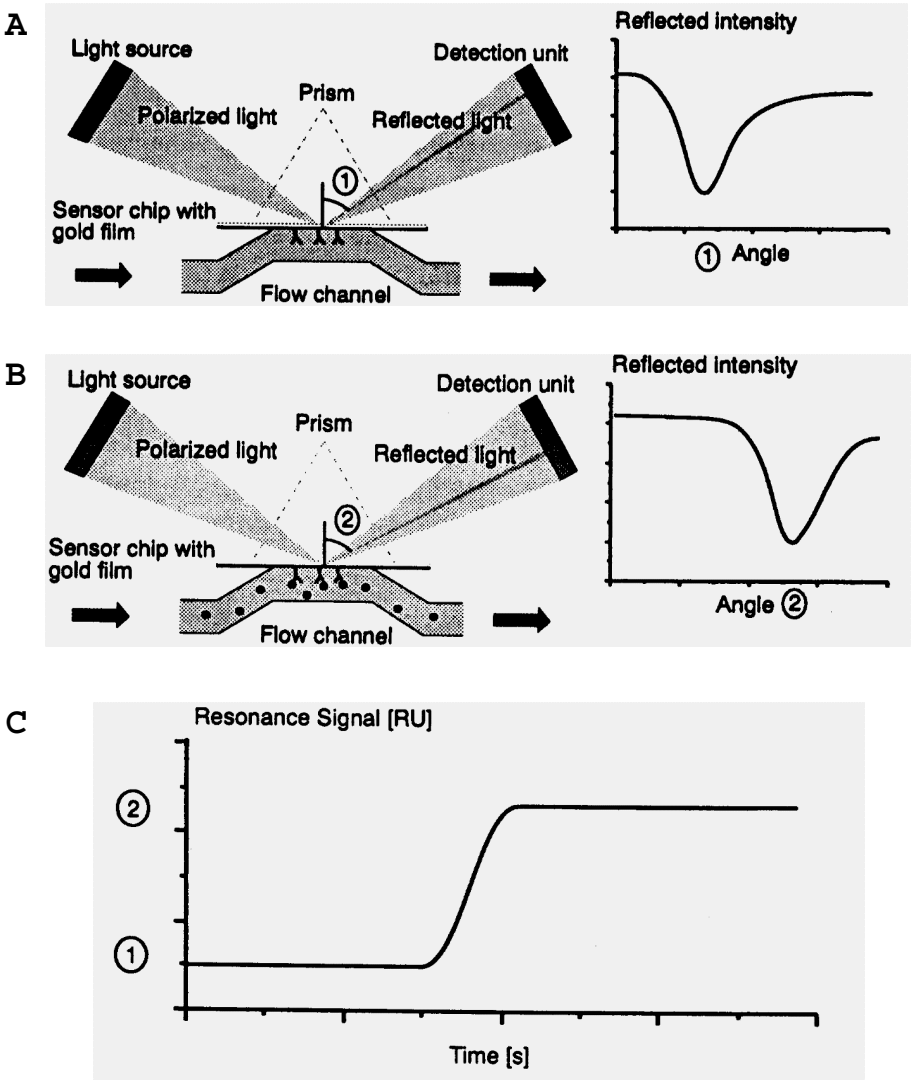


**FIG. 2.6.** Surface plasmon resonance detects changes in the refractive index of the surface layer of the sensor chip. The dips in the intensity of the reflected light occur at the specific angles of incidence; ***A***. No peptides has bound to the immobilized proteins and are detected at angle ①. ***B.*** When the peptides bind the mass and there by the refractive index on the sensor chip surface changes, causing a shift to angle ②. ***C***. Sensorgram plotted as the shift resonance signal versus time (from the manual of SPR, BIAcore AB [115]).

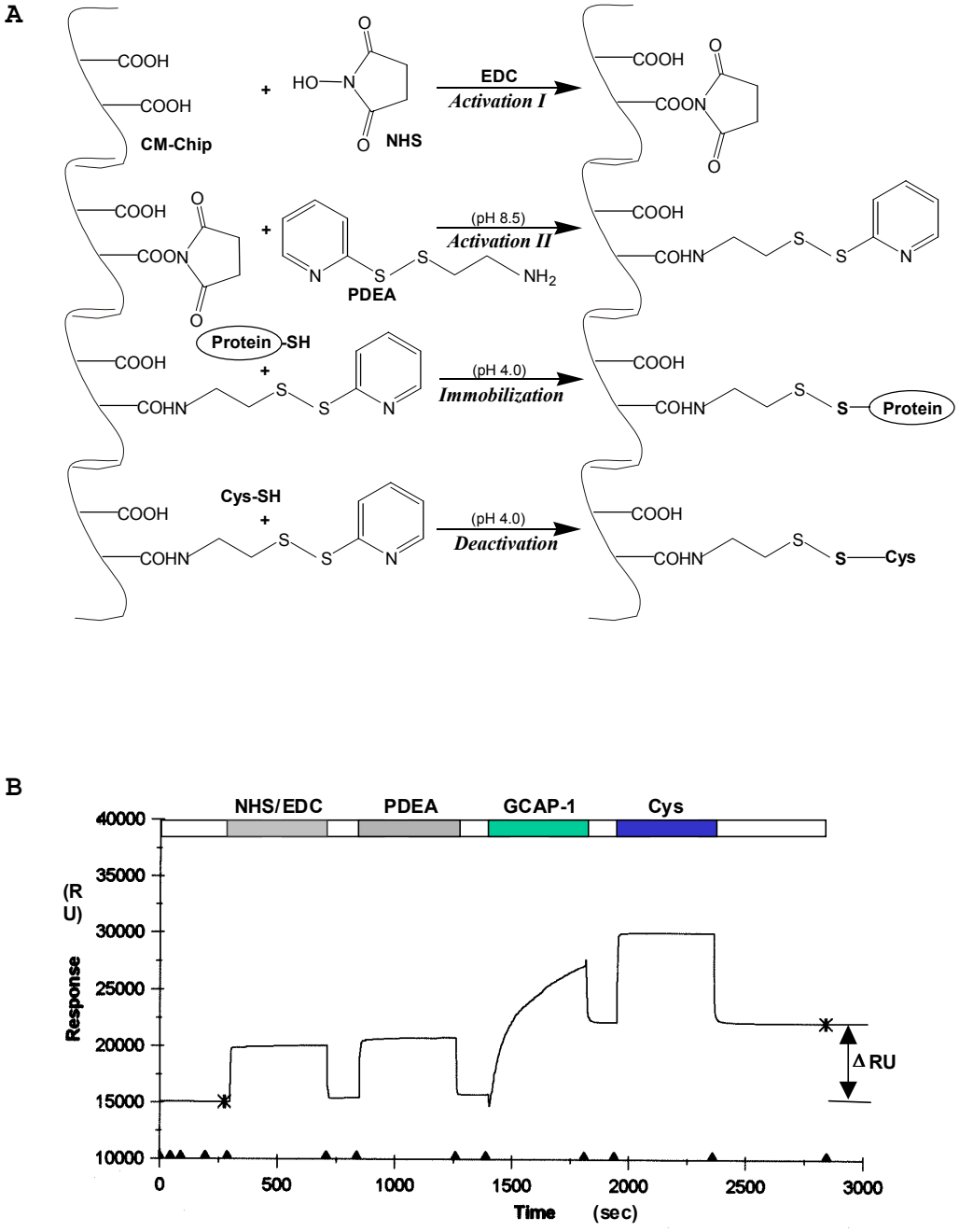


**FIG. 2.7.** The reaction of thiol coupling and a sensorgram showing the steps of activation, modification, coupling, and deactivation. ***A***. The coupling reaction of thiol disulfide exchange on SPR spectroscopy. The carboxylated dextran (CM) chip was first activated by NHS/EDC and then modified by PDEA in order to allow a thiol disulfide exchange reaction with the cysteine of the protein. After binding of the protein to the chip, excess reactive groups were deactivated by *L*-cysteine. ***B***. Sensorgram obtained during the immobilization of the cysteine mutants of GCAP-1.

# 3. RESULTS

The guanylate cyclase activating protein 1 (GCAP-1) activates the particulate membrane-bound guanylate cyclase 1 (ROS-GC1) to synthesize cGMP from GTP at low free $[Ca^{2+}]$ (<100 nM $[Ca^{2+}]_{free}$) [73]. In this dissertation, recombinant GCAP-1 was overexpressed in *E. coli* and purified by gel filtration chromatography and by anion ion exchange chromatography. Among investigations of the biochemical and biophysical properties of GCAP-1, the roles of cysteine residues and myristoylation were assessed focussing on activation of ROS-GC1, on $Ca^{2+}$-dependent conformational changes, and on interaction with peptides from the cytoplasmic part of ROS-GC1.

## 3.1 Preparation of Wild-type GCAP-1

### 3.1.1 Overexpression of Wild-type GCAP-1 in *Escherichia coli*

Some biochemical or biophysical experiments require a large amount of GCAP-1 (>10 mg). However, only about 10 µg native GCAP-1 can be extracted from 100 bovine eyes [14,73]. Therefore recombinant GCAP-1 was overexpressed in *E. coli*.

*E. coli* BL21-Condon Plus(DE3) cells were transformed with the T7 promoter-driven plasmid pET-11a, containing cDNA coding for GCAP-1. *E. coli* strain BL21-Condon Plus(DE3) encodes T7 RNA polymerase under the control of the IPTG-inducible *lac*UV5 promoter for efficient high-level expression of heterologous proteins [87].

To confirm the production of GCAP-1, single colonies were cultivated in a 50 ml culture volume and divided before induction. One part of the culture remained uninduced, whereas the other was supplemented with IPTG. After harvesting the cells they were disrupted by lysozyme. Aliquots of the cell lysates were examined by SDS-PAGE. Figure 3.1 shows that GCAP-1 is not expressed before induction. The most abundant protein in lysates is lysozyme with a molecular weight of ~14 kDa, by which the *E. coli* cells of uninduced cells have been disrupted (Fig. 3.1, *lane 2*). The induction of the plasmid with IPTG leads to the expression of recombinant GCAP-1 with a molecular mass of ~21 kDa

(Fig. 3.1, *lane 3*). As expected, the expressed proteins from *E. coli* containing solely pET-11a without cDNA of GCAP1 did not contain the ~21 kDa band (Fig. 3.1, *lane 4*).

For preparation of GCAP-1 on a large scale, the cells were induced in mid-logarithmic growth phase with 1 mM IPTG for 4 hours at 37°C. GCAP-1 was successfully expressed in soluble fractions with high yields (~100 mg of crude proteins were extracted from a culture volume of 500 ml). Native GCAP-1 contains a covalently attached myristate or related fatty acyl group on its N-terminus [63]. Post-translational fatty acylation of recombinant protein can be achieved by coexpression of N-terminal myristoyl transferase 1 (NMT1 from *S. cerevisiae*) in *E. coli* [116].

In this work, recombinant GCAP-1 was produced as nonmyristoylated GCAP-1 described as **nmGCAP-1**, and partially myristoylated GCAP-1 (**pmGCAP-1)** by coexpression with NMT. Fully myristoylated D$^{6}$S-GCAP-1 (**mD$^{6}$S-GCAP-1)** was obtained by coexpression with NMT. D$^{6}$S-GCAP-1 is a point mutant of GCAP-1, wherein an aspartate was substituted by a serine at position 6. It was kindly provided by Dr. C. Lange (IBI-1, Forschungszentrum Jülich). Substitution of aspartate by serine at position 6 creates a myristoylation consensus site for yeast NMT [72]. The experiments with mD$^{6}$S-GCAP-1 served as the positive control for the myristoylation. A detailed description of the properties of these GCAP-1 forms will be presented in the next chapter (Results 3.2.2).

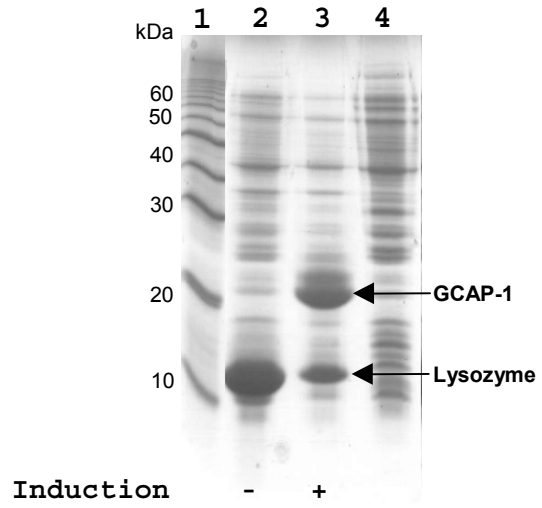


**FIG. 3.1.**Expression screening of GCAP-1. SDS–PAGE was performed on a 15% (w/v) polyacrylamide gel and the gel was stained with Commassie Blue. *Lane 1,* molecular mass standards (7 µg 10 kDa ladder); *lane 2*, total proteins in *E. coli* lysate before induction (4 µg protein + 3 µg lysozyme); *lane 3,* proteins in *E. coli* lysate, mainly containing GCAP-1 with a molecular weight of ~21 kDa, after induction with 1 mM IPTG (4 µg protein + 3 µg lysozyme); and *lane 4,* control, the expressed proteins from *E. coli* containing pET-11a (without cDNA of GCAP1) (7 µg protein).

### 3.1.2 Purification of Wild-type GCAP-1

GCAP-1, overproduced in 500 ml *E. coli* culture, was released by mechanical cell disruption in a volume of 5 ml lysis buffer. After three passages through a French pressure cell, all *E. coli* cells were completely disrupted as observed by optical microscopy. After ultracentrifugation, the supernatant was composed of more than 70% soluble GCAP-1 (Fig. 3.2 *C*, *lane 2*).

In the first purification step GCAP-1 was partially separated from contaminating *E. coli* proteins on HiLoad 16/60 Superdex 75 gel filtration column. GCAP-1 eluted in a wide peak with a retention volume of approx. 68 ml. By the gel filtration, about 25 ± 5 mg of proteins, were obtained in a purity of approx. 80% of GCAP-1, (Fig. 3.2 *A* and Fig. 3.2 *C*, *lane 3*).

In the second chromatographic step, pure fractions of GCAP-1 were eluted at NaCl concentrations of 290–370 mM from an Uno Q-6 ion exchange column. Approx. 12 ± 5 mg GCAP-1 was purified to more than 95% homogeneity (Fig. 3.2 *B* and Fig. 3.2 *C*, *lane 4* and *lane 5*). A summary of the purification steps is shown in Table 3.1.

**TABLE 3.1** Summary of purification steps of GCAP-1 from ~5 ml crude lysate (originating from 500 ml *E. coli* culture)

| Purification step | Volume (ml) | Protein concentration * (mg/ml) | Total protein (mg) |
|---|---|---|---|
| Crude extract | 5 ± 1 | 20 ± 5 | 100 ± 50 |
| Superdex 75 | 9 ± 1 | 3 ± 1 | 25 ± 5 |
| Uno Q-6 | 5 ± 3 | 2 ± 1 | 12 ± 5 |

* The protein concentration was determined by Coomassie blue dye binding [91] using BSA as a standard. After purification, the concentration of GCAP-1 was determined using a GCAP-1 concentration curve (refer to Methods 2.3.2.2). The given values are averaged from more than three experiments of different preparations.

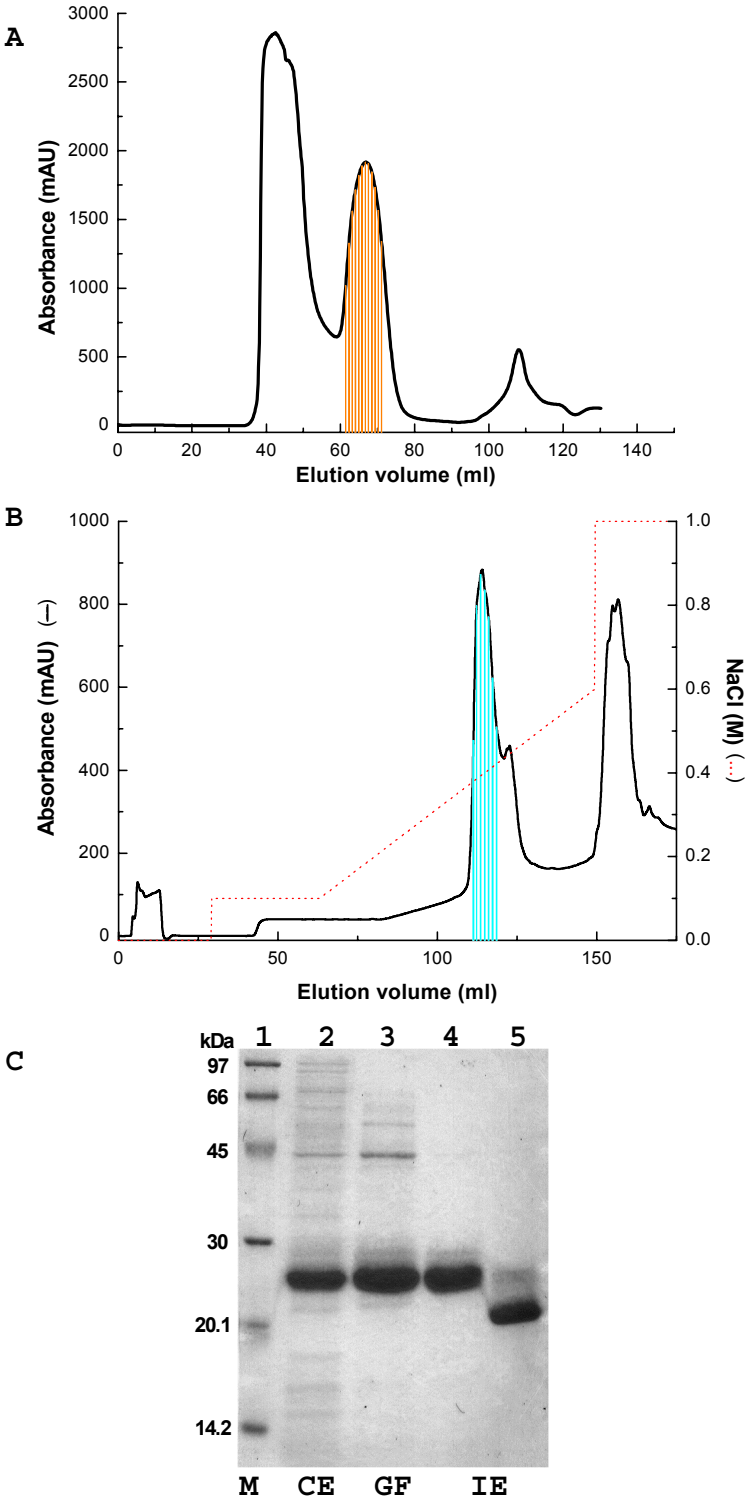


**FIG. 3.2.** Purification of recombinant GCAP-1. ***A.*** Gel filtration chromatography on Superdex 75 HiLoad 10/60. ***B.*** Ion exchange chromatography on Uno Q-6. ***C.*** Samples from each purification step were analyzed on 15% (w/v) SDS-PAGE and proteins were visualized by Commassie staining: *lane 1 (M),* low molecular mass standard (5 µg of standards); *lane 2 (CE),* the soluble fractions from *E. coli* cell lysate with 2.5 mM EGTA (10 µg total proteins); *lane 3 (GF*), pooled fractions from Superdex 75 with 2.5 mM EGTA (10 µg total proteins); *lane 4 (IE*), pooled fractions from Uno Q-6 with 2.5 mM EGTA (10 µg of GCAP-1); and *lane 5 (IE*), pooled from Uno Q-6 with 2 mM $CaCl_2$ added (10 µg of GCAP-1).

## 3.2 Properties of Wild-type GCAP-1

### 3.2.1 Myristoyl Attachment on GCAP-1

The attachment of a myristoyl group to GCAP-1 and the extent of myristoylation for the different forms of recombinant GCAP-1 were determined by matrix-assisted laser desorption/ionization time-of-flight (MALDI-TOF) mass spectrometry and by analytical high performance liquid chromatography (HPLC).

#### *3.2.1.1 MALDI-TOF mass spectrometry studies*

The molecular weights of proteins can be determined by a mass spectrometer, according to their mass-to-charge ratio (*m/z*) in the magnetic fields. Three types of purified recombinant GCAP-1, nmGCAP-1, pmGCAP-1, and mD$^{6}$S-GCAP-1, were characterized by MALDI-TOF-MS analysis. These measurements were performed by Dr. G. Dongmann (ICG-7, Forschungszentrum Jülich).

The spectra from MALDI-MS analysis are shown in Fig. 3.3. The following average isotopic molecular masses of nmGCAP-1, pmGCAP-1, and mD$^{6}$S-GCAP-1 are compared with the calculated molecular masses in Table 3.2.

The molecular mass of nmGCAP-1 was found to be 23349 ± 7.17 Da, in agreement with the calculated mass of 23379 Da, excluding the first Met$^{1}$ residue as methionine is removed during protein synthesis. The difference between the calculated mass and the experimental one of nmGCAP-1 is slight; $\Delta M = M_{cal}$ (nmGCAP-1) − $M_{exp}$ (nmGCAP-1) ≈ 30 Da. Therefore, this value is acceptable as the molecular mass of nmGCAP-1.

GCAP-1 isolated from bovine retinas has a putative site for N-terminal myristoylation at glycine at position 2, the actual N-terminal residue. For pmGCAP-1 coexpressed with NMT, the peak was at 23375 ± 22.57 Da, while the calculated mass for myristoylated GCAP-1 is 23587 Da, which is theoretically 210 Da more mass than nmGCAP-1. The experimental masses of pmGCAP-1 were not reproducible. For example, the difference of the measured mass of pmGCAP-1 and nmGCAP-1 was 117 Da; $\Delta M_{exp} = M_{exp}$ (pmGCAP-1) − $M_{exp}$ (nmGCAP-1) = 23370.33 – 23487.03 ≈ 117 Da, measured at the first day after sample delivery, however several days later the difference became smaller (1–10 Da); $\Delta M_{exp} = M_{exp}$

(pmGCAP-1) – $M_{exp}$ (nmGCAP-1) ≈ 1 Da. The corresponding $M_{exp}$ (pmGCAP-1) could be interpreted as an unresolved overlap of myristoylated and nonmyristoylated GCAP-1 peaks. All subsequent measurements on the same sample resulted in $\Delta M_{exp} \approx 0$, suggesting the myristoylation of pmGCAP-1 is unstable. This result suggests that wild-type GCAP-1 is not fully myristoylated when coexpressed with NMT and that it loses its attached myristoyl group very rapidly.

The peak of mD$^6$S-GCAP-1 was shifted in mass to 23533 ± 7.10 Da, in agreement with the calculated mass of 23561 Da. The shift of about 182 Da is in accord with the attachment of a myristoyl group.

These data suggested that GCAP-1 expressed in the presence of NMT contained a myristoyl group, but it was unstable or only partially myristoylated. In contrast, mD$^6$S-GCAP-1 was completely myristoylated and contained a stable myristoyl group.

**TABLE 3.2** Comparison of molecular masses of nmGCAP-1, pmGCAP-1, and mD$^6$S-GCAP-1 by MALDI-TOF mass spectrometric analysis

| **Type** | **$M_{average}$ (Da) (mean ± SD)** [a] | **$M_{cal}$ (Da)** [b] | **$\Delta M_{cal} - \Delta M_{exp}$** | **$\Delta M - \Delta M_{(nmGCAP-1)}$** |
|---|---|---|---|---|
| nmGCAP-1 | 23349 ± 7.17 | 23379 | 30 | - |
| pmGCAP-1 | 23375 ± 22.57 | 23587 | 212 | 26 |
| mD$^6$S-GCAP-1 | 23533 ± 7.10 | 23561 | 28 | 184 |

a. The mean and SD values were calculated from five to six independent measurements;

Mean is $\bar{x} = \sum_{i=1}^{n} \frac{x_i}{n}$ and SD is $\bar{s}_x = \sqrt{\sum_{i=1}^{n} \frac{(x_i - \bar{x})^2}{n-1}}$.

b. The theoretical mass for the protein sequence was calculated by the internet program 'Compute pI/Mw' of Protein Identification and Analysis Tools in the ExPASy Server at SWISS-PROT (http://expasy.ch/tools/pi_tool.html).

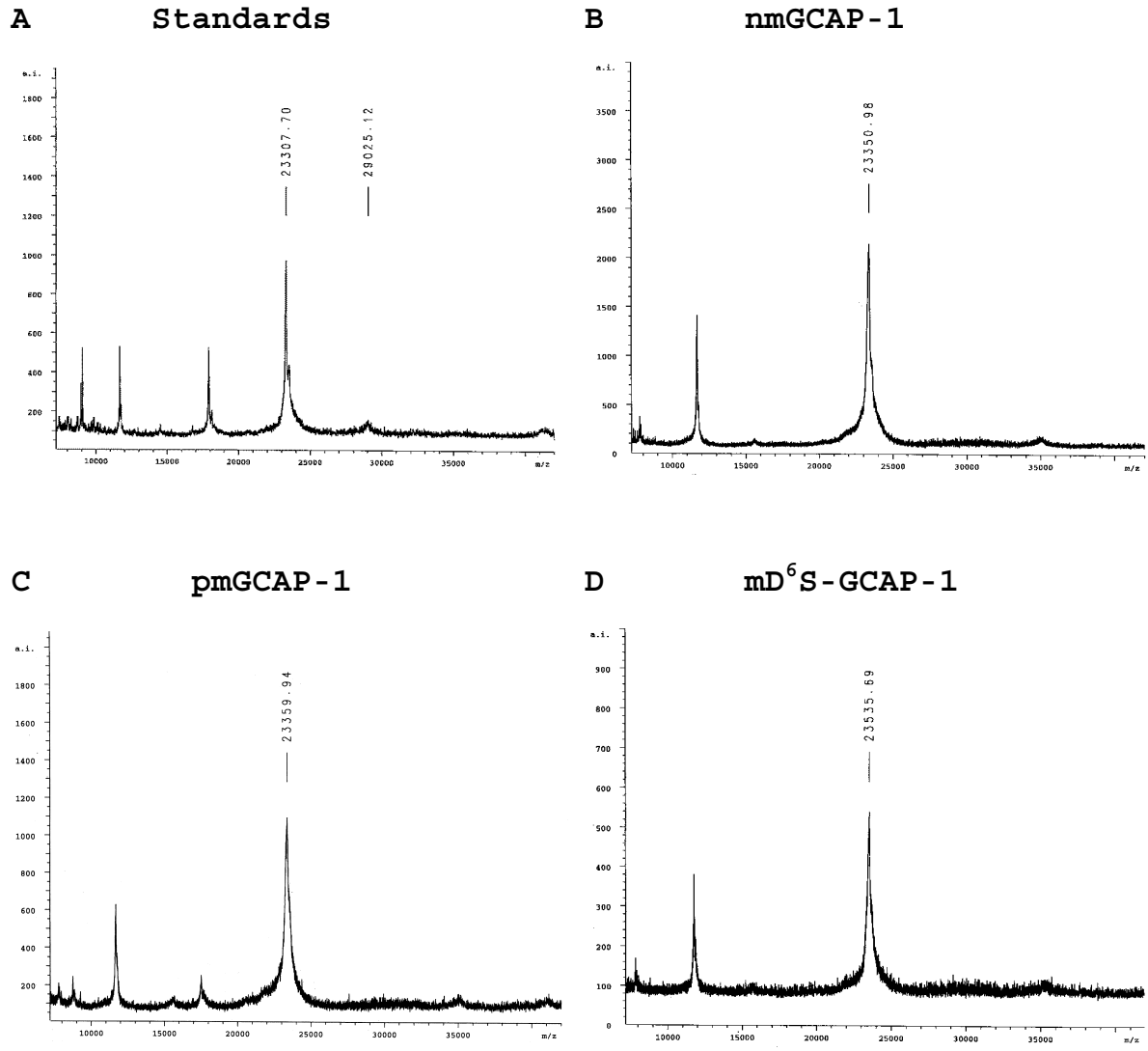


**FIG. 3.3.** MALDI-TOF mass spectra of standards and GCAP-1. One µl of the mixture (5 µl of protein solution + 5 µl of matrix solution) was deposited on the target on a Bruker Reflex TOF-MS instrument (dried droplet method). ***A.*** The molecular weights standards to calculate accurate protein average molecular weights: trypsin_$MH^+$ (23312 Da) and carbonic anhydrase_$MH^+$ (29025 Da). ***B***. nmGCAP-1 (23351 Da). ***C.*** pmGCAP-1 (23360 Da). ***D.*** mD$^6$S-GCAP-1 (23536 Da).

### *3.2.1.2 Analytical high-performance liquid chromatography (HPLC)*

In a second approach, the attachment of a myristoyl group to GCAP-1 and the extent of myristoylation were investigated by the HPLC analysis on a reversed-phase C18 column, shown in Fig. 3.4 (results communicated by Dr. C. Lange, IBI-1).

It was expected that pmGCAP-1 eluted at a higher retention volume compared with nmGCAP-1, since pmGCAP-1 is more hydrophobic. The pmGCAP-1 was eluted with the retention volume of ~52 ml as a main peak (>80%), which is comparable to the retention volume of nmGCAP-1 [58]. A minor peak was visible at ~57 ml (<20%) retention volume, which could be a minor fraction of myristoylated GCAP-1 (Fig. 3.4 *A*). These results indicate pmGCAP-1 is ineffectively carried out of myristoylation by NMT.

In contrast, the mD$^6$S-GCAP-1 was mainly eluted at ~55 ml (>90%). A minor peak was detected at ~52 ml (<10%) retention volume and identified as nonmyristoylated GCAP-1. This elution profile demonstrated that mD$^6$S-GCAP-1 was effectively myristoylated by NMT (Fig. 3.4 *B*). Thus the HPLC analysis complemented the results obtained by MALDI-TOF-MS analysis (refer to Results 3.2.1.1).

In summary, the results of MALDI-TOF-MS analysis and HPLC analysis showed: 1) GCAP-1 expressed without NMT is clearly nonmyristoylated (**nmGCAP-1)**, 2) GCAP-1 coexpressed with NMT is partially myristoylated, therefore this type of GCAP-1 is called **pmGCAP-1**, and 3) D$^6$S-GCAP-1 coexpressed with NMT is completely myristoylated, (**mD$^6$S-GCAP-1)**.

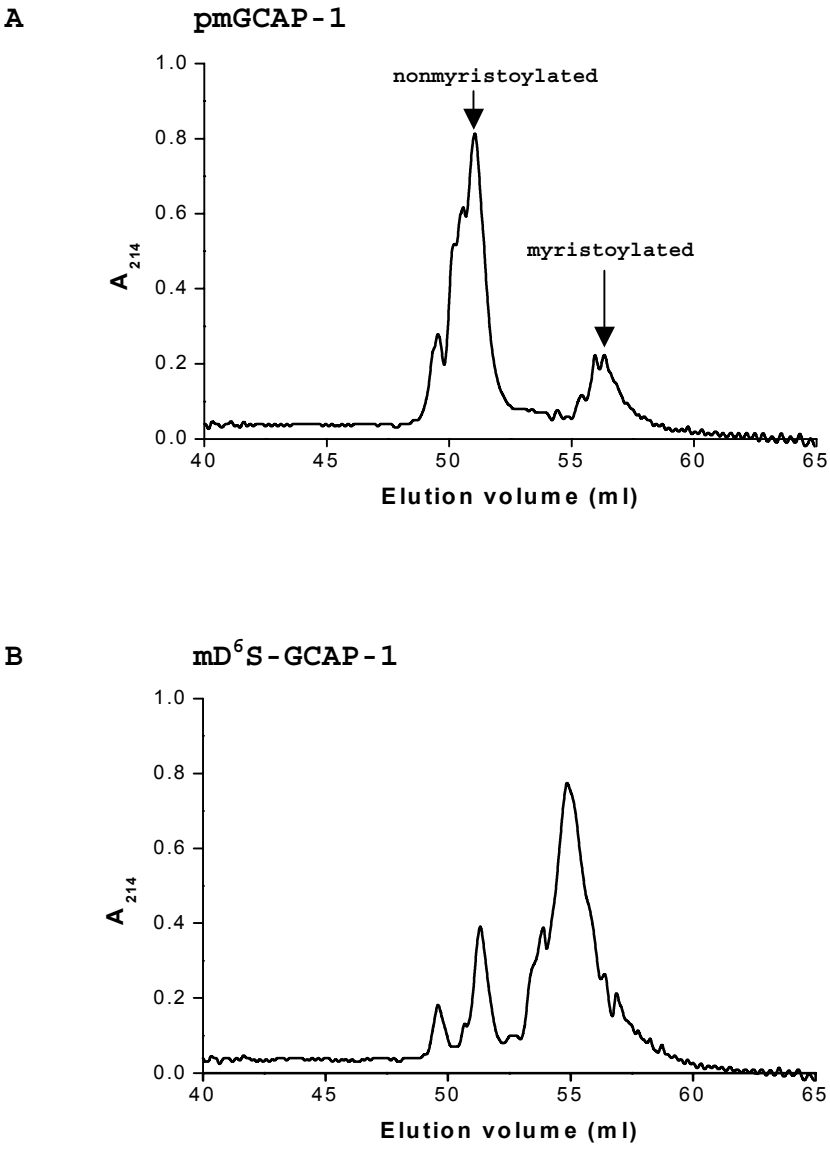


**FIG. 3.4.** HPLC elution profiles of GCAP-1 forms on an HPLC reversed-phase C18 column (250 × 4 mm). ***A***. pmGCAP-1 was mainly eluted at ~52 ml at about 40% (v/v) acetonitrile/0.118% (w/v) TFA. ***B***. mD$^{6}$S-GCAP-1 was mainly eluted at ~55 ml at about 70% (v/v) acetonitrile/0.109% (w/v) TFA. Fifty µg of each sample (1 mg/ml) were injected and eluted with a gradient of 0–100% (v/v) acetonitrile/0.13–0.1% (w/v) TFA at a flow rate of 0.8 ml/min. The retention times of nonmyristoylated GCAP-1 and myristoylated GCAP-1 are indicated.

### 3.2.2 Regulation of ROS-GC1 by GCAP-1

Washed ROS membranes were used for measuring the activation of ROS-GC1 (refer to Methods 2.4.3.1). These membranes contain ROS-GC1 without soluble activators GCAP-1 and GCAP-2. The basal ROS-GC1 activity in washed ROS membranes was about 3–4 nmol cGMP·min$^{-1}$·mg$^{-1}$ rhodopsin at low $[Ca^{2+}]_{free}$ and about 2–3 nmol cGMP·min$^{-1}$·mg$^{-1}$ rhodopsin at high $[Ca^{2+}]_{free}$. The regulation of ROS-GC1 activity by native GCAP-1 and wild-type GCAP-1 is illustrated in Figs. 3.5 and 3.6. These data are summarized in Tables 3.3 and 3.4.

In whole ROS, activation of ROS-GC1 at low $[Ca^{2+}]_{free}$ is mediated by mainly GCAP-1 and GCAP-2. The biological role of GCAP-3 is not known. In ROS isolated from bovine retinas GCAP-1 and GCAP-2 exist in the ratio of 1 to 1 (personal communication with Dr. K.-W. Koch, IBI-1). The maximal activity of ROS-GC1 by these endogenous GCAPs was ~17 nmol cGMP·min$^{-1}$·mg$^{-1}$ rhodopsin at low $[Ca^{2+}]_{free}$. Endogenous GCAPs in ROS stimulated ROS-GC1 activity 8-fold with high cooperativity ($n$ = 2.8) in the range from 100 nM to 1 µM free $[Ca^{2+}]$ ($IC_{50}$ = 264 nM) (Fig. 3.5).

Purified native GCAP-1 stimulated ROS-GC1 activity 5–10-fold with high cooperativity ($n$ = 2.5) in the range from 50 to 400 nM ($IC_{50}$ = 100 nM) [73]. Frins et al. reported that the recombinant GCAP-1 regulated the activation of ROS-GC1 differently; the degree of cooperativity was lower, $n$ = 2.0, and the $IC_{50}$-value had shifted to a higher value of 261 nM [97]. However, other $IC_{50}$-values reported in the literature by several groups range from 50 to 280 nM (see review 11).

In the presence of EGTA, maximal activity was 12.4 nmol cGMP·min$^{-1}$·mg$^{-1}$ rhodopsin with pmGCAP-1. This stimulation of ROS-GC1 by pmGCAP-1 was 6-fold. The $EC_{50}$-value for the ROS-GC1 activity upon the concentration of pmGCAP-1 was 0.9 µM in the presence of 2 mM EGTA (Fig. 3.6 *A*). The $Ca^{2+}$-dependence of ROS-GC1 activation differed significantly between native GCAP-1 and pmGCAP-1. The $IC_{50}$-value of pmGCAP-1 had shifted to a higher $[Ca^{2+}]_{free}$ value of 1.09 µM. The ROS-GC1 activity was stimulated 7-fold by pmGCAP with the lower cooperativity ($n$ = 1.1). The activity at ~10 µM $[Ca^{2+}]_{free}$ remained at ~26% (Fig. 3.6 *C*).

Stimulation of ROS-GC1 by nmGCAP-1 was only 3-fold with maximal activity of 8.1 nmol cGMP·min$^{-1}$·mg$^{-1}$ rhodopsin in the presence of EGTA. The $EC_{50}$-value for the ROS-GC1 activity upon the concentration of nmGCAP-1 was 0.9 µM in the presence of 2 mM EGTA (Fig. 3.6 *B*). The $IC_{50}$-value of pmGCAP-1 shifted to a higher value of 2.82 µM $[Ca^{2+}]_{free}$. The ROS-GC1 activity increased 5-fold in the presence of nmGCAP-1 of low $[Ca^{2+}]_{free}$. The cooperativity was lower ($n$ = 0.3). The activity at ~10 µM $[Ca^{2+}]_{free}$ still remained at ~43% (Fig. 3.6 *D*).

When the $[Ca^{2+}]_{free}$ was low with 2 mM EGTA the activities of ROS-GC1 depended on the concentration of GCAP-1. In the presence of 2 mM $CaCl_2$ the ROS-GC1 activity remained constant at varying concentration of wild-type GCAP-1. The $Ca^{2+}$-dependence of ROS-GC1 activation showed significant differences between native GCAP-1 and pmGCAP-1 as well as between pmGCAP-1 and nmGCAP-1.

**TABLE 3.3** Activation of ROS-GC1 by pmGCAP-1 and nmGCAP-1

| **Type** | **Activity at low $[Ca^{2+}]_{free}$ (nmol cGMP·mg$^{-1}$·min$^{-1}$ R)** [a] | **Activity at high $[Ca^{2+}]_{free}$ (nmol cGMP·mg$^{-1}$·min$^{-1}$ R)** [b] | **$EC_{50}$** [c] **[Protein] (µM)** |
|---|---|---|---|
| pmGCAP-1 | 12.39 | 2.14 | 0.85 |
| nmGCAP-1 | 8.09 | 2.50 | 0.88 |

a. with 2 mM EGTA

b. with 2 mM $CaCl_2$

c. The $EC_{50}$-value upon the concentration of proteins with 2 mM EGTA.

**TABLE 3.4** Stimulation of ROS-GC1 with GCAP-1 as a function of $[Ca^{2+}]_{free}$

| Type | Inhibition at high $[Ca^{2+}]_{free}$ | Maximal Activity (nmol cGMP·mg$^{-1}$·min$^{-1}$ R) | $IC_{50}$ $[Ca^{2+}]_{free}$ (μM) | $n$ to $Ca^{2+}$ |
|---|---|---|---|---|
| ROS-GCAPs | +/-* | 15.99 | 0.263 | 2.8 |
| Native GCAP-1 | + | 20 | 0.100 | 2.5 |
| pmGCAP-1 | - | 13.91 | 1.088 | 1.1 |
| nmGCAP-1 | - | 9.23 | 2.817 | 0.3 |

* In this experiment, the inhibitory effect of endogenous GCAP in ROS was slight, but some investigators reported observation of a significantly lower activity (inhibition) in the presence of endogenous GCAPs than in its absence.

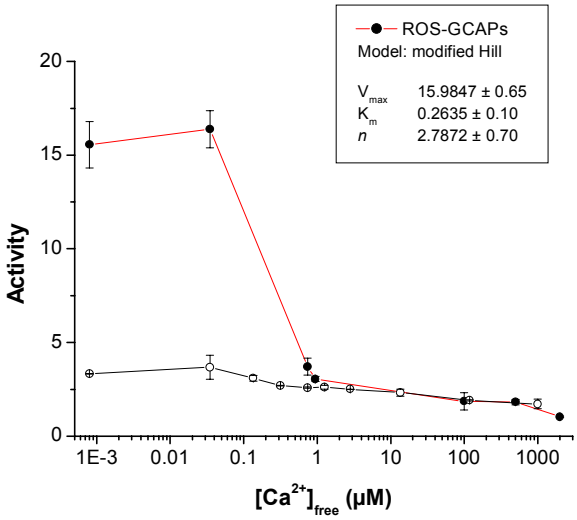


**FIG. 3.5.** Regulation of ROS-GC1 by endogenous GCAPs. The activity unit is nmol cGMP·mg$^{-1}$·min$^{-1}$ rhodopsin. The filled circles indicate data obtained in the presence of GCAPs and the open circles indicate data obtained in the absence of GCAPs. These data were averaged from at least three experiments. In box, $K_m$ corresponds to $IC_{50}$ of $Ca^{2+}$-dependent ROS-GC1 activity, $V_{max}$ is the maximal activity, and $n$ is the Hill cooperativity in the text.

**The general description for the figures of activities of ROS-GC1:** These data were averaged from at least three experiments. The activity unit is nmol cGMP·mg$^{-1}$·min$^{-1}$ rhodopsin. The data were fitted by the Hill equation; $V/V_{max} = [protein]^n/([protein]^n + K_{1/2}^n)$ or the modified Hill equation; $V/V_{max} = (Z \times [Ca^{2+}]^n)/([Ca^{2+}]^n + K_m^n) + 1$; $V$ is the activity of ROS-GC1, $V_{max}$ is the maximal activity of ROS-GC1, $n$ is the Hill cooperativity, $Z$ is a constant taking into account that ROS-GC1 activity is not zero at high free [$Ca^{2+}$], $K_{1/2}$ corresponds to $EC_{50}$ of ROS-GC1 activity upon the concentration of proteins, and $K_m$ corresponds to $IC_{50}$ of $Ca^{2+}$-dependent ROS-GC1 activity.

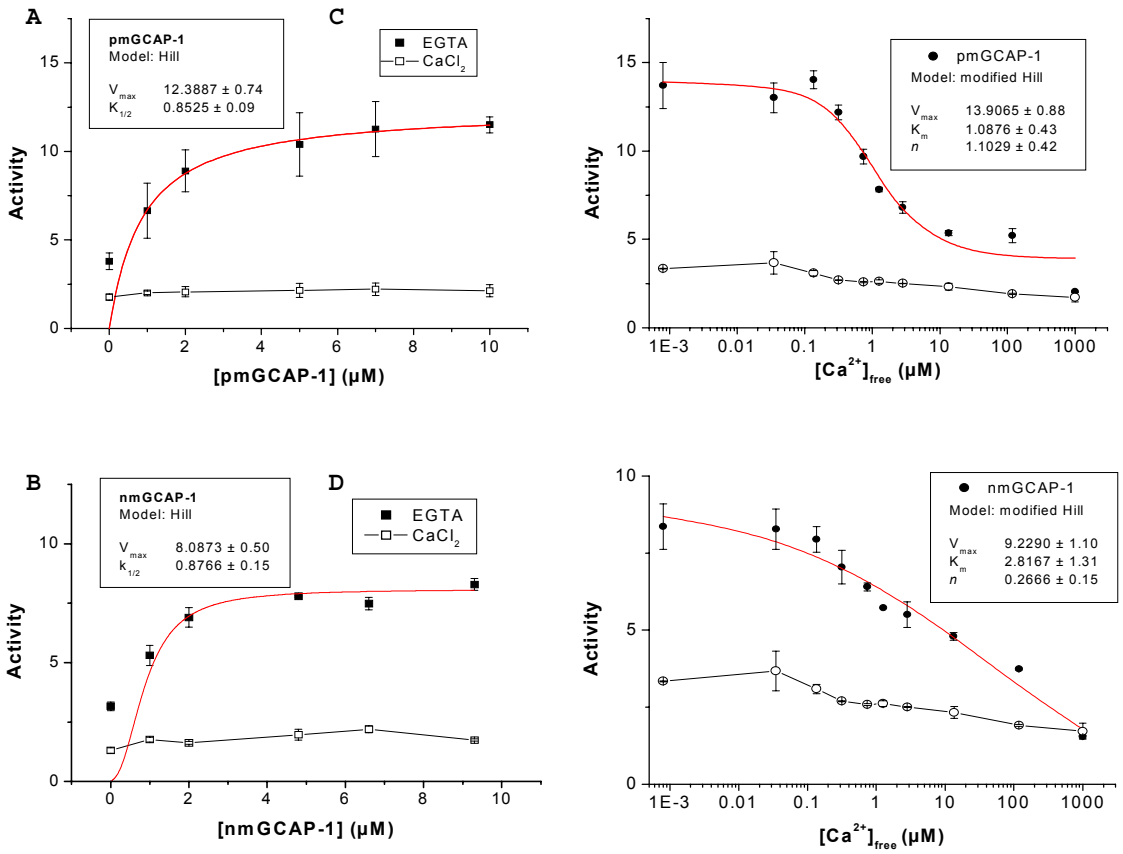


**FIG. 3.6.** Stimulation of ROS-GC1 by pmGCAP-1 and nmGCAP-1. Activities of ROS-GC1 ***A.*** as a function of pmGCAP-1 concentration and ***B.*** as a function of nmGCAP-1 concentration. Activities of ROS-GC1 ***C.*** by pmGCAP-1 and ***D.*** by nmGCAP-1 as a function of free [$Ca^{2+}$]. In figure *A* and *B*, the filled squares indicate data obtained in the presence of 2 mM EGTA and the open squares indicate data obtained with 2 mM $CaCl_2$. In *C* and *D*, the filled circles indicate data obtained with 10 μM GCAP-1 and the open circles indicate data obtained without protein.

### 3.2.3 $Ca^{2+}$-dependent Conformational Changes Measured by Circular Dichroism (CD) Spectroscopy

The secondary structure of GCAP-1 was evaluated by CD spectroscopy in order to investigate $Ca^{2+}$-dependent conformational changes and whether the myristoylation has an effect on these changes (refer to Methods 2.5.1). These measurements were performed by Dr. J. Grötzinger (Institute of Biochemistry, RWTH Klinikum Aachen). CD spectra of nmGCAP-1 and mD$^{6}$S-GCAP-1 revealed aspects of conformational changes upon $Ca^{2+}$-binding, shown in Figs. 3.7–3.9. The spectra of both proteins exhibited ellipticity minima at 222 and 208 nm and an ellipticity maximum at 195 nm. These far-UV CD profiles are typical for α-helical secondary structure.

Figure 3.7 *A* and *C* present the UV-CD spectra of nmGCAP-1 for $Ca^{2+}$-free and $Ca^{2+}$-bound forms. The near-UV spectra illustrate that the $Ca^{2+}$-free form of nmGCAP-1 is more exposed to the solvent with Tyr at $[\Theta]_{275}$ and Trp at $[\Theta]_{275}$ than the $Ca^{2+}$-bound one (Fig. 3.7 *A*). When the far-UV spectrum of the $Ca^{2+}$-bound form was compared with that of the $Ca^{2+}$-free, 8–10% increase in $[\Theta]_{222}$ and 10–15% increase in $[\Theta]_{208}$ were observed (Fig. 3.7 *C*). However, the shapes of $Ca^{2+}$-bound and $Ca^{2+}$-free spectra were virtually indistinguishable from each other. The amplitudes are different, showing characteristics of folded α-helical conformation. Analysis of the averaged UV-CD spectrum revealed an α?helical content of 42% in the presence of $Ca^{2+}$ and 38% in the absence of $Ca^{2+}$, using the method of Provencher and Glöckner [117].

In contrast, figure 3.7 *B* and *D* show different conformational aspects between $Ca^{2+}$-bound and $Ca^{2+}$-free conformation of myristoylated GCAP-1, mD$^{6}$S-GCAP-1. There is a slight change in the near-UV spectra that could be attributed to the conformational change depending on $Ca^{2+}$-binding. In the presence of $Ca^{2+}$ mD$^{6}$S-GCAP-1 has more positive ellipticity at ~275 nm and ~286 nm than in the absence of $Ca^{2+}$ (Fig. 3.7 *B*). The far-UV spectra of mD$^{6}$S-GCAP-1 were also typical of a largely α-helical protein with minima at ~222 nm and ~208 nm. In the presence of $Ca^{2+}$, the spectrum of mD$^{6}$S-GCAP-1 indicated a lower degree of helicity than in the absence of $Ca^{2+}$ (Fig. 3.7 *D*). This is the opposite result to that obtained with nmGCAP-1. The loss of CD intensity and the decrease of α-helical content for the $Ca^{2+}$-free form of nmGCAP-1 and the $Ca^{2+}$-bound form of mD$^{6}$S-GCAP-1 suggest that the α-helical secondary structure reduces upon the release of $Ca^{2+}$ for nonmyristoylated GCAP-1, while myristoylated GCAP-1 without $Ca^{2+}$ has more α-helical fixed conformation.

In summary, the UV-CD spectra illustrates that the α-helical content in GCAP-1 increases in the following order; nmGCAP-1 without $Ca^{2+}$ < mD$^{6}$S-GCAP-1 with $Ca^{2+}$ < nmGCAP-1 with $Ca^{2+}$ < mD$^{6}$S-GCAP-1 without $Ca^{2+}$.

Measurement of the ellipticity at 215 nm as a function of temperature indicates that the unfolding profiles were different between $Ca^{2+}$-free form and $Ca^{2+}$-bound form of GCAP-1. Figures 3.8 and 3.9 show the far-UV CD spectra measured at 25°C and at ~95°C after increasing the temperature: nmGCAP-1 with $Ca^{2+}$ (Fig. 3.8 *A* and *C*), nmGCAP-1 without $Ca^{2+}$ (Fig. 3.8 *B* and *D*), mD$^{6}$S-GCAP-1 with $Ca^{2+}$ (Fig. 3.9 *A* and *C*), and mD$^{6}$S-GCAP-1 without $Ca^{2+}$ (Fig. 3.9 *B* and *D*).

The change in ellipticity of nmGCAP-1 with $Ca^{2+}$ at 215 nm with temperature indicated that the helicity was decreased with increase in temperature from 25°C to 94°C, estimated by a difference of 10–15% in $[\Theta]_{215}$. The shape of CD spectrum of nmGCAP-1 with $Ca^{2+}$ at 94°C was similar to that at 25°C (Fig. 3.8 *C*). However, in the absence of $Ca^{2+}$ the change in ellipticity at 215 nm takes place in two-state melting of the secondary structure at ~44°C (Fig. 3.8 *B*). The CD spectra of nmGCAP-1 without $Ca^{2+}$ at 97°C showed the loss of α-helicity (Fig. 3.8 *D*). Similar to nonmyristoylated GCAP-1, mD$^{6}$S-GCAP-1 showed a different change in ellipticity at 215 nm as a function of temperature in the presence and absence of $Ca^{2+}$. The temperature-dependent UV-CD at 215 nm of mD$^{6}$S-GCAP-1 with $Ca^{2+}$ showed a higher single transition temperature ($T_m$ ~ over 95°C) (Fig. 3.9 *A*). The CD spectrum had a slight difference of the helicity (about 5% increase) between 25°C and 97°C (Fig. 3.9 *C*). However $T_m$-value shifted to ~40°C in the absence of $Ca^{2+}$ which is slightly lower than in the case of nmGCAP-1 (Fig. 3.9 *B*). $Ca^{2+}$-free mD$^{6}$S-GCAP-1 at 94°C showed an apparently different CD spectrum than at 25°C (Fig. 3.9 *D*), which indicated that mD$^{6}$S-GCAP-1 without $Ca^{2+}$ lost its helicity at 94°C and unfolded as a result of increasing the temperature.

Temperature affected the conformation of GCAP-1 with respect to the presence or absence of $Ca^{2+}$. The presence or absence of the myristoyl group had only slight effects. These data, obtained by varying the temperature, suggest that the conformation of GCAP-1 is stable through stepwise increase of the temperature from 25°C to ~95°C, and GCAP-1 is heat-resistant with $Ca^{2+}$-bound, but loses α-helicity upon increase of temperature above 45°C in the $Ca^{2+}$-free form. It indicates that α-helices of GCAP-1 are stabilized by $Ca^{2+}$-binding, i.e. $Ca^{2+}$-bound GCAP-1 is the most thermally stable form.

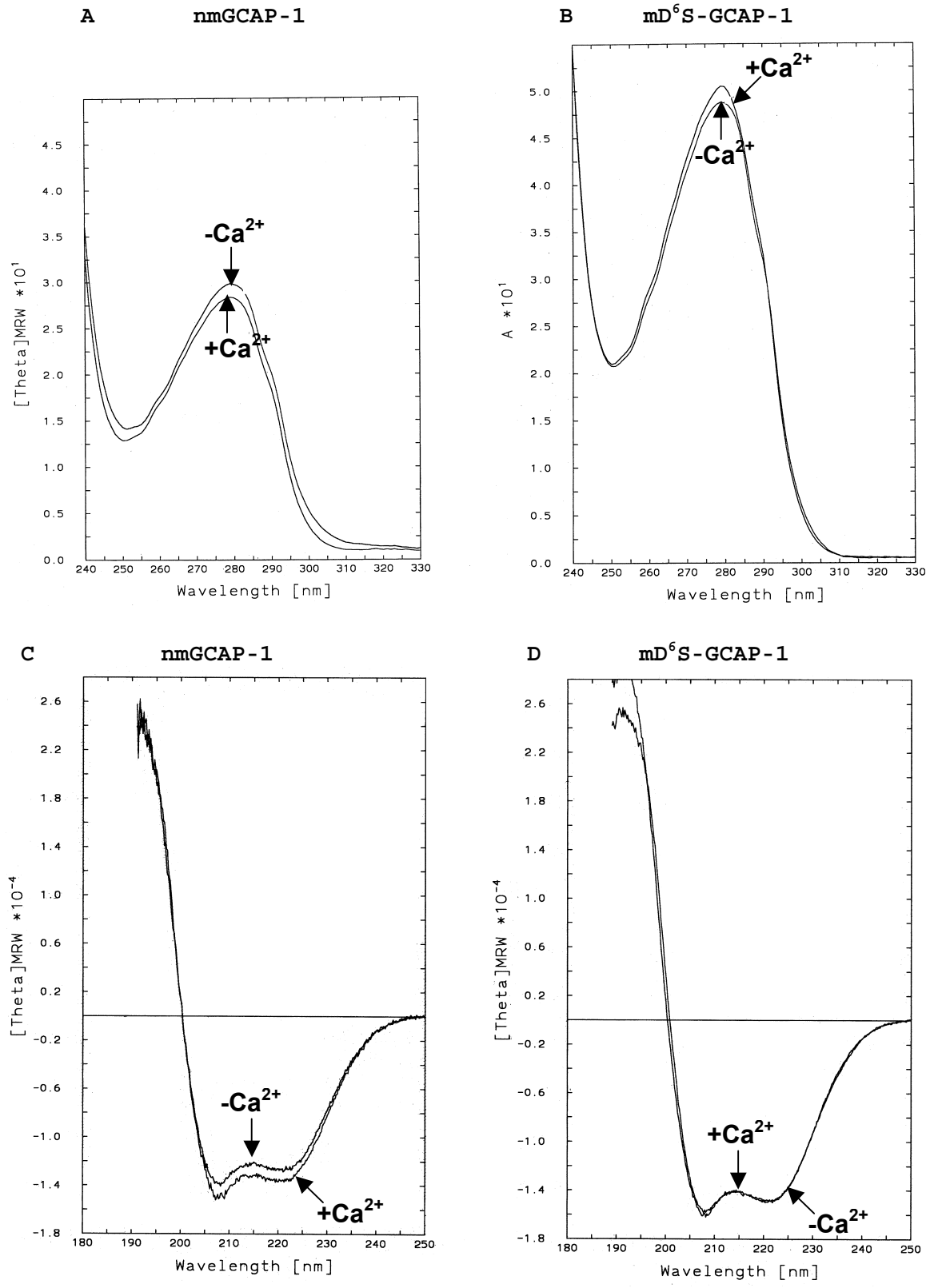


**FIG. 3.7.** The UV-CD spectra of nmGCAP-1 and mD$^6$S-GCAP-1. ***A.*** The near-UV CD spectra of nmGCAP-1 with 5 mM $CaCl_2$ and with 2 mM EGTA. ***B.*** The near-UV CD spectra of mD$^6$S-GCAP-1 with 5 mM $CaCl_2$ and with 2 mM EGTA. ***C.*** The far-UV CD spectra of nmGCAP-1 with 5 mM $CaCl_2$ and with 2 mM EGTA. ***D.*** The far-UV CD spectra of mD$^6$S-GCAP-1 1 with 5 mM $CaCl_2$ and with 2 mM EGTA.

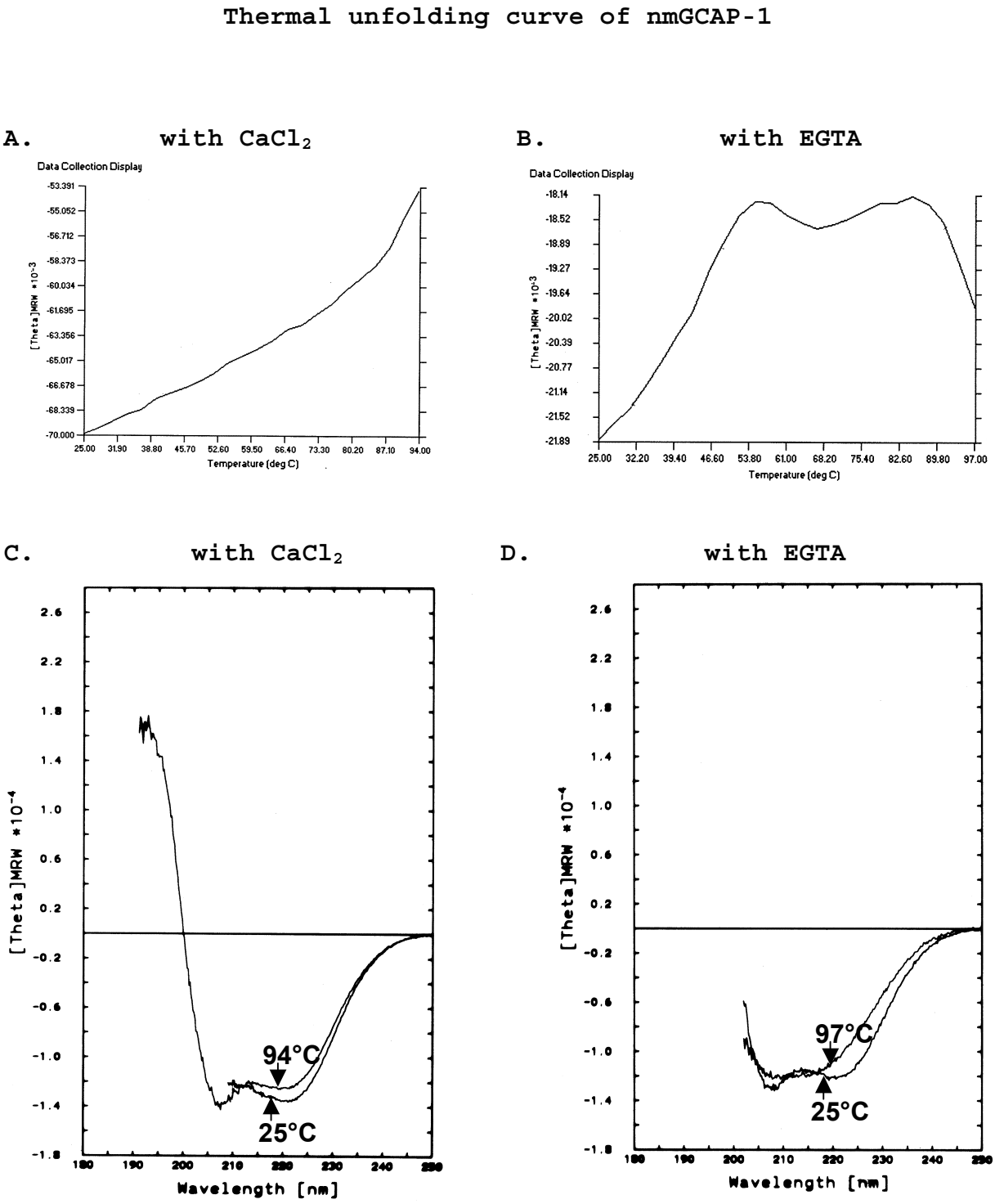


**FIG. 3.8.** Thermal sensitivity of nmGCAP-1 conformation (***A***) with $CaCl_2$ and (***B***) with EGTA changes in the ellipticity of nmGCAP-1 at 215 nm. The path length is 10 mm. The UV-CD spectra of nmGCAP-1 at 25°C and at 95°C (***C***) with $CaCl_2$ (***D***) with EGTA. The concentration of nmGCAP-1 is 15 μM. The path length is 1 mm.

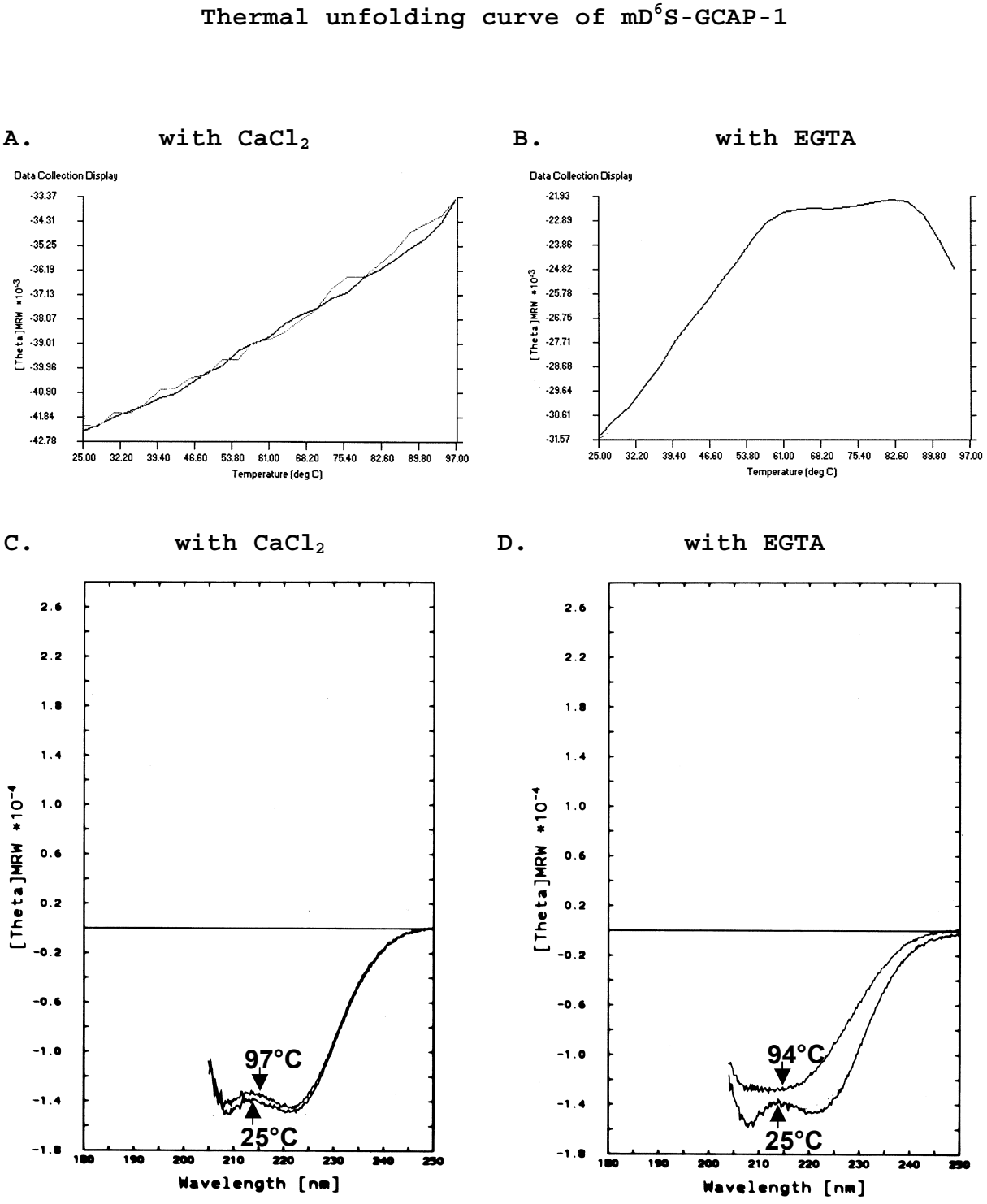


**FIG. 3.9.** Thermal sensitivity of mD$^6$S GCAP-1 conformation (***A***) with $CaCl_2$ and (***B***) with EGTA changes in the ellipticity of mD$^6$S GCAP-1 at 215 nm. The path length is 10 mm. The UV-CD spectra of nmGCAP-1 at 25°C and at 95°C (***C***) with $CaCl_2$ (***D***) with EGTA. The concentration of mD$^6$S GCAP-1 is 11 μM. The path length is 1 mm.

### 3.2.4 $Ca^{2+}$-dependent Gel-shifts of nmGCAP-1

One peculiar feature of calcium binding proteins, such as calmodulin, recoverin, and GCAPs, is a $Ca^{2+}$-dependent mobility shift during gel electrophoresis [73,118,119].

The purified recombinant wild-type GCAP-1 exhibited the typical $Ca^{2+}$-dependent mobility shift of the apparent molecular mass on SDS-PAGE (Fig. 3.10). The two forms of GCAP-1, $Ca^{2+}$-bound and $Ca^{2+}$-free, can be easily distinguished by their different electrophoretic mobilities. The $Ca^{2+}$-free form of GCAP-1 migrated at a higher molecular weight than the $Ca^{2+}$-bound form. Complexing $Ca^{2+}$ with 2 mM EGTA in GCAP-1 solution caused a gel shift from approx. 21 kDa to approx. 26 kDa (Fig. 3.10 and Table 3.5).

The SDS-PAGE separates proteins based primarily on their molecular weights under denaturing conditions. The anomalous electrophoretic mobility observed in the Laemmli sample buffer after 10-min boiling and in the presence of SDS, i.e. under protein denaturation conditions, indicates that GCAP-1 is able to interact with calcium in the presence of SDS and that the interaction is stable to boiling. GCAP-1 seems to be a heat-stable (or heat-resistant) protein, with calcium stabilizing its compact structure. A second band in addition to the GCAP-1 band was observed on the SDS-PAGE gels, indicated in Fig. 3.10 *A*, by the dotted arrows. This band showed the same calcium-dependent gel shift on SDS-PAGE as the GCAP-1 band at 21 kDa. Therefore, this band could be a GCAP-1 form of slightly slower electrophoretic mobility. I tested the identity of this band by Western blotting using an anti-GCAP-1 antibody (Fig. 3.11). The experiment showed that this band, slightly above GCAP-1, (Fig. 3.11, indicated by the arrow at **b**) is also GCAP-1. Interestingly, the antibody reacted also with a band of approx. 40 kDa, which would correspond to a dimer of GCAP-1 (Fig. 3.11, with the arrow at **c**).

**TABLE 3.5** The calculated molecular weights of GCAP-1 from the calibration of SDS-PAGE

| Proteins | M.W. (Da) | $R_f$ |
|---|---|---|
| Phosphorylase b | 97400 | 0.10 |
| Bovine serum albumin | 66000 | 0.16 |
| Ovalbumin | 45000 | 0.25 |
| Carbonic anhydrase | 29000 | 0.41 |
| Soybean trypsin inhibitor | 20100 | 0.55 |
| α-Lactalbumin | 14200 | 0.76 |
| ***GCAP-1 ( - $Ca^{2+}$)*** | ***25700*** | ***0.49*** |
| ***GCAP-1 ( + $Ca^{2+}$)*** | ***20900*** | ***0.56*** |

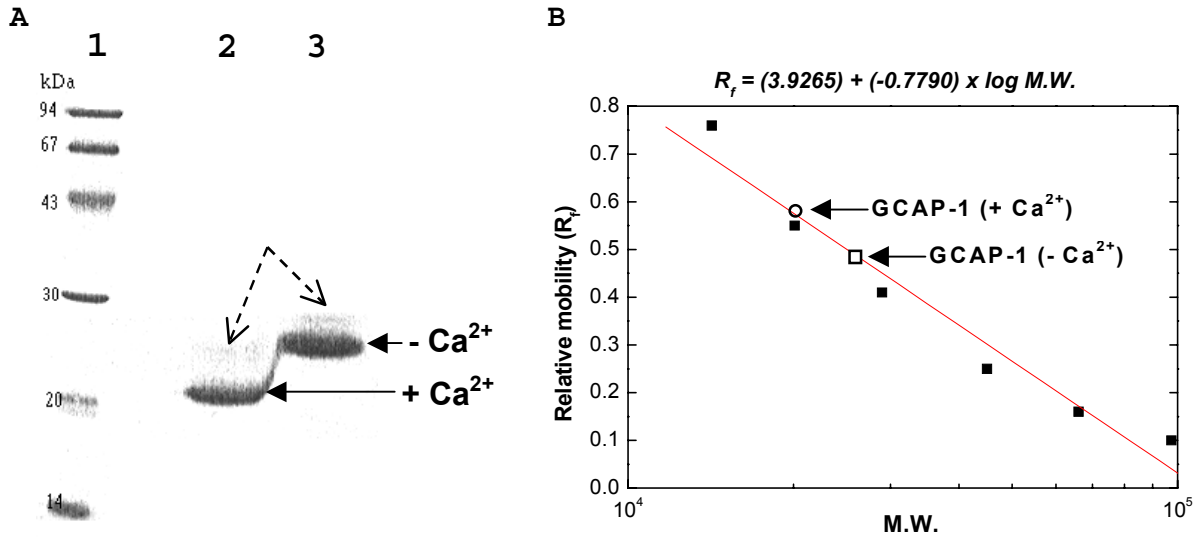


**FIG. 3.10.** The $Ca^{2+}$-dependent mobility gel-shift on SDS-PAGE. ***A.*** SDS–PAGE was performed on a 15% (w/v) polyacrylamide gel and the gel was stained with Commassie Blue: *lane 1*, 5 µg of low molecular mass standard marker; *lane 2,* 5 µg of purified nmGCAP-1 with 1 mM $CaCl_2$; *lane 3,* 5 µg of purified nmGCAP-1 with 2 mM EGTA. ***B.*** The calibration curve of the SDS-PAGE was plotted as the relative mobility ($R_f$) of the molecular weight standards versus the logarithmic functions of their molecular mass (log M.W.). The standards (■) are indicated as the $R_f$-value and corresponding M.W. of GCAP-1 with $Ca^{2+}$ as (○), and without $Ca^{2+}$ as (□).

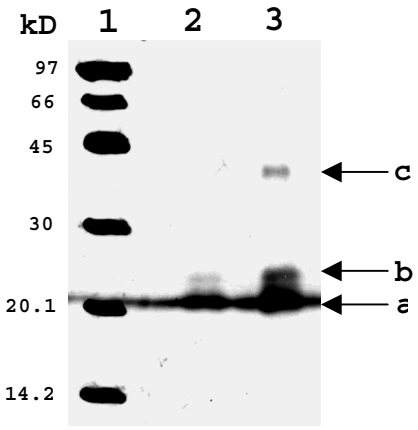


**FIG. 3.11.** Immunoblotting of GCAP-1. The purified GCAP-1 was run on a SDS-PAGE gel and was detected by the anti-GCAP-1 antibody (1:10000) after Western blotting. The blot was exposed on Kodak XAR-2 film for one second: *lane 1,* molecular mass standards drawn from the Commassie stained SDS-PAGE gel; *lane 2,* with 0.1 µg of purified nmGCAP-1; *lane 3,* with 0.5 µg of purified nmGCAP-1. (***a***) a band of ~21 kDa corresponding to GCAP-1, (***b***) diffuse bands, which are detected by the anti-GCAP-1 antibody, and (***c***) a band of ~40 kDa molecular weight, which can also be detected by the anti-GCAP-1 antibody.

### 3.2.5 Dimerization of nmGCAP-1

To investigate the distribution of monomers and dimers of GCAP-1 in the presence and the absence of $Ca^{2+}$ and to test the influence of a reducing agent, DTT or β-mercaptoethanol, ND-PAGE and size exclusion chromatography were performed. The chromatograms and the calibration curves are shown in Figs. 3.13 and 3.14, respectively. The estimated molecular masses of standard proteins and GCAP-1 are calculated and listed in Table 3.6.

In contrast to the results of SDS-PAGE, GCAP-1 showed a different behavior on a ND-PAGE gel. It moved faster with 2 mM EGTA than with 1 mM $CaCl_2$. The $Ca^{2+}$-free form of GCAP-1 migrated as a single band in the presence of β-mercaptoethanol, while in the absence of β-mercaptoethanol, two bands were found (Fig. 3.12).

In the presence of 1 mM $CaCl_2$ a diffuse band appeared. The diffuse staining was less in the absence of β-mercaptoethanol, and a band representing a dimer was clearly visible (Fig. 3.13, *lane 4*). In contrast, in the presence of EGTA a band of monomers was visible and the diffuse staining disappeared (Fig. 3.12, *lane 3*). The expected molecular weights, ~30 kDa and ~50 kDa, are consistent with a monomer and dimer of GCAP-1, respectively. Therefore, I tested dimer formation of GCAP-1 in the presence and absence of $Ca^{2+}$ by size exclusion chromatography.

First, a calibration experiment was used to estimate the molecular weight. Each calibration point is the result of two independent measurements in the same buffer containing 20 mM Tris, pH 8.0, 150 mM NaCl. $K_{av}$ values were plotted as a logarithmic function of molecular mass standard (log $M_r$) in Fig. 3.14 *A*. From this calibration curve the molecular weight of GCAP-1 was calculated according to its observed partition coefficient, $K_{av}$; $K_{av} = (2.0265) + (-0.3955) \times \log M_r$.

In the presence of 2 mM DTT, freshly prepared GCAP-1 was eluted from a main peak, corresponding to an estimated molecular mass of ~36 kDa, in the presence of 2 mM EGTA (Fig. 3.13 *B*), and ~66 kDa in the presence of $CaCl_2$ (Fig. 3.13 *C*). The peak at 10.8 ml (36 kDa) corresponded to a monomer and the peak at 9.1 ml (66 kDa) to a dimer.

To evaluate GCAP-1 after lyophilization, equivalent experiments have been done with this preparation. In the presence of 2 mM DTT, lyophilized protein eluted in a peak that corresponded to its monomer. However, in the absence of 2 mM DTT, it eluted in several

peaks (Fig. 3.13 *F* and *G*). A similar phenomenon was observed with $Ca^{2+}$-bound GCAP-1 (Fig. 3.13 *E*).

These results suggests that GCAP-1 exists predominantly in monomeric form in the absence of $CaCl_2$ and as a dimer in the presence of $CaCl_2$. Necessary for further investigation of this monomer/dimer equilibrium was the use of a fresh preparation with a reducing agent. Different results were obtained when lyophilized sample was used. In this case, the main portion of GCAP-1 eluted as a monomer when DTT was present. However, in the presence of $CaCl_2$, a dimer and multimers (aggregates) of higher molecular weights were detected (Fig. 3.13 *E*, see elution volume 7–10 ml). In the absence of DTT, formation of GCAP-1 dimers and aggregates increased. This effect was more pronounced in the presence of $CaCl_2$ (Fig. 3.13 *G*) than in the absence of $CaCl_2$ (Fig. 3.13 *F*).

Figure 3.14 *B* shows the calibration to estimate the Stokes' radius, the hydrodynamic radius [120]. The calculated values of $(-\log K_{av})^{1/2}$ were plotted as a function of Stokes' radius. From this calibration curve the Stokes' radius of GCAP-1 was calculated, $(-\log K_{av})^{1/2} = (0.3874) + (0.0158) \times (\text{Stokes' radius})$. The $Ca^{2+}$-free GCAP-1 eluted from the column with a Stokes' radius of ~27 Å and the $Ca^{2+}$-bound GCAP-1 eluted as a protein with a Stokes' radius of ~36 Å.

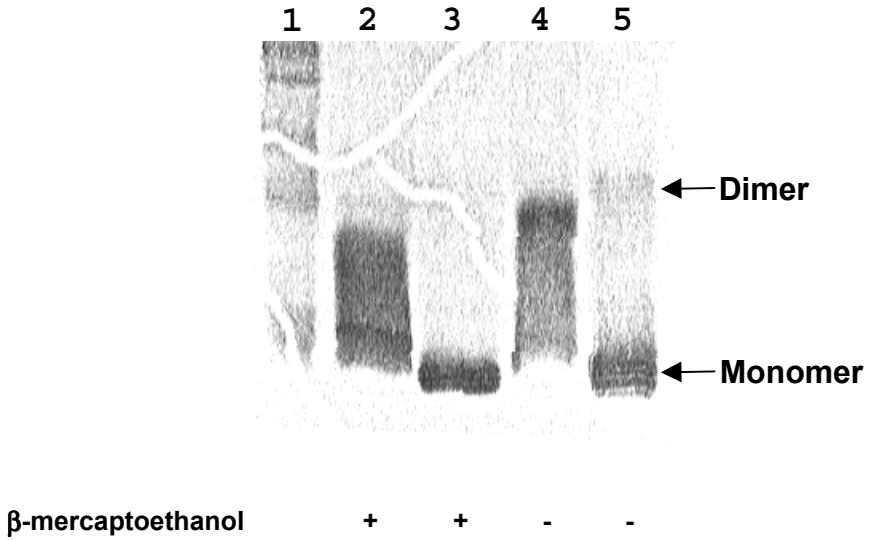


**FIG. 3.12.** Mobility of purified GCAP-1 on ND-PAGE. Samples (~10 μg) were run on 8% ND PAGE and proteins were visualized by Commassie staining. *Lane 1,* marker; *lane 2,* in the presence of 1 mM β-mercaptoethanol with 1 mM $CaCl_2$; *lane 3,* in the presence of 1 mM β-mercaptoethanol with 2 mM EGTA; *lane 4,* in the absence of 1 mM β-mercaptoethanol with 1 mM $CaCl_2$; and *lane 5,* in the absence of 1 mM β-mercaptoethanol with 2 mM EGTA.

**TABLE 3.6** The calculated partition coefficient and Stokes' radius of GCAP-1 from the calibration by the size exclusion chromatography

| **Standards** | **$M_r$ (Da)** [a] | **Elution volume (ml)** | **$K_{av}$** [b] | **$(-\log K_{av})^{1/2}$** | **Stokes' radius (Å)** [c] |
|---|---|---|---|---|---|
| Thyroglobulin | 669000 | 7.45 | 0.03 | 1.25 | 85.0 |
| BSA | 67000 | 9.05 | 0.12 | 0.96 | 35.5 |
| Ovalbumin | 43000 | 10.13 | 0.18 | 0.86 | 30.5 |
| Chymotrypsinogen | 25000 | 12.16 | 0.30 | 0.72 | 20.9 |
| Ribonuclease A | 13700 | 13.44 | 0.38 | 0.65 | 16.4 |
| Aprotinin | 6500 | 15.87 | 0.52 | 0.53 | - |
| ***GCAP-1 (as a dimer)*** | ***66000*** | ***9.10*** | ***0.12*** | ***0.95*** | ***35.8*** |
| ***GCAP-1 (as a monomer)*** | ***36000*** | ***10.80*** | ***0.22*** | ***0.81*** | ***26.5*** |

a. The standard from pharmania

b. $K_{av} = (V_x - V_o)/(V_t - V_o)$, where $V_o$ is the void volume, $V_t$ the total volume of the gel bed, and $V_x$ the elution volume of the protein.

c. See Reference 120.

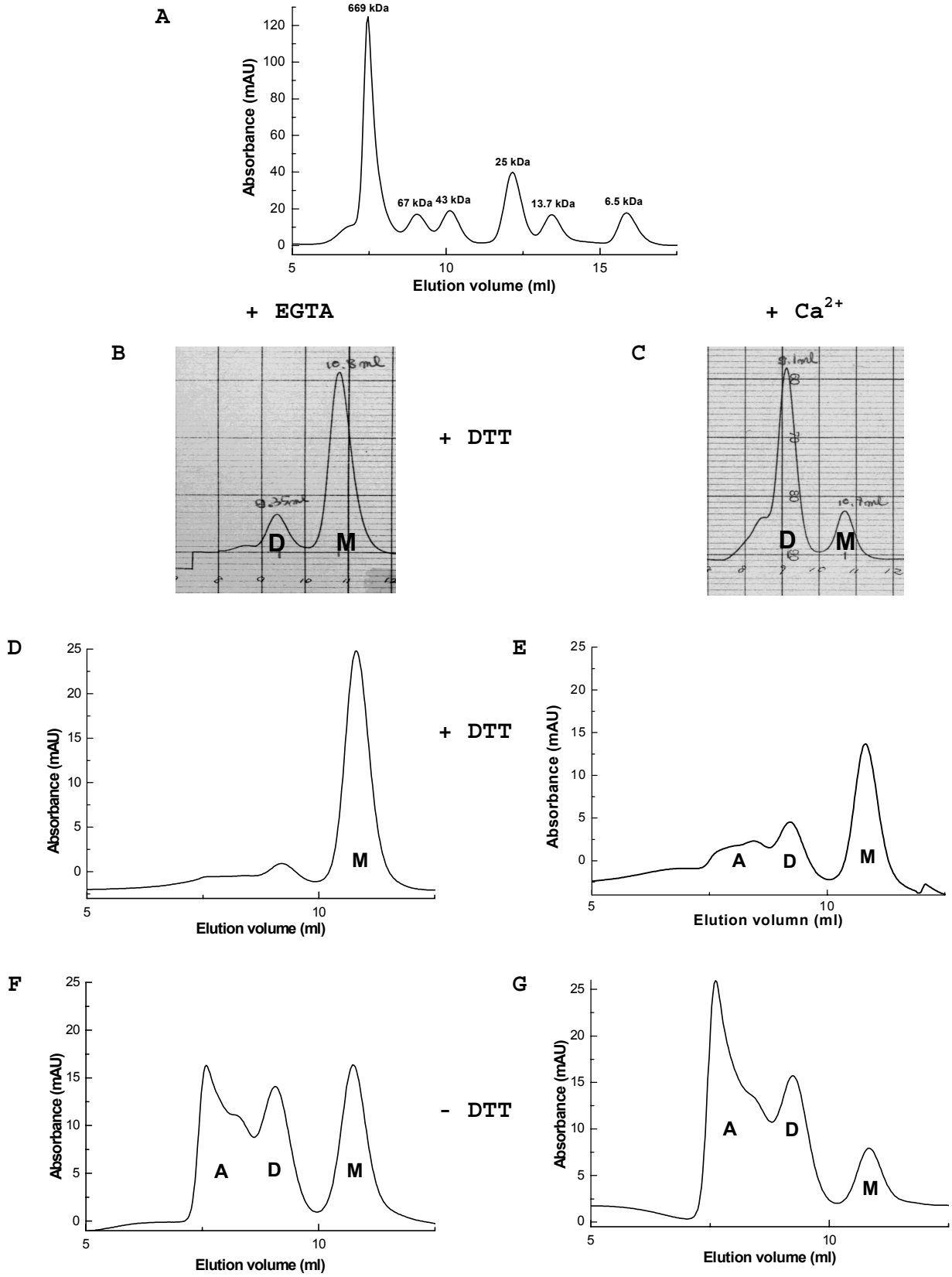


**FIG. 3.13.** The estimation of the molecular weights of GCAP-1 by size exclusion chromatography on Superdex 75 10/30. ***A.*** Standards (~1 mg of mixture) with 669 kDa thyroglobulin at 7.45 ml, 67 kDa of BSA at 9.05 ml, 43 kDa of ovalbumin at 10.13 ml, 25 kDa of chymotrysinogen at 12.16 ml, 13.7 kDa of RNase A at

13.44 ml, and 6.5 kDa of aprotinin at 15.87 ml. In the presence of 2 mM DTT, freshly purified GCAP-1 (50 µg) eluted ***B.*** at 10.8 ml with 2.5 mM EGTA and ***C.*** at 9.1 ml with 2 mM $CaCl_2$. In the presence of 2 mM DTT, lyophilized purified GCAP-1 (50 µg) eluted ***D.*** at 10.8 ml with 2.5 mM EGTA and ***E.*** with 2 mM $CaCl_2$. In the absence of 2 mM DTT, lyophilized purified GCAP-1 (50 µg) eluted ***F.*** with 2.5 mM EGTA and ***G.*** with 2 mM $CaCl_2$. In the figures, M or signifies the monomer, D the dimer, and A aggregates or multimers.

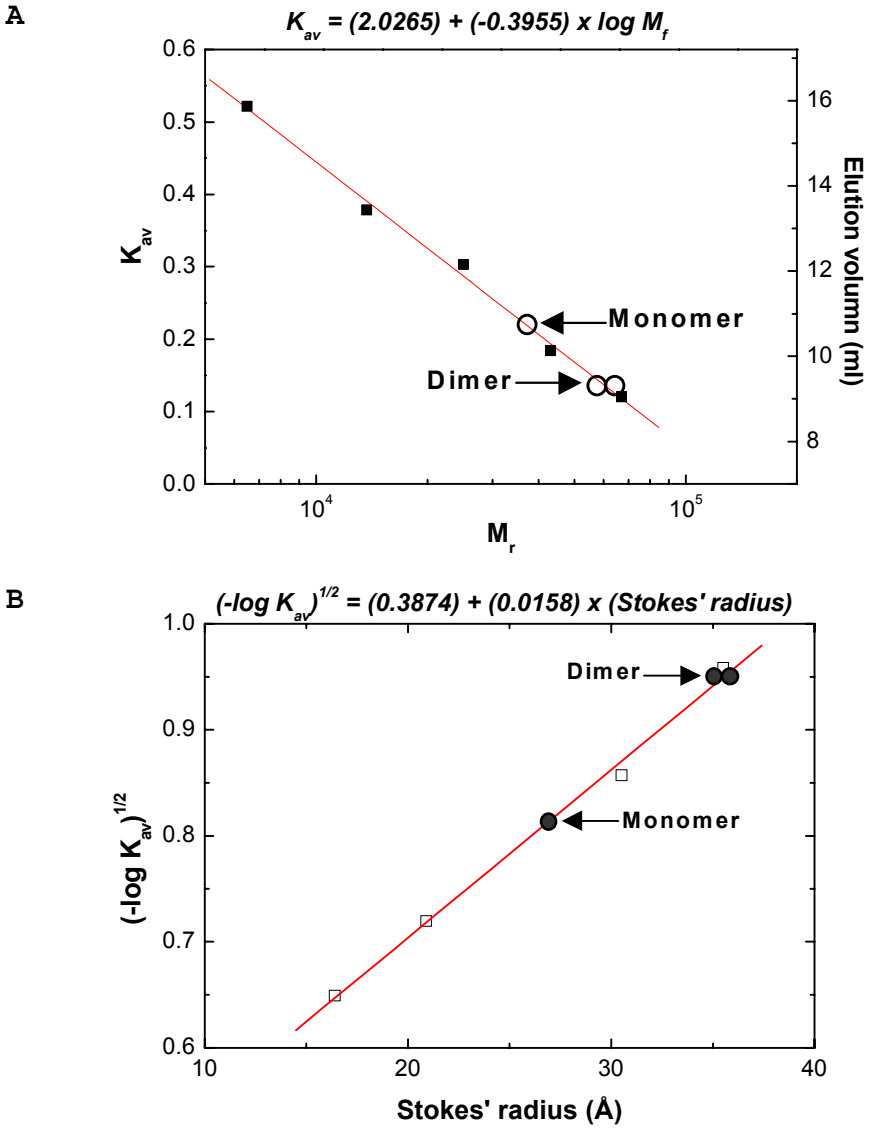


**FIG. 3.14.** The calibration curve of the standards by size exclusion chromatography on Superdex 75 10/30. ***A.*** The calibration curve of $K_{av}$ versus $M_r$ of standard proteins: (■), the $K_{av}$-value and corresponding relative molecular weight ($M_r$). of GCAP-1 without $Ca^{2+}$(○) as a monomer and with $Ca^{2+}$ (○○) as a dimer. ***B.*** The calibration curve $(-log\ K_{av})^{1/2}$ versus Stokes' radius of standard proteins. The standards (□) and the calculated $(-log\ K_{av})^{1/2}$-value corresponding to the Stokes' radius of GCAP-1 without $Ca^{2+}$(●) as a monomer and with $Ca^{2+}$ (●●) as a dimer.

### 3.2.6 Determination of Disulfide Bonds of nmGCAP-1 by Iodoacetate Derivatives

The numbers of disulfide bonds in a protein can be determined by the following strategy. Proteins with different numbers of cleaved disulfide bonds are alkylated with iodoacetamide (IAM) or iodoacetic acid (IAA) as the first step. The remaining disulfide bonds are reduced by DTT, and the resulting free sulfhydryl groups are alkylated with IAA or IAM as the second step [99] (refer to Methods 2.1.4.1 and Fig. 2.3 *A*).

After this treatment, the total numbers of disulfide bonds in a protein are determined by acid-urea non-denaturing PAGE, in which proteins are separated into distinct bands depending on the number of disulfide bonds cleaved [121]. Carboxymethylation with IAA induces new acidic group at each free cysteine residue, making the charge of the molecule more negative, however IAM reacts with SH groups to give a neutral moiety [100]. The usage of both blocking groups ensures that intermediates with different hydrodynamic radii or numbers of disulfides bonds can be distinguished [122].

To determine how many IAA molecules react with partially reduced GCAP-1, each sample was incubated with different concentrations of DTT (ranging from 1–10 mM) and alkylated in the first step with IAM and then in the second step with IAA. For 10 mM DTT, an additional experiment has been done in which the sample was first alkylated with IAA and then subsequently with IAM.

In these experiments, no significantly different mobilities were visible under various concentrations of the reducing agent (Fig. 3.15, *lanes 2–8*). To confirm the slight shifts on the gel (on *lanes 6–8*), all reactions were mixed and then loaded on the gel. The mixture of the sample of nmGCAP-1 had only one band (Fig. 3.15, *lane 10*), which corresponded to the number of the introduced IAA molecules. This result showed that nmGCAP-1 has no intramolecular disulfide bonds.

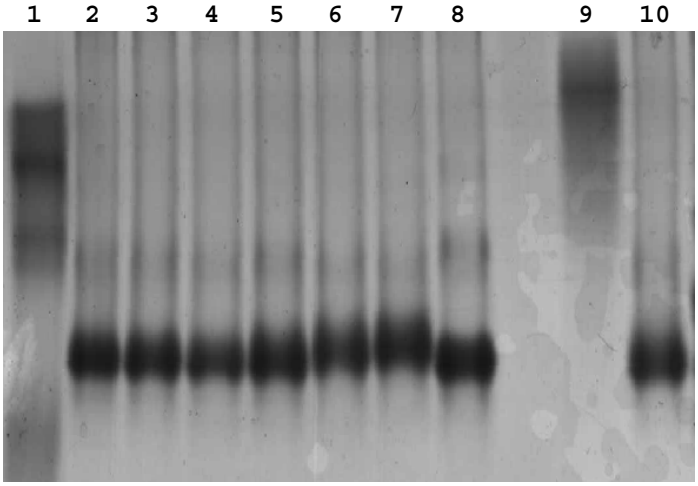


**FIG. 3.15.** Counting the disulfide bonds of nmGCAP-1 as a function of DTT on ND-PAGE. *Lanes 1* and *9*, marker; *lanes 2–7*, two alkylation steps with IAM and then IAA; *lane 2*, with 0 μM DTT ; *lane 3*, with 50 μM DTT; *lane 4*, with 100 μM DTT; *lane 5*, with 200 μM DTT; *lane 6*, with 500 μM DTT; *lane 7*, with 10 mM DTT; *lane 8*, with 10 mM DTT (two alkylation steps with IAA and then IAM); and *lane 10*, the mixture of all reactions.

### 3.2.7 Monitoring the Exposition of Thiol Groups of GCAP-1

The cysteine residues in GCAP-1 were titrated by 5,5´-dithio-bis-(2-nitrobenzoic acid) (DTNB) in either the presence or absence of $Ca^{2+}$. The reaction of DTNB with GCAP-1 caused a time-dependent labeling by 5-thio-2 nitrobenzoic acid (TNB) (see Fig. 2.4 *B*). The rate of covalent modification of free sulfhydryl groups with DTNB solution was dependent on the relative accessibility and the chemical environment of the cysteines. From the standard curve of thiol-reactivity, the number of reactive cysteines can be calculated (refer to Methods 2.4.4.2). A thiol solution of 5 µM has an absorbance of 0.08 at 412 nm. The reaction of GCAP-1 with DTNB as a function of time is illustrated in Fig. 3.16 and summarized in Table 3.7.

The absorbance at 412 nm ($A_{412}$) of 5 µM nmGCAP-1 with $CaCl_2$ is 0.205. This absorbance corresponds to 15 µM thiol group or free cysteine, i.e. 3 cysteine in nmGCAP-1. After 300 sec, injection of EGTA caused an additional increase in $A_{412}$ of 0.074, which corresponds to 5.4 µM of free thiol or one cysteine (Fig. 3.16 *A*). When the injection of $CaCl_2$ and EGTA was reversed, the change in $A_{412}$ was 0.290 with EGTA and after 300 sec, injection of $CaCl_2$ caused no change (Fig. 3.16 *B*). These data demonstrated that in the presence of $CaCl_2$, three cysteines are exposed to the solvent and one cysteine remains buried in nmGCAP-1. An additional reaction in the absence of calcium (with 2 mM EGTA) exposes the buried cysteine to the solvent. In contrast, when nmGCAP-1 first reacted with EGTA, all four cysteines were exposed and were already readily accessible to DTNB.

The difference in cysteine reactivity between nmGCAP-1 and pmGCAP-1 with DTNB in slight; 2.7 cysteines have reacted in the presence of $CaCl_2$ and then the remaining cysteine was exposed after additional injection with EGTA (Fig. 3.16 *C*). The reverse injection of EGTA and $CaCl_2$ showed that 3.6 cysteines of pmGCAP-1 were quickly exposed with EGTA and afterwards pmGCAP-1 had no more reactivity with injection of $CaCl_2$ (Fig. 3.16 *D*).

However, the reactivity of fully myristoylated GCAP-1 (m$D^6$S-GCAP-1) towards DTNB was different than that of nmGCAP-1. Figure 3.16 *E* showed that two of the four cysteine residues in m$D^6$S-GCAP-1 reacted with DTNB in the presence of $Ca^{2+}$. When EGTA was injected after 300 sec, one cysteine reacted with DTNB while the other cysteine still remained buried. The reactivity of exposed cysteines with DTNB in the absence of $Ca^{2+}$ is

shown in Fig. 3.16 *F*, which indicates that three of the four cysteines in mD$^{6}$S-GCAP-1 reacted. The presence of a myristoyl group in GCAP-1 apparently has a shielding effect, burying one cysteine of GCAP-1.

**TABLE 3.7** Summary of cysteine reactivities of nmGCAP-1, pmGCAP-1, and mD$^{6}$S-GCAP-1

| Type | Treatment | Time (sec) | $A_{412}$ | [-SH] (μM) | No. of –SH (mole/protein) |
|---|---|---|---|---|---|
| nmGCAP-1 * | $CaCl_2$ | 300 | 0.205 | 15.0 | 3 |
| | EGTA | 600 | + 0.074 | 5.4 | 1.1 |
| | EGTA | 300 | 0.290 | 21.0 | 4.2 |
| | $CaCl_2$ | 600 | + 0.017 | 1.3 | - |
| pmGCAP-1 * | $CaCl_2$ | 300 | 0.187 | 13.8 | 2.7 |
| | EGTA | 600 | + 0.074 | 5.4 | 1 |
| | EGTA | 300 | 0.180 | 19.2 | 3.8 |
| | $CaCl_2$ | 600 | + 0.005 | - | - |
| mD$^{6}$S-GCAP-1 * | $CaCl_2$ | 300 | 0.124 | 9.1 | 2 |
| | EGTA | 600 | + 0.058 | 4.3 | 1 |
| | EGTA | 300 | 0.186 | 18.2 | 3 |
| | $CaCl_2$ | 600 | + 0.001 | - | - |

* In these experiments, the protein concentration of nmGCAP-1, pmGCAP-1, and mD$^{6}$S-GCAP-1 were 5 μM, 5 μM, and 4.5 μM, respectively.

**The general description for the figures of cysteine reactivity of GCAP-1 towards DTNB:** The cysteine reactivity is able to determine the free thiol groups of proteins stoichiometrically (Fig. 2.4 B). A thiol group reacts with one molecule of DTNB in solution and generates one molecule of TNB anion which can be measured by the absorbance at 412 nm. Figure 2.5 B demonstrates the standard curve of thiol reactivity*;* $A_{412} = (0.0152) + (0.0138) \times [thiol](\mu M)$, for example, absorbance of 0.08 at 412 nm corresponds to 5 μM thiol group. Reactivity of each protein with DTNB was measured at 412 nm in the presence of $CaCl_2$ for 300 sec and then measured further for 300 sec after injection of EGTA. As the reverse injection of EGTA and $CaCl_2$, the measurement was performed at 412 nm in the presence of EGTA for 300 sec and then measured further for 300 sec after injection of $CaCl_2$. Each injection is indicated with the arrow.

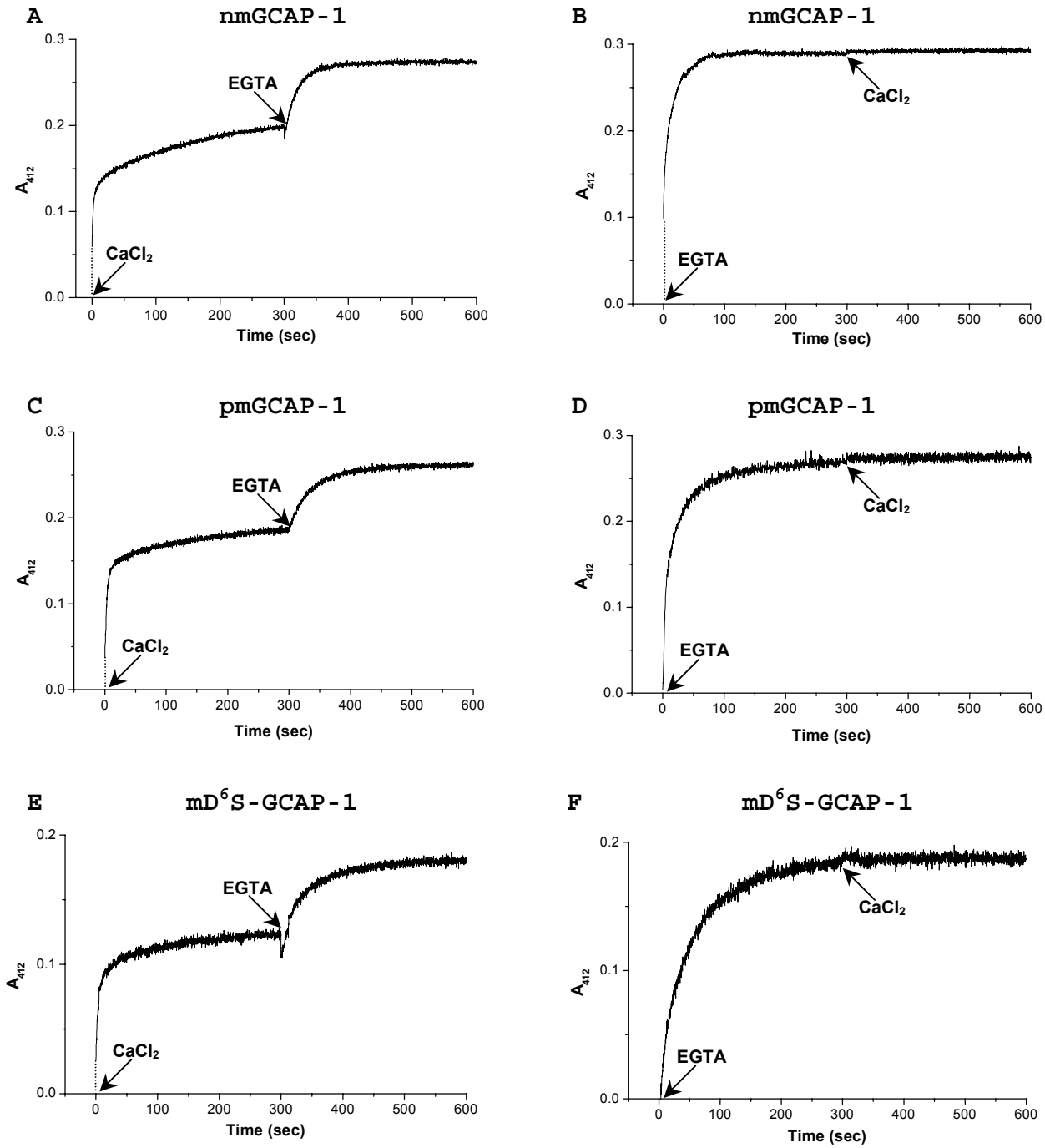


**FIG. 3.16.** Cysteine reactivity of GCAP-1 towards DTNB. The injection of $CaCl_2$ or EGTA is indicated with the arrows. ***A.*** $A_{412}$ of 5 µM nmGCAP-1 is 0.205 in the presence of $Ca^{2+}$ and 0.279 in the absence of $Ca^{2+}$. ***B.*** $A_{412}$ of 5 µM nmGCAP-1 is 0.290 in the absence of $Ca^{2+}$ and dose not change in the presence of $Ca^{2+}$. ***C.*** $A_{412}$ of 5 µM pmGCAP-1 is 0.187 in the presence of $Ca^{2+}$ and 0.074 in the absence of $Ca^{2+}$. ***D.*** $A_{412}$ of 5 µM pmGCAP-1 is 0.180 in the absence of $Ca^{2+}$ and dose not change in the presence of $Ca^{2+}$. ***E.*** $A_{412}$ of 4.5 µM mD$^6$S-GCAP-1 is 0.124 in the presence of $Ca^{2+}$ and 0.182 in the absence of $Ca^{2+}$. ***F.*** $A_{412}$ of 4.5 µM mD$^6$S-GCAP-1 is 0.186 in the absence of $Ca^{2+}$ and dose not change in the presence of $Ca^{2+}$.

## 3.3 Preparation of Cysteine Mutants of GCAP-1

Previously, bovine retinal cDNA of GCAP1 was isolated and cloned into pGEX-2T, in frame behind the coding region of glutathione S-transferase. The linker region between both genes contains coding sequences for six additional amino acids [73]. The fusion protein, glutathione S-transferase + GCAP-1 (GST-GCAP-1), was cleaved by thrombin. The additional amino acids remain at the N-terminus of GCAP-1. This recombinant GCAP-1 was characterized by Dr. S. Frins (IBI-1, Forschungszentrum Jülich) [97]. However, several difficulties arose during purification of large amounts of protein for biochemical and biophysical studies. GCAP-1 showed unexpected proteolysis by thrombin. Proteinase cleavage was observed not just between GST and GCAP-1 but also within GCAP-1 molecules. Therefore the yield of purified GCAP-1 was low.

To overcome these problems, GCAP-1 was designed to be expressed natively, without any additional amino acids, and, optionally, with substitution of cysteine residues.

### 3.3.1 Cloning Cysteine Mutants of GCAP-1

The experiments described in the previous section showed that a) no disulfide bond exists in GCAP-1 and b) GCAP-1 tends to form aggregates very easily, probably induced by oxidative processes after storage at 4°C for more than two days. Several attempts to crystallize GCAP-1 have failed because large aggregates formed after two days.

Due to the redox-sensitive formation of aggregates (see Results 3.2.5), it was reasoned that intermolecular disulfide bonds had formed. Therefore I constructed several cysteine to alanine exchange mutants to prevent the formation of disulfide bonds. Additionally, these mutants can help to clarify whether cysteines in GCAP-1 play a role for its function. Furthermore, cysteine exchange mutants in GCAP-1 can be used for monitoring conformational changes (see Results 3.2.7).

Site-directed mutagenesis was done by replacement of the triplet TGC coding for a cysteine at positions 18, 29, 106, and 125 against the triplets GCG or GCC coding for an alanine (see Fig. 6.1, the genetic code). The first cysteine $Cys^{18}$ is located in the α-helix of the non-functional EF-1, $Cys^{29}$ in the loop of EF-1, $Cys^{106}$ in the loop of the functional EF-3, and $Cys^{125}$ between the functional EF-3 and EF-4 (see Fig. 1.6). The single mutants were termed

as C18A, C29A, C106A, and C125A. The four double mutants were termed C18·29A, C18·106A, C18·125A, and C106·125A. The triple mutants, where three cysteines were replaced by alanines, were termed CAAA (C29·106·125A), ACAA (C18·106·125A), AACA (C18·29·125A), and AAAC (C18·29·106A). In the quad mutant, termed AAAA, all four cysteines were substituted by alanines (Table 3.8).

In all, thirteen cysteine mutants of GCAP-1 were cloned. Cysteine substitution mutations of GCAP-1 were performed using the different mutagenesis strategies shown in Fig. 3.18. All cysteine mutants of GCAP-1 were overexpressed successfully in *E. coli*.

The single mutants, C18A, C106A, and C125A, were constructed by using suitable mutant oligonucleotide primers #3–6 (refer to Methods 2.1.3.1) in PCR reaction. The double mutants, C18·29A, C18·106A, C18·125A, and C106·125A, were generated using the single mutants as templates and suitable mutant primers #3–6 (refer to Methods 2.1.3.1) to introduce the second mutation. The triple mutants, ACAA, AACA, and AAAC, were cloned using the single mutant as the template and mutant primers with two mutations or using the double mutant as the template and the mutant primers with one mutation. The quad mutant, AAAA, was constructed using the double mutant, C106·125A, as template and the mutant primers #3 and #4 [123] (Fig. 3.17 *A*).

In order to construct the triple mutant, CAAA, the quad mutant and C106·125A were used. A *Bsp*HI/*Bam*HI-fragment restricted from the quad mutant was used as a primer in a PCR reaction. C106·125A served as the template DNA (Fig. 3.17 *B*).

The single mutant, C29A, was constructed combining the upstream part of CAAA with the downstream part of wild-type GCAP1 by using restriction enzyme *Bsa*I [124] (Fig. 3.17 *C*).

All amplified PCR fragments were ligated into pCR-blunt (excluding the single mutant, C29A, which did not result from PCR). All mutants were identified by automated DNA sequencing using sequencing primer #7–8 (see Methods 2.1.3.1). The correct DNA fragments containing the individual mutations were released from pCR-blunt using the restriction enzymes *Nde*I and *Bam*HI, and respectively inserted into corresponding sites of the vector pET-11a. The modified GCAP1 sequences were confirmed again by sequencing using sequencing primer #9–10 (see Methods 2.1.3.1).

**TABLE 3.8** Location of the cysteine substitution with alanine of GCAP-1 and the list of cysteine-exchange mutants of GCAP-1

| No | EF-1 (α-helix) ($E^{17}$–$F^{25}$) | EF-1 (loop) ($M^{26}$–$E^{39}$) | EF-3 (loop) ($D^{100}$–$E^{111}$) | In-between of EF-3 and EF-4 ($R^{120}$–$E^{134}$) | Name of mutants | Type |
|---|---|---|---|---|---|---|
| | ECHQWYKKF | MTECPSGQLTLYE | DVDGNGCIDRDE | RAINPCSDSTMTAEE | WT | Wild-type |
| 1 | A | | | | C18A | Single mutants |
| 2 | | A | | | C29A | |
| 3 | | | A | | C106A | |
| 4 | | | | A | C125A | |
| 5 | A | A | | | C18·29A | Double mutants |
| 6 | A | | A | | C18·106A | |
| 7 | A | | | A | C18·125A | |
| 8 | | | A | A | C106·125A | |
| 9 | | A | A | A | CAAA | Triple mutants |
| 10 | A | | A | A | ACAA | |
| 11 | A | A | | A | AACA | |
| 12 | A | A | A | | AAAC | |
| 13 | A | A | A | A | AAAA | Quad mutant |

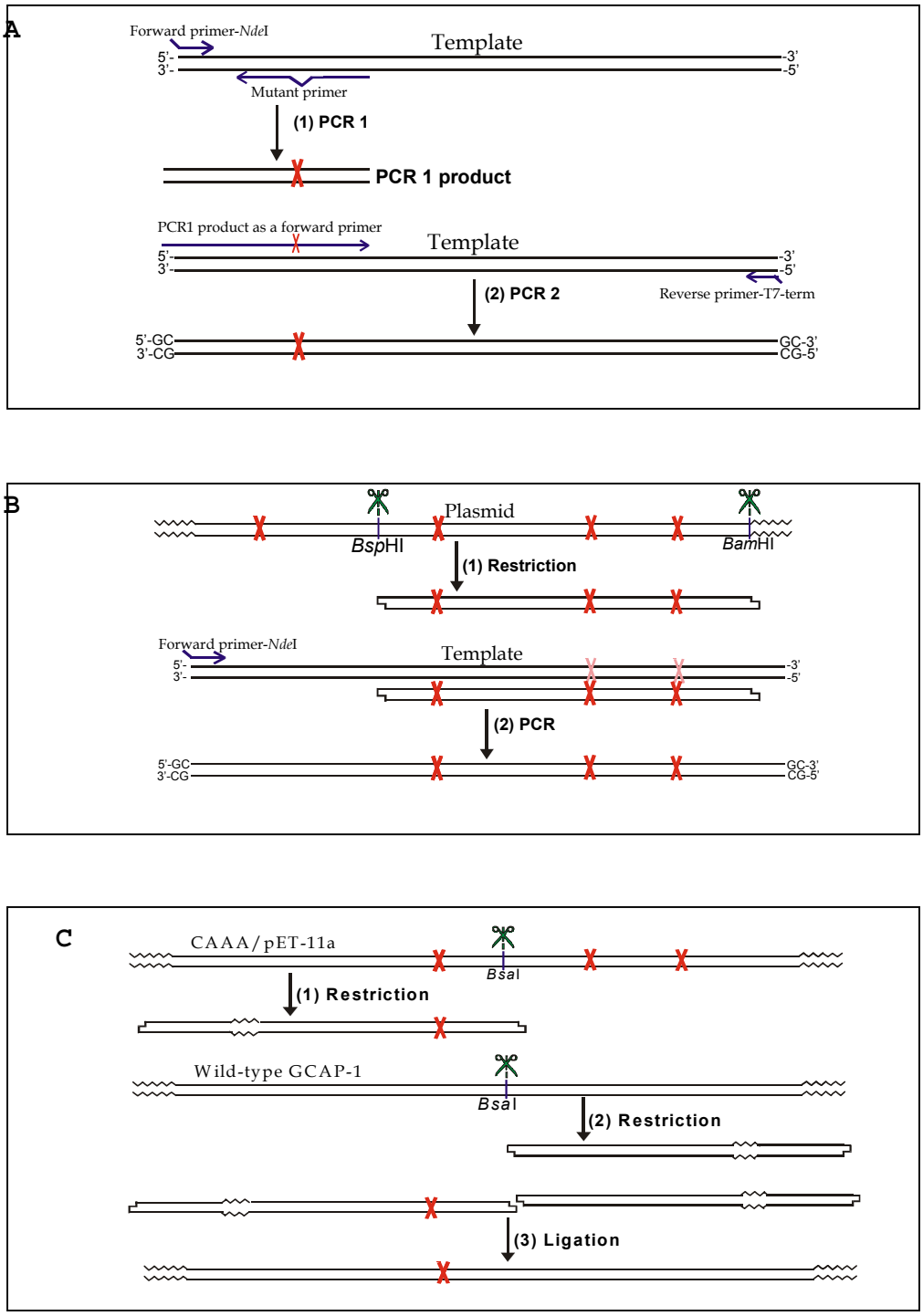


**FIG. 3.17.** The schematic description of the mutagenesis strategies. ***A.*** PCR-mediated oligonucleotide-directed mutagenesis strategies for the single mutants, C18A, C106A, and C125A; the double mutants, C18·29A, C18·106A, C18·125A, and C106·125A; the triple mutants, ACAA, AACA, and AAAC; and the quad mutant, AAAA. ***B.*** Use of an already mutagenized GCAP1 fragments as a primer in a PCR reaction, in order to generate CAAA. ***C.*** Combining fragments of different GCAP1 at *Bsa*I restriction site to generate C29A. The mutation sites are indicated by X and the used restriction sites by ✂ .

### 3.3.2 Overexpression and Preparation of Cysteine Mutants of GCAP-1

Overexpression of cysteine mutants of GCAP-1 was achieved in *E. coli* strain BL21-Codon Plus(DE3) as described before for the wild-type GCAP-1 (refer to Results 3.1.1). A part of the expressed proteins was seen in the insoluble fraction after cell lysis; only the soluble fraction was used for purification and further studies. As described previously, more than one hundred milligrams of crude proteins were obtained from a 500 ml culture (refer to Results 3.1.2).

All cysteine mutants exhibited the same $Ca^{2+}$-dependent electrophoretic mobility shift as seen in the wild-type (21 kDa in the presence of $Ca^{2+}$ and 26 kDa in the absence of $Ca^{2+}$). Two examples, the mutants C18A and CAAA, are shown in Fig. 3.18. The prominent bands in the *E. coli* lysates were identified as GCAP1 with a polyclonal anti-GCAP-1 antibody by Western blotting.

The cysteine mutants of GCAP-1 can be purified by the same procedures as the wild-type GCAP-1. Purified protein showed the same $Ca^{2+}$ mobility shift and diffuse bands on the SDS-PAGE as observed for wild-type GCAP-1 (refer to Results 3.1.2).

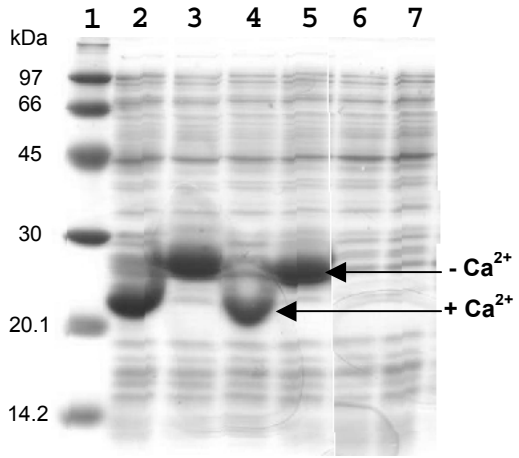


**FIG. 3.18.** Expression of two cysteine mutants of GCAP-1, C18A and CAAA. Proteins were separated on a 15% (w/v) polyacrylamide gel and visualized by staining with Commassie Blue: *lane 1,* molecular weight markers (7 µg standards); *lane 2,* C18A with $Ca^{2+}$ (~10 µg protein); *lane 3,* C18A without $Ca^{2+}$ (~10 µg protein); *lane 4,* CAAA with $Ca^{2+}$ (~10 µg protein); *lane 5,* CAAA without $Ca^{2+}$ (~10 µg protein); *lane 6,* control (soluble fraction of *E. coli* containing pET-11a) with $Ca^{2+}$ (~5 µg protein); *lane 7,* control without $Ca^{2+}$ (~5 µg protein).

## 3.4 Properties of Cysteine Mutants of GCAP-1

### 3.4.1 Regulation of ROS-GC1 by Cysteine Mutants of GCAP-1

The calcium-dependent activation of ROS-GC1 by cysteine mutants of GCAP-1 was tested at free [$Ca^{2+}$] ranging from 1 nM to 1 mM. The $Ca^{2+}$ sensitivity of ROS-GC1 stimulation by wild-type GCAP-1 was previously described (refer to Results 3.2.2 and Reference 73). The activity of ROS-GC1 with native GCAP-1 effectively increased about 10-fold, when $[Ca^{2+}]_{free}$ was below 100 nM. The regulation of ROS-GC1 by native GCAP-1 was fit with a modified Hill equation, resulting in a coefficient of ~2 and half-maximal activation at ~100 nM $Ca^{2+}$. Increasing the $Ca^{2+}$ concentration above 300 nM resulted in a slight inhibition, i.e. ROS-GC1 activity with GCAP is lower than basal activity in washed ROS membranes (see Fig. 3.5). However, the activity of ROS-GC1 was regulated by nmGCAP-1 with a lower degree of cooperativity (Hill coefficient $n$ = 0.3) and half-maximal activation at ~2.82 µM $[Ca^{2+}]_{free}$. At high $[Ca^{2+}]_{free}$ (>1 µM), the activity had no inhibitory effect (see Fig. 3.6 *B* and *D*).

Single cysteine mutants of GCAP-1 were expressed without NMT, and therefore those mutants have no myristoylation. Slight differences between nmGCAP-1 and single cysteine mutants (C18A, C29A, C106A, and C125A) were noticed. The regulation of ROS-GC1 activity by single cysteine mutants is illustrated in Fig. 3.19 and summarized in Tables 3.9 and 3.10.

Stimulation of ROS-GC1 by C18A was 4-fold with maximal activity of 10.1 nmol cGMP·$min^{-1}$·$mg^{-1}$ rhodopsin in the presence of EGTA. The $EC_{50}$-value for the ROS-GC1 activity upon [C18A] was 0.5 µM in the presence of 2 mM EGTA (Fig. 3.19 *A*). The $IC_{50}$-value of C18A shifted higher to 10.4 µM $[Ca^{2+}]_{free}$. The ROS-GC1 activity increased 5-fold with C18A of low $[Ca^{2+}]_{free}$. Cooperativity was low ($n$ = 0.6). The activity at ~10 µM $[Ca^{2+}]_{free}$ still remained at ~51% (Fig. 3.19 *E*). The ROS-GC1 activity increased 4-fold with C29A at lower $[Ca^{2+}]_{free}$.

Stimulation of ROS-GC1 by C29A was 5-fold with maximal activity of 8.3 nmol cGMP·$min^{-1}$·$mg^{-1}$ rhodopsin in the presence of EGTA. The $EC_{50}$-value for the ROS-GC1 activity upon [C29A] was 0.4 µM in the presence of 2 mM EGTA (Fig. 3.19 *B*). The $IC_{50}$-value of C29A shifted higher to 5.2 µM $[Ca^{2+}]_{free}$. The ROS-GC1 activity increased

4-fold with C29A of low $[Ca^{2+}]_{free}$. Cooperativity was low ($n$ = 0.7). The activity at ~10 µM $[Ca^{2+}]_{free}$ still remained at ~46% (Fig. 3.19 *E*).

Stimulation of ROS-GC1 by C106A was 5-fold with maximal activity of 6.0 nmol cGMP·min$^{-1}$·mg$^{-1}$ rhodopsin in the presence of EGTA. The $EC_{50}$-value for the ROS-GC1 activity upon [C106A] was 0.4 µM in the presence of 2 mM EGTA (Fig. 3.19 *C*). The $IC_{50}$-value of C106A shifted slightly lower to 2.1 µM $[Ca^{2+}]_{free}$. The ROS-GC1 activity increased 3-fold with C106A ot low $[Ca^{2+}]_{free}$. Cooperativity was low ($n$ = 1.2). The activity at ~10 µM $[Ca^{2+}]_{free}$ still remained at ~46% (Fig. 3.19 *F*).

Stimulation of ROS-GC1 by C125A was 6-fold with maximal activity of 18.0 nmol cGMP·min$^{-1}$·mg$^{-1}$ rhodopsin in the presence of EGTA. The $EC_{50}$-value for the ROS-GC1 activity upon [C125A] was 0.4 µM in the presence of 2 mM EGTA (Fig. 3.19 *D*). The $IC_{50}$-value of C125A shifted higher to 4.3 µM $[Ca^{2+}]_{free}$. The ROS-GC1 activity increased 9-fold with C18A of low $[Ca^{2+}]_{free}$. Cooperativity was low ($n$ = 1.0). The activity at ~10 µM $[Ca^{2+}]_{free}$ still remained at ~36% (Fig. 3.19 *G*).

The activity of ROS-GC1 increased about 5-fold (± 1) at saturating GCAP-1 single cysteine mutants in the absence of $Ca^{2+}$ (Table 3.8 and Fig. 3.19 *A–D*). The $IC_{50}$-values of single mutants shifted to a higher free $[Ca^{2+}]$. The degrees of cooperativity were higher. The single cysteine mutants had no inhibitory effects on ROS-GC1. The activity at high $[Ca^{2+}]_{free}$ (~10 µM) remained at ~36%.

The triple mutants of GCAP-1 (CAAA, ACAA, AACA, and AAAC) activate ROS-GC1 in a similar fashion as native GCAP-1, while the single cysteine mutants had different stimulation from wild-type GCAP-1. Significant differences between nmGCAP-1 and these triple cysteine mutants were noticed. The regulation of ROS-GC1 activity by triple cysteine mutants is illustrated in Fig. 3.20 and summarized in Tables 3.9 and 3.10.

Stimulation of ROS-GC1 by CAAA was 6-fold with maximal activity of 10.0 nmol cGMP·min$^{-1}$·mg$^{-1}$ rhodopsin in the presence of EGTA. The $EC_{50}$-value for the ROS-GC1 activity upon [CAAA] was 0.8 µM in the presence of 2 mM EGTA (Fig. 3.20 *A*). The $IC_{50}$-value of CAAA shifted to a lower value of 499 nM $[Ca^{2+}]_{free}$. The ROS-GC1 activity increased 5-fold with CAAA of low $[Ca^{2+}]_{free}$. Cooperativity was higher (Fig. 3.20 *D*).

Stimulation of ROS-GC1 by ACAA was 4-fold with maximal activity of 9.0 nmol cGMP·min$^{-1}$·mg$^{-1}$ rhodopsin in the presence of EGTA. The $EC_{50}$-value for the ROS-GC1 activity upon [ACAA] was 0.8 µM in the presence of 2 mM EGTA (Fig. 3.19 *B*). The

$IC_{50}$-value of ACAA shifted to lower values to 721 nM $[Ca^{2+}]_{free}$. The ROS-GC1 activity increased 5-fold with ACAA of low $[Ca^{2+}]_{free}$. Cooperativity was higher ($n$ = 1.5) (Fig. 3.20 *E*).

Stimulation of ROS-GC1 by AACA was 11-fold with maximal activity of 11.8 nmol cGMP·min$^{-1}$·mg$^{-1}$ rhodopsin in the presence of EGTA. The $EC_{50}$-value for the ROS-GC1 activity upon [AACA] was 0.5 µM in the presence of 2 mM EGTA (Fig. 3.20 *C*). The $IC_{50}$-value of AACA shifted to lower value to 551 nM $[Ca^{2+}]_{free}$. The ROS-GC1 activity increased 7-fold with AACA at low $[Ca^{2+}]_{free}$. Cooperativity was higher ($n$ = 1.5) (Fig. 3.20 *F*).

Stimulation of ROS-GC1 by AAAC was 8-fold with maximal activity of 12.9 nmol cGMP·min$^{-1}$·mg$^{-1}$ rhodopsin in the presence of EGTA. The $EC_{50}$-value for the ROS-GC1 activity upon [AAAC] was 0.5 µM in the presence of 2 mM EGTA (Fig. 3.20 *D*). The $IC_{50}$-value of AAAC shifted to 1.1 µM $[Ca^{2+}]_{free}$. The ROS-GC1 activity increased 6-fold with AAAC of low $[Ca^{2+}]_{free}$. Cooperativity was higher ($n$ = 1.5) (Fig. 3.20 *G*).

The stimulation of ROS-GC1 was about 7-fold (± 3) with the triple cysteine mutants of GCAP-1 in the absence of $CaCl_2$ (Fig. 3.20 *A–D*). The $IC_{50}$-values are shifted to higher $[Ca^{2+}]_{free}$ compared to native GCAP-1 (100 nM) and to lower $[Ca^{2+}]_{free}$ compared to those of recombinant wild-type nmGCAP-1 ($IC_{50}$ of nmGCAP-1 = 2.8 µM) and single cysteine mutants. The cooperativity of ROS-GC1 activity by triple cysteine mutants is lower than that of native GCAP-1 ($n$ = 2.5) and higher than those of the recombinant wild-type and the single mutants of GCAP-1 at $[Ca^{2+}]_{free}$. Some triple cysteine mutants have slight inhibitory effects above 5 µM $[Ca^{2+}]_{free}$ (Fig. 3.20 *E–G*).

The quad cysteine mutant of GCAP-1 (AAAA) increased ROS-GC1 activity ~6-fold at low $[Ca^{2+}]_{free}$. The maximal activity of ROS-GC1 by AAAA was ~12 nmol cGMP·min$^{-1}$·mg$^{-1}$ rhodopsin at low $[Ca^{2+}]_{free}$. The half-maximal activation of AAAA was 0.7 µM (Fig. 3.22 *A*). The $IC_{50}$ of its $Ca^{2+}$-dependent activation was 293 nM and the Hill coefficient was at $n$ = 1.7. AAAA shows a marked inhibitory effect on ROS-GC1 in the µM range of free $[Ca^{2+}]$. (Fig. 3.22 *B*). AAAA of GCAP-1 stimulated ROS-GC1 most similarly to native GCAP-1 in whole ROS even though this protein has no myristoylation on its N-terminus.

**TABLE 3.9** The comparison of the activation of ROS-GC1 according to the stimulation of concentration of cysteine mutants of GCAP-1. Summary of Fig. 3.19 *A-D*, Fig. 3.20 *A–D*, and Fig 3.21 *A*.

| Type | Activity at low $[Ca^{2+}]_{free}$ (nmol cGMP·mg$^{-1}$·min$^{-1}$ R) [a] | Activity at high $[Ca^{2+}]_{free}$ (nmol cGMP·mg$^{-1}$·min$^{-1}$ R) [b] | $EC_{50}$ [c] [Protein] (μM) |
|---|---|---|---|
| nmGCAP-1 | 12.39 | 2.14 | 0.85 |
| C18A | 10.13 | 2.86 | 0.53 |
| C29A | 8.28 | 1.77 | 0.41 |
| C106A | 6.01 | 1.34 | 0.36 |
| C125A | 17.97 | 2.80 | 0.35 |
| CAAA | 9.98 | 1.51 | 0.78 |
| ACAA | 9.47 | 1.71 | 0.82 |
| AACA | 11.84 | 1.12 | 0.49 |
| AAAC | 12.85 | 1.72 | 0.49 |
| AAAA | 12.23 | 1.22 | 0.68 |

a. with 2 mM EGTA

b. with 2 mM $CaCl_2$

c. The $EC_{50}$-value upon the concentration of proteins with 2 mM EGTA.

**TABLE 3.10** The comparison of the stimulation of ROS-GC1 with cysteine mutants of GCAP-1 as a function of $[Ca^{2+}]_{free}$. Summary of Fig. 3.19 *E–H*, Fig. 3.20 *E–H*, and Fig. 3.21 *B*.

| Type | Inhibition at high $[Ca^{2+}]_{free}$ | Maximal activity (nmol cGMP·mg$^{-1}$·min$^{-1}$ R) | $IC_{50}$ $[Ca^{2+}]_{free}$ (μM) | $n$ to $Ca^{2+}$ |
|---|---|---|---|---|
| nmGCAP-1 | - * | 9.23 | 2.817 | 0.3 |
| C18A | - | 10.51 | 10.368 | 0.6 |
| C29A | - | 8.84 | 5.190 | 0.7 |
| C106A | (-) | 6.72 | 2.083 | 1.2 |
| C125A | - | 17.07 | 4.254 | 1.0 |
| CAAA | + | 9.45 | 0.499 | 1.7 |
| ACAA | + | 9.01 | 0.721 | 1.5 |
| AACA | + | 12.97 | 0.551 | 1.5 |
| AAAC | (+) | 11.62 | 1.052 | 1.5 |
| AAAA | ++ | 12.18 | 0.293 | 1.7 |

* '+' indicates that each sample has inhibitory effect to be lower activity than the basal activity at high $[Ca^{2+}]_{free}$, while '–' means that each sample still has activity at high $[Ca^{2+}]_{free}$ (>10 μM).

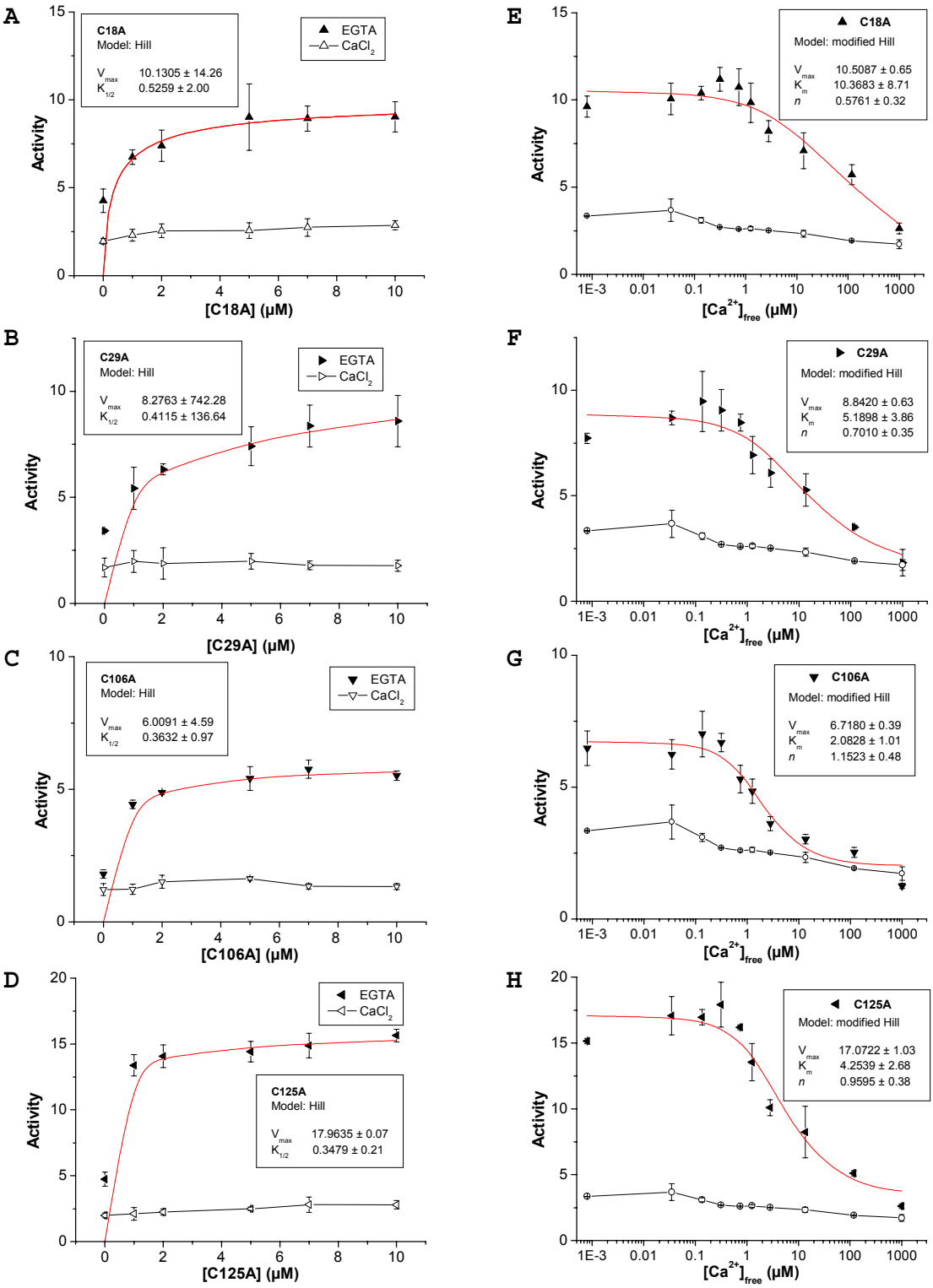


**FIG. 3.19.** Stimulation of ROS-GC1 with single cysteine mutants of GCAP-1. **Left panels**; as a function of protein concentration; *A.* C18A, *B.* C29A, *C* C106A, and *D.* C125A. The filled triangles indicate data acquired in the presence of 2 mM EGTA, and the open triangles indicate data obtained with 2 mM $CaCl_2$. **Right panels**; *E.* by C18A, *F.* by C29A, *G.* by C106A, and *H.* by C125A as a function of free [$Ca^{2+}$]. The filled triangles indicate data obtained by 10 μM protein, and the open circles indicate data obtained in the absence of protein.

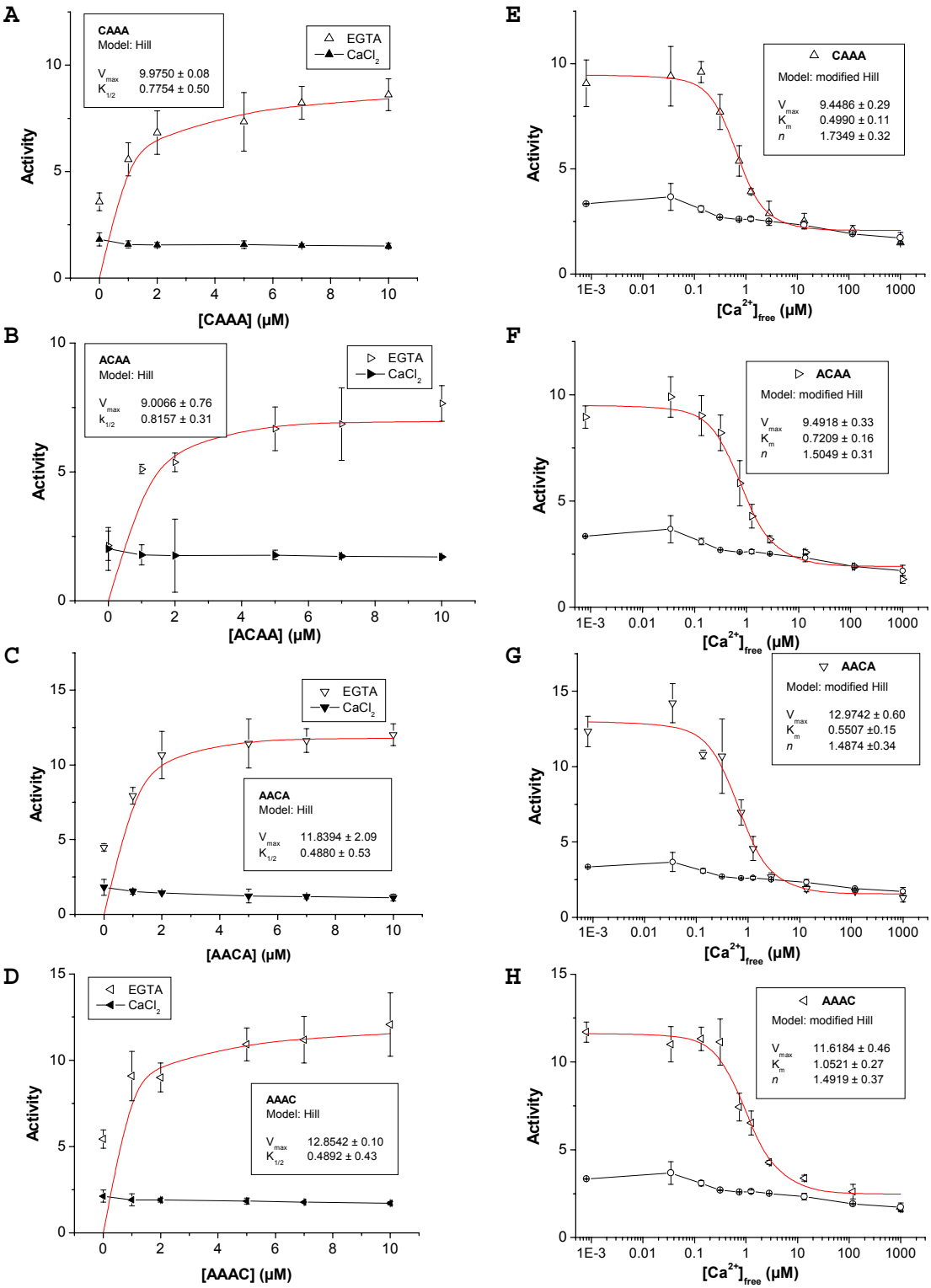


**FIG. 3.20.** Stimulation of ROS-GC1 with triple cysteine mutants of GCAP-1. **Left panels**; as a function of protein concentration; *A.* CAAA, *B.* ACAA, *C.* AACA, and *D.* AAAC. The open triangles indicate data acquired in the presence of 2 mM EGTA, and the filled triangles indicate data obtained with 2 mM $CaCl_2$. **Right panels**; *E.* by CAAA, *F.* by ACAA, *G.* by AACA, and *H.* by AAAC as a function of free [$Ca^{2+}$]. The open triangles indicate data obtained by 10 μM protein, and the open circles indicate data obtained in the absence of protein.

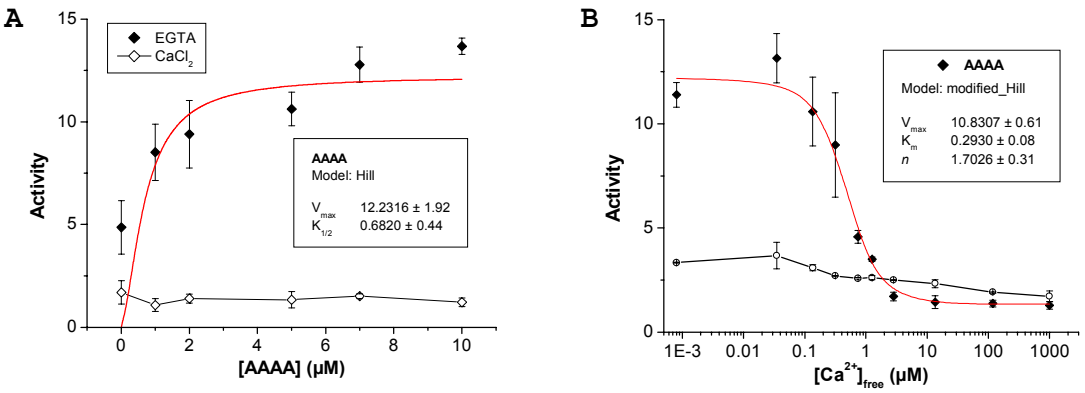


**FIG. 3.21.** Stimulation of ROS-GC1 by quad cysteine mutant of GCAP-1. ***A.*** ROS-GC1 activity as a function of AAAA concentration. The filled diamonds indicate data obtained with 2 mM EGTA and the open diamonds indicate data obtained with 2 mM $CaCl_2$. ***B.*** The $Ca^{2+}$-titration versus ROS-GC1 activity with AAAA at saturating concentrations. The filled diamonds indicate data obtained with 10 µM protein and the open circles indicate without protein.

## 3.4.2 Monitoring the Exposition of Cysteine Residues towards DTNB

As previously described in Results 3.2.7, three cysteines in nmGCAP-1 were exposed in the presence of $CaCl_2$. On the other hand, when EGTA was added, all four cysteines rapidly reacted with DTNB. The single cysteine mutants were used to explore which of the four cysteine residues is buried in the $Ca^{2+}$-binding form of GCAP-1.

### *3.4.2.1 Reactivity of single cysteine mutants*

Figure 3.22 illustrates the reactivity of the single cysteine mutants with DTNB. The absorbance at 412 nm ($A_{412}$) of 10 µM C18A with $CaCl_2$ is 0.205, which corresponds to 12.7 µM thiol group of free cysteine or one cysteine. After 300 sec, injection of EGTA caused an additional increase in $A_{412}$ of 0.076, which corresponds to 5.6 µM of free thiol or half a cysteine (Fig. 3.22 *A*). These data demonstrate that in the presence of $CaCl_2$ one cysteine in C18A is slowly exposed to the solvent and the additional reaction with 2 mM EGTA quickly exposes a cysteine to the solvent, however, only half population of the molecules may have reacted. Figure 3.22 *B* shows that in the presence of $CaCl_2$, two cysteines in C18A are quickly exposed to the solvent, and the additional reaction after injection of 2 mM EGTA starts with the other cysteine to be extruded to the solvent. Figure 3.22 *C* shows that in the presence of $CaCl_2$, all three cysteines in C106A are relatively slowly exposed to the solvent. No increase of absorbance was observed by subsequent addition of EGTA. Therefore the cysteine residue at position 106 must be the buried cysteine in GCAP-1. Figure 3.22 *D* shows that in the presence of $CaCl_2$, two cysteines in C125A were slowly exposed to the solvent and the subsequent reaction with 2 mM EGTA quickly gets the other cysteine exposed to the solvent.

The mutants C18A, C29A, and C125A contain two cysteines that are accessible at high $Ca^{2+}$ and one cysteine that is accessible upon subsequent addition of EGTA. The C106A mutant exposed three cysteines in the presence of $Ca^{2+}$. No reactivity towards DTNB was observed after subsequent addition of EGTA.

**TABLE 3.11** Summary of cysteine reactivities of single mutants of GCAP-1

| Type | Treatment | Time (sec) | $A_{412}$ | [-SH] (μM) | No. of –SH (mole/protein) | Reactivity |
|---|---|---|---|---|---|---|
| C18A * | $CaCl_2$ | 300 | 0.173 | 12.7 | 1 | slow |
| | EGTA | 600 | + 0.076 | 5.6 | 0.5 | fast |
| C29A * | $CaCl_2$ | 300 | 0.283 | 20.8 | 2 | fast |
| | EGTA | 600 | + 0.130 | 9.6 | 1 | fast |
| C106A * | $CaCl_2$ | 300 | 0.170 | 12.5 | 3 | relatively slow |
| | EGTA | 600 | + 0.006 | 0.4 | - | no |
| C125A * | $CaCl_2$ | 300 | 0.246 | 18.0 | 2 | slow |
| | EGTA | 600 | + 0.118 | 8.7 | 1 | fast |

* The protein concentrations of C18A, C28A, C106A, and C125A are 10 μM, 12 μM, 5 μM, and 8 μM, respectively.

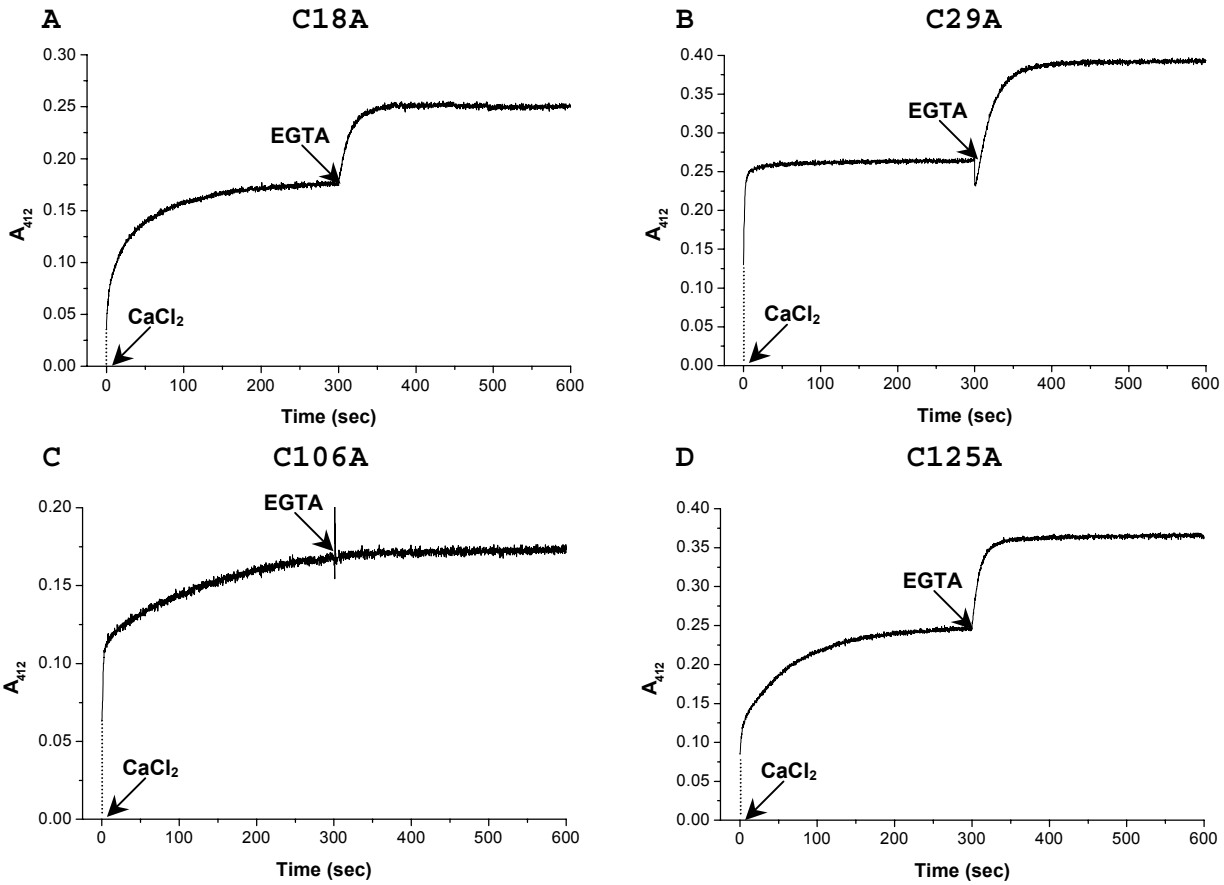


**FIG. 3.22.** Cysteine reactivity of single cysteine mutants of GCAP-1 towards DTNB. The injection of $CaCl_2$ or EGTA is indicated with the arrows. ***A.*** $A_{412}$ of 10 μM C18A is 0.173 in the presence of $CaCl_2$ and 0.249 in the presence of EGTA. ***B.*** $A_{412}$ of 12 μM C29A is 0.283 in the presence of $CaCl_2$ and 0.413 in the presence of EGTA. ***C.*** $A_{412}$ of 5 μM C106A is 0.170 in the presence of $CaCl_2$ and 0.176 in the presence of EGTA. ***D.*** $A_{412}$ of 8 μM C125A is 0.246 in the presence of $CaCl_2$ and 0.364 in the presence of EGTA.

### *3.4.2.2 Reactivity of triple cysteine mutants*

To monitor the reactivity of each cysteine residue respectively, the triple mutants were used. Figure 3.23 *A* illustrates the reactivity of the unique cysteine of CAAA towards DTNB. The absorbance at 412 nm ($A_{412}$) of 6 µM CAAA with $CaCl_2$ is 0.044, which corresponds to 3.2 µM thiol group. This corresponds to a stoichiometric ratio of 0.5 cysteine, meaning that one cysteine exposes to the solvent, however, only half population of molecules is reacted. After 300 sec, injection of EGTA caused no change. Figure 3.23 *B* showed that in the presence of $CaCl_2$ the cysteine of ACAA is exposed to the solvent and reacted with slow kinetics. It is apparent from Figure 3.23 *C* that there is no reaction of the cysteine in AACA in the presence of $CaCl_2$. However, in the presence of EGTA the cysteine in AACA is rapidly exposed to the solvent. This observation supported the results from Fig. 3.22 *C* that the cysteine residue at position 106 is the buried one in GCAP-1 and it becomes exposed in the absence of $CaCl_2$. Figure 3.23 *D* showed that in the presence of $CaCl_2$, the cysteine of AAAC is exposed to the solvent quickly. The results are summarized in Table 3.12.

In summary, the cysteine in CAAA and AAAC were rapidly exposed in the presence of $Ca^{2+}$, whereas cysteine in ACAA slowly reacted with DTNB in the presence of $Ca^{2+}$. Only the cysteine of AACA is buried within GCAP-1 when $Ca^{2+}$ is bound, and it is exposed after EGTA addition.

**TABLE 3.12** Summary of cysteine reactivities of triple mutants of GCAP-1

| Type | Treatment | Time (sec) | $A_{412}$ | [-SH] (μM) | No. of –SH (mole/protein) | Reactivity |
|---|---|---|---|---|---|---|
| CAAA * | $CaCl_2$ | 300 | 0.044 | 3.2 | 0.5 | fast |
| | EGTA | 600 | + 0 | - | - | no |
| ACAA * | $CaCl_2$ | 300 | 0.095 | 7.0 | 1 | slow |
| | EGTA | 600 | + 0.010 | 0.7 | - | no |
| AACA * | $CaCl_2$ | 300 | 0.017 | 1.3 | - | no |
| | EGTA | 600 | + 0.109 | 8.0 | 1 | fast |
| AAAC * | $CaCl_2$ | 300 | 0.134 | 9.9 | 1 | fast |
| | EGTA | 600 | + 0 | - | - | no |

* The protein concentrations of CAAA, ACAA, AACA, and AAAC were 6 μM, 6 μM, 10 μM, and 10 μM, respectively.

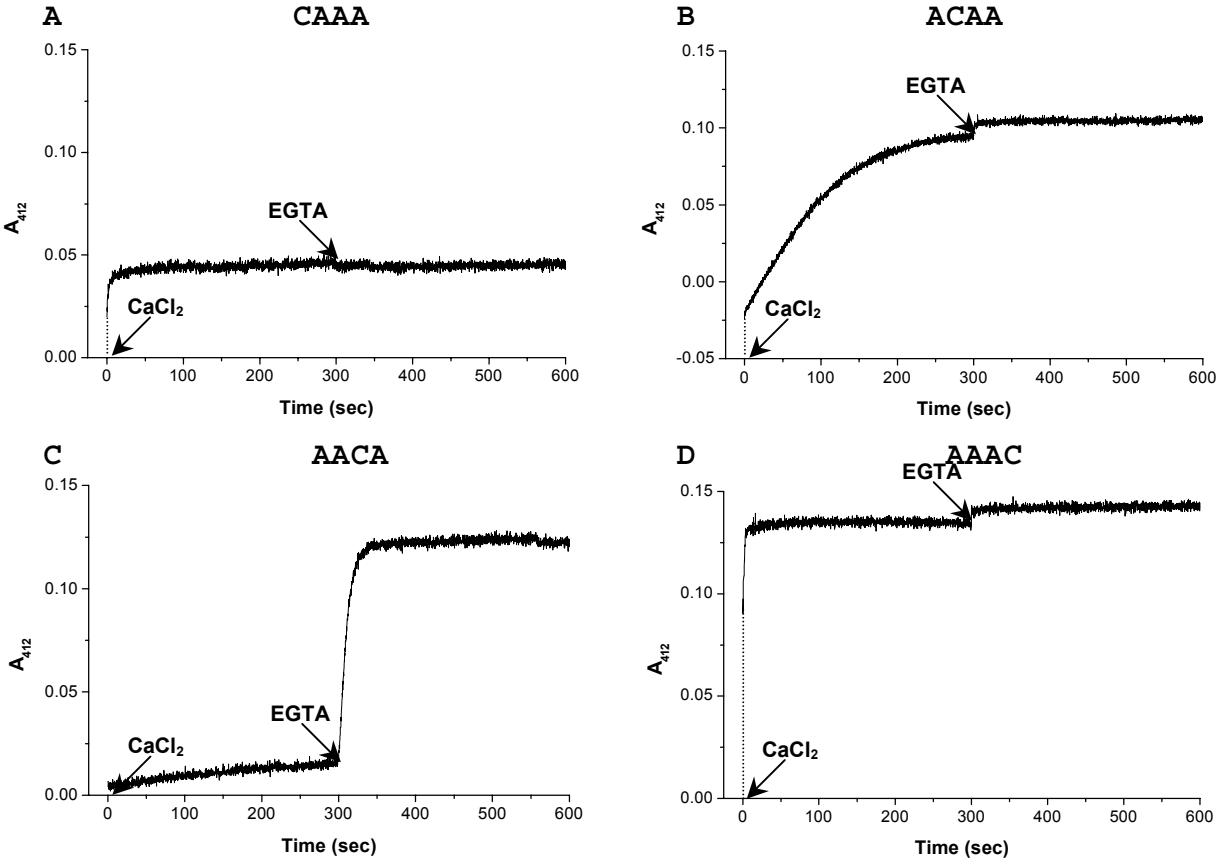


**FIG. 3.23.** Cysteine reactivity of triplet cysteine mutants GCAP-1 towards DTNB. The injection of $CaCl_2$ or EGTA is indicated with the arrows. ***A.*** $A_{412}$ of 6 μM CAAA is 0.044 in the presence of $CaCl_2$ and dose not change in the presence of EGTA. ***B.*** $A_{412}$ of 6 μM ACAA is 0.095 in the presence of $CaCl_2$ and 0.105 in the presence of EGTA. ***C.*** $A_{412}$ of 10 μM AACA is 0.017 in the presence of $CaCl_2$ and 0.126 in the presence of EGTA. ***D.*** $A_{412}$ of 10 μM AAAC is 0.134 in the presence of $CaCl_2$ and dose not change in the presence of EGTA.

### *3.4.2.3 Thiol reactivity of ACAA and AACA as a function of $[Ca^{2+}]_{free}$*

The results with the triple cysteine mutants indicated different kinetics of DTNB reactivity as a function of $[Ca^{2+}]_{free}$ (compare ACAA and AACA in Fig. 3.23 *B* and *C*). These two triple mutants (ACAA and AACA) were used to compare the reactivities of cysteines at position 29 and 106, respectively, measured as a function of time, varying the concentration of $[Ca^{2+}]_{free}$ (Fig. 3.24 *A* and *B*).

The accessibility of the cysteine in ACAA is clearly dependent on $[Ca^{2+}]_{free}$. The change in accessibility as a function of $[Ca^{2+}]_{free}$ can be seen in different reaction rates of DTNB in Fig. 3.24 *A*. I determined different time constants by fitting the raw data to a single exponential. Plotting the time constants as a function of $[Ca^{2+}]_{free}$ yielded an $EC_{50}$ = 55 µM and a Hill coefficient of $n$ = 0.5 (Fig. 3.24 *C*).

A different titration was obtained with the triple mutant AACA (Fig. 3.24 *B* and *D*). Almost no reactivity was observed at high $[Ca^{2+}]_{free}$. At intermediate $[Ca^{2+}]_{free}$ (3 µM), the reaction towards DTNB occurred at a slow rate when compared with ACAA. Finally, at low $[Ca^{2+}]_{free}$ the reaction proceeded with similar fast kinetics as in the case of ACAA.

A summary of the fit results is shown in Table 3.13.

**TABLE 3.13** The thiol reactivity of ACAA and AACA with respect to the $[Ca^{2+}]_{free}$

| Type | $t1_{max}$ (sec) | $K_{1/2}$ $[Ca^{2+}]_{free}$ (µM) | $n$ to $Ca^{2+}$ |
|---|---|---|---|
| ACAA | 135 | 54.47 | 0.5 |
| AACA | 993 | 2.69 | 1.6 |

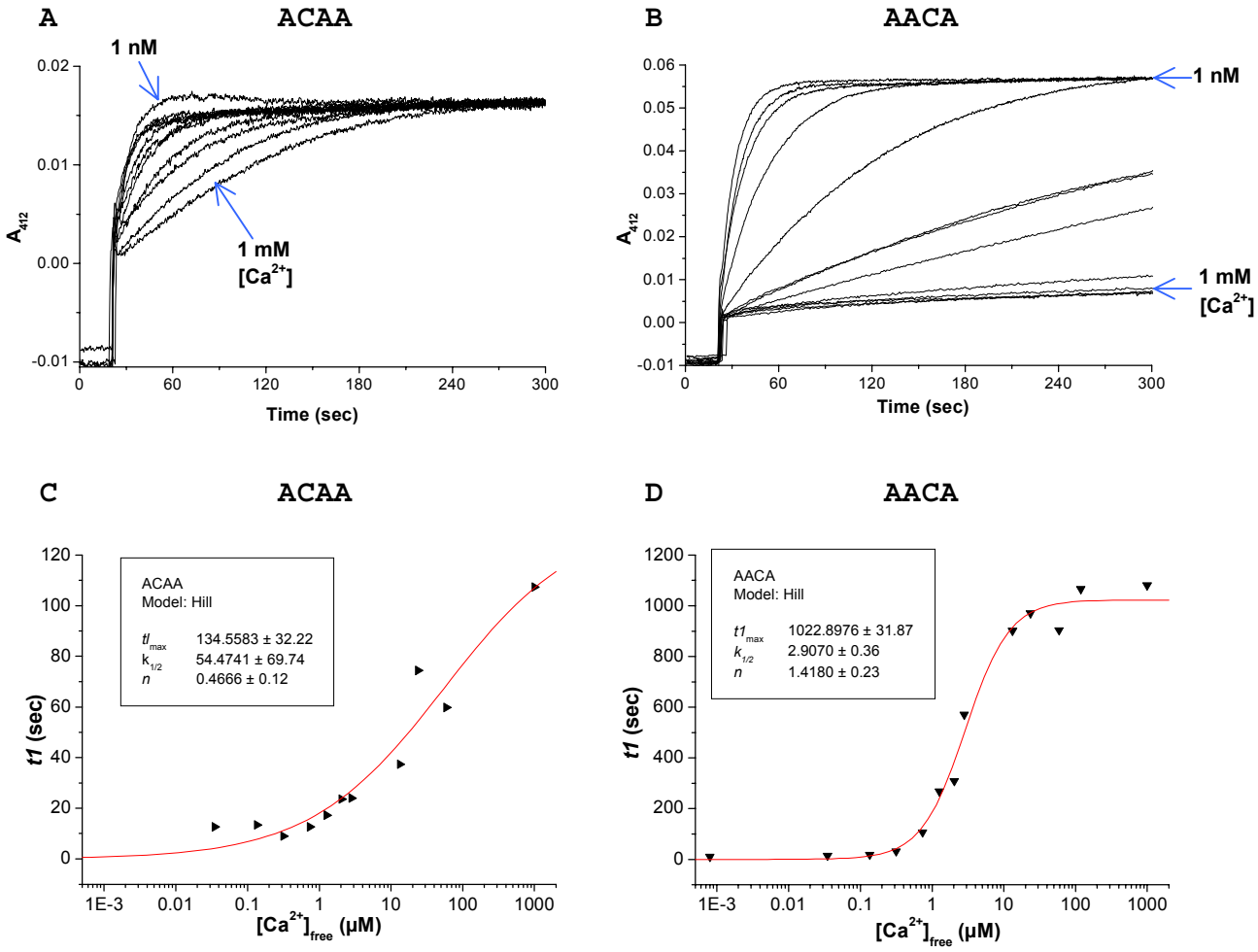


**FIG. 3.24.** Cysteine reactivity of ACAA and AACA towards DTNB as a function of time and calcium concentration. ***A.*** ACAA and ***B.*** AACA. These data were fitted to a modified exponential growth for nonlinear curve fitting; $y = y_o - A_1 * e^{-x/t1}$. ***C.*** and ***D.*** The calculated time constants (*t1*) were plotted against $[Ca^{2+}]_{free}$. The solid line represents the best fit to the Hill equation. Thiol reactivity was measured for various concentrations of $Ca^{2+}$/EGTA buffer (refer to Table 2.2). The reaction was started by the addition of DTNB directly to the cuvette to a final concentration of 100–250 µM and immediately monitored using an SLM-Aminco DW-2000 UV/VIS spectrophotometer in dual wavelength mode with monochromators set at 412 nm and 750 nm.

## 3.5 Interaction of GCAP-1 with Peptides from ROS-GC1

### 3.5.1 Monitoring the Exposition of Cysteine Residues

Cysteine residues in GCAP-1 can be used to monitor conformational changes. Therefore, I also tested whether the interaction of GCAP-1 with peptides from the cytoplasmic part of ROS-GC1 can be monitored by a change in thiol reactivity towards DTNB. Cysteine reactivity of nmGCAP-1 was investigated at high and low $[Ca^{2+}]_{free}$ in the absence and presence of peptides. Peptides obtained from Dr. M. Beyermann (Forschungsinstitut für Molekulare Pharmakologie, Berlin) had been synthesized automatically on MiliGen 9050 peptide synthesizer [125].

Figure 3.25 *A* shows that 2.3 cysteines of nmGCAP-1 are exposed in the presence of #34a in the presence of $CaCl_2$ and then 1.5 cysteines with subsequent addition of EGTA. In the absence of $Ca^{2+}$, all four cysteines were exposed to the solvent (Fig. 3.25 *B*). Addition of S #71 led to the exposure of only 1.7 cysteines in the presence of $Ca^{2+}$ and an additional 1.0 cysteine with subsequent addition of EGTA (Fig. 3.25 *C*). All four cysteines in nmGCAP-1 in the presence of S # 71 are exposed to the solvent when EGTA is added before DTNB (Fig. 3.25 *D*).

Addition of peptides had consequences for the thiol reactivity of the single cysteines. The presence of both peptides decreased the reactivity of one cysteine in the presence of $Ca^{2+}$, whereas in the presence of EGTA (before changing to high $[Ca^{2+}]_{free}$), all four cysteines were rapidly exposed. Furthermore, addition of S #71 prevented the exposure of one cysteine when the experiment was first carried out in the presence of $Ca^{2+}$.

To monitor the reactivity of each cysteine residue separately, the triple mutants were used. Thiol reactivities of the triple mutants, CAAA, ACAA, AACA and AAAC, were slightly different between experiments in which the peptide #34a or the peptide S #71 was added (Figs. 3.26 and 3.27).

With peptide #34a half a cysteine of CAAA is exposed in the presence of $CaCl_2$ relatively fast (Fig. 3.26 *A*). Also half a cysteine of ACAA is slowly exposed under the same conditions (Fig. 3.26 *B*). About 70% of the cysteine of AACA is rapidly exposed by the

addition of 2 mM EGTA (Fig. 3.26 *C*), whereas the whole cysteine residue of AAAC is quickly exposed in the presence of $CaCl_2$ (Fig. 3.26 *D*).

In the presence of the peptide S #71, 60% of the cysteine of CAAA was exposed in the presence of $CaCl_2$ (Fig. 3.27 *A*), 40% cysteine of ACAA was slowly exposed (Fig. 3.27 *B*), 70% of AACA was rapidly exposed upon EGTA addition (Fig. 3.27 *C*), and the whole cysteine of AAAC rapidly reacted in the presence of $CaCl_2$ (Fig. 3.27 *D*).

In summary, two triple mutants, ACAA and AACA, had a reduced thiol reactivity of their single cysteines in the presence of peptides, when the results were compared with the experiments without peptides (Table 3.12 vs. Tables 3.15 and 3.16). Thus, these two cysteines appear to be buried or shielded when GCAP-1 interacts with ROS-GC1 peptides.

**TABLE 3.14** Summary of cysteine reactivities of nmGCAP-1 with DTNB in the presence of peptides as indicated

| Type | Treatment | Time (sec) | $A_{412}$ | [-SH] (μM) | No. of –SH (mole/protein) |
|---|---|---|---|---|---|
| nmGCAP-1 | $CaCl_2$ | 300 | 0.035 | 2.6 | 2.3 |
| with #34a * | EGTA | 600 | + 0.023 | 1.7 | 1.5 |
| | EGTA | 300 | 0.065 | 4.6 | 4 |
| | $CaCl_2$ | 600 | - | - | - |
| nmGCAP-1 | $CaCl_2$ | 300 | 0.026 | 2.0 | 1.7 |
| with S #71 * | EGTA | 600 | + 0.018 | 1.1 | 1.0 |
| | EGTA | 300 | 0.066 | 4.6 | 4 |
| | $CaCl_2$ | 600 | - | - | - |

* The concentration of protein was 5 μM, and the concentrations of peptides were 50 μM.

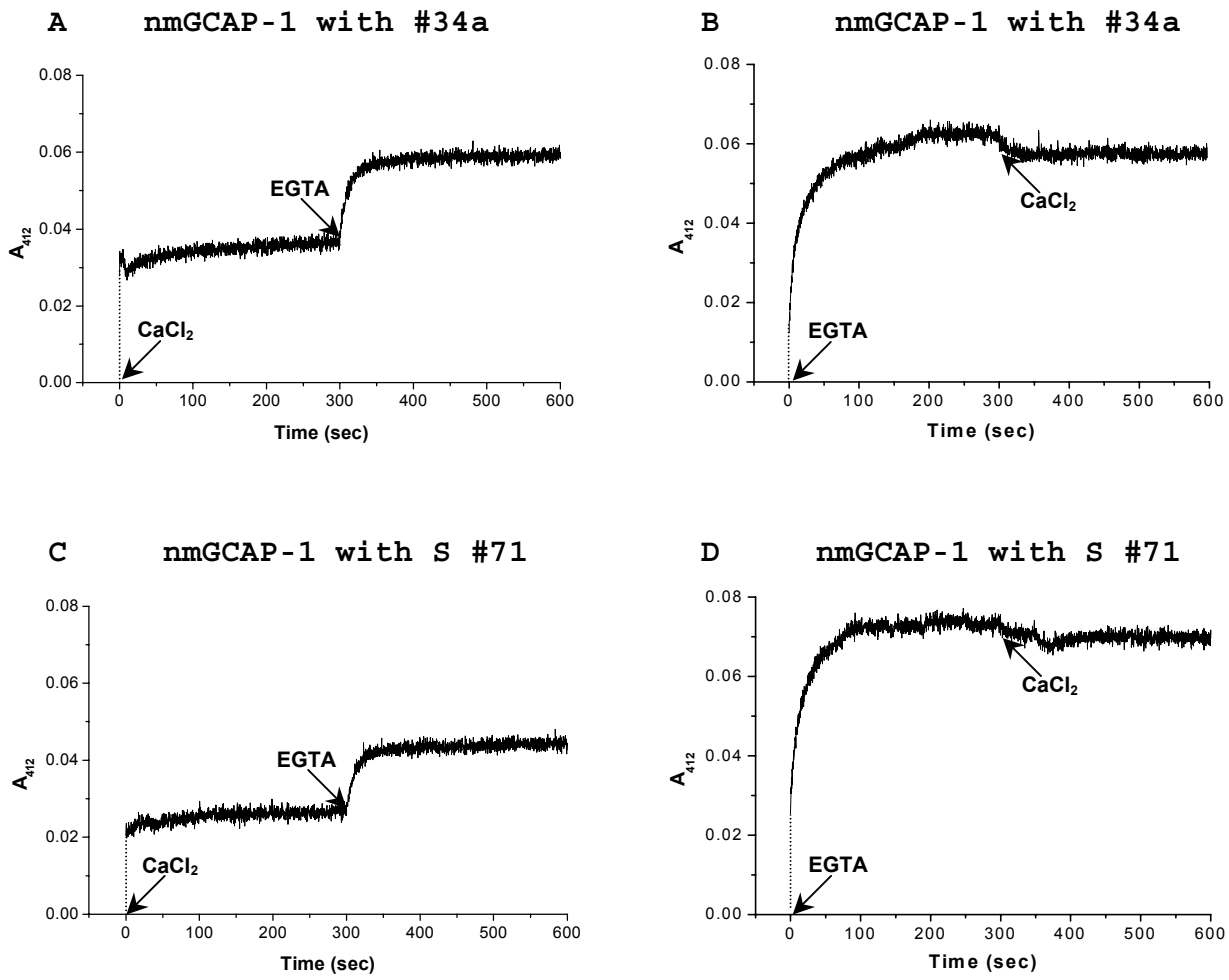


**FIG. 3.25.** Cysteine reactivity of 5 μM nmGCAP-1 towards DTNB in the presence of peptides. ***A.*** DTNB reactivity was measured in the presence of 50 μM #34a. The first 300 sec were reacted in the presence of $CaCl_2$ and the following 300 sec in the presence of EGTA. ***B.*** The reverse injection in the presence of #34a. ***C.*** Reactivity with DTNB with the injection of $CaCl_2$ and then injection of EGTA in the presence of 50 μM S #71. ***D.*** The reverse injection in the presence of 50 μM S #71.

**TABLE 3.15** Summary of cysteine reactivities of triple mutants of GCAP-1 in the presence of the peptide #34a

| Type | Treatment | Time (sec) | $A_{412}$ | [-SH] (μM) | No. of –SH (mole/protein) | Reactivity |
|---|---|---|---|---|---|---|
| CAAA * | $CaCl_2$ | 300 | 0.037 | 2.8 | 0.6 | relatively fast |
| | EGTA | 600 | - | - | - | - |
| ACAA * | $CaCl_2$ | 300 | 0.031 | 2.3 | 0.5 | slow |
| | EGTA | 600 | - | - | - | - |
| AACA * | $CaCl_2$ | 300 | - | - | - | - |
| | EGTA | 600 | 0.050 | 3.5 | 0.7 | fast |
| AAAC * | $CaCl_2$ | 300 | 0.078 | 5.5 | 1.1 | fast |
| | EGTA | 600 | - | - | - | - |

* The protein concentrations of each protein were 5 μM and the peptide concentration was 50 μM.

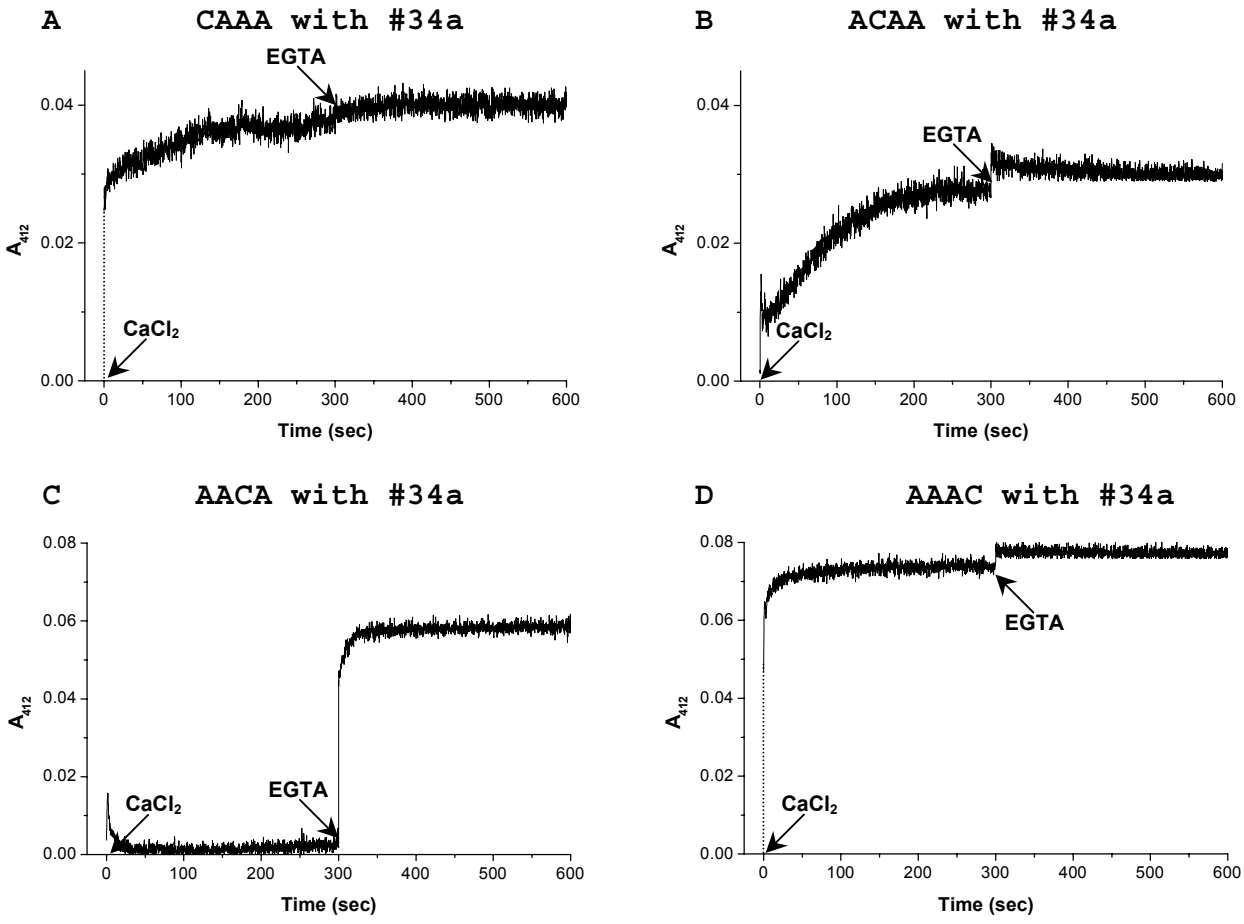


**FIG. 3.26.** Cysteine reactivity of the triplet cysteine mutants of GCAP-1 towards DTNB in the presence of peptide #34a. ***A.*** Reactivity of 5 μM CAAA in the presence of $CaCl_2$. ***B.*** Reactivity of 5 μM ACAA in the presence of $CaCl_2$. ***C.*** Reactivity of 10 μM AACA in the presence of EGTA. ***D.*** Reactivity of 5 μM AAAC in the presence of $CaCl_2$.

**TABLE 3.16** Summary of cysteine reactivities of triple mutants of GCAP-1 in the presence of the peptide S #71

| Type | Treatment | Time (sec) | $A_{412}$ | [-SH] (μM) | No. of –SH (mole/protein) | Reactivity |
|---|---|---|---|---|---|---|
| CAAA * | $CaCl_2$ | 300 | 0.037 | 2.8 | 0.6 | fast |
| | EGTA | 600 | - | - | - | - |
| ACAA * | $CaCl_2$ | 300 | 0.024 | 1.8 | 0.4 | slow |
| | EGTA | 600 | - | - | - | - |
| AACA * | $CaCl_2$ | 300 | - | - | - | - |
| | EGTA | 600 | 0.051 | 3.6 | 0.7 | fast |
| AAAC * | $CaCl_2$ | 300 | 0.070 | 5.0 | 1.0 | fast |
| | EGTA | 600 | - | - | - | - |

* The protein concentrations of each protein were 5 μM and the peptide concentration was 50 μM.

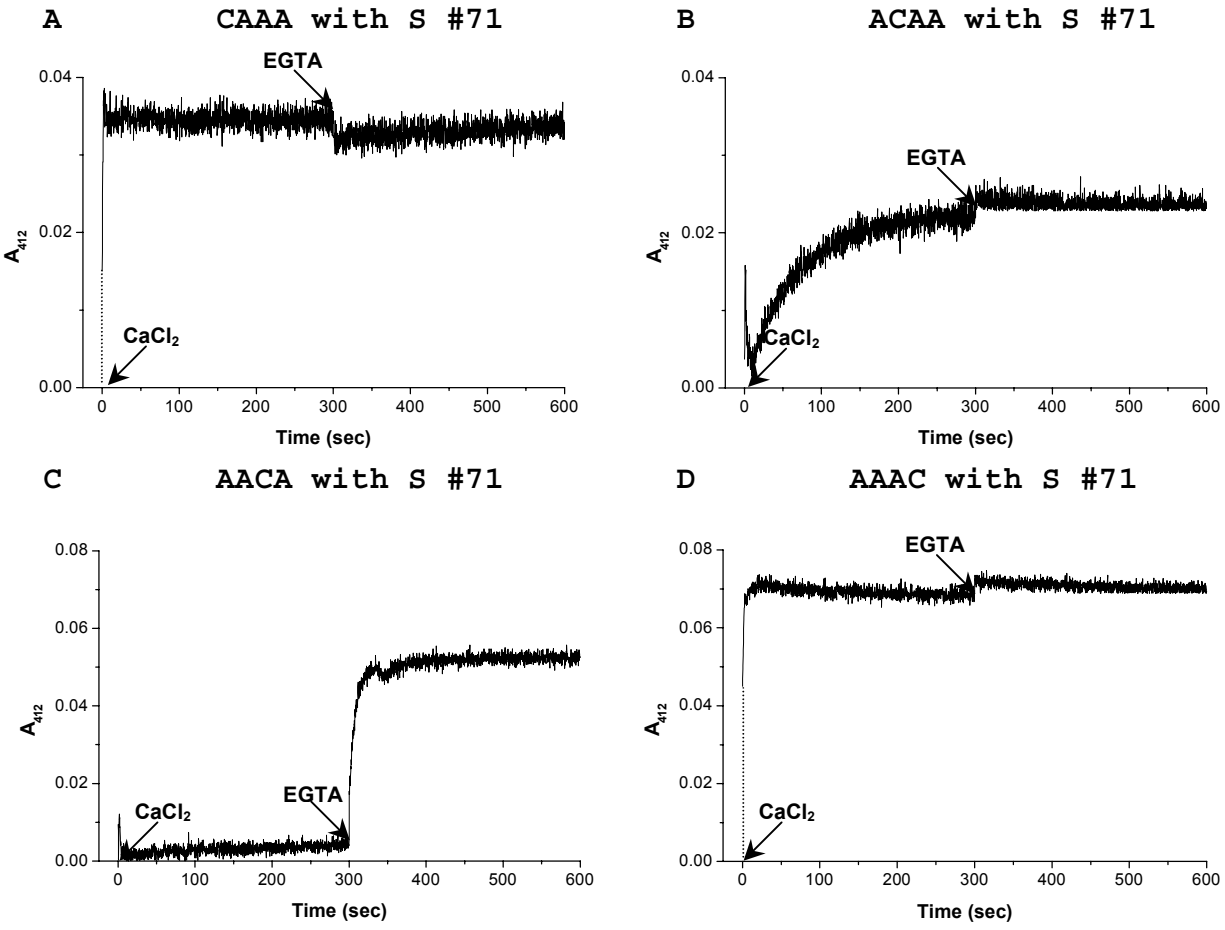


**FIG. 3.27.** Cysteine reactivity of the triplet cysteine mutants of GCAP-1 towards DTNB in the presence of peptide Sokal #71. ***A.*** Reactivity of 5 μM CAAA in the presence of $CaCl_2$. ***B.*** Reactivity of 5 μM ACAA in the presence of $CaCl_2$. ***C.*** Reactivity of 10 μM AACA in the presence of EGTA. ***D.*** Reactivity of 5 μM AAAC in the presence of $CaCl_2$.

### 3.5.2 Surface Plasmon Resonance (SPR) Studies

Surface plasmon resonance spectroscopy is suitable for real-time studies of molecular interactions, and was therefore chosen to study binding between GCAP-1 and ROS-GC1 peptides. The target domains of GCAP-1 in ROS-GC1, peptide #34a and peptide S #71, are located in the JMD and CCD, respectively. Previous attempts to study the interaction of immobilized GCAP-1 and hypothetical target domains of ROS-GC1 resulted in sensorgrams that were difficult to analyze. Due to the presence of four cysteines in wild-type GCAP-1, thiol coupling led to a heterogeneous surface [58]. The advantage of the triple mutants is that they can be used for selective immobilization on the sensor surface via a single cysteine. Successful immobilization of triple cysteine mutants of GCAP-1 was achieved by thiol disulfide exchange reaction. An example for the immobilization of the triple mutants of GCAP-1 on the sensor chip is shown in Fig. 2.5 *B* (refer to Methods 2.5.3). Changes in resonance units (RU) correspond to changes in bulk refractive index during the steps of activation, immobilization, and deactivation. Covalent attachment of the protein to the dextran layer (CM5) resulted in ΔRU of 1528–7691 RU which corresponds to 0.07–0.33 pmol/mm$^2$ (1000 RU ≅ 1 μg protein/mm$^2$). Figure 3.28 shows how triplet cysteine mutants of GCAP-1 are immobilized on SPR chips.

Peptides #34a and S #71 bound to all four triple mutants in a concentration dependent manner. Interestingly, binding was observed in the presence and absence of $Ca^{2+}$ (see Figs. 3.29–32). Sensorgrams were only evaluated by the determination of $RU_{eq}$ at the end of the injection time (black bar). Attempts to fit the data according to a simple Langmuir binding model (monoexponential 1:1 binding model, see the Biacore manual) failed. More complex binding models were not applied because experimental evidence supporting their use is so far lacking. The values obtained from the SPR study are summarized in Table 3.17.

Binding affinities were in all cases rather low, as indicated by the apparent binding constants ($K_{1/2}$ in Table 3.17) in the micromolar to millimolar range (panels *A–D*). Inspection of the sensorgrams and of the data evaluation (panel *E–H*) showed that, in some cases, no saturation during a titration experiment was achieved (3.29 *A*, 3.30 *B*, 3.30 *D*, 3.31 *F*, 3.32 *B* and *D*). Therefore, apparent binding constants obtained by fitting (panel *E–H*) were very high (millimolar range). At high peptide concentration, nonspecific binding of peptides to the sensor chip surface might have occurred and contributed to the amplitude of sensorgrams. This is concluded from control experiments with immobilized calmodulin and recoverin

which showed binding of peptides despite the fact that these proteins do not interact with ROS-GC1.

Another striking result is that $K_{1/2}$ values showed large differences when different triple mutants were compared. Interestingly, in the absence of $Ca^{2+}$ both peptides interacted with all mutants with rather similar apparent binding constants (0.6–1.2 mM for peptide #34a and 0.86–1.1 mM for peptide S #71 in Table 3.17). In the presence of $Ca^{2+}$, large differences were seen. Values for $K_{1/2}$ differed for peptide #34a from 0.78 mM to 8.3 mM and for peptide S #71 from 1.5 mM to 15.5 mM. The decrease of apparent affinity was most striking in the interaction of mutant ACAA with S #71 and in the interaction of mutant AACA with peptide #34a.

In conclusion, the SPR studies indicated that the site of immobilization had no influence on the interaction of mutants with #34a and S #71 in the absence of $Ca^{2+}$. However, in the presence of $Ca^{2+}$ the site of immobilization via a single cysteine can significantly disturb the binding process which leads to a decrease in affinity. The observed low affinities measured with single peptides is consistent with the view that GCAP-1 interacts with ROS-GC1 via a multipoint attachment [59]. Single peptides will only display a low affinity site for GCAP-1. However, in the whole protein, at least two or possibly more binding sites will create a high affinity interaction site.

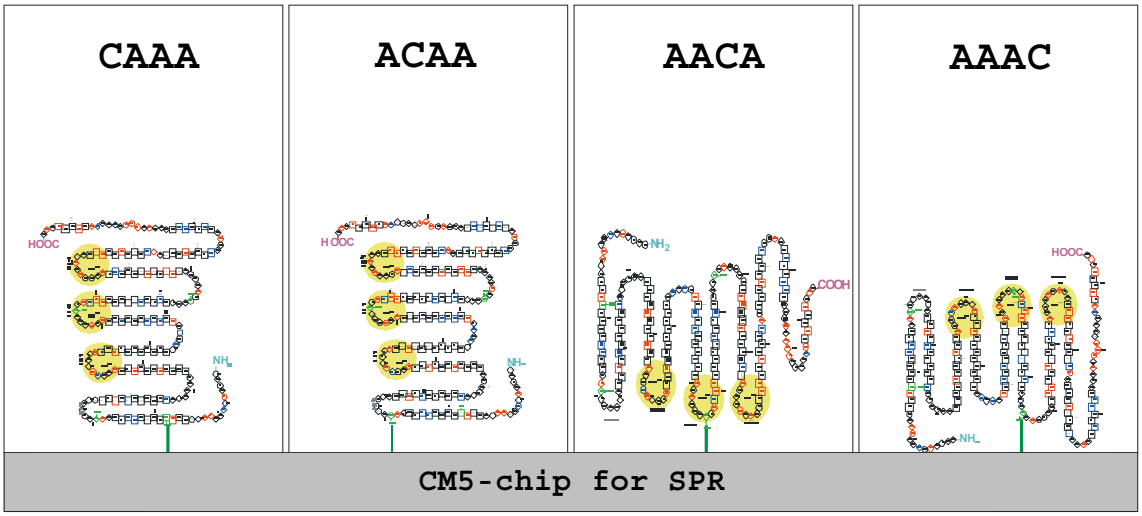


**FIG. 3.28.** A speculative description of triplet cysteine mutants of GCAP-1 on SPR chips by thiol couplings. EF-hands with calcium binding sites are highlighted in yellow. The N-terminus is represented in cyan, and the C-terminus in magenta. The thiol coupling of cysteine residues of proteins on activated carboxylated dextran (CM) chip is shown with green lines.

**TABLE 3.17** Summary of SPR studies on the interaction of the triple cysteine mutants of GCAP-1 with the peptide #34a and the peptide S #71

| Type | Peptide | Buffer | $RU_{max}$ * (RU) | $K_{1/2}$ [Peptide] (µM) |
|---|---|---|---|---|
| CAAA * | #34a | EGTA | 10014 | 1225 |
| | | $CaCl_2$ | 8505 | 778 |
| | S #71 | EGTA | 6314 | 1113 |
| | | $CaCl_2$ | 5130 | 5130 |
| ACAA * | #34a | EGTA | 10782 | 639 |
| | | $CaCl_2$ | 15812 | 2260 |
| | S #71 | EGTA | 8010 | 928 |
| | | $CaCl_2$ | 432908 | 15501 |
| AACA * | #34a | EGTA | 9391 | 771 |
| | | $CaCl_2$ | 182145 | 8279 |
| | S #71 | EGTA | 6809 | 922 |
| | | $CaCl_2$ | 8031 | 1553 |
| AAAC * | #34a | EGTA | 9117 | 1018 |
| | | $CaCl_2$ | 266711 | 6474 |
| | S #71 | EGTA | 5277 | 860 |
| | | $CaCl_2$ | 7504 | 1587 |

* The maximal values of the curve fitting using the Hill equation from sensorgrams

**The general description for the figures of the surface plasmon resonance studies: Left panels, (*A–D*);** one representative set of sensorgrams for the real time interaction analysis of the peptide #34a and the peptide S #71 to immobilized triple cysteine mutants of GCAP-1, (CAAA, ACAA, AACA, and AAAC). Immobilization densities are indicated in the corresponding figure legends. Sensorgrams were recorded with varying concentrations of peptides (50–2000 µM) in the running buffer during the association phase. Dissociation of GCAP-1/peptides interaction was initiated by omitting peptides in the buffer. Horizontal filled black bars represent the presence of peptides in the running buffer. Horizontal gray bars represent flow of running buffer in the absence of peptides. Presence or absence of $Ca^{2+}$ in the running buffer is always indicated. **Right panels, (*E–H*);** $R_{eq}$ values versus the varying concentration of peptides were plotted using data of the sensorgrams in the left panels. Data point represent the mean and SD values from one to three independent experiments. The curves were fitted in the data using the Hill equation. Main results of the fitting procedure are seen in the inset boxes.

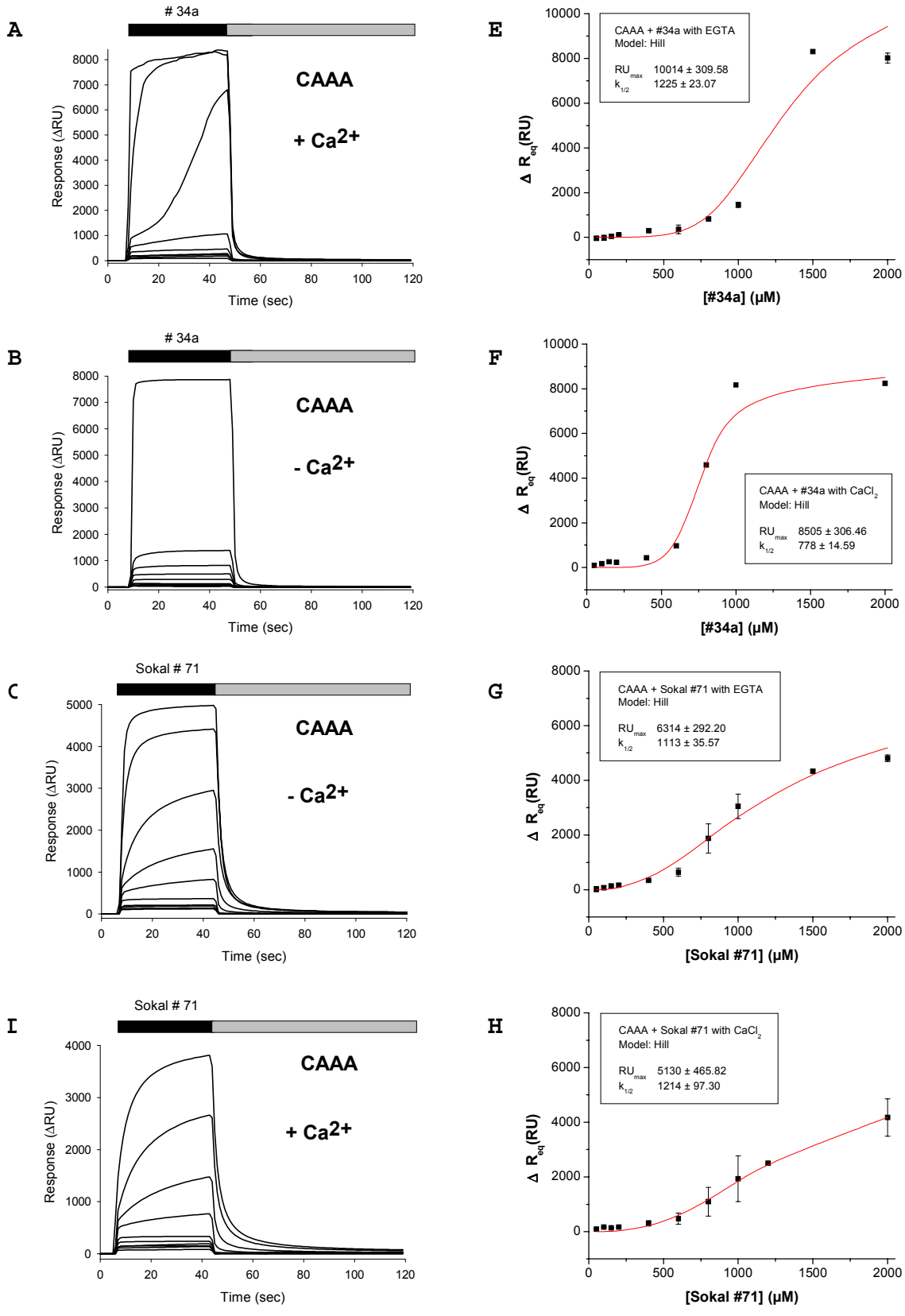


**FIG. 3.29.** Real time interaction analysis of peptides to immobilized CAAA and the plots $R_{eq}$ values vs. [peptide]. Covalent attachment of CAAA on the dextran layer (CM5) resulted in ΔRU of 1528 RU.

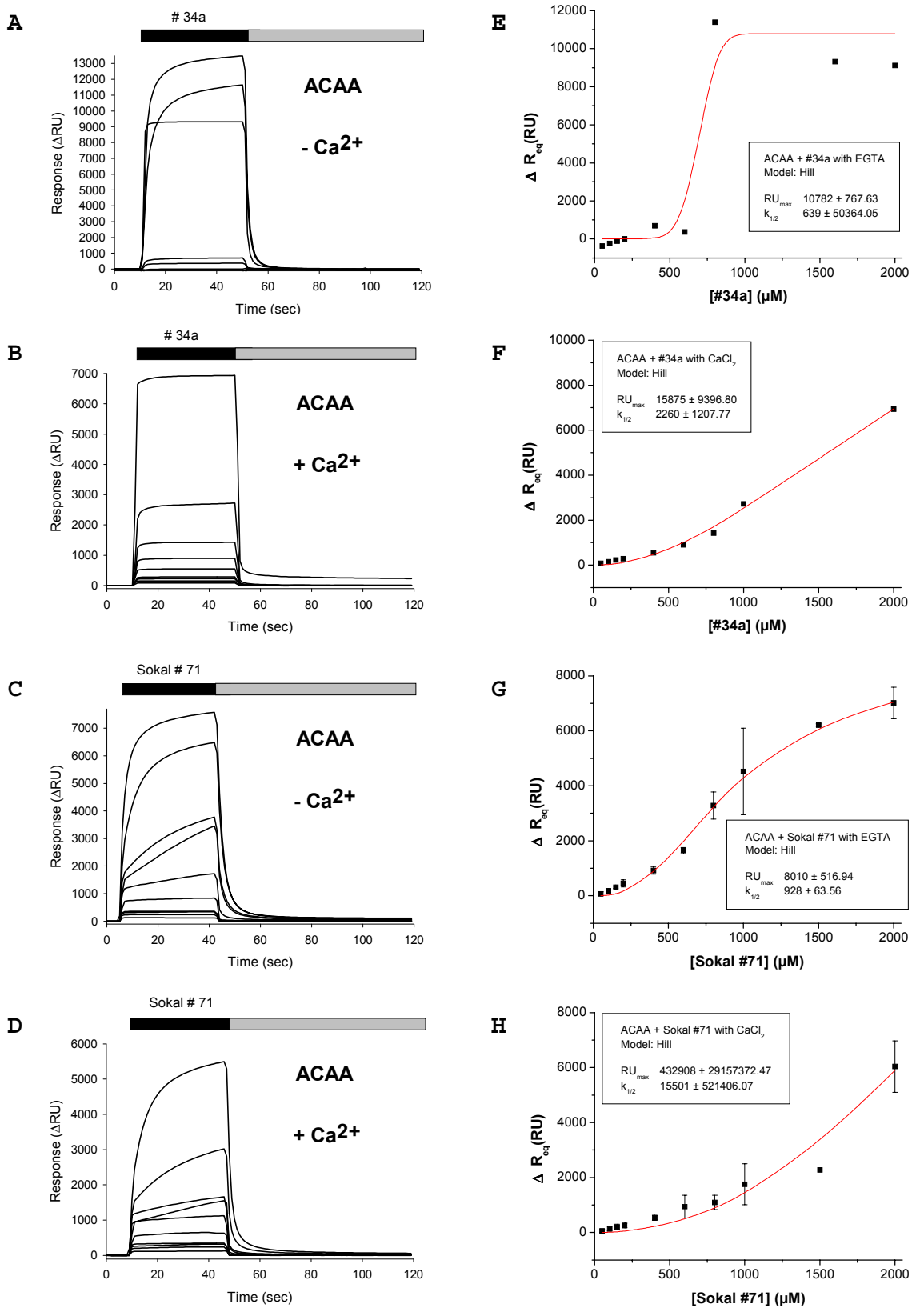


**FIG. 3.30.** Real time interaction analysis of peptides to immobilized ACAA and the plots $R_{eq}$ values vs. [peptide]. Covalent attachment of ACAA on CM5 resulted in ΔRU of 7691 RU.

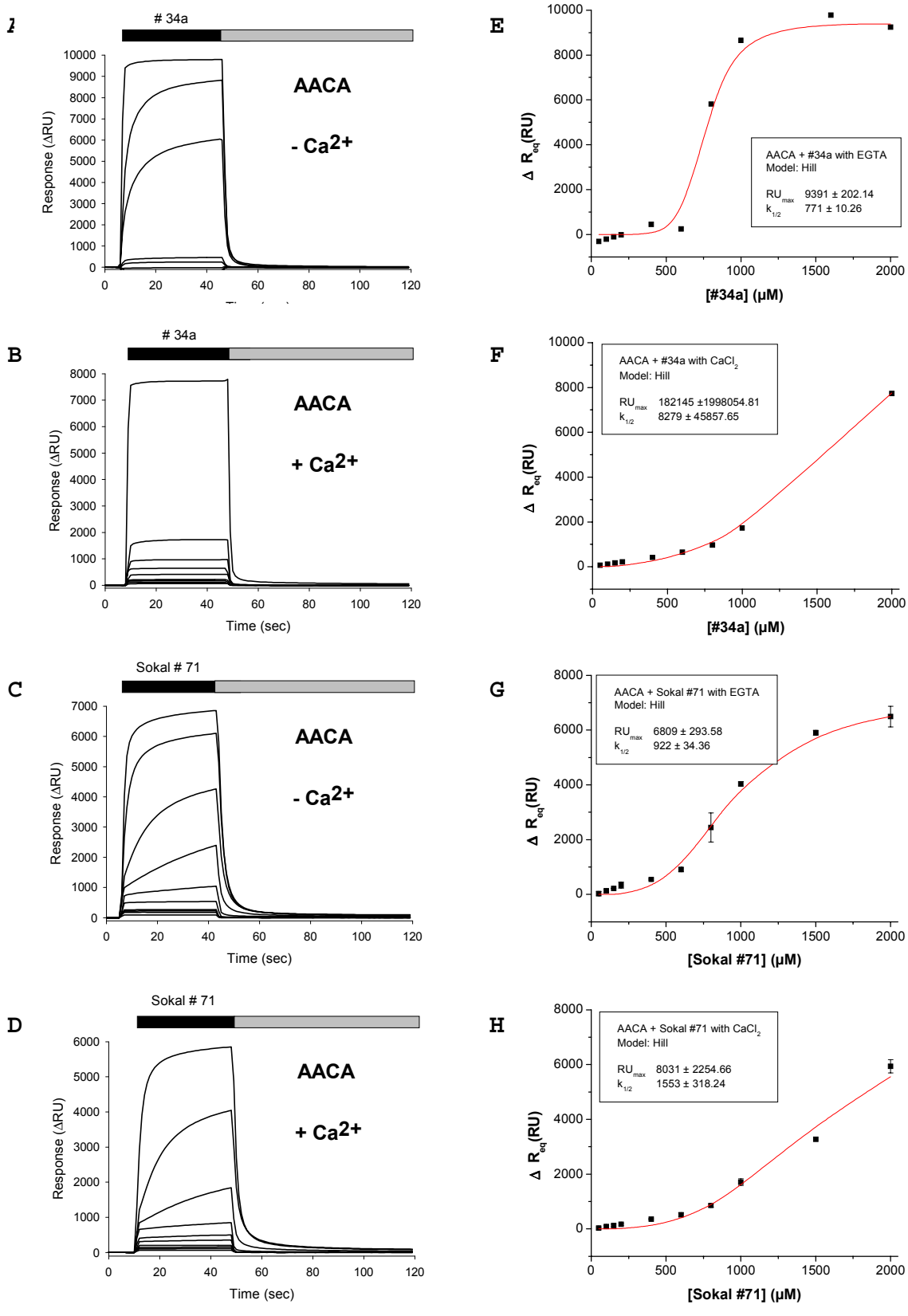


**FIG. 3.31.** Real time interaction analysis of peptides to immobilized AACA and the plots $R_{eq}$ values vs. [peptide]. Covalent attachment of AACA on CM5 resulted in ΔRU of 4973 RU.

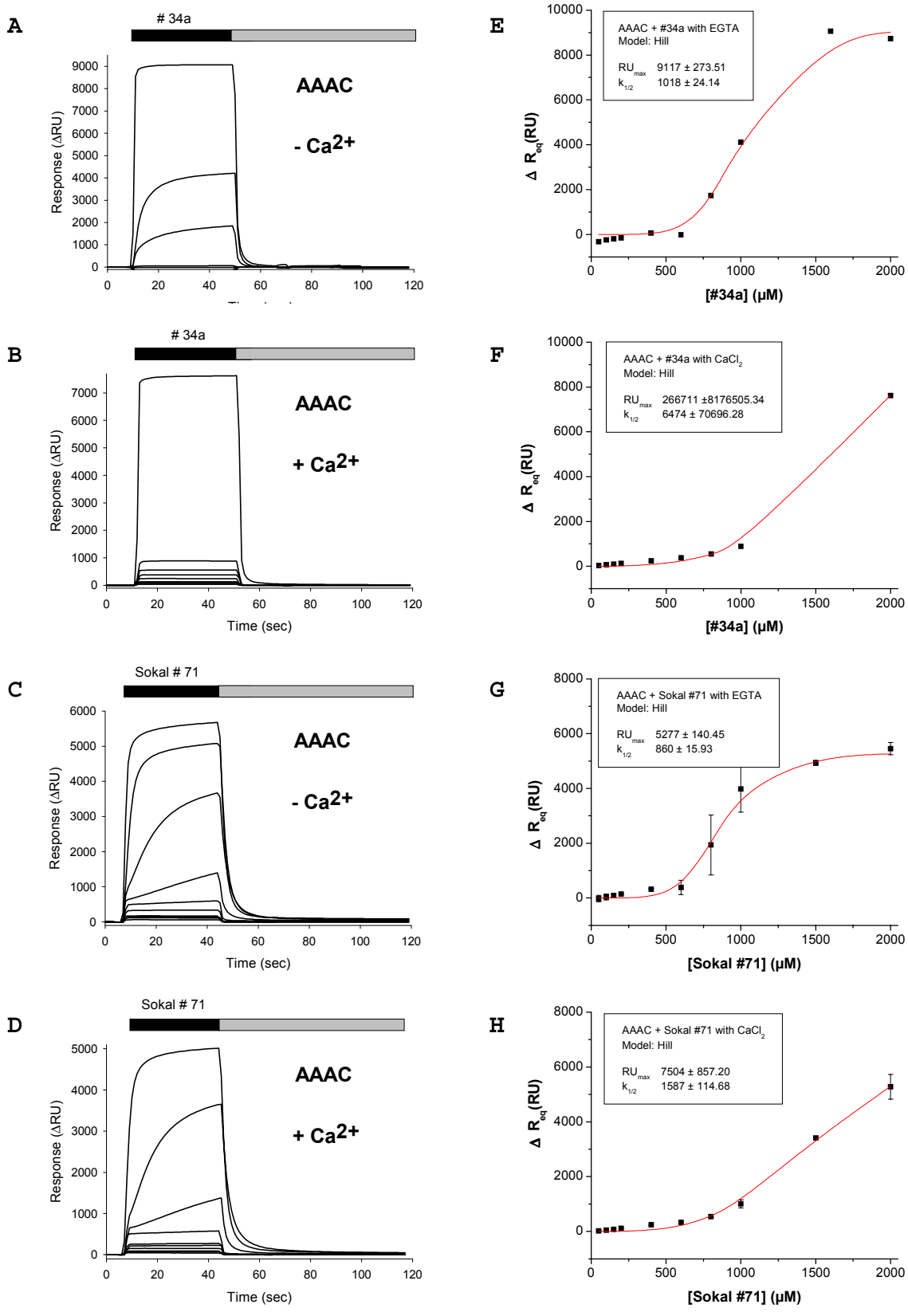


**FIG. 3.32.** Real time interaction analysis of peptides to immobilized AAAC and the plots $R_{eq}$ values vs. [peptide]. Covalent attachment of AAAC on CM5 resulted in ΔRU 2014 RU.

# 4. DISCUSSION

In this dissertation, each of the four cysteines of GCAP-1 was substituted with alanine using several mutagenesis strategies. GCAP-1 and its cysteine mutants were overexpressed in *E. coli* and purified by gel filtration chromatography and anion exchange chromatography. In order to explain the functional and structural properties of GCAP-1, the biochemical and biophysical properties of three types of wild-type GCAP-1 (nonmyristoylated GCAP-1, partially myristoylated GCAP-1, and myristoylated $D^{6}S$-GCAP-1) and nine types of cysteine mutants of GCAP-1 (four single-cysteine-exchange mutants, four triple-cysteine-exchange mutants, and one quad-cysteine-exchange mutant) were investigated by analytical HPLC, MALDI-TOF-MS, gel electrophoresis, analytical SEC, CD spectroscopy, UV/VIS spectrophotometer, and SPR spectroscopy. The stimulation of ROS-GC1 by wild-type GCAP-1 and its cysteine mutants was compared. The $Ca^{2+}$-dependent conformational changes of GCAP-1 and its cysteine mutants were monitored. The functional interaction of GCAP-1 with the peptides from ROS-GC1 were tested by the chemical modification of the cysteine residues and by spectroscopic methods.

## 4.1 Structural Aspects of GCAP-1

Guanylate cyclase activating protein 1 (GCAP-1) is a $Ca^{2+}$-binding protein from vertebrate photoreceptors. It contains three distinct functional EF-hands (EF-2, EF-3, and EF-4) and one EF-hand-related structure (EF-1). GCAP-1 contains a consensus sequence recognized by the N-terminal myristoyl transferase which transfers a myristoyl group on the N-terminus [74]. GCAP-1 has four cysteines. The first cysteine $Cys^{18}$ is located in the α-helix of non-functional EF-1, $Cys^{29}$ in the non $Ca^{2+}$-binding loop of EF-1, $Cys^{106}$ in the loop of the functional EF-3, and the last $Cys^{125}$ between the functional EF-3 and EF-4. Figure 4.1 presents a speculative illustration of the two-dimensional structure of GCAP-1, highlighting three functional EF-hands, myristoylation on its N-terminus, and four cysteine residues. Figure 4.2 shows an alignment of GCAP-1 from various species to elucidate the conservative amino acid sequences.

The canonical EF-hand consists of a consensus sequence of 29 amino acid residues. EF-hand is a helix-loop-helix motif, i.e. an α-helix (helix E, residues 1–10), a loop wrapped around the $Ca^{2+}$ ion (residues 10–21), and a second α-helix (helix F, residues 19–29). The name for E-F hand originates from parvalbumin, whose helices labeled E and F contained the first identifiable $Ca^{2+}$-binding motif of this kind [126]. The $Ca^{2+}$ ion is coordinated by residues within a loop region that separates two helices and forms a pentagonal bipyramid with six to seven oxygen atoms and with the surrounding water molecules. The $Ca^{2+}$-binding loop is composed of the side chains of residues 10 (*x*), 12 (*y*), 14 (*z*), 16 (-*y*), 18 (-*x*), and 21 (-*z*). The ligand at vertex -*y* is the carbonyl oxygen of residue 16. The carboxyl side chains of aspartate at the first position *x* and glutamate at the last position -*z* of an EF-hand are essential for coordinating a $Ca^{2+}$ ion. A number of side chains (*n*) form a hydrophobic core between the α-helices [298].

A number of recent structural studies have revealed substantial differences in $Ca^{2+}$-induced conformational changes among the EF-hand domains of some $Ca^{2+}$-binding proteins [128]. Comparison of the three-dimensional structures of these proteins determined by NMR spectroscopy or X-ray crystallography brings information to understand the structure/function relationships in GCAP-1. GCAP-1 and GCAP-2 have 40% sequence homology, but most of this homology resides in $Ca^{2+}$-binding EF-hands. The C- and N-termini of GCAP-1 and GCAP-2 are quite different [129]. The sequence homologies of GCAP-1 with recoverin and neurocalcin are 34% and 41%, respectively [130,131] (see Fig. 1.6 and Table 1.3). A superposition of the main chain structures of nonmyristoylated, $Ca^{2+}$-bound GCAP-2 (red), recoverin (cyan), and neurocalcin (green) are shown in Fig. 4.3 *A*.

Both C- and N-terminal domains of calmodulin undergo large structural rearrangements upon binding of $Ca^{2+}$, from the closed conformation in which the two helices of each EF-hand are almost anti-parallel to the open conformation in which the two helices are more perpendicular. Several $Ca^{2+}$-binding proteins, the $Ca^{2+}$-induced transition from closed to open has been analyzed [132]. It is possible that GCAP-1 is closed upon $Ca^{2+}$-binding and open in the absence of $Ca^{2+}$.

Recoverin has a concave hydrophobic surface formed by residues in EF-1 and EF-2. The nonpolar aliphatic surface residues emerging from the second helix of EF-4 of a symmetry-related molecule fit snugly into this hydrophobic patch. These exposed nonpolar residues could form a binding site for the covalently attached myristoyl group of retinal recoverin or for a target protein [80].

The three-dimensional structure of GCAP-2 determined by NMR spectroscopy is shown in Fig. 4.3 *B* [129]. The overall main chain structure of GCAP-2 is similar to that of $Ca^{2+}$-bound recoverin except for structural differences near the N-terminus and the binding site of $Ca^{2+}$ in EF-4. An exposed hydrophobic patch of residues belonging to EF-1 and EF-2 may play a role in regulating ROS-GC. GCAP-2 is a compact protein (radius of gyration, 17 Å) made of two domains separated by a flexible linker. EF-1 and EF-2 interact to form the N-terminal domain, and EF-3 and EF-4 form the C-terminal domain. The first helix of EF-2 packs against the helices of EF-3 at the interface between the two domains, thereby forming a cleft. Two additional helices occur near the N-terminus and C-terminus. There are two pairs of short strands at the interfaces between pairs of EF-hands. The linker between the domains is U-shaped, which positions the four EF-hands in a compact tandem array [129].

The loop of EF-1 does not bind a $Ca^{2+}$ ion, i.e. it is a non-functional EF-hand. EF-1 is distorted from a favorable $Ca^{2+}$-binding geometry by $Cys^{29}$ and $Pro^{30}$ at position 13 of the loop. This is not suitable for ligating $Ca^{2+}$ because the bulky sulfhydryl group sterically blocks the entry of $Ca^{2+}$.

The region around the EF-3 motif becomes more exposed to solvent in the $Ca^{2+}$-free form of GCAP-1 in consensus to the results of Sokal et al. using Trp fluorescence spectroscopy [133]. In the $Ca^{2+}$-binding loop of EF-3, a significant reorientation occurs when allowed to coordinate with $Ca^{2+}$ or to interact with ROS-GC1 as $Ca^{2+}$-free form. The reorientation results in a dramatic change, e.g. the exposure of either the loop in EF-3 or the of hydrophobic residues in EF-2 and EF-3 (see Fig. 4.1). These have been proposed as key regions for the interaction with ROS-GC1, providing an attractive target-recognition site or close spatial proximity.

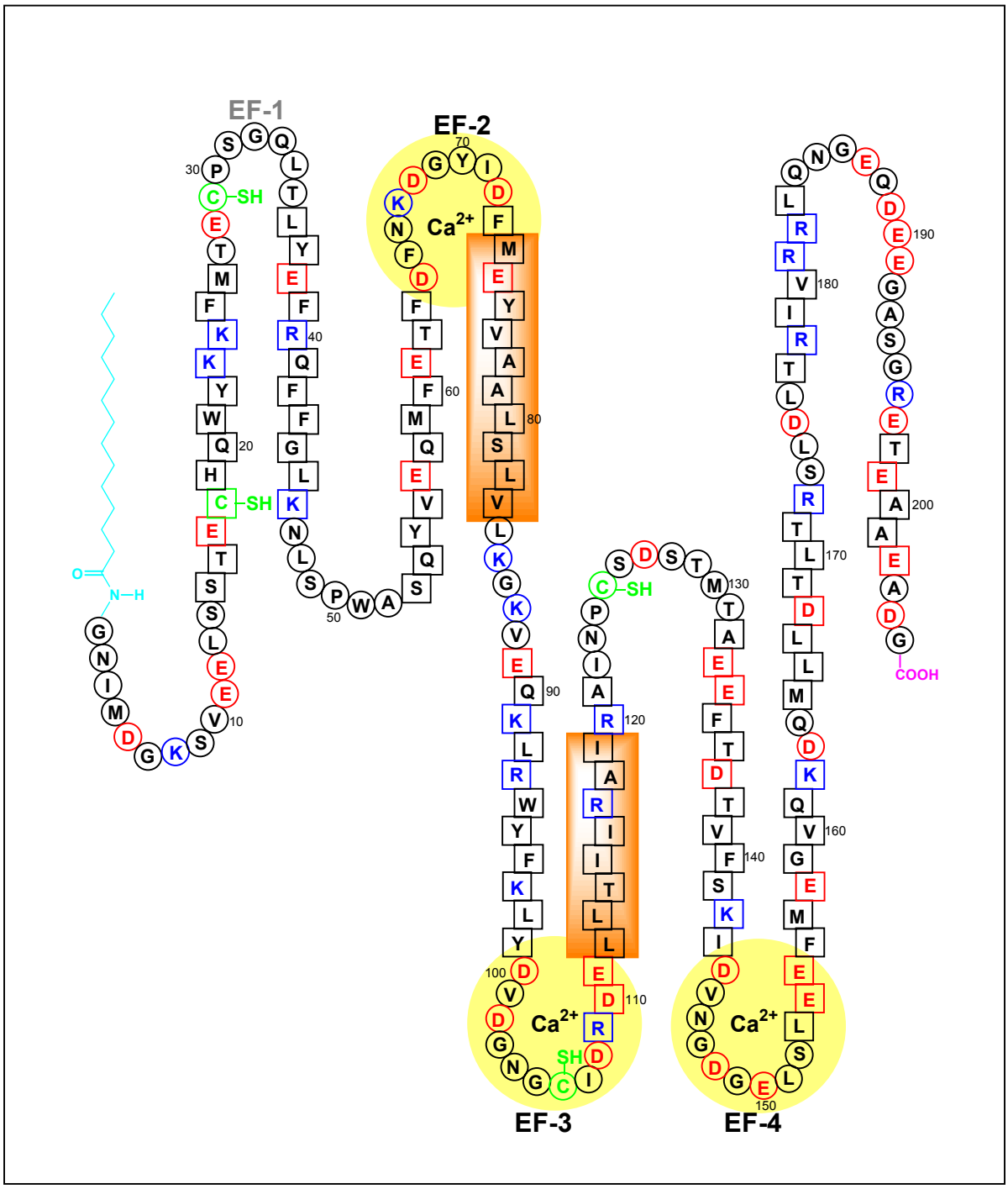


**FIG. 4.1.** A speculative description of the two-dimensional structure of GCAP-1. Basic amino acids are shown in blue, acidic amino acids in red, neutral amino acids in black, cysteine residues in green, the N-terminal myristoyl group in cyan, and the C-terminus in magenta. Squares depict amino acids contributing to putative α-helices. EF-hands with $Ca^{2+}$-binding sites are highlighted with yellow color. The hydrophobic patches are highlighted with the scarlet-colored boxes.

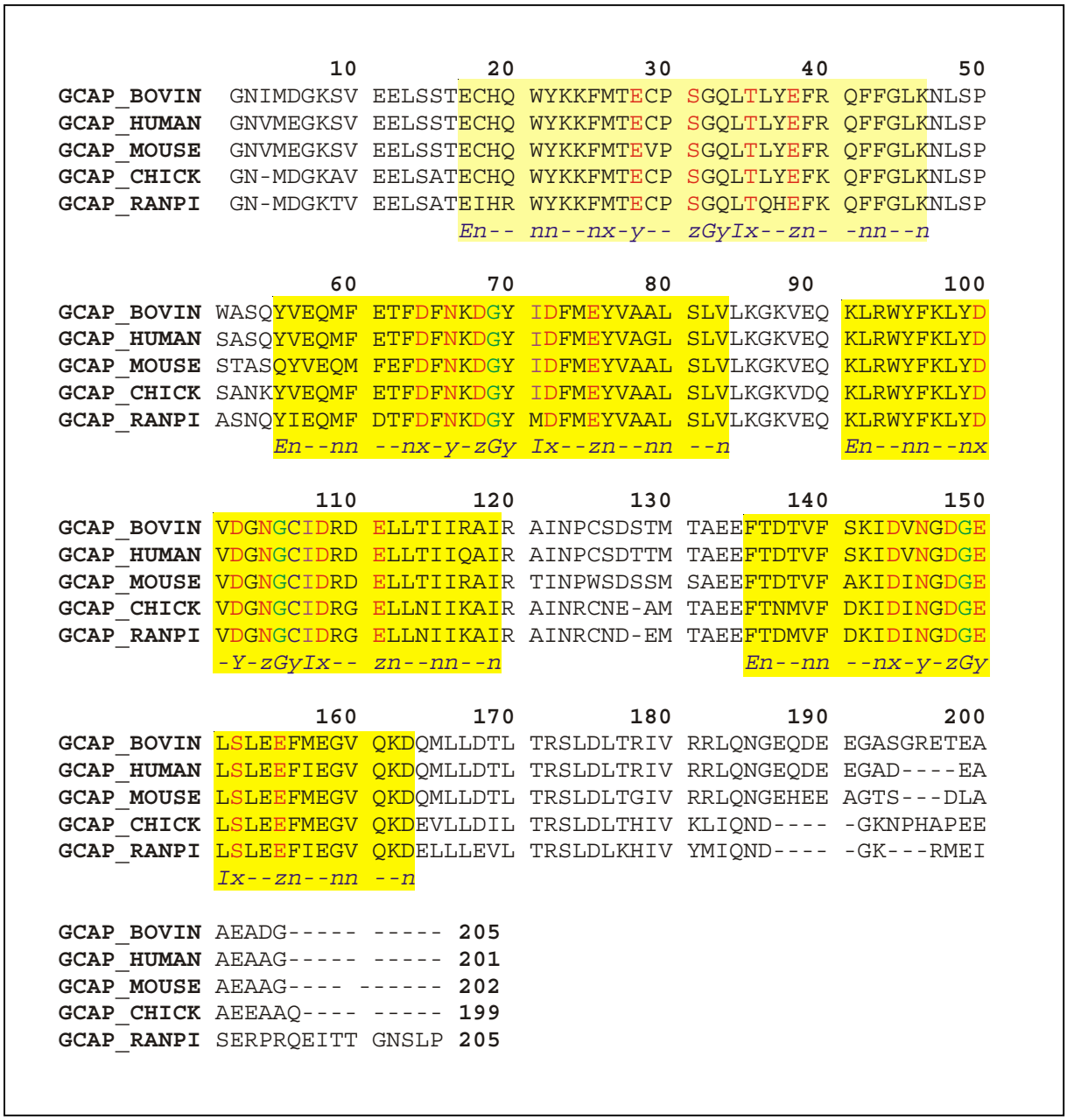


**FIG. 4.2.**Alignment of GCAP-1 from the various species. GCAP_BOVIN (the access number: P46065), GCAP_HUMAN (P43080), GCAP_MOUSE (P43081), GCAP_CHICK (P79880), and GCAP_RANPI (O73761). The sequence of each protein was from SWISS-PROT and TrEMBL Protein Sequence Databases (http://expasy.ch/cgi-bin/sprot-search-ac). The sequence alignment was carried out using CLUSTAL W (1.8) Multiple Sequence Alignment Software in internet. The 29-residue EF-hand motifs are highlighted with yellow color. Consensus sequence for $Ca^{2+}$-binding loops in EF-hands is shown in colored letters. The helix-loop-helix regions with the characterized letters are shown underneath sequences. The $Ca^{2+}$-binding loop is composed of the side chains of residues 10 (*x*), 12 (*y*), 14 (*z*), 16 (*y*), 18 (*x*), and 21 (*z*). A number of side chains (*n*) form a hydrophobic core between the α-helices.

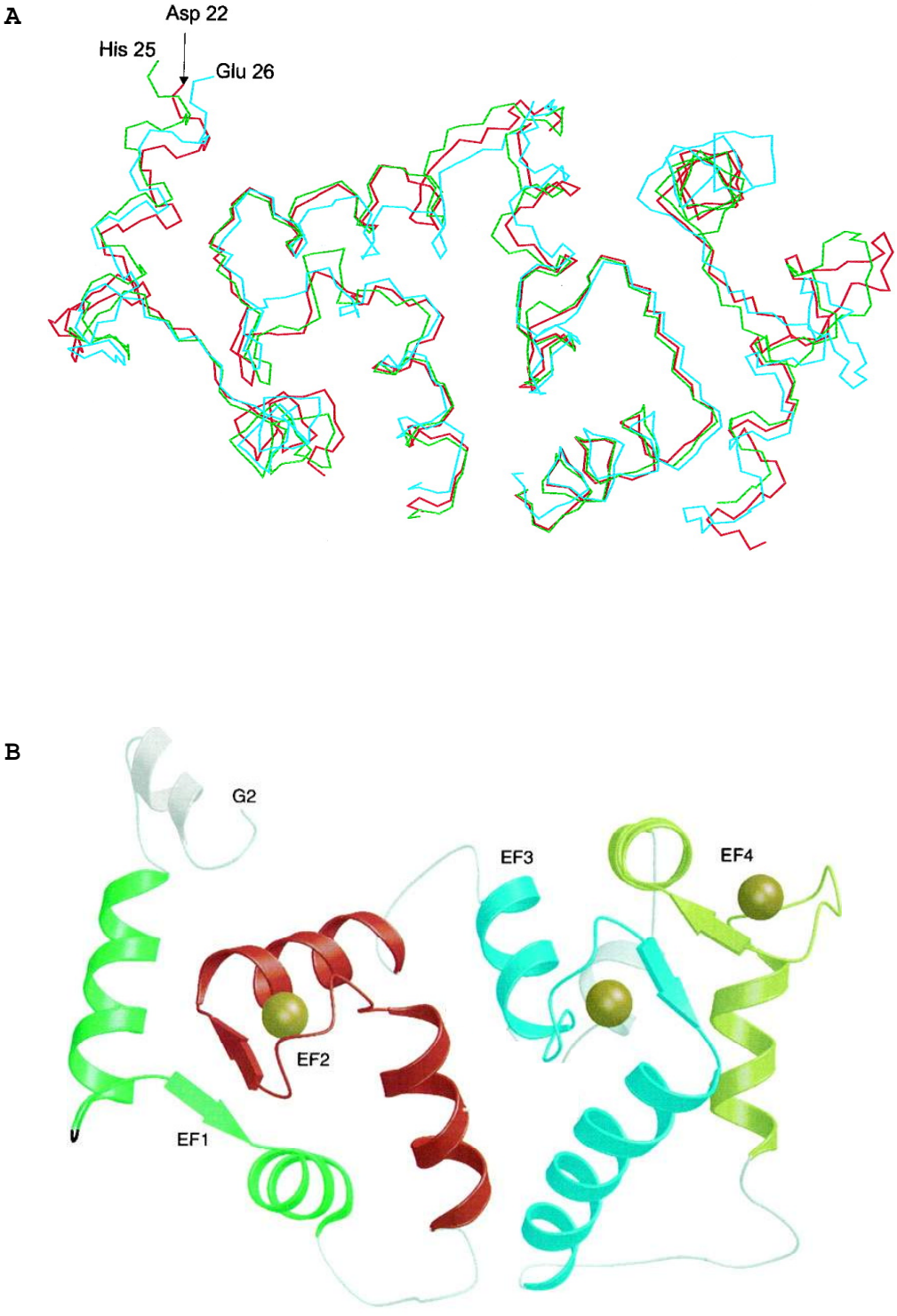


**FIG. 4.3.** The know three-dimensional structure of some $Ca^{2+}$-binding proteins. ***A.*** Superposition of the main chain structures of the EF-hand motifs of $Ca^{2+}$-bound nonmyristoylated GCAP-2 (red, PDB id 1jba), recoverin (cyan, PDB id 1jsa), and neurocalcin (green, PDB id 1bjf) [129]. ***B.*** Schematic ribbon representation of the energy-minimized average NMR structure of nonmyristoylated GCAP-2 from Ames et al. [129].

## 4.2 $Ca^{2+}$-dependent Conformational Changes of GCAP-1

A comparison of the $Ca^{2+}$-bound and $Ca^{2+}$-free GCAP-1 is shown in Table 4.1.

From SDS-PAGE the $Ca^{2+}$-bound and $Ca^{2+}$-free forms of GCAP-1 showed different electrophoretic mobility than predicted by their apparent molecular weights. The $Ca^{2+}$-free form of GCAP-1 migrates more slowly than the $Ca^{2+}$-bound form, whereas complexing $Ca^{2+}$ with 2 mM EGTA in the protein sample causes a gel shift from approx. 21 kDa to approx. 26 kDa. This abnormal mobility can be explained by a more compact structure and less negative charge for GCAP-1 as a result of $Ca^{2+}$-binding, causing faster migration (see Results 3.2.4).

All protein samples of wild-type GCAP-1 and its cysteine mutants with $Ca^{2+}$ showed the same $Ca^{2+}$-dependent gel-shifts of about 5 kDa (see Results 3.3.2). This result demonstrates that the mutations of the cysteine residues are not important for any $Ca^{2+}$-induced change in conformation of GCAP-1.

Comparison of the CD spectra of the $Ca^{2+}$-bound and $Ca^{2+}$-free forms of nonmyristoylated GCAP-1 demonstrates that it undergoes a significant conformational change upon $Ca^{2+}$-binding (see Fig. 3.7 *C*). The shapes of the two spectra are characteristic for a folded α-helical protein. The 8–15% enhancement of CD intensity and the decrease of α-helical content upon the $Ca^{2+}$-free form of GCAP-1 suggest that nonmyristoylated GCAP-1 has a lower degree of α-helicity in the absence of $Ca^{2+}$, i.e. less α-helical secondary structure than that in the presence of $Ca^{2+}$. In the case of nonmyristoylated GCAP-1, there are potential complications due to the limited solubility in the presence of calcium. Therefore, the change in CD intensity could arise from dimerization or aggregation. This observation is a consequence of $Ca^{2+}$-induced aggregation of the protein, since higher concentrations of calcium ultimately lead to precipitation.

Interestingly, the CD spectra of myristoylated GCAP-1 upon $Ca^{2+}$-binding differs from that of nonmyristoylated GCAP-1 (see above), myristoylated GCAP-2 [134], and myristoylated recoverin [135]. Under close scrutiny myristoylated GCAP-1 has more α-helical content in the absence of $Ca^{2+}$ than in the presence of $Ca^{2+}$ (see Results 3.2.3). The CD spectra of recoverin upon $Ca^{2+}$-binding are the same for both nonmyristoylated and myristoylated forms [135].

The unfolding curves indicating the thermal stability of GCAP-1 suggest that GCAP-1 is heat-resistant or thermophilic in the $Ca^{2+}$-bound form and that it easily loses α-helicity and leads to denaturation, aggregation, or precipitation of the protein in the $Ca^{2+}$-free form [136,137]

(see Results 3.2.3). It indicates that α-helices of GCAP-1 are stabilized by binding $Ca^{2+}$ ions. These results support the observed SDS-PAGE shift of GCAP-1 upon $Ca^{2+}$-binding. Even though the samples for SDS-PAGE were boiled, GCAP-1 has a different mobility with $Ca^{2+}$ than without $Ca^{2+}$.

Furthermore, the results of SEC and ND-PAGE suggested 1) that GCAP-1 prefers a monomeric form in the absence of $CaCl_2$ with a reducing agent in a fresh preparation, 2) that nonmyristoylated GCAP-1 can exist in a multimeric form in the presence of $CaCl_2$ without a reducing agent, and 3) that oxidation, lyophilization, and long-term storage of GCAP-1 can induce aggregation (see Results 3.2.5).

This aggregation phenomenon of GCAP-1 could be due to 1) some intra- or inter-molecular disulfide bonds (covalent homodimers), or 2) packing of hydrophobic patches between molecules (non-covalent homodimers). Since four cysteine residues do not form any intra disulfide bonds in GCAP-1, it is likely that disulfide bridges could instantly form between molecules, i.e. intermolecular-disulfide bonds (see Results 3.2.6). The most plausible residues in GCAP-1 to form these intermolecular disulfide bonds are $Cys^{29}$ and $Cys^{125}$ because in the presence of calcium, because $Cys^{106}$ is buried (see Results 3.2.7 and 3.4.2) and $Cys^{18}$ could be shielded by myristoylation (see below for further discussion). Aggregation occurs by specific interaction of certain conformations of folding intermediates rather than by nonspecific coaggregation of hydrophobic patches on folding intermediates in the $Ca^{2+}$-binding forms [138]. The rearrangement of the hydrophobic residues at high concentration of $Ca^{2+}$ could allow two molecules of GCAP-1 to form a dimer. This bulky dimer could obstruct the dimerization of ROS-GC1, which is a necessary condition for synthesizing cGMP from GTP (see Fig. 4.4). The monomer/dimer equilibrium may operate as a switch mechanism to change GCAP-1 function from an activator to inhibitor of ROS-GC1.

Another physiological function of dimerization of GCAP-1 could be to protect the protein from heat denaturation, damage by radical oxygen species, etc. Rudnicka-Nawrot et al. [139] observed that the $Ca^{2+}$-bound form of GCAP-1 is more stable to proteolysis than the $Ca^{2+}$-free form, which is consistent with the conclusion that $Ca^{2+}$ induces dimerization of GCAP-1 which results in less accessibility to a protease. Interestingly, GCAP-2 also undergoes a monomer/dimer switch [140]. However, the $Ca^{2+}$-dependence of this switch is opposite to what I observed in the case of GCAP-1. This difference could indicate that GCAP-1 and GCAP-2 control activity of ROS-GC1 by a different mechanism.

**TABLE 4.1** Comparison of the $Ca^{2+}$-bound and $Ca^{2+}$-free GCAP-1

| | **$Ca^{2+}$-free** | **$Ca^{2+}$-bound** | **Evidence** |
|---|---|---|---|
| **Molecular weight** | ~ 26000 Da | ~ 21000 Da | SDS-PAGE |
| **Mobility** | slower | faster | SDS-PAGE |
| **Conformation** | flexible | compact (more folding) | CD, (NMR) |
| **α-helicity** | less helical (+ myr) | more helical (+ myr) | CD |
| **Stability** | unstable at high temp. | temperature-resistant | CD |
| **Molecule** | monomer (+ DTT) | dimer (+ DTT) | ND-PAGE, SEC |
| **Stokes' radii** | 26.5 Å | 35.8 Å | SEC |
| **Relative molecular mass** | 36 kDa | 66 kDa | SEC |
| **Surface hydrophobicity** | more hydrophilic | more hydrophobic | (hypothetical) |
| **Surface charge** | less negative | more negative | SDS-PAGE |
| **Cysteine reactivity** | four cysteines exposed | three cysteines exposed and one cysteine ($Cys^{106}$) buried | Elleman's reagent |
| **Regulation of ROS-GC1** | activation | inhibition | ROS-GC assay |
| **Interaction with peptides** | higher affinity | lower affinity | SPR |
| **Conclusion** | relaxed monomer to interact with ROS-GC1 | compact dimer to stabilize GCAP-1 itself | |

**TABLE 4.2** Comparison of myristoylated and nonmyristoylated GCAP-1

| | **+ Myr** | **- Myr** | **Evidence** |
|---|---|---|---|
| **Molecular weight** | ~ 20500 Da | ~ 21000 Da | (SDS-PAGE) |
| **Mobility** | faster | slower | (SDS-PAGE) |
| **Mass** | 23349 ± 7.17 Da | 23533 ± 7.10 Da | MS |
| **Hydrophobicity** | more hydrophobic | less hydrophobic | HPLC, (NMR) |
| **α-helicity** | more helical | less helical | CD |
| **$Ca^{2+}$-dependent conformational change** | slight difference | more different changes | CD |
| **Cysteine reactivity in the presence of $Ca^{2+}$** | two cysteines exposed and two cysteines buried | three cysteines exposed and one cysteine buried | Ellman's reagent |
| **Cysteine reactivity in the absence of $Ca^{2+}$** | three cysteines exposed and one cysteine buried | four cysteines exposed | Ellman's reagent |
| **Regulation of ROS-GC1** | more active | less active | ROS-GC assay |
| **Conclusion** | better activator of ROS-GC1 with proper conformation to interact with ROS-GC1 | less active on ROS-GC1 activity | |

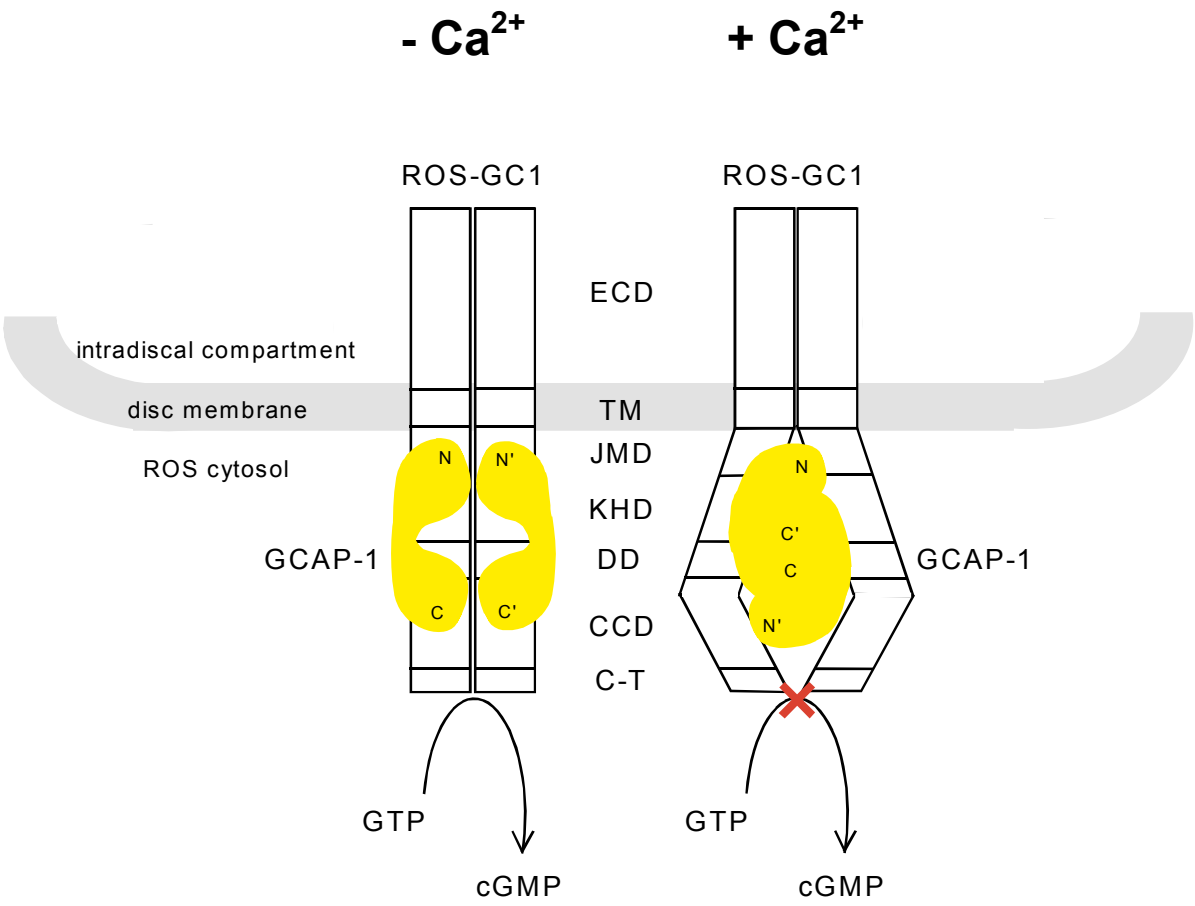


**FIG. 4.4.**Schematic representation for the speculative conformational changes of $Ca^{2+}$-free and $Ca^{2+}$-bound GCAP-1. GCAP-1 prefers a monomeric form in the absence of $CaCl_2$. The rearrangement of the hydrophobic residues at high concentration of $Ca^{2+}$ could allow two molecules of GCAP-1 to form a dimer. This bulky dimer could obstruct the dimerization of ROS-GC1, which is a necessary condition for synthesizing cGMP from GTP.

## 4.3 Myristoyl-induced Changes of GCAP-1

A comparison of the myristoylated and nonmyristoylated GCAP-1 is shown in Table 4.2. Otto-Bruc et al. reported that myristoylated GCAP-1 has slightly faster electrophoretic mobility than nonmyristoylated GCAP-1 [141]. Consistent with this result, the nonmyristoylated GCAP-1 runs approx. 1 kDa higher than the myristoylated GCAP-1 in spite of the fact that the molecular mass of myristoylated GCAP-1 is 210 Da larger than that of nonmyristoylated (data not shown). The nonmyristoylated GCAP-1 has a lower electrophoretic mobility compared with the wild-type protein. I could only observe a marginally difference between both GCAP-1 forms.

Another difference between GCAP-1 and GCAP-2 is apparent in the function of the myristoyl groups. It has been reported that myristoylation has only a minor effect on the ability of GCAP-2 to stimulate ROS-GCs [72]. Myristoylation does not affect $Ca^{2+}$-sensitive stimulation of ROS-GC by GCAP-2 and it does not influence the membrane binding properties of GCAP-2 [72]. In contrast, it has been reported that myristoylation of GCAP-1 has an effect on its structural stability and its interaction with ROS-GC1.

These results reveal that the presence of myristoyl groups has significant effects on the structural stability and on the biological function of GCAP-1 (for summary, see Table 4.2). First, the CD spectra reveal that calcium addition leads to only slight changes in helicity for myristoylated GCAP-1 (see Results 3.2.3). In the presence of $Ca^{2+}$, the spectrum of myristoylated GCAP-1 demonstrated a lower degree of helicity than in the absence of $Ca^{2+}$. The loss of CD intensity and the decrease of α-helical content suggest that myristoylated GCAP-1 without $Ca^{2+}$ has more fixed α-helical content. This is the opposite result of what was obtained with nonmyristoylated GCAP-1.

Second, the reactivity of myristoylated GCAP-1 towards DTNB showed that two of four cysteine residues reacted with DTNB in the presence of $Ca^{2+}$. The reactivity of exposed cysteines with DTNB in the absence of $Ca^{2+}$ indicates that three cysteines in myristoylated GCAP-1 are not buried. The presence of a myristoyl group in GCAP-1 apparently has a shielding effect, burying one cysteine of GCAP-1. Third, the stimulation of ROS-GC1 activity by nonmyristoylated GCAP-1 has shifted to higher $[Ca^{2+}]_{free}$ than by myristoylated GCAP-1. The maximal activity of ROS-GC1 by nonmyristoylated GCAP-1 is lower than by myristoylated GCAP-1. These results are consistent with the observations of other

investigators [141]. The myristoylation of GCAP-1 has an effect on the stimulation of ROS-GC1 activity and on the $Ca^{2+}$ sensitivity.

The concept of $Ca^{2+}$-myristoyl switch is based on the conformational changes of recoverin according to $Ca^{2+}$-induced and myristoyl group induced different forms [75,142]. The binding of $Ca^{2+}$ is postulated to induce the extrusion of the myristoyl group of recoverin and lead to the exposure of other hydrophobic residues [143,144]. Nonmyristoylated recoverin is monomeric and globular in solution in the presence of $Ca^{2+}$, while N-terminal myristoylation causes aggregation. In the absence of $Ca^{2+}$, nonmyristoylated recoverin tends to aggregate, while myristoylated recoverin becomes monomeric and globular. These observations indicate that recoverin changes its surface properties depending on both $Ca^{2+}$-binding and N-terminal myristoylation [135]. It is unclear whether GCAP-1 undergoes the same types of $Ca^{2+}$-myristoyl switch as recoverin. Results from experiments with DTNB, especially the shielding effect of the myristoyl group (see above) indicate that no $Ca^{2+}$-myristoyl switch operates in GCAP-1.

## 4.4 Roles of Cysteine Residues of GCAP-1

The cysteine exchange mutants showed different accessibilities to solvent. Hence, it is possible to derive some structural aspects of GCAP-1. When GCAP-1 was incubated with $CaCl_2$, three cysteines reacted with DTNB. However, all four cysteines rapidly reacted in the presence of EGTA. Although in the closed state three thiol groups in GCAP-1 were DTNB-sensitive in the presence of $Ca^{2+}$, all four thiol groups were detected by DTNB as being in the open state in the presence of EGTA.

It is of interest to compare the time course of reaction of those triple mutants with DTNB at various free $Ca^{2+}$ concentrations. The results indicate that $Ca^{2+}$-dependent changes in the rate of reaction could reflect an apparent affinity constant of $Ca^{2+}$ for a particulate EF-hand. The accessibility of the cysteine in ACAA located in EF-1 is reflected in the apparent $Ca^{2+}$-binding constant at 55 μM $[Ca^{2+}]_{free}$. The cysteine of AACA located in EF-3 is accessible to solvent at 3 μM intermediate $[Ca^{2+}]_{free}$.

Affinities of EF-hands in GCAP-1 for $Ca^{2+}$ are not reported so far. Only for GCAP-2, a macromolecular binding constant was estimated. $Ca^{2+}$-binding measurements using equilibrium dialysis and tryptophan fluorescence titrations showed that three calcium ions bind to unmyristoylated GCAP-2 [129]. The apparent affinity is 300 ± 40 nM, and the Hill coefficient is 2.1 ± 0.2. A stoichiometry of three $Ca^{2+}$-bound to GCAP-2 is also supported by

site-directed mutagenesis studies of the EF-hand motifs. Substituting glutamine for glutamate at position 12 of the EF-hand loops (EF-2, EF-3, EF-4) prevents the binding of $Ca^{2+}$ and produces a constitutively active form of GCAP-2 [129]. It would be interestingly to use cysteine residues in the vicinity of EF-hands to determine apparent $Ca^{2+}$-binding constants by the DTNB method.

## 4.5 Regulation of ROS-GC1 Activity by GCAP-1

The $Ca^{2+}$-dependent regulation of ROS-GC1 activity by four types of wild-type GCAP-1 from different preparations, four types of single cysteine mutants, four types of triple cysteine mutants, and the quad cysteine mutant is compared in Fig. 4.5.

There are significant differences in the $EC_{50}$-values of the stimulation upon the calcium concentration between native GCAP-1 and single cysteine mutants. Those $EC_{50}$-values of single mutants have shifted to extremely high values in the μM range (Fig. 4.5 *B* and *F*). Remarkably, nonmyristoylated GCAP-1 showed the same $Ca^{2+}$-dependent regulation as the single cysteine mutants (Fig. 4.5 *E* and *F*). In contrast, myristoylated GCAP-1 and the triple mutants activated ROS-GC1 in a similar manner (Fig. 4.5 *E*, *G*, and *H*), although no myristoylation was present in the cysteine mutants. It appears that the myristoylation somehow protects the structural integrity of GCAP-1 and this integrity can be disturbed by the cysteine residues. Results from section 3.2.6, however, show that cysteines in wild-type GCAP-1 do not form intramolecular disulfide bonds. However, SEC experiment described in Results 3.2.5 indicated that dimerization and aggregation was facilitated in a medium without reducing agents. This could mean that intermolecular disulfide bridges had formed. In line with these arguments are the results with the triple mutants, where only one cysteine is present and a lesser chance to form disulfide bridges exist.

Interestingly, the stimulation of ROS-GC1 activity by all-cysteine-exchange mutant, AAAA, of GCAP-1 is very similar with that by native GCAP-1, even though this mutant is nonmyristoylated. Without cysteine residues and without myristoylated groups, the quad mutant, AAAA-GCAP-1 stimulates ROS-GC1 activity as does myristoylated GCAP-1 purified from inclusion bodies. From these results it could be speculated that the myristoyl group of GCAP-1 may play a role in the proper folding of GCAP-1 for interaction with ROS-GC1 and $Ca^{2+}$, preventing inappropriate inter- or intramolecular binding of GCAP-1's thiol groups. With misfolding due to the wrong disulfide pairs the conformation of GCAP-1

lost the ability of binding with $Ca^{2+}$, so that it stimulates ROS-GC1 in a higher range of $[Ca^{2+}]_{free}$. Therefore, an ideal mutant of GCAP-1 without myristoylation should be formed in a quadruple cysteine mutant which is actually the case (see Results 3.4.1 ). I suspect that the the quad mutant was properly folded, and therefore suitable for crystallization trials of GCAP-1.

The lack of myristoylation substantially reduces the ability of GCAP-1 to activate ROS-GC1 [141]. This observation of Otto-Bruc et al. was consistent with the results of this thesis, which shows that myristoylated GCAP-1 stimulated ROS-GC1 at lower free $[Ca^{2+}]$ than nonmyristoylated. However, it is not clear whether myristoylation directly influences the ability of GCAP-1 to regulate ROS-GCs or if it is merely required for proper folding of GCAP-1. Myristoylation of GCAPs may be important for other aspects of GCAP function *in vivo* such as compartmentalization and transport [40].

## 4.6 Folding and Refolding of GCAP-1

Surprisingly, different activation patterns of ROS-GC1 has been observed, depending on the preparation of wild-type GCAP-1. Three different preparations were used: inclusion bodies, supernatants, guanidine hydrochloride treated. The protein quality from each preparation were distinguished by the regulation assay.

Dr. C. Lange (IBI-1, Forschungszentrum Jülich), isolated nonmyristoylated GCAP-1 and myristoylated GCAP-1 from the inclusion bodies using the chaotrope reagent, guanidine hydrochloride for protein unfolding in order to minimize aggregation and to increase the yield of properly folded protein. Dialysis of the guanidine hydrochloride solution resulted in properly refolded protein. These proteins, purified from inclusion bodies, stimulate ROS-GC1 activity more than those isolated from supernatant (refer Fig. 4.5 *A*). The preparations differ in the $EC_{50}$-value for $[Ca^{2+}]_{free}$ and in the Hill coefficient (Fig. 4.5 *A* and *E*). Remarkably, a preparation obtained from inclusion bodies was most similar to native GCAP-1 (see Results 3.2.2 and Reference 97). Why did GCAP-1 that was isolated from the *E. coli* supernatant show a shift in the $Ca^{2+}$ sensitivity as compared native GCAP-1? GCAP-1 could be misfolded with incorrect disulfide bonds. These possible intermolecular disulfide bridges could have formed spontaneously after protein synthesis and after cell lysis and an extraction step. I tried to analyze this problem by a denaturation/renaturation cycle.

After purifying nonmyristoylated GCAP-1 and partially myristoylated GCAP-1 from supernatant, both proteins were refolded by denaturating with guanidine hydrochloride in the presence of high concentration of reducing agent and then dialyzing to remove guanidine hydrochloride [146]. However, activation of ROS-GC1 by both proteins was the same as before refolding proceeding. Therefore, I conclude that additional factors, e.g. saturating $CaCl_2$ or EGTA, are needed for optimal conditions in a refolding experiment.

The presence of the proper N-terminus on the myristoyl group might somehow prevent incorrect pairing of disulfide bonds. There could be a higher risk of misfolding and mismatching for the single cysteine mutants with odd numbers of cysteine residues. However, the triple mutants, which have unpaired cysteine residues, also have the possibility to make intermolecular disulfide bonds, and, therefore, those mutants show shifts in their $EC_{50}$-values to higher $[Ca^{2+}]_{free}$ than that of native GCAP-1.

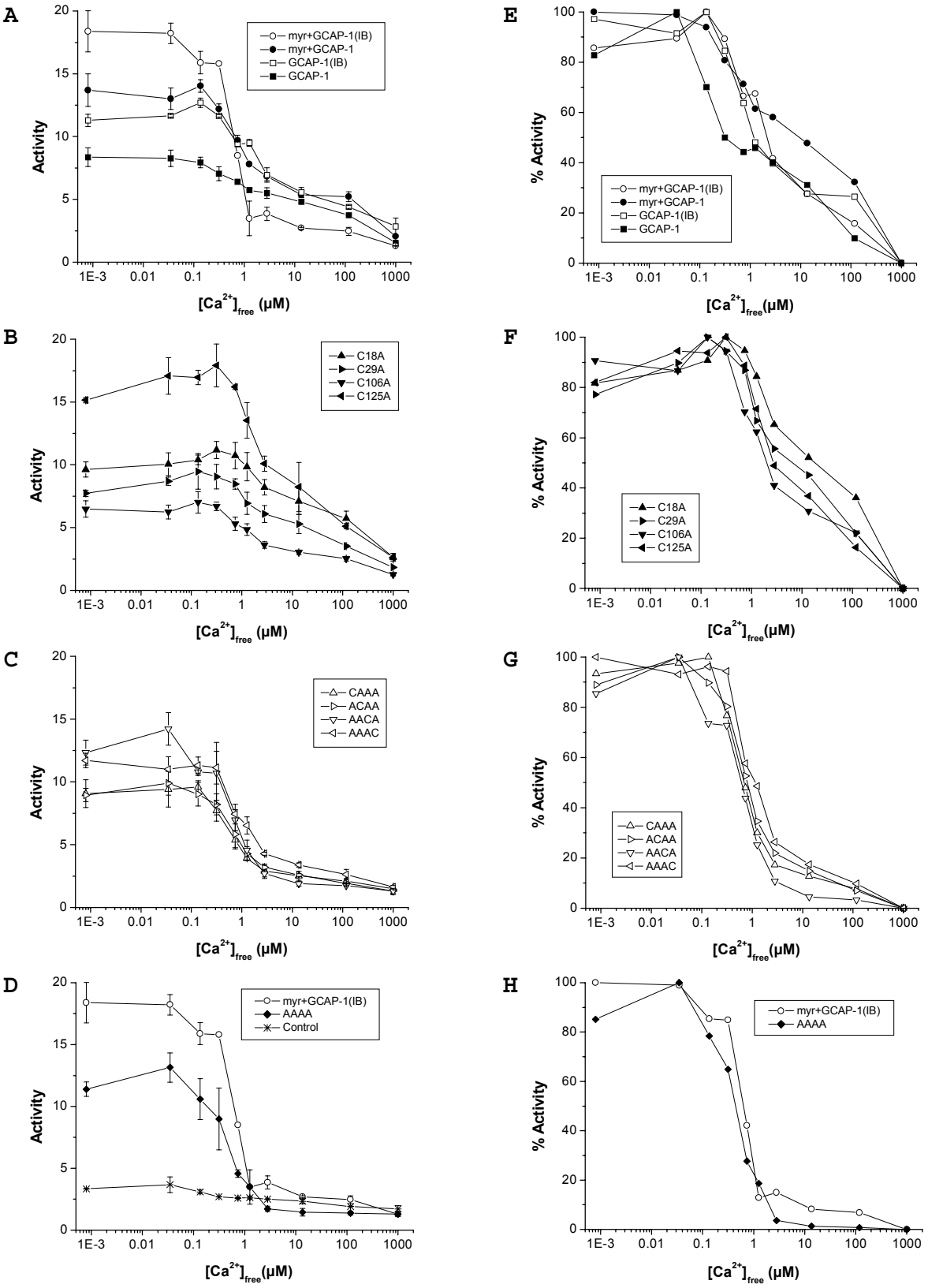


**FIG. 4.5.** Regulation of ROS-GC1 by GCAP-1 and its mutants. Left panels (***A–D***) show $Ca^{2+}$-dependent regulation of ROS-GC1 activity. Right panels (***E–H***) show the adjusted activity to percentage. Maximal ROS-GC activity at low $[Ca^{2+}]_{free}$ was set to 100% and minimal ROS-GC activity at high $[Ca^{2+}]_{free}$ was set to 0%. IB indicates the preparations purified from the inclusion bodies.

## 4.7 Perspectives

In this thesis, the apparent $Ca^{2+}$-binding affinity constants of EF-1 and EF-3 of GCAP-1 were determined, using the advantages of monitoring the cysteine reactivity towards DTNB. To understand the $Ca^{2+}$-binding affinity of further EF-hands, EF-2 and EF-4, a similar approach can be used. If additional amino acids are substituted to cysteines in EF-2 and EF-4, the $Ca^{2+}$-induced conformational changes and $Ca^{2+}$ sensitivity of the respective EF-hands could be understood. This would give a more complete picture of $Ca^{2+}$-binding behavior of GCAP-1.

A novel approach to studying the activator/inhibitor switch of GCAP-1 (and GCAP-2) involves chimeric mutants, whose parts of GCIP (guanylate cyclase inhibitory protein) are exchanged for corresponding regions in GCAP-1. It might also be possible to convert a nonfunctional EF-hand into a functional one, using corresponding amino acid motifs present in the prototype EF-hand protein, calmodulin.

Recent advances in the three-dimensional structural analysis of various EF-hand proteins have led to new insights into the structural and functional relationships of this large family of $Ca^{2+}$-binding proteins, providing valuable information about the $Ca^{2+}$-induced conformational changes for their correlation with target recognition. Ultimately, the three-dimensional structure of GCAP-1, $Ca^{2+}$-bound or $Ca^{2+}$-free form, would yield wealth of information about the function of GCAP-1. In this thesis, examination of the monomer/dimer equilibrium with size exclusion chromatography suggests that monomer and dimers co-exist in presence and absence of $Ca^{2+}$ but that dimerization is favored in the presence of $Ca^{2+}$. This observed dimerization may explain why attempts have thus far failed to determine the three-dimensional structure of GCAP-1 by NMR studies or X-ray crystallography. The stimulation of ROS-GC1 activity by all-cysteine-exchange (i.e. cysteine-free) mutant, AAAA, of GCAP-1 is very similar to that of native GCAP-1. This quad mutant therefore shows promise for further pursuits of crystallization trials and other three-dimensional structural studies of GCAP-1.

Several mutations of human GCAP-1 were recently found to be linked to autosomal dominant cone rod dystrophy that causes a decrease in visual acuity and loss of color vision [68-70,147]. The understanding of the structure and function of GCAP-1 could bring a hopeful prospect of relevance to clinical therapeutics for some eye diseases.

# 5. APPENDIX

## 5.1. Amino Acid Residues

**TABLE 5.1** Some properties of individual amino acid residues [4,148,149]

| Amino Acids | | pK | Mass (Da) | Hydro-phobicity (kcal/mol) | Preference | | |
|---|---|---|---|---|---|---|---|
| | | | | | α-helix | β-sheet | Turn |
| Glycine | Gly (G) | - | 57.05 | 0 | 0.43 | 0.58 | 1.77 |
| Alanine | Ala (A) | - | 71.09 | –0.25 | 1.41 | 0.72 | 0.82 |
| Valine | Val (V) | - | 99.14 | –1.30 | 0.90 | 1.87 | 0.41 |
| Leucine | Leu (L) | - | 113.16 | –1.82 | 1.34 | 1.22 | 0.57 |
| Isoleucine | Ile (I) | - | 113.16 | –1.82 | 1.09 | 1.67 | 0.47 |
| Proline | Pro (P) | - | 97.12 | –0.99 | 0.34 | 0.31 | 1.32 |
| Serine | Ser (S) | - | 87.08 | 1.24 | 0.57 | 0.96 | 1.22 |
| Threonine | Thr (T) | - | 101.11 | 1.00 | 0.76 | 1.17 | 0.90 |
| Cysteine | Cys (C) | 9.3 | 103.15 | –0.25 | 0.66 | 1.40 | 0.54 |
| Methionine | Met (M) | - | 131.19 | –0.96 | 1.30 | 1.14 | 0.52 |
| Aspartate | Asp (D) | 3.9 | 115.09 | 3.81 | 0.99 | 0.39 | 1.24 |
| Asparagine | Asn (N) | - | 114.11 | 1.91 | 0.76 | 0.48 | 1.34 |
| Glutamiate | Glu (E) | 4.3 | 129.12 | 2.91 | 1.59 | 0.52 | 1.01 |
| Glutamine | Gln (Q) | - | 128.14 | 1.30 | 1.27 | 0.98 | 0.84 |
| Lysine | Lys (K) | 10.0 | 128.17 | 2.77 | 1.23 | 0.69 | 1.07 |
| Arginine | Arg (R) | 12.0 | 156.19 | 3.95 | 1.21 | 0.84 | 0.90 |
| Histidine | His (H) | 6.5 | 137.14 | 0.64 | 1.05 | 0.80 | 0.81 |
| Phenylalanine | Phe (F) | - | 147.18 | –2.27 | 1.16 | 1.33 | 0.59 |
| Tyrosine | Tyr (Y) | 10.2 | 163.18 | –1.47 | 0.74 | 1.45 | 0.76 |
| Tryptophan | Trp (W) | - | 186.21 | –2.13 | 1.02 | 1.35 | 0.65 |

# 5.2. Full Restriction Map of DNA Sequence of GCAP1

It was carried out by DNA Strider™ 1.2 software in Macintosh. Positions of restriction endonucleases sites and unique sites underlined are indicated.

**GCAP1 → Full Restriction Map**

DNA sequence 626 b.p. CATATGGGTAAC ... CGGCTAGGATCC linear

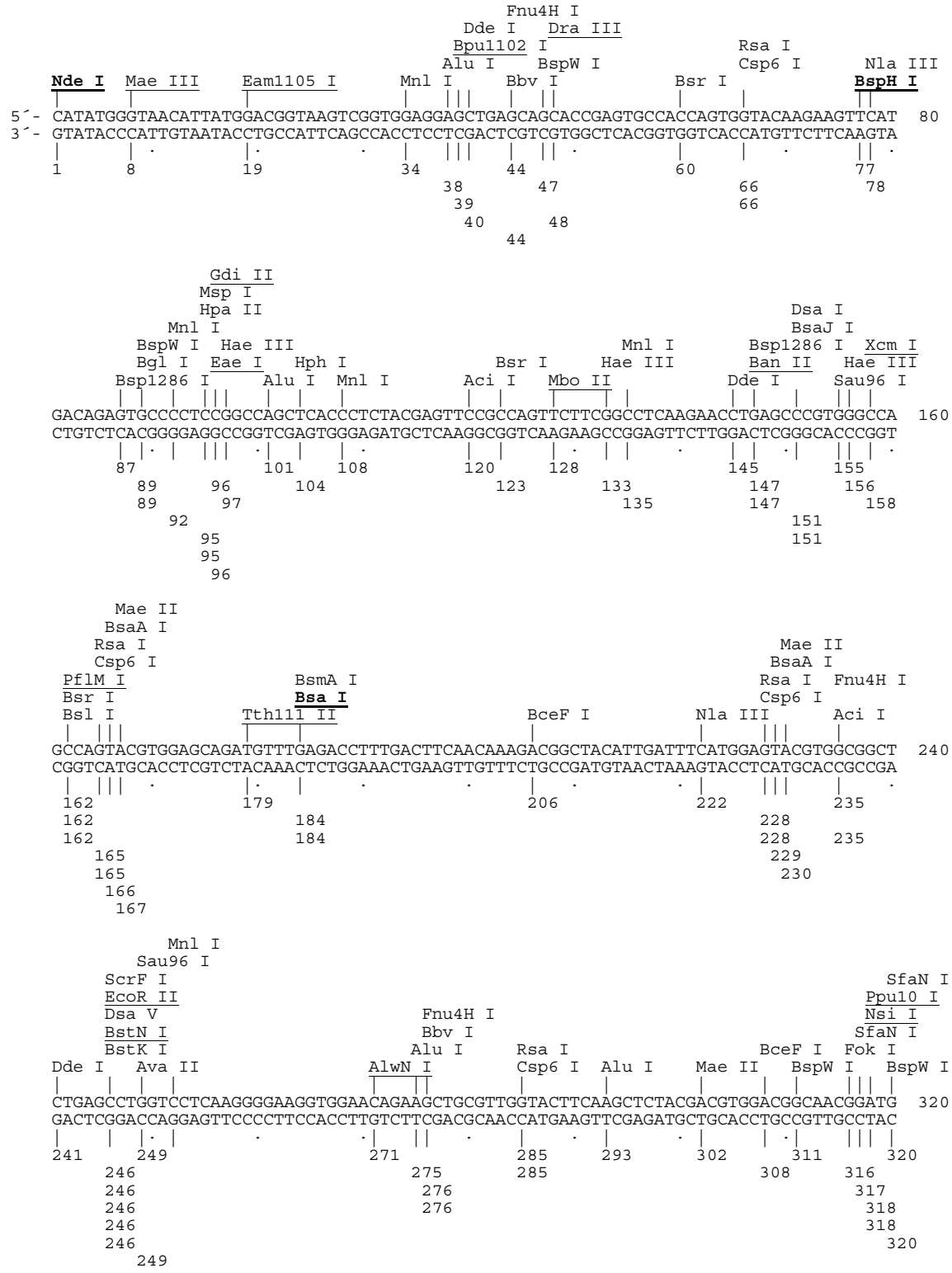

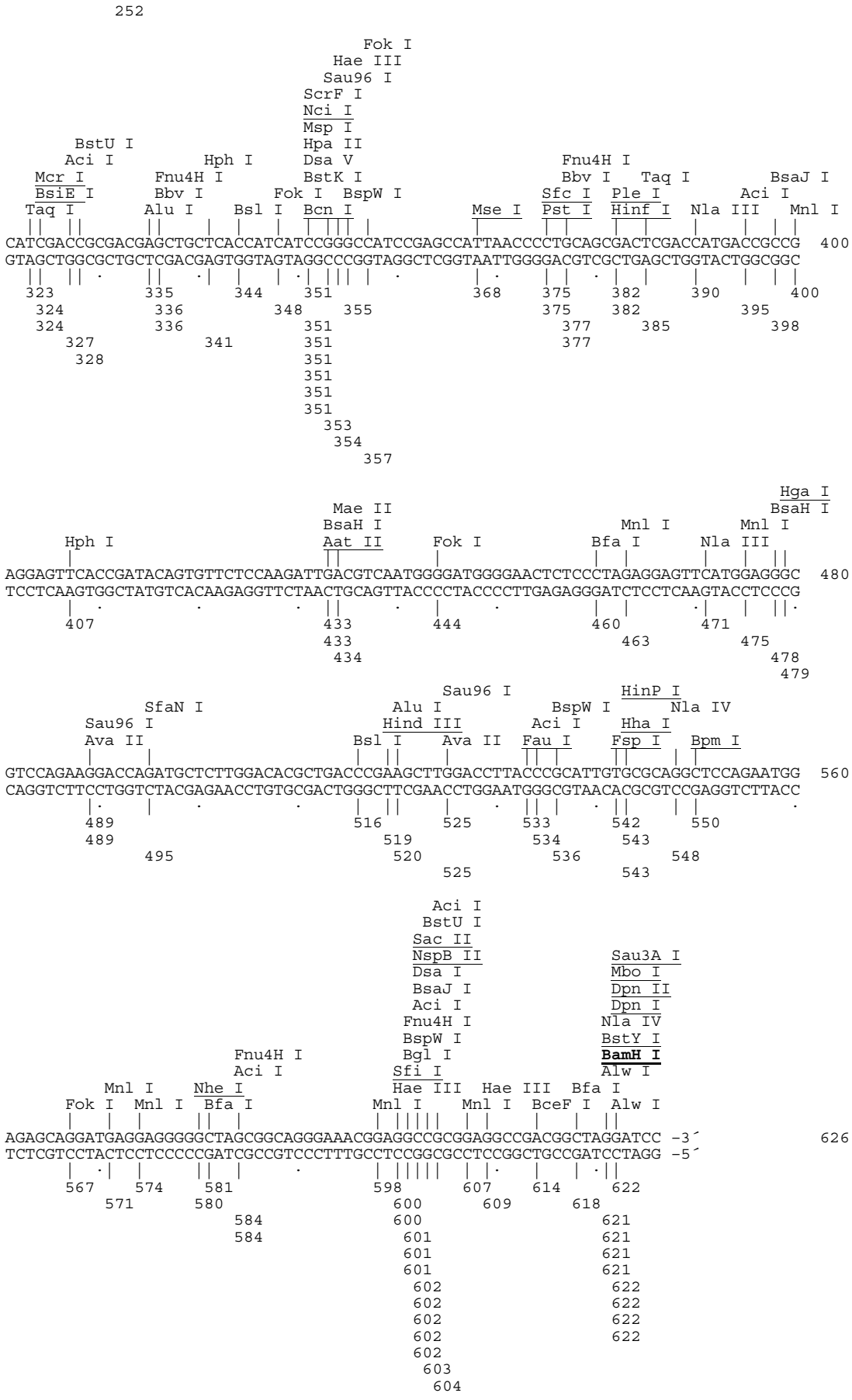
Fok I
Hae III
Sau96 I
ScrF I
Nci I
Msp I
Hpa II
Dsa V
BstU I
Aci I
Hph I
Mcr I
BsiE I
Fnu4H I
Bbv I
BstK I
Fok I
BspW I
Fnu4H I
Bbv I
Taq I
Sfc I
Ple I
BsaJ I
Aci I
Taq I
Alu I
Bsl I
Bcn I
Mse I
Pst I
Hinf I
Nla III
Mnl I
CATCGACCGCGACGAGCTGCTCACCATCATCCGGGCCATCCGAGCCATTAACCCCTGCAGCGACTCGACCATGACCGCCG 400
GTAGCTGGCGCTGCTCGACGAGTGGTAGTAGGCCCGGTAGGCTCGGTAATTGGGGACGTCGCTGAGCTGGTACTGGCGGC
323 335 344 351 368 375 382 390 400
324 336 348 355 375 382 395
324 336 351 377 385 398
327 341 351 377
328 351
351
351
351
353
354
357
Hga I
BsaH I
Mae II
BsaH I
Mnl I
Mnl I
Hph I
Aat II
Fok I
Bfa I
Nla III
AGGAGTTCACCGATACAGTGTTCTCCAAGATTGACGTCAATGGGGATGGGGAACTCTCCCTAGAGGAGTTCATGGAGGGC 480
TCCTCAAGTGGCTATGTCACAAGAGGTTCTAACTGCAGTTACCCCTACCCCTTGAGAGGGATCTCCTCAAGTACCTCCCG
407 433 444 460 471
433 463 475
434 478
479
Sau96 I
HinP I
SfaN I
Alu I
BspW I
Nla IV
Sau96 I
Hind III
Aci I
Hha I
Ava II
Bsl I
Ava II
Fau I
Fsp I
Bpm I
GTCCAGAAGGACCAGATGCTCTTGGACACGCTGACCCGAAGCTTGGACCTTACCCGCATTGTGCGCAGGCTCCAGAATGG 560
CAGGTCTTCCTGGTCTACGAGAACCTGTGCGACTGGGCTTCGAACCTGGAATGGGCGTAACACGCGTCCGAGGTCTTACC
489 516 525 533 542 550
489 519 534 543
495 520 536 548
525 543
Aci I
BstU I
Sac II
NspB II
Dsa I
BsaJ I
Aci I
Fnu4H I
BspW I
Bgl I
Sfi I
Hae III
Hae III
Bfa I
Sau3A I
Mbo I
Dpn II
Dpn I
Nla IV
BstY I
BamH I
Alw I
Fnu4H I
Aci I
Mnl I
Nhe I
Fok I
Mnl I
Bfa I
Mnl I
Mnl I
BceF I
Alw I
AGAGCAGGATGAGGAGGGGGCTAGCGGCAGGGAAACGGAGGCCGCGGAGGCCGACGGCTAGGATCC -3´ 626
TCTCGTCCTACTCCTCCCCCGATCGCCGTCCCTTTGCCTCCGGCGCCTCCGGCTGCCGATCCTAGG -5´
567 574 581 598 607 614 622
571 580 600 609 618
584 600 621
584 601 621
601 621
601 621
602 622
602 622
602 622
602 622
602
603
604

## 5.3. Encoded Amino Acids of GCAP-1 According to the DNA Sequence of GCAP1

It was carried out by DNA Strider™ 1.2 software in Macintosh. The cysteine sites are shown in bold.

**GCAP1 → 1-phase Translation**

DNA sequence 618 b.p. ATGGGTAACATT ... GCCGACGGCTAG linear

```
1/1                                             31/11
ATG GGT AAC ATT ATG GAC GGT AAG TCG GTG GAG GAG CTG AGC AGC ACC GAG TGC CAC CAG
Met Gly Asn Ile Met Asp Gly Lys Ser Val Glu Glu Leu Ser Ser Thr Glu Cys His Gln
61/21                                           91/31
TGG TAC AAG AAG TTC ATG ACA GAG TGC CCC TCC GGC CAG CTC ACC CTC TAC GAG TTC CGC
Trp Tyr Lys Lys Phe Met Thr Glu Cys Pro Ser Gly Gln Leu Thr Leu Tyr Glu Phe Arg
121/41                                          151/51
CAG TTC TTC GGC CTC AAG AAC CTG AGC CCG TGG GCC AGC CAG TAC GTG GAG CAG ATG TTT
Gln Phe Phe Gly Leu Lys Asn Leu Ser Pro Trp Ala Ser Gln Tyr Val Glu Gln Met Phe
181/61                                          211/71
GAG ACC TTT GAC TTC AAC AAA GAC GGC TAC ATT GAT TTC ATG GAG TAC GTG GCG GCT CTG
Glu Thr Phe Asp Phe Asn Lys Asp Gly Tyr Ile Asp Phe Met Glu Tyr Val Ala Ala Leu
241/81                                          271/91
AGC CTG GTC CTC AAG GGG AAG GTG GAA CAG AAG CTG CGT TGG TAC TTC AAG CTC TAC GAC
Ser Leu Val Leu Lys Gly Lys Val Glu Gln Lys Leu Arg Trp Tyr Phe Lys Leu Tyr Asp
301/101                                         331/111
GTG GAC GGC AAC GGA TGC ATC GAC CGC GAC GAG CTG CTC ACC ATC ATC CGG GCC ATC CGA
Val Asp Gly Asn Gly Cys Ile Asp Arg Asp Glu Leu Leu Thr Ile Ile Arg Ala Ile Arg
361/121                                         391/131
GCC ATT AAC CCC TGC AGC GAC TCG ACC ATG ACC GCC GAG GAG TTC ACC GAT ACA GTG TTC
Ala Ile Asn Pro Cys Ser Asp Ser Thr Met Thr Ala Glu Glu Phe Thr Asp Thr Val Phe
421/141                                         451/151
TCC AAG ATT GAC GTC AAT GGG GAT GGG GAA CTC TCC CTA GAG GAG TTC ATG GAG GGC GTC
Ser Lys Ile Asp Val Asn Gly Asp Gly Glu Leu Ser Leu Glu Glu Phe Met Glu Gly Val
481/161                                         511/171
CAG AAG GAC CAG ATG CTC TTG GAC ACG CTG ACC CGA AGC TTG GAC CTT ACC CGC ATT GTG
Gln Lys Asp Gln Met Leu Leu Asp Thr Leu Thr Arg Ser Leu Asp Leu Thr Arg Ile Val
541/181                                         571/191
CGC AGG CTC CAG AAT GGA GAG CAG GAT GAG GAG GGG GCT AGC GGC AGG GAA ACG GAG GCC
Arg Arg Leu Gln Asn Gly Glu Gln Asp Glu Glu Gly Ala Ser Gly Arg Glu Thr Glu Ala
601/201
GCG GAG GCC GAC GGC TAG
Ala Glu Ala Asp Gly AMB
```

## 5.4. Used Vectors for Cloning GCAP1

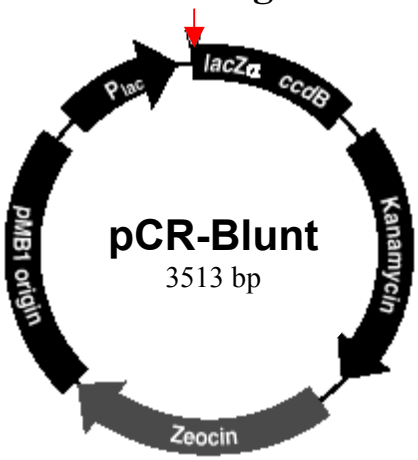


**FIG. 5.1.** pCR-Blunt as the cloning vector

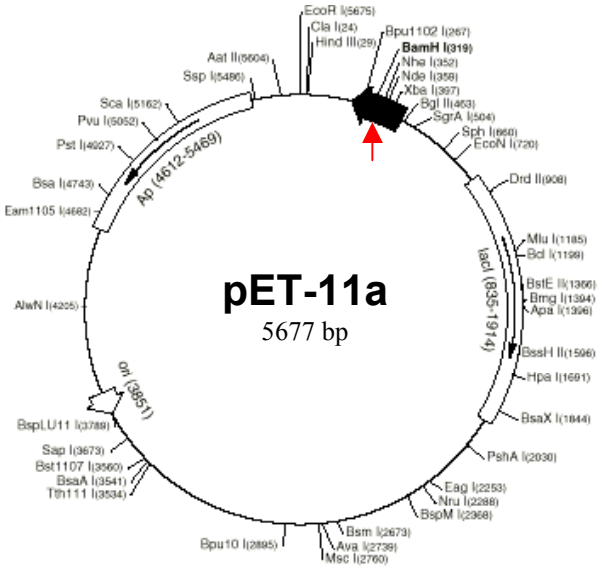


**FIG. 5.2.** pET-11a as the expression vector

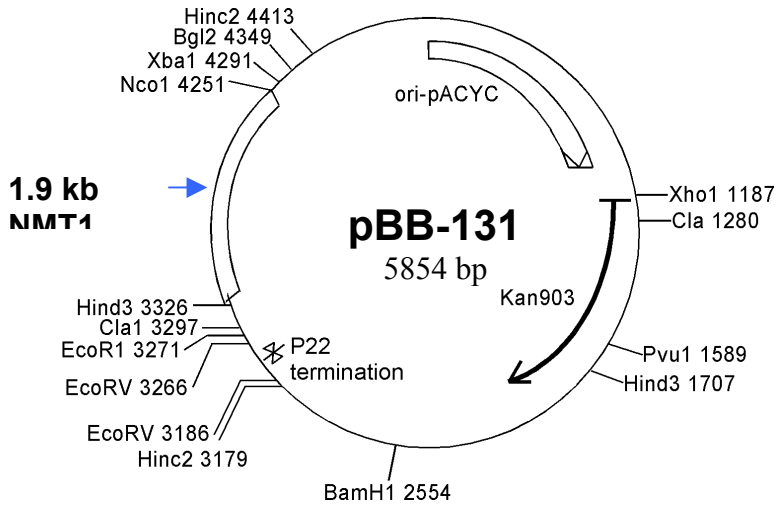


**FIG. 5.3.** pBB-131 as the coexpression vector

## 5.5. Amino Acids of ROS-GC1

The apparent molecular weight of ROS-GC1 is ~112000 on SDS-PAGE. The calculated molecular mass is ~120 kDa containing the 56-amino acids of an N-terminal signal peptide (LS), which is cleaved of in the mature protein. The LS is indicated with dash-and-dot underlining. The peptide #34a ($Leu^{559}$–$Ile^{578}$) is indicated with solid underlining and the peptide Sokal #71 ($Gly^{966}$–$Gly^{983}$) with dotted underlining.

```
MTACTFLAGG LRDPGLCGPT RWAPSPPGLP PIPPRPRLRL RPPLLLLLLL PRSVLSAVFT    60
VGVLGPWACD PIFARARPDL AARLAASRLN HAAALEGGPR FEVALLPEPC RTPGSLGAVS   120
SALTRVSGLV GPVNPAACRP AELLAQEAGV ALVPWGCPGT RAAGTTAPVV TPAADALYAL   180
LRAFRWAHVA LVTAPQDLWV EAGHALSTAL RARGLPVALV TSMEPSDLSG AREALRRVQD   240
GPRVRAVIMV MHSVLLGGEE QRCLLEAAEE LGLADGSLVF LPFDTLHYAL SPGPDALAVL   300
ANSSQLRKAH DAVLTLTRHC PLGGSVRDSL RRAQEHRELP LDLNLQQVSP LFGTIYDSVF   360
LLAGGVARAR VAAGGGWVSG AAVARHIRDA RVPGFCGALG GAEEPSFVLL DTDATGDQLF   420
ATYVLDPTQG FFHSAGTPVH FPKGGRGPGP DPSCWFDPDT ICNGGVEPSV VFIGFLLVVG   480
MGLAGAFLAH YCRHRLLHIQ MVSGPNKIIL TLDDITFLHP HGGNSRKVAQ GSRTSLAARS   540
ISDVRSIHSQ LPDYTNIGLY EGDWVWLKKF PGDRHIAIRP ATKMAFSKIR ELRHENVALY   600
LGLFLAGGAG GPAAPGEGVL AVVSEHCARG SLQDLLAQRD IKLDWMFKSS LLLDLIKGIR   660
YLHHRGVAHG RLKSRNCVVD GRFVLKVTDH GHGRLLEAQR VLPEPPSAED QLWTAPELLR   720
DPVLERRGTL AGDVFSLGII MQEVVCRSAP YAMLELTPEE VVKRVQSPPP LCRPSVSIDQ   780
APMECIQLMK QCWAEQPELR PSMDRTFELF KSINKGRKMN IIDSMLRMLE QYSSNLEDLI   840
RERTEELELE KQKTDRLLTQ MLPPSVAEAL KMGTPVEPEY FEEVTLYFSD IVGFTTISAM   900
SEPIEVVDLL NDLYTLFDAI IGSHDVYKVE TIGDAYMVAS GLPQRNGHRH AAEIANMALD   960
ILSAVGTFRM RHMPEVPVRI RIGLHSGPCV AGVVGLTMPR YCLFGDTVNT ASAMESTGLP  1020
YRIHVNRSTV QILSALNEGF LTEVRGRTEL KGKGAEETYW LVGRRGFNKP IPKPPDLQPG  1080
ASNHGISLHE IPPDRRQKLE KARPGQFSGK
```

# 6. REFERENCES


1. Dowling, J. E.: *The retina: An approachable part of the brain*. Cambridge: Belknap Press (1987).

2. Müller, F. & Kaupp, U. B.: Signaltransduktion in Sehzellen (Signal transduction in photoreceptor cells). *Naturwissenschaften* **85**, 49-61 (1998).

3. Baylor, D. A. & Hodgkin, A. I.: Detection and resolution of visual stimuli by turtle photoreceptors. *J Physiol* **234**, 163-198 (1973).

4. Stryer, L.: *Biochemistry*, 4$^{th}$ ed. New York: W. H. Freeman and Company (1995).

5. Pugh, E. N. Jr. & Lamb, T. D.: Amplification and kinetics of the activation steps in phototransduction. *Biochim Biophys Acta* **1141**, 111-149 (1993).

6. Schnetkamp, P. P. & Szerencsei, R. T.: Effect of potassium ions and membrane potential on the $Na^+$-$Ca^{2+}$, $K^+$ exchanger in isolated intact bovine rod outer segments. *J Biol Chem* **266**, 189-197 (1991).

7. Schnetkamp, P. P.: Sodium ions selectively eliminate the fast component of guanosine cyclic 3',5'-phosphate induced $Ca^{2+}$ release from bovine rod outer segment disks. *Biochemistry* **26**, 3249-3253 (1987).

8. Yau, K.-W.: Phototransduction mechanism in retinal rods and cones. *Invest Ophthalmol Vis Sci* **35**, 9-32 (1994).

9. He, W., Cowan, C. W. & Wensel, T. G.: RGS9, a GTPase accelerator for phototransduction. *Neuron* **20**, 95-102 (1998).

10. Koutalos, Y. & Yau, K.-W.: Regulation of sensitivity in vertebrate rod photoreceptors by calcium. *TINS* **19**, 73-81 (1996).

11. Pugh, E. N. Jr., Duda, T., Sitaramayya, A. & Sharma, R. K.: Photoreceptor guanylate cyclases: a review. *Biosci Rep* **17**, 429-473 (1997).

12. Kawamura, S.: Rhodopsin phosphorylation as a mechanism of cyclic GMP phosphodiesterase regulation by S-modulin. *Nature* **362**, 855-857 (1993).

13. Koch, K.-W. & Stryer, L.: Highly cooperative feedback control of retinal rod guanylate cyclase by calcium ions. *Nature* **334**, 64-66 (1988).

14. Gorczyca, W. A., Gray-Keller, M. P., Detwiler, P. B. & Palczewski, K.: Purification and physiological evaluation of a guanylate cyclase activating protein from retinal rods. *Proc Natl Acad Sci U S A* **91**, 4014-4018 (1994).

15. Hsu, Y. T. & Molday, R. S.: Modulation of the cGMP-gated channel of rod photoreceptor cells by calmodulin. *Nature* **361**, 76-79 (1993).

16. Dowling, J. E.: Organization of vertebrate retinas. *Invest Ophthalmol* **9**, 655-680 (1970).

17. Howes, K., Bronson, J. D., Dang, Y. L., Li, N., Zhang, K., Ruiz, C., Helekar, B., Lee, M., Subbaraya, I., Kolb, H., Chen, J. & Baehr, W.: Gene array and expression of mouse retina guanylate cyclase activating proteins 1 and 2. *Invest Ophthalmol Vis Sci* **39**, 867-875 (1998).

18. Koutalos, Y., Nakatani, K., Tamura, T. & Yau, K.-W.: Characterization of guanylate cyclase activity in single retinal rod outer segments. *J Gen Physiol* **106**, 863-890 (1995).

19. Koch, K.-W.: Control of photoreceptor proteins by $Ca^{2+}$. *Cell Calcium* **18**, 314-321 (1995).

20. Palczewski, K., Polans, A., Baehr, W. & Ames, J. B.: $Ca^{2+}$-binding proteins in the retina: structure, function, and the etiology of human visual diseases. *BioEssays* **22**, 337-350 (2000).

21. Pugh, E. N. Jr., Nikonov, S. & Lamb, T. L.: Molecular mechanisms of vertebrate photoreceptor light adaptation. *Current Opinion in Neurobiology* **9**, 410-418 (1999).

22. Koch, K.-W.: Calcium as modulator of phototransduction in vertebrate photoreceptor cells. *Rev Physiol Biochem Pharmac* **125**, 149-192 (1994).

23. Stryer, L.: Visual excitation and recovery. *J Biol Chem* **266**, 10711-10714 (1991).

24. Koch, K.-W.: Biochemical mechanism of light adaptation in vertebrate photoreceptors. *TIBS* **17**, 307-311 (1992).

25. Molday, R. S.: Phtotoreceptor membrane proteins, phototransduction, and retinal degenerative disease. *Invest Ophthalmol Vis Sci* **39**, 2493-2513 (1998).

26. Polans, A. S., Baehr, W. & Palczewski, K.: Turned on by $Ca^{2+}$! The physiology and pathology of $Ca^{2+}$-binding proteins in the retina. *Trends Neurosci* **19**, 547-554 (1996).

27. Dizhoor, A. M.: Regulation of cGMP synthesis in photoreceptors: role in signal transduction and congenital diseases of the retina. *Cell Signal* **12**, 711-719 (2000).

28. Koesling, D.: Studying the structure and regulation of soluble guanylyl cyclase. *Methods* **19**, 485-493 (1999).

29. Foster, D. C. & Garbers, D. L.: Dual role for adenine nucleotides in the regulation of the atrial natriuretic peptide receptor, guanylyl cyclase-A. *J Biol Chem* **273**, 16311-16318 (1998).

30. Suga, S., Nakao, K., Hosoda, K., Mukoyama, M., Ogawa, Y., Shirakami, G., Arai, H., Saito, Y., Kambayashi, Y. & Inouye, K.: Receptor selectivity of natriuretic peptide family, atrial natriuretic peptide, brain natriuretic peptide, and C-type natriuretic peptide. *Endocrinology* **130**, 229-239 (1992).

31. Singh, S., Singh, G., Heim, J. M. & Gerzer, R.: Isolation and expression of a guanylate cyclase-coupled heat stable enterotoxin receptor cDNA from a human colonic cell line. *Biochem Biophys Res Commun* **179**, 1455-1463 (1991).

32. Koch, K.-W.: Purification and identification of photoreceptor guanylate cyclase. *J Biol Chem* **266**, 8634-8637 (1991).

33. Yang, R. B., Foster, D. C., Garbers, D. L. & Fulle, H. J.: Two membrane forms of guanylyl cyclase found in the eye. *Proc Natl Acad Sci U S A* **92**, 602-606 (1995).

34. Fulle, H. J., Vassar, R., Foster, D. C., Yang, R. B., Axel, R. & Garbers, D. L.: A receptor guanylyl cyclase expressed specifically in olfactory sensory neurons. *Proc Natl Acad Sci U S A* **92**, 3571-3575 (1995).

35. Schulz, S., Wedel, B. J., Matthews, A. & Garbers, D. L.: The cloning and expression of a new guanylyl cyclase orphan receptor. *J Biol Chem* **273**, 1032-1037 (1998).

36. Shyjan, A. W., de Sauvage, F. J., Gillett, N. A., Goeddel, D. V. & Lowe, D. G.: Molecular cloning of a retina-specific membrane guanylyl cyclase. *Neuron* **9**, 727-737 (1992).

37. Margulis, A., Goraczniak, R. M., Duda, T., Sharma, R. K. & Sitaramayya, A.: Structural and biochemical identity of retinal rod outer segment membrane guanylate cyclase. *Biochem Biophys Res Commun* **194**, 855-861 (1993).

38. Yang, R. B., Fulle, H. J. & Garbers, D. L.: Chromosomal localization and genomic organization of genes encoding guanylyl cyclase receptors expressed in olfactory sensory neurons and retina. *Genomics* **31**, 367-372 (1996).

39. Lowe, D. G., Dizhoor, A. M., Liu, K., Gu, Q., Spencer, M., Laura, R., Lu, L. & Hurley, J. B.: Cloning and expression of a second photoreceptor-specific membrane retina guanylyl cyclase (RetGC), RetGC-2. *Proc Natl Acad Sci U S A* **92**, 5535-5539 (1995).

40. Dizhoor, A. M. & Hurley, J. B.: Regulation of photoreceptor membrane guanylyl cyclases by guanylyl cyclase activator proteins. *Methods* **19**, 521-531 (1999).

41. Haeseleer, F., Sokal, I., Li, N., Pettenati, M., Rao, N., Bronson, D., Wechter, R., Baehr, W. & Palczewski, K.: Molecular characterization of a third member of the guanylyl cyclase- activating protein subfamily. *J Biol Chem* **274**, 6526-6535 (1999).

42. Duda, T., Goraczniak, R. M. & Sharma, R. K.: Molecular characterization of S100A1-S100B protein in retina and its activation mechanism of bovine photoreceptor guanylate cyclase. *Biochemistry* **35**, 6263-6266 (1996).

43. Pozdnyakov, N., Goraczniak, R., Margulis, A., Duda, T., Sharma, R. K., Yoshida, A. & Sitaramayya, A.: Structural and functional characterization of retinal calcium-dependent guanylate cyclase activator protein (CD-GCAP): identity with S100beta protein. *Biochemistry* **36**, 14159-14166 (1997).

44. Laura, R. P., Dizhoor, A. M. & Hurley, J. B.: The membrane guanylyl cyclase, retinal guanylyl cyclase-1, is activated through its intracellular domain. *J Biol Chem* **271**, 11646-11651 (1996).

45. Schrem, A., Lange, C., Beyermann, M. & Koch, K.-W.: Identification of a domain in guanylyl cyclase-activating protein 1 that interacts with a complex of guanylyl cyclase and tubulin in photoreceptors. *J Biol Chem* **274**, 6244-6249 (1999).

46. Yuen, P. S., Graeff, R. M., Walseth, T. F. & Goldberg, N. D.: Non-identity of cGMP as the guanine nucleotide stimulated to bind to ROS by light and ATP. *Exp Eye Res* **49**, 75-85 (1989).

47. Seno, K., Kishigami, A., Ihara, S., Maeda, T., Bondarenko, V. A., Nishizawa, Y., Usukura, J., Yamazaki, A. & Hayashi, F.: A possible role of RGS9 in phototransduction. A bridge between the cGMP-phosphodiesterase system and the guanylyl cyclase system. *J Biol Chem* **273**, 22169-22172 (1998).

48. Li, N., Fariss, R. N., Zhang, K., Otto-Bruc, A., Haeseleer, F., Bronson, D., Qin, N, Yamazaki, A., Subbaraya, I., Milam, A. H., Palczewski, K. & Baehr, W.: Guanylate-cyclase-inhibitory protein is a frog retinal $Ca^{2+}$-binding protein related to mammalian guanylate-cyclase-activating proteins. *Eur J Biochem* **252**, 591-599 (1998).

49. Yu, H., Olshevskaya, E., Duda, T., Seno, K., Hayashi, F., Sharma, R. K., Dizhoor, A. M. & Yamazaki, A.: Activation of retinal guanylyl cyclase-1 by $Ca^{2+}$-binding proteins involves its dimerization. *J Biol Chem* **274**, 15547-15555 (1999).

50. Yang, R. B. & Garbers, D. L.: Two eye guanylyl cyclases are expressed in the same photoreceptor cells and form homomers in preference to heteromers. *J Biol Chem* **272**, 13738-13742 (1997).

51. Duda, T., Goraczniak, R., Surgucheva, I., Rudnicka-Nawrot, M., Gorczyca, W. A., Palczewski, K., Sitaramayya, A., Baehr, W. & Sharma, R. K.: Calcium modulation of bovine photoreceptor guanylate cyclase. *Biochemistry* **35**, 8478-8482 (1996).

52. Laura, R. P. & Hurley, J. B.: The kinase homology domain of retinal guanylyl cyclases 1 and 2 specifies the affinity and cooperativity of interaction with guanylyl cyclase activating protein-2. *Biochemistry* **37**, 11264-11271 (1998).

53. Duda, T., Venkataraman, V., Goraczniak, R., Lange, C., Koch, K.-W. & Sharma, R. K.: Functional consequences of a rod outer segment membrane guanylate cyclase (ROS-GC1) gene mutation linked with Leber's congenital amaurosis. *Biochemistry* **38**, 509-515 (1999).

54. Duda, T., Krishnan, A., Venkataraman, V., Lange, C., Koch, K.-W. & Sharma, R. K.: Mutations in the rod outer segment membrane guanylate cyclase in a cone-rod dystrophy cause defects in calcium signaling. *Biochemistry* **38**, 13912-13919 (1999).

55. Tucker, C. L., Woodcock, S. C., Kelsell, R. E., Ramamurthy, V., Hunt, D. M. & Hurley, J. B.: Biochemical analysis of a dimerization domain mutation in RetGC-1 associated with dominant cone-rod dystrophy. *Proc Natl Acad Sci U S A* **96**, 9039-9044 (1999).

56. Kelsell, R. E., Gregory-Evans, K., Payne, A. M., Perrault, I., Kaplan, J., Yang, R. B., Garbers, D. L., Bird, A. C., Moore, A. T. & Hunt, D. M.: Mutations in the retinal guanylate cyclase (RETGC-1) gene in dominant cone-rod dystrophy. *Hum Mol Genet* **7**, 1179-1184 (1998).

57. Liu, Y., Ruoho, A. E., Rao, V. D. & Hurley, J. H.: Catalytic mechanism of the adenylyl and guanylyl cyclases: modeling and mutational analysis. *Proc Natl Acad Sci U S A* **94**, 13414-13419 (1997).

58. Lange, C.. Identifizierung regulatorischer Regionen in der partikulären Guanylatzyklase aus Photorezeptoraußensegmenten ROS-GC1. IBI-1, *Forschungzentrum Jülich* (1999).

59. Lange, C., Duda, T., Beyermann, M., Sharma, R. K. & Koch, K.-W.: Regions in vertebrate photoreceptor guanylyl cyclase ROS-GC1 involved in $Ca^{2+}$-dependent regulation by guanylyl cyclase-activating protein GCAP-1. *FEBS Lett* **460**, 27-31 (1999).

60. Sokal, I., Haeseleer, F., Arendt, A., Adman, E. T., Hargrave, P. A. & Palczewski, K.: Identification of a guanylyl cyclase-activating protein-binding site within the catalytic domain of retinal guanylyl cyclase 1. *Biochemistry* **38**, 1387-1393 (1999).

61. Dizhoor, A. M., Olshevskaya, E. V., Henzel, W. J., Wong, S. C., Stults, J. T., Ankoudinova, I. & Hurley, J. B.: Cloning, sequencing, and expression of a 24-kDa $Ca^{2+}$-binding protein activating photoreceptor guanylyl cyclase. *J Biol Chem* **270**, 25200-25206 (1995).

62. Dizhoor, A. M., Lowe, D. G., Olshevskaya, E. V., Laura, R. P. & Hurley, J. B.: The human photoreceptor membrane guanylyl cyclase, RetGC, is present in outer segments and is regulated by calcium and a soluble activator. *Neuron* **12**, 1345-1352 (1994).

63. Palczewski, K., Subbaraya, I., Gorczyca, W. A., Helekar, B. S., Ruiz, C. C., Ohguro, H., Huang, J., Zhao, X., Crabb, J. W. & Johnson, R. S.: Molecular cloning and characterization of retinal photoreceptor guanylyl cyclase-activating protein. *Neuron* **13**, 395-404 (1994).

64. Subbaraya, I., Ruiz, C. C., Helekar, B. S., Zhao, X., Gorczyca, W. A., Pettenati, M. J., Rao, P. N., Palczewski, K. & Baehr, W.: Molecular characterization of human and mouse photoreceptor guanylate cyclase-activating protein (GCAP) and chromosomal localization of the human gene. *J Biol Chem* **269**, 31080-31089 (1994).

65. Surguchov, A., Bronson, J. D., Banerjee, P., Knowles, J. A., Ruiz, C., Subbaraya, I., Palczewski, K. & Baehr, W.: The human GCAP1 and GCAP2 genes are arranged in a tail-to-tail array on the short arm of chromosome 6 (p21.1). *Genomics* **39**, 312-322 (1997).

66. Müller, F. & Koch, K.-W.: Calcium-binding proteins and nitric oxide in retinal function and disease. *Acta Anat* **162**, 142-150 (1998).

67. Kachi, S., Nishizawa, Y., Olshevskaya, E., Yamazaki, A., Miyake, Y., Wakabayashi, T., Dizhoor, A. & Usukura, J.: Detailed localization of photoreceptor guanylate cyclase activating protein-1 and -2 in mammalian retinas using light and electron microscopy. *Exp Eye Res* **68**, 465-473 (1999).

68. Payne, A. M., Downes, S. M., Bessant, D. A. R., Taylor, R., Holder, G. E., Warren, M. J., Bird, A. C. & Bhattacharya, S. S.: A mutation in guanylate cyclase activator 1A (GUCA1A) in an

autosomal dominant cone dystrophy pedigree mapping to a new locus on chromosome 6p21.1. *Hum Mol Genet* **7**, 273-277 (1998).

69. Payne, A. M., Downes, S. M., Bessant, D. A. R., Plant, C., Moore, T., Bird, A. C. & Bhattacharya, S. S.: Genetic analysis of the guanylate cyclase activator 1B (GUCA1B) gene in patients with autosomal dominant retinal dystrophies. *J Med Genet* **36**, 691-693 (1999).

70. Downes, S. M., Holder, G. E., Fitzke, F. W., Payne, A. M., Warren, M. J., Bhattacharya, S. S. & Bird AC: Autosomal dominant cone and cone-rod dystrophy with mutations in the guanylate cyclase activator 1A gene-encoding guanylate cyclase activating protein-1. *Arch Ophthalmol* **119**, 96-105 (2001).

71. Sokal, I., Li, N., Verlinde, C. L., Haeseleer, F., Baehr, W. & Palczewski, K.: $Ca^{2+}$-binding proteins in the retina: from discovery to etiology of human disease(1). *Biochim Biophys Acta* **1498**, 233-251 (2000).

72. Olshevskaya, E. V., Hughes, R. E., Hurley, J. B. & Dizhoor, A. M.: Calcium binding, but not a calcium-myristoyl switch, controls the ability of guanylyl cyclase-activating protein GCAP-2 to regulate photoreceptor guanylyl cyclase. *J Biol Chem* **272**, 14327-14333 (1997).

73. Frins, S., Bönigk, W., Muller, F., Kellner, R. & Koch, K.-W.: Functional characterization of a guanylyl cyclase-activating protein from vertebrate rods. Cloning, heterologous expression, and localization. *J Biol Chem* **271**, 8022-8027 (1996).

74. Rocque, W. J., McWherter, C. A., Wood, D. C. & Gordon, J. I.: A comparative analysis of the kinetic mechanism and peptide substrate specificity of human and *Saccharomyces cerevisiae* myristoyl-CoA: protein N-myristoyltransferase. *J Biol Chem* **268**, 9964-9971 (1993).

75. Zozulya, S. & Stryer, L.: Calcium-myristoyl protein switch. *Proc Natl Acad Sci U S A* **89**, 11569-11573 (1992).

76. Lange, C. & Koch, K.-W.: Calcium-dependent binding of recoverin to membrane monitored by surface plasmon resonance spectroscopy in real time. *Biochemistry* **36**, 12019-12026 (1997).

77. Gorodovikova, E. N., Senin, I. I. & Philippov, P. P.: Calcium-sensitive control of rhodopsin phosphorylation in the reconstituted system consisting of photoreceptor membranes, rhodopsin kinase and recoverin. *FEBS Lett* **353**, 171-172 (1994).

78. Calvert, P. D., Klenchin, V. A. & Bownds, M. D.: Rhodopsin kinase inhibition by recoverin. Function of recoverin myristoylation. *J Biol Chem* **270**, 24127-24129 (1995).

79. Kumar, V. D., Vijay-Kumar, S., Krishnan, A., Duda, T. & Sharma, R. K.: A second calcium regulator of rod outer segment membrane guanylate cyclase, ROS-GC1: neurocalcin. *Biochemistry* **38**, 12614-12620 (1999).

80. Flaherty, K. M.,, Zozulya, S., Stryer, L. & Mckay, D. B.: Three-dimensional structure of recoverin, a calcium sensor in vision. *Cell* **75**, 709-716 (1993).

81. Means, A. R., Tash, J. S. & Chafouleas, J. G.: Physiological implications of the presence, distribution, and regulation of calmodulin in eukaryotic cells. *Physiol Rev* **62**, 1-39 (1982).

82. Sambrook, J., Fritsch, E. F. & Maniatis, R.: *Molecular Cloning, A Laboratory Manual*, 2nd ed. NY: Cold Spring Harbor (1989).

83. Tsien, R. & Pozzan, T.: Measurement of cytosolic free $Ca^{2+}$ with Quin2. In *Biomembranes (Part T: Transport Theory: Cells and Model Membranes)*. Edited by Fleisher, S. & Fleisher, B., San Diego: Academic Press, 230-262 (1989).

84. Schoenmakers, T. J., Visser, G. J., Flik, G. & Theuvenet, A. P.: CHELATOR: an improved method for computing metal ion concentrations in physiological solutions. *Biotechniques* **12**, 870-879 (1992).

85. Hanahan, D.: Techniques for Transformation of E.coli. In *DNA Cloning*, Edited by Rickwood, D. & Hames, B. D., IRL Press 109-135 (1985).

86. Studier, F. W. & Moffatt, B. A.: Use of bacteriophage T7 RNA polymerase to direct selective high-level expression of cloned genes. *J Mol Biol* **189**, 113-130 (1986).

87. Carstens, C.-P. & Waesche, A.: Codon bias-adjusted BL21 derivatives for protein expression. *Strategies* **12**, 49-51 (1999).

88. Studier, F. W., Rosenberg, A. H., Dunn, J. J. & Dubendorff, J. W.: Use of T7 RNA polymerase to direct expression of cloned genes. In *Gene Expression Technology*. Edited by Goeddel, D. V., San Diego: Academic Press, 60-89 (1990).

89. Gordon, J. I., Duronio, R. J., Rudnick, D. A., Adams, S. P. & Gokel, G. W.: Protein N-myristoylation. *J Biol Chem* **266**, 8647-8650 (1991).

90. Pace, C. N. & Schmid, F. X.: How to determine the molar absorbance coefficient of a protein. In *Protein Structure - A Practical Approach*, 2nd ed. Edited by Creighton, T.E., Oxford: IRL Press at Oxford University Press, 253-260 (1997).

91. Bradford, M. M.: A rapid and sensitive method for the quantitation of microgram quantities of protein utilizing the principle of protein-dye binding. *Anal Biochem* **72**, 248-254 (1976).

92. Laemmli, U. K.: Cleavage of structural proteins during the assembly of the head of the bacteriophage T4. *Nature* **227**, 680-685 (1970).

93. Weber, K. & Osborn, M.: The reliability of molecular weight determinations by dodecyl sulfate-polyacrylamide gel electrophoresis. *J Biol Chem* **244**, 4406-4412 (1969).

94. Bollag, D. M., Rozycki, M. D. & Edelstein, S. J.: *Protein Methods*, 2nd ed. NY: Wiley-Liss (1996).

95. Goldenberg, D. P.: Analysis of protein conformation by gel electrophoresis. In *Protein Structure - A Practical Approach*, 2nd ed. Edited by Creighton, T. E., Oxford: IRL Press at Oxford University Press, 187-218 (1997).

96. Lambrecht, H. G. & Koch, K.-W.: A 26 kd calcium binding protein from bovine rod outer segments as modulator of photoreceptor guanylate cyclase. *EMBO J* **10**, 793-798 (1991).

97. Frins, S.. Funktionelle Charakterisierung eines Guanylatzyklase-aktivierenden Proteins aus Photorezeptorzellen von Wirbeltieren. IBI-1, *Forschungzentrum Jülich* (1996).

98. Protein Purification Methods - A Practical Approach. Edited by Harris, E. L. V. & Angal, S., Oxford: IRL Press at Oxford University Press (1995).

99. Hirose, M., Takahashi, N., Oe, H. & Doi, E.: Analysis of intramolecular disulfide bonds in proteins by polyacrylamide gel electrophoresis following two-step alkylation. *Anal Biochem* **168**, 193-201 (1988).

100. Hollecker, M.: Counting integral numbers of residues by chemical modification. In *Protein Structure - A Practical Approach*, 2nd ed. Edited by Creighton, T. E., Oxford: IRL Press at Oxford University Press, 151-164 (1997).

101. Ellman, G. L.: Tissue sulfhydryl group. *Arch Biochem Biophys* **82**, 70-77 (1959).

102. Hermanson, G. T.: *Bioconjugate Techniques*. San Diego: Academic Press (1996).

103. Colman, R. F.: Affinity labelling . In *Protein Function - A Practical Approach*, 2nd ed. Edited by Creighton, T. E., Oxford: IRL Press at Oxford University Press, 155-183 (1997).

104. *Circular Dichroism and the Conformational Analysis of Biomolecules*. Edited by Fasman, G. D., New York: Plenum Press (1996).

105. Rodger, A. & Nordén, B.: *Circular Dichroism and Linear Dichroism*. Oxford University Press (1997).

106. Wollmer, A.: ORD and CD Spectroscopy. In *Biophysics*. Edited by Hoppe, W., Lohmann, W., Markl, H. & Ziegler, H., Berlin Heidelberg: Springer-Verlag, 144-151 (1983).

107. Marin, S. R.: Circular dichroism. In *Proteins*. Edited by Price, N. C., Oxford: BIOS Scientific Publishers jointly by Academic Press, 195-204 (1996).

108. Schmid, F. X.: Optical spectroscopy to characterize protein conformation and conformational changes. In *Protein Structure - A Practical Approach*, 2nd ed. Edited by Creighton, T. E., Oxford: IRL Press at Oxford University Press, 261-298 (1997).

109. Jensen, O. N., Shevchenko, N. & Mann, M.: Protein analysis by mass spectrometry. In *Protein Structure - A Practical Approach*, 2nd ed. Edited by Creighton, T. E., Oxford: IRL Press at Oxford University Press, 29-58 (1997).

110. Siuzdak, G.: *Mass Spectrometry for Biotechnology*. Academic Press (1996).

111. Myszka, D. G.: Kinetic analysis of macromolecular interactions using surface plasmon resonance biosensors. *Current Opinion in Biotechnology* **8**, 50-57 (1997).

112. Schuck, P.: Use of surface plasmon resonance to probe the equilibrium and dynamic aspects of interactions between biological macromolecules. *Annu Rev Biophys Biomol Struct* **26**, 541-566 (1997).

113. Koch, K.-W.: Identification and characterization of calmodulin binding sites in cGMP-gated channel using surface plasmon resonance spectroscopy. In *Vertebrate Phototransduction and the Visual Cycle (Part A)*. Edited by Palczewski, K.. Washington: Academic Press, 785-797 (2000).

114. Levitzki, A.: Ligand binding. In *Protein Function - A Practical Approach*, 2nd ed. Edited by Creighton, T. E., Oxford: IRL Press at Oxford University Press, 101-129 (1997).

115. *Real-time BIA, Biomolecular interaction analysis; BIAcore™ methods manuel*. Uppsala, Sweden: Biacore (1993).

116. Duronio, R. J., Jackson-Machelski, E., Heuckeroth, R. O., Olins, P. O., Devine, C. S., Yonemoto, W., Slice, L. W., Taylor, S. S. & Gordon, J. I.: Protein N-myristoylation in *Escherichia coli*: reconstitution of a eukaryotic protein modification in bacteria. *Proc Natl Acad Sci U S A* **87**, 1506-1510 (1990).

117. Provencher, S. W. & Glöckner, J.: Estimation of globular protein secondary structure from circular dichroism. *Biochemistry* **20**, 33-37 (1981).

118. Burgess, W. H., Jemiolo, D. K. & Kretsinger, R. H.: Interaction of calcium and calmodulin in the presence of sodium dodecyl sulfate. *Biochim Biophys Acta* **623**, 257-270 (1980).

119. Lambrecht, H. G. & Koch, K.-W.: Recoverin, a novel calcium-binding protein from vertebrate photoreceptors. *Biochim Biophys Acta* **1160**, 63-66 (1992).

120. Siegel, L. M. & Monty, K. J.: Determination of molecular weights and frictional ratios of proteins in impure systems by use of gel filtration and density gradient centrifugation. Application to crude preparations of sulfite and hydroxylamine reductases. *Biochim Biophys Acta* **112,** 346-362 (1966).

121. Hollecker, M.: Counting integral numbers of residues by chemical modification. In *Protein Structure - A Practical Approach*, 2nd ed. Edited by Creighton, T. E., Oxford: IRL Press at Oxford University Press, 151-164 (1997).

122. Ewbank, J. J. & Creighton, T. E.: Pathway of disulfide-coupled unfolding and refolding of bovine alpha-lactalbumin. *Biochemistry* **32**, 3677-3693 (1993).

123. Blacklow, S. C. & Knowles, J. R.: Spiked oligonucleotide mutagenesis. In *Directed Mutagenesis: A Practical Approach*. Edited by McPherson, M. J., Oxford: IRL Press, 177-198 (1991).

124. Richards, J. H.: Cassette mutagenesis. In *Directed Mutagenesis: A Practical Approach*. Edited by McPherson, M. J., Oxford: IRL Press, 199-216 (1991).

125. Zoche, M., Bienert, M., Beyermann, M. & Koch, K.-W.: Distinct molecular recognition of calmodulin-binding sites in the neuronal and macrophage nitric oxide synthases: a surface plasmon resonance study. *Biochemistry* **35**, 8742-8747 (1996).

126. Kretsinger, R. H.: Structure and evolution of calcium-modulated proteins. *CRC Crit Rev Biochem* **8**, 119-174 (1980).

127. Kretsinger, R. H.: EF-hands reach out. *Nat Struct Biol* **3**, 12-15 (1996).

128. Burgoyne, R. D. & Weiss, J. L.: The neuronal calcium sensor family of $Ca^{2+}$-binding proteins. *Biochem J* **353**, 1-12 (2001).

129. Ames, J. B., Dizhoor, A. M., Ikura, M., Palczewski, K. & Stryer, L.: Three-dimensional structure of guanylyl cyclase activating protein-2, a calcium-sensitive modulator of photoreceptor guanylyl cyclases. *J Biol Chem* **274**, 19329-19337 (1999).

130. Ray, S., Zozulya, S., Niemi, G. A., Flaherty, K. M., Brolley, D., Dizhoor, A. M., Mckay, D. B., Hurley, J. B. & Stryer, L.: Cloning, expression, and crystallization of recoverin, a calcium sensor in vision. *Proc Natl Acad Sci U S A* **89**, 5705-5709 (1992).

131. Vijay-Kumar, S. & Kumar, V. D.: Crystal structure of recombinant bovine neurocalcin. *Nat Struc Biol* **6**, 80-88 (1999).

132. Ikura, M.: Calcium binding and conformational response in EF-hand proteins. *TIBS* **21**, 14-17 (1996).

133. Sokal, I., Otto-Bruc, A., Surgucheva, I., Verlinde, C. L., Wang, C. K., Baehr, W. & Palczewski, K.: Conformational changes in guanylyl cyclase-activating protein 1 (GCAP1) and its tryptophan mutants as a function of calcium concentration. *J Biol Chem* **274**, 19829-19837 (1999).

134. Hughes, R. E., Brzovic, P. S., Dizhoor, A. M., Klevit, R. E. & Hurley, J. B.: $Ca^{2+}$-dependent conformational changes in bovine GCAP-2. *Protein Sci* **7**, 2675-2680 (1998).

135. Kataoka, M., Mihara, K. & Tokunaga, F.: Recoverin alters its surface properties depending on both calcium-binding and N-terminal myristoylation. *J Biochem (Tokyo)* **114**, 535-540 (1993).

136. Hunter, M. J. & Chazin, W. J.: High level expression and dimer characterization of the S100 EF-hand proteins, migration inhibitory factor-related proteins 8 and 14. *J Biol Chem* **273**, 12427-12435 (1998).

137. Christova, P., Cox, J. A., Craescu, C. T.: Ion-induced conformational and stability changes in Nereis Sarcoplasmic calcium binding protein: evidence that the APO state is a molten globulen. *Proteins: Structure, Function, and Genetics* **40**, 177-184 (2000).

138. Speed, M. A., Wang, D. I. & King, J.: Specific aggregation of partially folded polypeptide chains: the molecular basis of inclusion body composition. *Nat Biotechnol* **14**, 1283-1287 (1996).

139. Rudnicka-Nawrot, M., Surgucheva, I., Hulmes, J. D., Haeseleer, F., Sokal, I., Crabb, J. W., Baehr, W. & Palczewski, K.: Changes in biological activity and folding of guanylate cyclase-activating protein 1 as a function of calcium. *Biochemistry* **37**, 248-257 (1998).

140. Olshevskaya, E. V., Ermilov, A. N. & Dizhoor, A. M.: Dimerization of guanylyl cyclase-activating protein and a mechanism of photoreceptor guanylyl cyclase activation. *J Biol Chem* **274**, 25583-25587 (1999).

141. Otto-Bruc, A., Buczylko, J., Surgucheva, I., Subbaraya, I., Rudnicka-Nawrot, M., Crabb, J. W., Arendt, A., Hargrave, P. A., Baehr, W. & Palczewski, K.: Functional reconstitution of photoreceptor guanylate cyclase with native and mutant forms of guanylate cyclase-activating protein 1. *Biochemistry* **36**, 4295-4302 (1997).

142. Ames, J. B., Ishima, R., Tanaka, T., Gordon, J. I., Stryer, L. & Ikura, M.: Molecular mechanics of calcium-myristoyl switches. *Nature* **389**, 198-202 (1997).

143. Ames, J. B., Tanaka, T., Stryer, L. & Ikura, M.: Portrait of a myristoyl switch protein. *Curr Opin Struct Biol* **6**, 432-438 (1996).

144. Taylor, T., Ames, J. B., Harvey, T. S., Stryer, L. & Ikura, M.: Sequestration of the membrane-targeting myristoyl group of recoverin in the calcium-free state. *Nature* **376**, 444-447 (1995).

145. Yap, K. L., Ames, J. B., Swindells, M. B. & Ikura, M.: Diversity of conformational states and changes within the EF-hand protein superfamily. *Proteins* **37**, 499-507 (1999).

146. Marston, F. A.: The purification of eukaryotic polypeptides synthesized in *Escherichia coli*. *Biochem J* **240**, 1-12 (1986).

147. Duda, T., Venkataraman, V., Jankowska, A., Lange, C., Koch, K.-W. & Sharma, R. K.: Impairment of the rod outer segment membrane guanylate cyclase dimerization in a cone-rod dystrophy results in defective calcium signaling. *Biochemistry* **39**, 12522-12533 (2000).

148. Creighton, T. E.: *Proteins : Structures and molecular properties*, 2nd ed. New York: W.H. Freeman and Company (1996).

149. Branden, C. & Tooze, J.: *Introduction to protein structure*, 2nd ed. New York: Garland Publishing (1999)

# ACKNOWLEDGEMENTS

First of all I would like to express gratitude to my supervisor, Professor Georg Büldt, for invaluable guidance and unconditional support and also to my adviser, Priv. Doz. Dr. Karl-Wilhelm Koch, for countless and tireless discussions, for sharing his vast knowledge and experiences, and for introducing me to so many interesting themes in the field of biochemistry. In addition, I am grateful to Dr. Ramona Schlesinger for her advise and coaching in the field of molecular biology. She provided me valuable training of mutagenesis to construct mutants, which resulted in nice studies presented in this thesis.

I would like to thank the following people for experiments and discussions: Dr. Christian Lange (IBI-1, Forschungszentrum Jülich) for provision of mD$^{6}$S-GCAP-1 and for kind communication, Dr. Michael Beyermann (Forschungsinstitut für Molekulare Pharmakologie, Berlin) for synthesis of the peptides, Dr. Joachim Grötzinger (Institut für Biochemie, RWTH Klinikum Aachen) for measurement of CD spectroscopy, Dr. Gerd Dongmann and Van Dy Nguyen (ICG-7, Forschungszentrum Jülich) for MALDI-TOF mass spectrometry, and Dr. Bernd König for NMR spectroscopy. I appreciate Dr. Joachim Herberle for many useful discussions about macromolecular spectroscopy and Drs. Jörg Labahn and Joachim Granzin for their clear explanations of crystallography and three-dimensional structure of proteins.

I must thank all the past and present members in IBI-1 and IBI-2 in Research Centre Jülich for their generous help, useful discussions, and harmonious atmosphere for working in laboratories and offices. They are Karin Abarca-Heidemann, Carsten Bolwien, Petra Censarek, Anne Cousin, Anita Eckert, Andreas Eckhoff, Ulf Eidhoff, Rudi Esser, Dirk Fasterman, Nicole Ficek, Torsten Fischer, Sandra Frins, Ellisabeth Fuß, Dominic Hehn, Dirk Heitbrink, Annika Helbig, Doris Höppner-Heitmann, Birgit Gehrmann, Ralf Geßenich, Verena Kehren, Rainer Kofahl, Bianca Krafft, Christian Lange, Andy Mahoney, Ilona Ritter, Annette Sasse, Alexander Schrem, Dimitri Traenker, Dietmar Weitz, Martin Zoche, et al.

I appreciate Karin Abarca-Heidemann, Petra Censarek, and Annette Sasse for sparing no efforts on finishing up this work. Especially I must thank Rebecca Nyquist (Uni. Illinois, Urbana) for neverending correction and counsels of this thesis and Dr. Samuel K. H. Jun (IPV, Forschungszentrum Jülich) for worthy manuscripts, critical correction, prominent compilation, and several days' overnight work for my thesis.

I would like to gratefully acknowledge the DAAD (Deutscher Akademischer Austauschdienst) scholarship to support and promote this doctoral program for three years and to provide me with the great opportunities of visiting the German course at the Goethe institute in Göttingen in 1997 and taking part in the symposium with 20 Nobel Prize in chemistry winners in Lindau in 1998.

Special thanks go to Professor Hui-Woog Choe (Chonbuk National University, Korea and Charité / Humboldt Universität Berlin, Germany) for his encouragement and guidance in the world of biochemistry and the life of enterprise. He provided me with great opportunities to work and train in his laboratory as a graduate student in Chonbuk National University and to come to Germany to study in Jülich. I am grateful to his wife, Jung-Hee Kim, and two sons, Jin-Gon and Sung-Gon, in Berlin for their warm hearts. I really feel that they are like my family.

Above all things, I would like to give thanks to my parents for their endless patience, sacrifices, support, encouragement, and love to me, their only daughter. Without spiritual and material help and the support of my parents, teachers, colleagues, and friends, this doctoral thesis could not be completed.

Finally, I dedicate all my honor and glory to the Lord, Jesus Christ.

# *Curriculum Vitae*


**Name** : Ji-Young Hwang

**Date of Birth** : Jan. 25th, 1972

**Place of Birth** : Seoul, S. Korea

**Present Address** : Bocksgasse 9, 52428 Jülich, Germany

**Address of Institute** : IBI-2, Forschungszentrum Jülich, 52425 Jülich, Germany

**Telephone No. :** +49-2461-618069

**Fax No. :** +49-2461-614216

**E-Mail :** j.hwang@fz-juelich.de


## Educational Achievement

Feb. 1994 : B. S., Department of Chemistry, Chonbuk National University, Chon-Ju, S. Korea

Feb. 1996 : M. S., Department of Chemistry, Chonbuk National University, Chon-Ju, S. Korea
Theme of <*Biochemical Studies on Proteinase K Inhibitor-1 from Wheat Germ*>

Sep. 1997 : DSH (Deutsche Sprachprüfung für den Hochschulzugang ausländischer Studienbewerber), Goethe Institute, Göttingen, Germany

## Academic Activities

Mar. 1990 ~ Feb. 1996 : Membership, Association of the Personal Computer users, Chonbuk National University, Chon-Ju, S. Korea

Aug. 1995 ~ Dec. 1995 : Teaching Assistant, Department of Chemistry, Chonbuk National University, Chon-Ju, S. Korea

Oct. 1996 ~ May 1996 : Visiting Researcher, IBI-2 (Institute of Structural Biology), Forschungszentrum Jülich, Jülich, Germany

Jun. 1996 ~ Sep. 1996 : Participant of German Course, Goethe Institute, Göttingen, Germany

Jun. 1997 ~ Sep. 2000: Grant of DAAD (Deutscher Akademischer Austauschdienst)

Oct. 1997 ~ Jul. 2001 : Doctoral Student, Department of Biology, Heinrich-Heine-Universität Düsseldorf, Düsseldorf, Germany

Oct. 1996 ~ Jul. 2001 : Researcher as a Ph.D. Student, IBI-2 (Institute of Structural Biology), Forschungszentrum Jülich, Jülich, Germany